Mycobacterium amidases: Biological function and putative role in cell wall remodeling

Nombeko Sikhosana (551945)

M.Sc. report submitted to the Faculty of Health Science, University of the Witwatersrand, Johannesburg, in fulfillment of the requirements for the degree of Master of Science in Medicine.

March 2018

Declaration

I, Sikhosana Nombeko declare that this Dissertation is my own work. It is being submitted for M.Sc. (Medicine) degree in Health Sciences, University of the Witwatersrand, Johannesburg. This paper has not been submitted before for a Degree or examination at any university or this.

Nombeko Sikhosana

MSc. Candidate

Date

Presentations from this study

Conference Molecular Biosciences Research Thrust Research Day
Presentation: Poster presentation
Date: 08 December 2016
Wits Club, West campus, University of the Witwatersrand

Conference 8th Cross-Faculty Graduate Symposium
Presentation: Oral presentation
Date: 25 October 2017
School of Public Health Auditorium, University of the Witwatersrand

Conference Molecular Biosciences Research Thrust Research Day
Presentation: Poster presentation
Date: 30 November 2017
Wits Club, West campus, University of the Witwatersrand

Abstract

Mycobacterium tuberculosis, the causative agent of tuberculosis, uses macrophages to cross host mucosal barriers and initiate infection at sterile sites in the alveoli, where it establishes infection and evades immune detection. Despite significant effort, the mechanism through which mycobacteria replicate and persist within host tissues remains enigmatic. Bacterial replication requires substantive rearrangement of the cell surface and in this context, the bacterial cell wall and the enzymes that remodel the various polymers present in this structure are of particular interest. Within the cell wall, the bacterial peptidoglycan (PG) layer has been the subject of intense research, given the therapeutic benefit of targeting this macromolecule in various diseases. PG hydrolases specifically, *N*-acetylmuramyl-L-alanine amidases (amidases) in other bacterial species have been shown to contribute to essential cell division processes and pathogenesis. In this study, the role of mycobacterial amidases in cell growth and division was investigated to assess their function in *Mycobacterium smegmatis*, a model organism routinely used for tuberculosis research. For this, putative amidase-encoding genes *ami3*, *ami4* and *ami5* were individually deleted using homologous recombination. The resulting mutant strains were then phenotypically characterized by investigating nascent cell wall incorporation, cell elongation and division mechanisms. Deletion of *ami3* resulted in severe cell division defects, in many cases these were associated with mislocalization of the cell elongation and division apparatus. In addition to this, cell wall permeability was severely affected, with the strain displaying increased susceptibility to cell wall targeting antibiotics. Deletion of *ami4* resulted in the formation of twisted and morphologically atypical cells, some of which died after the first cell division event. In contrast, deletion of *ami5* resulted in the formation of short cells, suggesting that this enzyme plays a role in cell growth/elongation. Collectively, these data describe novel and non-redundant roles for amidases in mycobacterial cell growth and division, thus validating them as potential new drug targets for tuberculosis disease

Acknowledgments

I would like to Thank Prof Bavesh D. Kana and Dr. Melissa D. Chengalroyen for giving me the opportunity to work with them, mentoring me and playing a significant role in my growth during my Postgraduate studies. May their teachings be manifested in all I do.

I would like to express my sincerest gratitude to my financial sponsors (National Research Foundation [NRF]) and University of the Witwatersrand.

Lastly, I would like to thank the CBTBR staff members.

Table of contents

Declaration.....II
Presentations from this MSc. ……III
Abstract IV
Acknowledgements.....V
Nomenclature/List of Abbreviations and symbols……..……...XII
List of Figures XV
List of Tables…….XIX

1. Introduction

1.1. Background……...1

1.2 TB infection - Persistence and immune evasion……1

1.3 Anti-TB strategies……..4

1.4 The mycobacterial cell wall: novel drug target…….....5

1.5 Peptidoglycan biosynthesis……....5

1.6 Targeting PG biosynthesis for drug development…….8

1.7 PG modification: Benefits for fitness……....9

1.8 Peptidoglycan modifications during dormancy……10

1.9 Role of PG and its hydrolases in virulence…….....11

1.10 PG modifying hydrolases……11

1.10.1 Glucosidases as servants of beta lactamase expression……12

1.10.1.1 *N*-acetyl-β-D-glucosaminidases…….....12

1.10.1.2 *N*-acetyl β-D-muramidases (Lysozymes)…….13

1.10.1.3 Lytic transglycosylases……..13

1.10.1.4 Resuscitation promoting factors……....14

1.10.2 Peptidases…….14

1.10.2.1 Endopeptidases……..15

1.10.2.2 Carboxypeptidases…….15

1.10.3 Amidases*: N*-acetylmuramyl-L-alanine amidases……16

1.10.3.1 Role of amidases in bacterial cell differentiation……..16

1.10.3.2 The role of amidases in bacterial pathogenesis…….18

1.10.3.3 Use of amidase as biomarkers, antibacterial agents and vaccine candidates……21

1.10.3.4 The role of amidases in cell wall recycling and antibiotic resistance……...22

1.10.3.5 The role of amidases in symbiosis……23

1.11 Cell division and division site placement in mycobacteria…….24

1.12 The Elongation complex…….26

1.13 Hypothesis……...28

1.14 Aims and objectives……28

Materials and Methods

2.0 Bacterial strains, plasmids, chemicals and growth conditions……..30

2.0.1 Bacterial strains and culture conditions…….....30

2.0.2 Growth conditions of *E. coli* DH5α strain……..…34

2.0.3 Growth conditions of *M. smegmatis* strains……....35

2.1 DNA manipulation…….35

2.1.1 Mycobacterial DNA extraction……...35

2.1.1.1 Cetyltrimethylammonium bromide DNA extraction (CTAB) protocol……..35

2.1.1.2 Small scale mycobacterial DNA extraction…….36

2.1.2 *E.* coli plasmid DNA extraction……..36

2.1.2.1 Plasmid bulk DNA extraction……..36

2.1.2.2 Small scale plasmid extraction…….37

2.1.3 DNA purification and removal of contaminating proteins……..37

2.1.3.1 Sodium Acetate precipitation……...37

2.1.4 Nucleic acid quantification and visualization…….38

2.1.5 DNA amplification-Polymerase chain reaction and PCR Fragment purification……...38

2.1.5.1 Roche Applied Science, United States FastStart Taq PCR……..38

2.1.5.2 Q5 High-Fidelity DNA polymerase PCR…….39

2.1.6 PCR Fragment Purification…….39

2.1.7 DNA Manipulation…….39

2.1.7.1 Restriction digestion of plasmid DNA and PCR products……...39

2.1.7.2 Phosphorylation and Dephosphorylation of DNA fragments…….….40

2.1.7.3 DNA ligations…….……..40

2.1.8 Bacterial transformation……...41

2.1.8.1 Preparation of *E. coli* chemically competent cells for transformation…….....41

2.1.9 Preparation and Transformation of *M. smegmatis* competent cells for electroporation...41

2.2 Generation of *M. smegmatis* strains used in the study…….42

2.2.1. Two-step allelic exchange homologous recombination for construction of knockout deletion mutants……..42

2.2.2 Generation of *M. smegmatis* complementation strains……44

2.2.3 Genotypic verification of the parental and mutant strain……45

2.2.3.1 Southern blot analyses…….45

2.2.3.2 Probe synthesis Electro blotting……...……...45

2.2.3.3 DNA hybridization and detection……46

2.3 Generation of amidase overexpressing strains…….....47

2. 4 Analysis of gene expression……....48

2.4.1 RNA extraction……..48

2.4.2 Reverse Transcriptase PCR (RT-PCR)/ first strand cDNA synthesis……...48

2.4.3 Quantitative real time PCR……49

2.5 Sequencing of gene fragments…….....49

2.6 Phenotypic analysis of *M. smegmatis* knockout strains……50

2.6.1 Growth kinetic analysis of *M. smegmatis* knockout strains……...50

2.6.2 Biofilm formation……..50

2.6.3 Crystal violet biomass estimation assay……..…….50

2.6.4 Minimum inhibitory concentration determination…….....51

2.6.5 The ethidium bromide assay…….51

2.7 Identification of amidase interacting partners using a bacterial 2-hybrid system (M-PFC assay)…….....52

2.7.1 Plasmid construction for the M-PFC assay…….....53

2.7.2 Mycobacterial protein fragment complementation assay…….53

2.8 Microscopy……..54

2.8.1 Copper Click reaction with D-alanine analogue……...54

2.8.2 DMN-Trehalose staining……..55

2.8.3 Scanning Electron Microscopy……56

2.8.4 Time-lapse microscopy……57

2.9 A description of the bioinformatics analyses tools used in this investigation……57

2.9.1 The BioCyc Pathway/ Genome database collection……57

2.9.2 Protein family database (pFAM) ……57

2.9.3 KEGG: Kyoto Encyclopaedia of Genes and Genomes…….....57

2.9.4 Uniprot…….....58

2.9.5 National Centre for Biotechnology Information (NCBI) Basic Local Alignment Search (BLAST) Tool…….....58

2.9.6 SMEGMALIST…….58

2.9.7 TUBERCULIST……58

2.9.8 CLUSTAL Omega…….58

2.9.9 Interactive Tree of life (ITOL) …….59

2.9.10 Search Tool for the Retrieval of Interacting Genes/Proteins (STRING) …….....59

2.9.11SignalP4.1 Server…….....59

2.9.12 Iterative Threading Assembly Refinement (I-TASSER) …….……...59

2.9.13 PyMOL…….……...60

Results

3.1.1 Identification of *M. smegmatis* amidase_2 domain containing proteins…….61

3.1.2 Phylogenetic analysis and domain conservation…….64

3.1.3 Domain organization of the amidase_2 and amidase_3 domain containing proteins….66

3.1.3.1 Amidase_2 domain proteins: Tertiary structure predictions……....67

3.2 Strategy used for the generation of *M. smegmatis* amidase gene deletions……....69

3.2.1 Construction of *M. smegmatis ami3* deletion constructs…….69

3.2.2 Construction of *M. smegmatis ami4* deletion constructs…….69

3.2.3 Construction of *M. smegmatis ami5* deletion constructs…….69

3.3 Strategy for the generation of the *M. smegmatis* amidase deletion mutant strains……....71

3.3.1 Generation of *M. smegmatis* Δ*ami3* strain……..72

3.3.2 Generation of Δ*ami4 M. smegmatis* strain……..73

3.3.3 Generation of the Δ*ami5 M. smegmatis* strain……74

3.4.1 Generation of *M. smegmatis* Δ*ami3* complementation strains ……..75

3.4.2 Construction of Δ*ami4* genetic complementation strain…….77

3.4.3 Genetic Complementation of *M. smegmatis* Δ*ami5* strain……..79

3.5 Phenotypic characterization of the Amidase_2 domain mutant *M. smegmatis* strains…..80

3.6 *M. smegmatis* Δ*ami*3 phenotypic characterization…….81

3.6.1 Mycobacterial Ami3 is dispensable for growth……..81

3.6.2 *M. smegmatis* Ami3 plays a role in biofilm formation and cell wall permeability…....82

3.6.3 Increased ethidium bromide transport across the cell wall correlates with increased antibiotic susceptibility……83

3.6.4 Maintenance of cell length is dependent on Ami3 activity……....84

3.6.5 Defective septal placement and cell division is evident in an *ami3* mutant……86

3.6.6 Ectopic polar growth in the Δ*ami3* strain as a result of DivIVA mislocalization……88

3.6.7 Mycobacterial cell wall proteins potentially interact with Ami3 to coordinate bacterial cell wall synthesis and cell division……..90

3.7 Phenotypic characterization of Δ*ami4* strain……93

3.7.1 Loss of ami4 has no effect on *M. smegmatis* growth in axenic culture…….93

3.7.2 Loss of Ami4 affects biofilm formation and teicoplanin tolerance……94

3.7.3 Ami4 has a role in PG synthesis coordination……95

3.7.4 Loss of Ami4 results in cell death……...96

3.7.5 Mislocalization of DivIVA alters mycobacterial growth dynamics……97

3.8 Role of the amidase_2 domain containing protein, Ami5, in bacterial cell length maintenance and cell wall homeostasis…….98

3.8.1 Loss of Ami5 has no effect on *M. smegmatis* growth in axenic culture……98

3.8.2 Loss of Ami5 results in inherited resistance to ethambutol and vancomycin……..…99

3.8.3 Loss of Ami5 results in the formation of mini cells……...101

3.8.4 Loss of Ami5 leads to the formation of short cells….....102

3.8.5 Loss of Ami5 leads to formation of viable short cells……....103

Discussion

4.1 Mycobacterium amidase bioinformatics review……105

4.2 Role of mycobacterial Ami3 in coordinating cell elongation and division……...106

4.3 Ami3 interactions reveal a link between the elongasome and divisome complexes and PG-Lipid layer biosynthesis……...107

4.4 Mycobacterial biomass and biofilm formation possibly depend on Ami3 function…….110

4.5 The deletion of Ami4 causes dysregulated cell wall remodeling and the release of cell wall material accompanied by cell death…….112

4.6 The role of *M. smegmatis* Ami5 in cell wall homeostasis and cell death…….113

Conclusion ……...114

Future work……..116

Supplementary Figures……117

Appendices……..131

References……137

Turnitin Report……138

Abbreviations

Ami	amidase
AAP	antarctic alkaline phosphatase
DIG	digoxigenin
DNA	deoxyribonucleic acid
hr/s	hour/s
LA	Luria-Bertani agar
LB	Luria-Bertani
MA	mycolic acid
µ	micro
Mtb	*Mycobacterium tuberculosis*
Msm	*Mycobacterium smegmatis*
NAG/GlcNac	*N*-acetylglucosamine
NAM/MurNac	*N*-acetylmuramic acid
PCR	polymerase chain reaction
PG	peptidoglycan
TRIM	Trimethoprim

List of Figures

Introduction Figures

Figure 1.1: Estimated new TB cases per 100 000 population per year as indicated by the WHO global TB report 2016

Figure 1.2: Mycobacterial host immune evasion strategies during colonization of host alveolar macrophages

Figure 1.3: Diagrammatic representation of the mycobacterial cell and cell wall layer composed of distinct macromolecules

Figure 1.4: Schematic representation of bacterial PG synthesis

Figure 1.5: Diagrammatic representation of peptidoglycan (PG) structure and hydrolases responsible for remodeling during bacterial growth

Figure 1.6: Representation of the multiprotein complex known as the divisome which responsible for coordinating bacterial cell division

Figure 1.7: Schematic representation of the mycobacterial cell elongation complex

Materials and Methods Figures

Figure 2.1: Diagrammatic representation of two step allelic exchange homologous recombination

Figure 2.2: Flow chart depicting the process involved in the analysis of cell wall stability using antibiotics (MIC) susceptibility and ethidium bromide accumulation in the cytosplasmic space

Figure 2.3: Schematic representation of the M-PFC assay for protein-protein interaction screening

Figure: 2.4: Flow diagram depicting the process involved in spatially identifying areas of new PG growth

Figure 2.5: Schematic representation of mycobacterial cell wall DMN-Trehalose staining process and the incorporation of trehalose analog

Results Figures

Figure 3.0: Flow Diagram of the study of Amidase_2 family of proteins in *M. smegmatis*

Figure 3.1: Multiple sequence alignment of the Amidase_2 domain family of proteins using Clustal Omega analysis

Figure 3.2: Phylogenetic analysis of the amidase_2 family of proteins

Figure 3.3: Domain organization of PG *N*-acetylmuramoyl-L-alanine amidases (Amidases) in *E. coli*, *M. smegmatis* and *M. tuberculosis*

Figure 3.4: Tertiary structure of the amidase_2 domain family of proteins in *E. coli* and *M. smegmatis*

Figure 3.5: Generation of amidase deletion suicide constructs

Figure 3.6: Restriction profile of p2NIL_pG17_*ami5*

Figure 3.7: Genotypic characterization of *M. smegmatis* Δ*ami3*

Figure 3.8: Genotypic characterization of *M. smegmatis* Δ*ami4*

Figure 3.9: Genotypic characterization of *M. smegmatis* Δ*ami5*

Figure 3.10: Restriction profile of pMV306H::*ami3*

Figure 3.11Genetic complementation of *M. smegmatis* Δ*ami3* with pMV306H::*ami3*

Figure 3.12: Restriction profile of pTweety::*ami4*

Figure 3.13: Genetic complementation of *M. smegmatis* Δ*ami4* mutant with pTweety::*ami4*

Figure 3.14: Restriction profiling of pMV306H::*ami5*

Figure 3.15: Growth kinetic analysis of the Δ*ami3* strain in relation to wild-type and the complement strain

Figure 3.16: Biofilm formation after 7 days in Sauton's minimal media

Figure 3.17: Analysis of cell wall permeability of the Δ*ami3* strain

Figure 3.18: *M. smegmatis ami3* modulates cell shape and division

Figure 3.19: Scanning electron micrographs of Δ*ami3* and fluorescence microscopy of mycobacterial cytoskeletal elements in the Δ*ami3* background

Figure 3.20: Mycobacterial DivIVA localization in Δa*mi3* background

Figure 3.21: Time-lapse microscopy analysis of mycobacterial cell branching and coiling in the *ami3* mutant

Figure 3.22: Time lapse microscopic images for DivIVA-rsEGFP localization

Figure 3.23: Schematic representation of possible Ami3 interacting partners as determined by the SRING database

Figure 3.24: Ami3 interacting partner screening using the M-PFC assay

Figure 3.25: Growth kinetic analyses of Δ*ami4 M. smegmatis* strain

Figure 3.26: Biofilm formation, antibiotic susceptibility and ethidium bromide diffusion in the am*i4* mutant

Figure 3.27: *M. smegmatis* Ami4 modulates cell length and shape

Figure 3.28: Time-lapse microscopy analysis of cell branching, bulging and bursting in the *ami4* mutant

Figure 3.29: DivIVA fails to properly assemble in the Δ*ami4* strain

Figure 3.30: Growth kinetic analysis of Δ*ami5* strain in relation to wild-type and complement

Figure 3.31: Drug susceptibility assay and ethidium bromide diffusion in *Δami5 M. smegmatis* strain

Figure 3.32: *M. smegmatis ami5* modulates cell shape

Figure 3.33: Scanning electron microscopy of wild-type, Δ*ami5* and Δ*ami5::ami5* strains

Figure 3.34: Time-lapse microscopy analysis of Δ*ami5* strain pole rounding and cell death

Figure 3.36: Confocal microscopy showing FtsZ localization in wild-type and Δ*ami5* strains

Discussion Figures

Figure 4.1: Model for mycobacterium Ami3 role in cell elongation and division

Figure 4.2: Proposed model for the role of Ami4 in mycobacterium cell size homeostasis

Figure 4.3: Model for the roles of mycobacterium amidase Ami5 in bacterial programmed cell death and cell size homeostasis

Supplementary Figures

Supplementary Figure 1: Multiple sequence alignment of the amidase_2 domain family of proteins in different organisms.

Supplementary Figure 2: SignalP analysis of Amidase_2 family of proteins in *M. smegmatis* (Ami3, Ami4 and Ami5) to determine presence of a signal peptide

Supplementary Figure 3: Restriction profile of p2NIL_pG17_*ami3*.

Supplementary Figure 4: Restriction profile of *ami4p2NILpG17*.

Supplementary Figure 5: Predicted Ami3 interacting partners using bioinformatics tool SPRING.

Supplementary Figure 6: *M. smegmatis ami3* modulates cell shape. Fluorescence microscopy carried out to determine alterations in cell wall synthesis using DMN-tre (Trehalose)

Supplementary Figure 7: Fluorescence microscopy of mycobacterial DivIVA localization in Δ*ami4* background.

Supplementary Figure 8: Scanning electron microscopy of mc^2155 (Wild-type), Δ*ami4* and Δ*ami4*:: *ami4* strains.

Supplementary Figure 9: Time-lapse microscopy of *M. smegmatis ami3* deficient strain and the resulting flat poles.

Supplementary Figure 10: Time-lapse microscopy of *M. smegmatis ami4* deficient strain and dysregulated cell wall synthesis

Supplementary Figure 11: Restriction profile of pUAB400_*mmpl*.

Supplementary Figure 12: Restriction profile of pUAB400_*pap2*

Supplementary Figure 13: Restriction profile of pUAB400_*glft*

Supplementary Figure 14: Restriction profile of pUAB400_*erp*.

Supplementary Figure 15: Restriction profile of pUAB300_*ami3*

Supplementary Figure 16: Restriction profile of pUAB400_*ponA1*.

List of tables

Table 2.1: List of plasmids used and generated in this study

Table 2.2: List of strains generated and used in this study

Table 3: Primer3 parameters for primer design

Table 4: Description of formula

Appendix A, Table 1: Media and recipes used in this study

Appendix A, Table 2: Reagents used in this study

Appendix A, Table 3: All primers used in the study

Appendix A, Table 4: Primers for *ami3*, *ami4* and *ami5* complementation

1. Introduction

1.1. Background

Mycobacterium tuberculosis (*Mtb*) was identified by Robert Koch in 1884 as the etiological agent of Tuberculosis (TB). TB is one of the top 10 causes of death worldwide, latently infecting a third of the world's population, which collectively serve as reservoir for future active TB cases (Lin and Flynn, 2010). Extensive programs have been implemented by the World Health Organization (WHO) to eradicate the TB pandemic, with over 36 million people being treated for TB. Despite these efforts, TB remains a global health issue, causing 10.7 million infections and 1.4 million deaths, whilst an estimated 600 000 multidrug resistant/Rifampicin (MDR/RIF) resistant cases were reported in 2016 (WHO, 2017). According to the WHO, global TB incidence is declining at 2% per year, however, an accelerated annual decline of 4-5% is needed to reach the 2030 milestone of the End TB Strategy, which aims to reduce TB incident cases by 90% (WHO, 2017). The slow rate of decline can be ascribed to the rise of HIV infections, poor diagnostics, inadequate linkage to care, poor access to drugs and treatment failure, particularly in resource limited regions such as Sub-Saharan Africa. Considering this, South Africa is among the seven countries with the highest TB incidence (Figure 1.1), despite having implemented one of the largest diagnostics and treatment programs in the world. Apart from the rise in the HIV pandemic, Type-2-diabetes, the use of immunosuppressive agents, aging and malnutrition also conribute to compromising the host's ability to control *Mtb* infection (Esmail *et al*., 2014). Furthermore, the continuing emergence and global spread of MDR-TB necessitates a thorough investigation of host-pathogen interactions and possible novel drug targets for the development of new therapeutic interventions and host directed therapies.

1.2 TB infection - Persistence and immune evasion

Mtb infection is characterized by the interplay between the host immune response and bacterial survival strategies (Sasindran and Torrelles, 2011). The initial stage of infection encompasses inhalation of *Mtb* as tiny hydrophobic aerosol droplets, released into the air when a patient with active TB coughs, these are inhaled by a close contact for the establishment of new infection in a healthy individual (Sasindran and Torrelles, 2011). Within the lung, *Mtb* is phagocytosed by

resident alveolar macrophages. However, *Mtb* possesses numerous immune evasion and virulence systems enabling survival and consequent disease progress (Simmons *et al*., 2010).

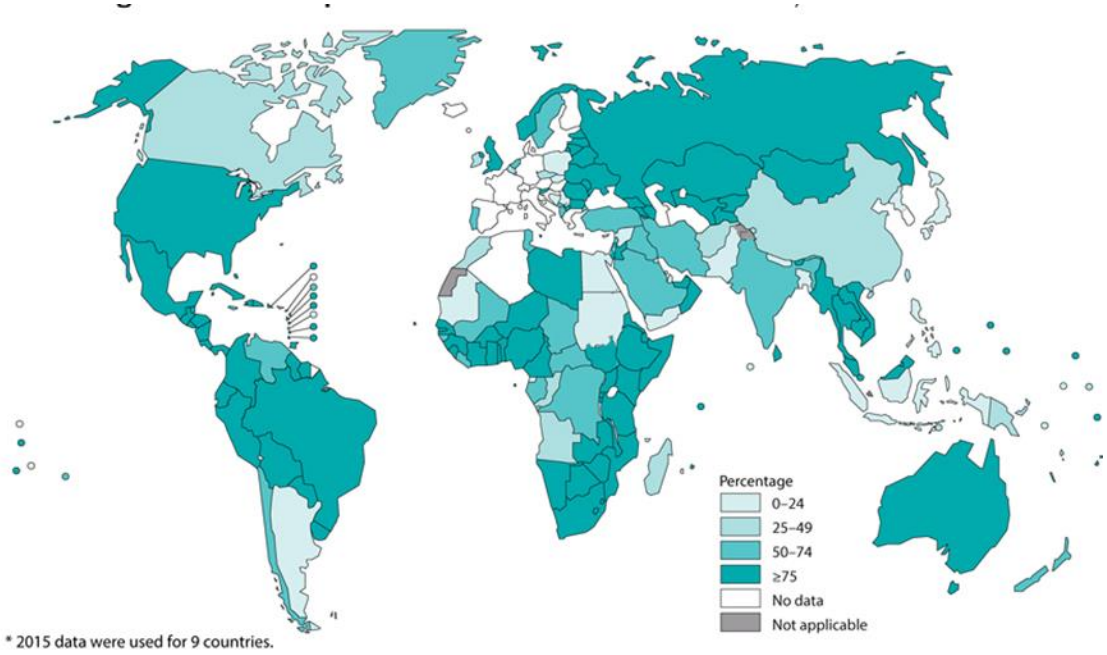

Figure 1.1: Estimated new TB cases per 100 000 population per year as indicated by the WHO global TB report 2016. The darkened regions show the highest TB incidence rates, with the Sub Saharan African region having one of the highest TB burdens. Taken from WHO 2017 report.

These mechanisms are summarized in Figure 1.2. One of the major immune evasion strategies employed by *Mtb* is the production of the cell wall -linked glycolipid pthiocerol dimycoceroserate (PDIM) which masks pathogen activated molecular patterns (PAMPs) on the bacterial surface in order to evade detection by the innate immune system (Cambier *et al*., 2014). The virulence factor phenolic glycolipid (PGL) is then used to induce macrophage chemokines such as CCL2, which recruit macrophages permissive for *Mtb* growth (Cambier *et al*., 2017). Activated alveolar macrophages may effectively clear out the infection however, *Mtb* has evolved several strategies to escape host immune clearance and survive within activated macrophages. An important mechanism related to this is the blocking of phagosome-lysosomal fusion (phagolysosome formation), which aids in the elimination of tubercle bacilli (Russel *et al*., 2002). The inhibition of phagosome maturation by *Mtb* is believed to protect the bacilli from exposure to lysosomal hydrolases and low pH, among other stressful conditions (Goldberg, Saini and Porcelli, 2014). Some mycobacterial phagosomes do undergo lysosomal fusion and *Mtb* is

able to survive under these hostile environments (Goldberg, Saini and Porcelli, 2014). Survival under acidic and nitro-oxidative niches is facilitated by mechanisms that detoxify reactive oxygen/nitrogen intermediates and repair the damage caused by these radicals (Ehrt and Schnappinger, 2009). These detoxification mechanisms include use of the KatG catalase-peroxidase, which detoxifies H_2O_2 (hydrogen peroxide) by converting it into water and oxygen, thus protecting the bacterium (Ng *et al*., 2004). Another noteworthy mechanism is the outer membrane protein OmpATb, which is responsible for providing acid resistance by decreasing the permeability of the cell envelope (Molle *et al*., 2006). These evasion strategies allow *Mtb* to escape the bactericidal effect of activated macrophages, resulting in further recruitment of activated monocytes (alveolar macrophages and dendritic cells) and neutrophils to the site of infection, which may still fail to completely neutralize the bacteria (Molle *et al*., 2006). *Mtb* also possesses potent mechanisms that disrupt the processing and presentation of antigens to $CD4^+$ T cells (Harding, Ramachandra and Wick, 2003). This is facilitated by the previously mentioned blockage of phagolosysomal formation, which restricts intracellular trafficking of *Mtb* antigens, thus reducing their access to the machinery generating major histocompatibility class II (MHC class II) complexes responsible for presenting mycobacterial epitopes. This ultimately restricts the development of an effective bactericidal $CD4^+$ T cell response (Goldberg, Saini and Porcelli, 2014).

Failure to effectively activate infected macrophages and dendritic cells aids in escape of the tubercle bacilli from the bactericidal effect of the macrophage, resulting in further recruitment of activated monocytes and neutrophils to the site of infection (Goldberg, Saini and Porcelli, 2014). At this stage *Mtb* grows within the damaged lung tissue causing migration of activated $CD4^+$ T cells to the site of infection, this results in the formation of a granuloma (Ulrichs and Kaufmann, 2006). As inflammation proceeds in the lung, granulomatous structures can progress to become necrotic, followed by breakdown of the peripheral cuff of lymphocytes. This can disrupt the structure of the granuloma resulting in the formation of lung cavities and pulmonary TB disease (Sansindran and Torrelles, 2011).

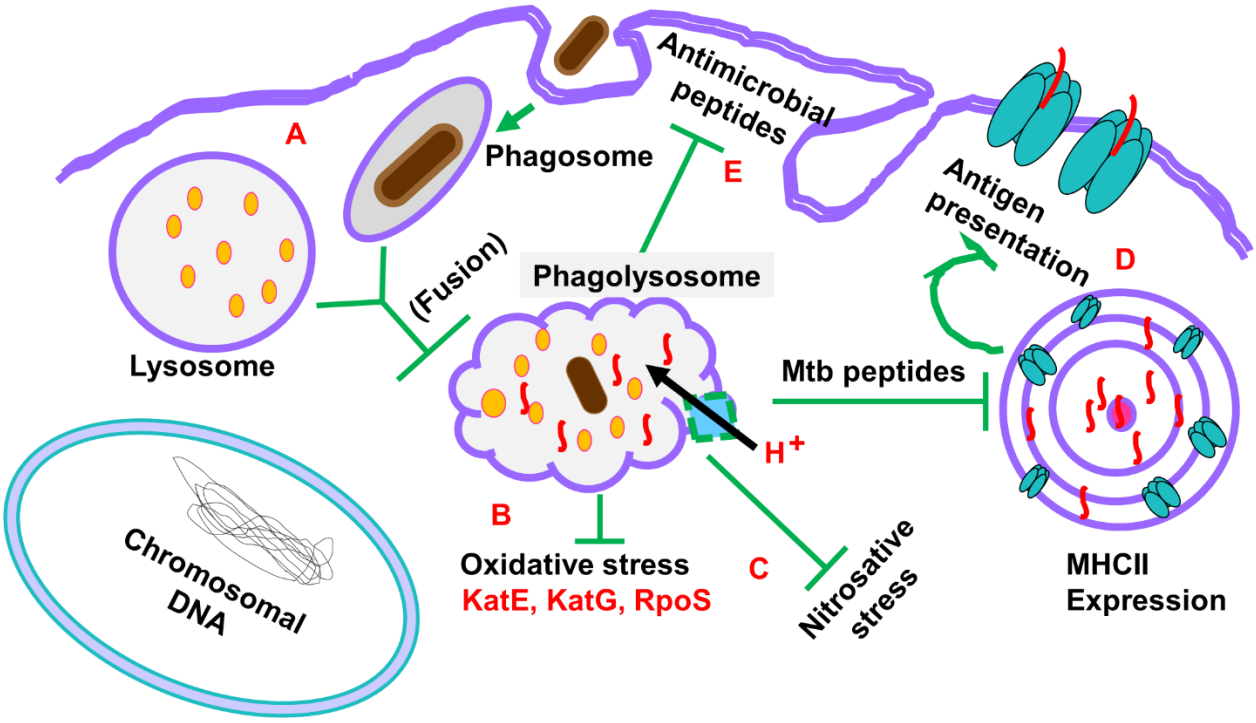

Figure 1.2: Mycobacterial host immune evasion strategies during colonization of host alveolar macrophages: *Mtb* bacilli (brown rods) phagocytized by alveolar macrophages are usually primed for degradation through endocytic pathways. However, *Mtb* has developed diverse strategies to modulate, exploit and avoid annihilation by the host endocytic pathway. (A) *Mtb* inhibits lysosome-phagosome fusion and this aids in bacterial proliferation in the non-acidified endosome compartment. (B and C) *Mtb* resists the acidic environment of the phagolysosome by production of proteins such as KatG and RpoS. D) *Mtb* inhibits MHC class II mediated antigen presentation which aids in further recognition of the pathogenic invader by the host immune system. (E) *Mtb* also resists degradation by antimicrobial peptide by limiting innate immune recognition. Adapted from Goldberg, Saini and Porcelli (2014). Figure drawn by student.

1.3 Anti-TB strategies

Failure to eradicate the TB epidemic can be attributed to the development of MDR and extensively drug resistant (XDR) (MDR TB that is resistant to second line TB drugs, including an aminoglycoside and an injectable fluoroquinolone) strains, which have prompted the need to look at other avenues for TB treatment. One comprehensive approach is the development of potent vaccines. Currently, the only licensed vaccine against TB is Bacille Calmette-Guérin (BCG) however, the BCG vaccine is not protective against adult TB, prompting a search for new

vaccines (McShane, 2011). Despite this drive, efforts to develop new effective vaccines have proven unsuccessful, with promising vaccine candidates failing human clinical trials (Gopal and Khader, 2013). In addition, host directed therapies, which act to support anti-TB treatment, possibly by shortening treatment duration or by increasing host immune clearance of TB are currently being investigated. The main goal would be to impede further tissue damage associated with TB infection (Maiga *et al*., 2012). To promote the realization of the WHO 2030 goal, a wide range of candidate targets have been investigated, including the investigation of mycobacterial cell wall components, which remains a high priority target for development of new anti-TB drugs and vaccines (Sarathy, Dartois and Lee, 2012).

1.4 The mycobacterial cell wall: novel drug targets

To prevent cell lysis due to external pressures, nearly all bacteria have developed a protective outer layer known as the cell wall. Mycobacteria are encased in an exoskeletal-like cell wall composed of the mycolic acid layer (MA) and a highly branched polysaccharide known as the arabinogalactan (AG), which is covalently linked to peptidoglycan (PG) (Figure 1.3). The mycolic acids dampen host immune detection, whilst PG maintains cell shape and fortifies the cell wall contributing to overall cell viability (Marrakchi *et al*., 2014; Hett and Rubin, 2008 and Brennan, 2003). Among the most effective anti-TB drugs are the cell wall targeting antibiotics such as Isoniazid (INH), Ethambutol (EMB), Ethionamide (ETH) and D-cyclosserine. Surprisingly, no drugs in the current regimen target PG, which is regrettable given the massive therapeutic benefit in targeting this macromolecule for other disease (Jackson, McNeil and Brennan, 2013). The rise of MDR-TB has spurred the search for more potential drug targets in the mycobacterial cell wall, including the pathways required for PG synthesis and remodeling.

1.5 Peptidoglycan biosynthesis

Bacterial PG is a critical component of the cell wall, providing structural support and protection from turgor pressure (Kieser and Rubin, 2014 and Typas *et al*, 2012). The mechanisms of PG synthesis adopted by mycobacteria have not been extensively studied (Kieser and Rubin, 2014). Mycobacterial PG is composed of alternating sugars namely, *N*-acetylmuramic acids (Mur*NA*c) and *N*-acetylglucosamine (Glc*NA*c) linked via β-1,4-glycosidic bonds (Heijenoort, 2001).

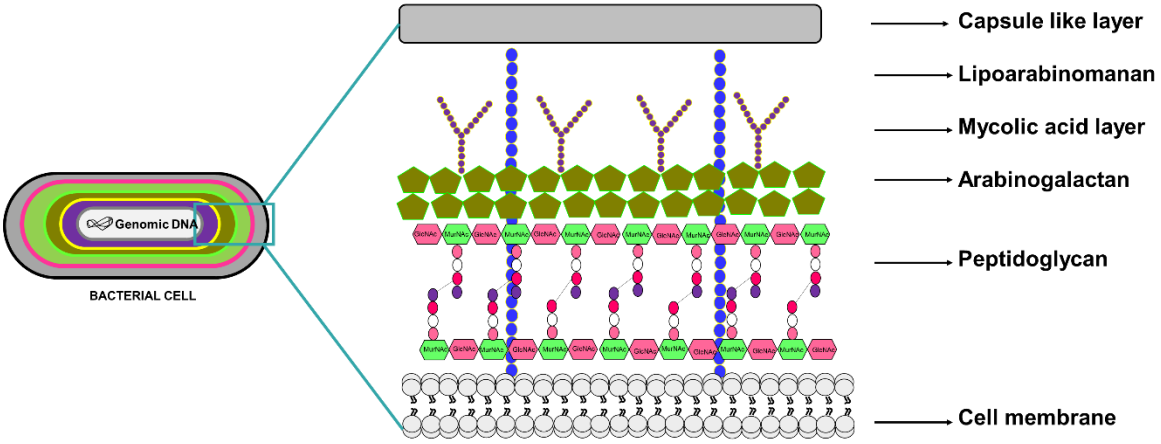

Figure 1.3: Diagrammatic representation of the mycobacterial cell and cell wall layer composed of distinct macromolecules. The cell wall includes the capsule layer (grey with black lining) composed of glucose polymers, lipoarabinomannan (blue circles), mycolic acid layer (purple circles) made up of lipids, arabinogalactan (green), peptidoglycan (pink and green) composed of alternating sugars cross-linked by stem peptides and the inner most layer, which is the cell membrane (light grey). Adapted from Hett and Rubin (2008). Figure drawn by student.

The Mur*NA*c is oxidized, thus forming *N*-glycolylmuramic acid, which is thought to provide further support to the mycobacterial cell wall and increase resistance towards lysozyme (Mahapatra, Scherman, and Crick, 2005). Mur*NA*c is attached to pentapeptides (L-alanine, D-*iso*-glutamine, *meso*-diaminopimelic acid and 2 X D-alanine), which cross-link with an adjacent Mur*NA*c-peptapeptide, forming the mesh-like network of the PG. These cross-links exist in two conformations, the 3-4 cross-links [between *meso*-diaminopimelic acid (*m*-DAP) and D-alanine at position 4] and the 3-3 cross-link between *meso*-DAP and *meso*-DAP of the opposite strand (Vollmer, Blanot and De Pedro, 2008). The synthesis of PG initially takes place in the cytoplasm and following this, the PG monomer, Lipid II, is then polymerized with pre-existing PG in the periplasm (Hett and Rubin, 2008). PG synthesis involves the biosynthesis of the nucleotide precursors i.e., UDP-*N*-Acetylmuramic acid (UDP-Mur*NA*c) from UDP-Glc*NA*c through the addition of enoylpyruvate to the 3rd position of the Glc*NA*c residue of UDP-Glc*NA*c. Following this, is a reduction step to form UDP-Mur*NA*c (Figure 1.4), through the action of the MurA and MurB enzymes (Lovering, Safadi and Strynadka 2012). Subsequently, in a sequential manner, MurC adds the L-alanine onto UDP-Mur*NA*c followed by the activity of MurD, MurE and MurF

adding D-iso-glutamine, meso-diaminopimelic and D-alanyl-D-alanine dipeptide, respectively, thus forming UDP-Mur*NA*c-pentapeptide (Lipid I) (Lovering, Safadi and Strynadka 2012).

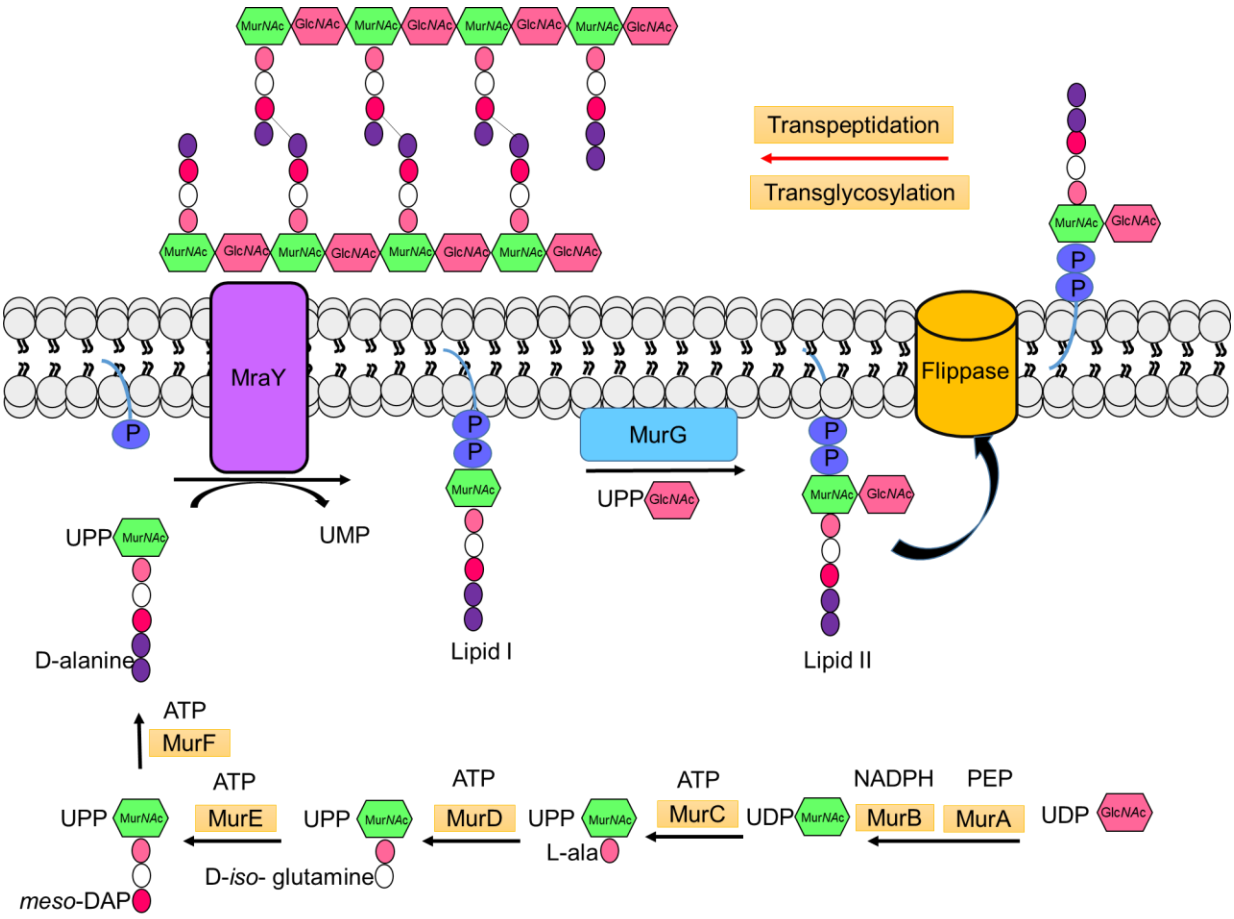

Figure 1.4: Schematic representation of bacterial PG synthesis. Schematic representation of bacterial PG synthesis. PG precursors are initially synthesized in the cytoplasm and the final precursor is linked to the transport lipid (undecaprenyl phosphate), which is exported across the cell membrane to the periplasmic space where it is polymerized to pre-existing PG. Initially, UDP-Murn*NA*c is synthesized from UDP-Glc*NA*c by MurA and MurB. Subsequently, L-alanine addition to UDP-Mur*NA*c is catalyzed by MurC, thereby forming UDP-Mur*NA*c-L-ala. MurD catalyzes the addition of D-glutamine to the Mur*NA*c-monopeptide moiety, resulting in UDP-Mur*NA*c-L-ala-D-glu. Subsequently, MurE adds meso-diaminopimelate acid to the UDP-Mur*NA*c dipeptide, forming UDP-Mur*NA*c-L-ala-D-glu-meso-DAP. Lastly, the D-alanine dipeptide is added by MurF to form UDP-Mur*NA*c-L-ala-D-glu-meso-DAP-D-ala-D-ala (Lipid I). Lipid I is then transferred to undecaprenyl phosphate after which, Glc*NA*c is added to Mur*NA*c by MurG, forming Lipid II. A Flippase translocates the PG precursor to the periplasm, incorporating it into pre-existing PG with the aid of both the transpeptidases and transglycosylases (Ldts and PonAs). Adapted from Lovering, Safadi and Strynadka (2012). Figure drawn by student.

Phosphoryl-Mur*NA*c is then transferred to undecaprenyl phosphate and thereafter Glc*NA*c is added via the action of MurG, forming Lipid II, which is translocated from the cytoplasmic space to the perisplasmic space (Lovering, Safadi and Strynadka 2012). Lipid II is then assembled into the pre-existing PG via activity of tansglycosylases such as PonA1 and PonA2, which not only assemble the glycan but also form cross-links between D-alanine and meso-DAP. Ld-transpeptidases form the 3-3 cross-links, possibly in response to stressful conditions (Lovering, Safadi and Strynadka 2012).

1.6 Targeting PG biosynthesis for drug development.

Although thought of as static, bacterial PG need to be flexible aiding in the maintenance of cell structure and to allow for growth processes (Doyle and Marguis, 1994). Research by multiple groups has shown the essentiality of the PG and its modifications in ensuring pathogen survival, antimicrobial resistance, evasion of immune detection and exacerbating virulence (Davis and Weiser, 2011; Swim *et al*, 1983). Mammals do not possess PG components and thus have evolved strategies to detect intact fragments of PG, signaling the presence of host invaders (Allison and Lambert, 2015). As a result, drugs targeting the PG layer would be highly selective (Allison and Lambert, 2015). Muropeptides, PG precursors also play a significant role in modulating host responses in favor of the pathogen (Humann and Lenz, 2009), making the PG a suitable novel drug target.

1.7 PG modification: Benefits for fitness

Bacterial infections are normally accompanied by host innate immune response, in which host antimicrobial agents, i.e. lysozymes are released, resulting in bacterial lysis and the release of cell components, particularly PG fragments. These can be recognized by host receptors resulting in the production of pro-inflammatory cytokines and chemokines and further recruitment of host immune cells to the site of infection. However, a plethora of bacterial pathogens have evolved mechanisms to evade host recognition by modifying the PG, preventing PG cleavage and cell lysis, thus ensuring pathogen fitness (Davis and Weiser, 2011). PG modifications such as the *N*-deacetylation of Glc*NA*c residues in *Streptococcus pneumoniae* and *Bacillus anthracis* contribute to lysozyme resistance in these organisms (Lacks and Neuberger, 1975; Ohno *et al*, 1982;

Zipperle *et al*, 1984). Furthermore, *O*-acetylation of *Neisseria gonorrhoeae* also confers resistance to lysozyme (Swim *et al*, 1983; Rosenthal *et al*, 1982). Mycobacterial PG is modified through the glycolylation of PG-derived muramyl dipeptide (MDP) by the action of NamH (Coulombe *et al*, 2009). By abrogating *namH* gene function, Coulombe *et al*, 2009 demonstrated a role for this modification in promoting NOD2 (member of the Nod-like receptor family involved in PG detection) mediated innate responses to *M. smegmatis* PG. The decreased NOD2 mediated response lead to the activation of the NF-kB pathway and ultimately the production of proinflammatory cytokines and TNF-α (Coulombe *et al*., 2009). Furthermore, extended investigation in *Mtb* by deleting the *Mtb namH* gene corroborated the *M. smegmatis* findings, indicating that abrogating muropeptide glycolylation resulted in decline of NOD-2 mediated responses (Hansen *et al*., 2014). The authors further indicate that these modifications enhance immune recognition, leading to *Mtb* persistence within the host (Hansen *et al*, 2014). This process is highly useful when *Mtb* escapes the granuloma for transmission to the next host (Hansen *et al*, 2014). Furthermore, bacteria can reutilize their own cell wall through the metabolic process of PG recycling (Park and Uehara, 2008). This process not only saves energy and resources allowing bacteria to survive under adverse environments but also aids in evading detection by the host immune system (Humann and Lenz, 2009). Cell wall fragments have important messenger functions in bacterial communication and as signaling molecules in spore resuscitation and germination in some gram-positive bacteria (Johnson, Fisher, and Mobashery, 2013; Boudreau, Fisher, and Mobashery, 2012). In eukaryotes, the detection of muropeptides via PG recognizing proteins and NOD receptors initiates an immune response (Johnson, Fisher, and Mobashery, 2013). The bacterial recovery of cell wall muropeptides suppresses this response, suggesting that PG recycling may also contribute to immune evasion (Johnson, Fisher, and Mobashery, 2013).

1.8 Peptidoglycan modifications during dormancy

As mentioned above, bacterial pathogens modify PG to aid them to thrive within the host. In addition, these modifications assist in the transition from an actively growing state to a quiescent or spore form during stressful conditions. Zhou and Cegelski (2012) demonstrated that when *Staphylococcus aureus* encounters nutrient depletion, it decreases the amount of pentaglycine bridges, which are responsible for crosslinking PG. This results in a relatively thicker PG.

Similarly, *Bacillus subtilis* limits the gradient of crosslinking by removing the peptide side chains from MurNAc, thus aiding spore formation (Atrih *et al*., 1996). An altered degree of PG crosslinks was also observed in *Mtb* under stressful conditions and during stationary phase where PG, which is predominantly crosslinked by 4-3 linkages, accumulates 3-3 crosslinks (Lavollay *et al*., 2008). This is proposed to confer resistance to β-lactam antibiotics as the formation of 3-3 crosslinks is mediated by the β-lactam insensitive L,D-transpeptidase Rv2518c (Erdemli *et al*., 2012). However, contrary findings by Kumar *et al*, 2012 argue that 3-3 crosslinks are present in a similar abundance throughout all bacterial growth phases. In addition to this, previous work has shown that stress induced by hypoxia also leads to the thickening of the mycobacterial cell wall, reducing cell wall permeability and the uptake of certain antibiotics into quiescent *Mtb*, when compared to actively growing cells (Sarathy *et al*., 2013).

PG fragments released during spore germination play a pivotal role in the induction of spore germination in *B. subtilis* (Pompeo, Foulquier and Galinier, 2016). Actively growing cells release PG fragments, which are detected by the *B. subtilis* PrkC, a Ser/Thr kinase, which induces spore germination (Pompeo, Foulquier and Galinier, 2016). Similar proteins are expressed in *Mtb* and have been proposed to be involved in the regulation of bacterial growth by sensing PG fragments (Gee *et al*., 2012). These proteins could also have a role in *Mtb* resuscitation as seen in the reactivation of dormant *Mtb* by mycobacterial culture filtrate, which is presumed to contain secreted PG fragments (Mukamolova *et al*., 1998). In addition, recent work demonstrated that the addition of anhydromuropeptides resulted in resuscitation of dormant mycobacteria (Nikitushkin *et al*., 2015).

1.9 Role of PG and its hydrolases in virulence

Extensive research on cell wall hydrolases has confirmed a role for these proteins in modulating prey invasion, controlling cell shape and facilitating lysis of competitor cells (Wyckoff *et al*, 2012). In addition, PG hydrolases may serve as useful drug targets given their role in bacterial pathogenesis and ultimately fitness. Three main classes of PG hydrolases have been identified, these include the glycosidases responsible for cleaving the PG glycan backbone and the second group includes the peptidases, which cleave the peptide bonds within the stem peptide from the Mur*NA*c moiety and amidases, which cleave the stem peptide bonds between the Mur*N*Ac and stem peptide (Firczuk and Bochtler, 2007) (Figure 1.5). Peptidases also comprise enzymes such

as carboxypeptidases, which cleave the terminal D-alanine in the stem peptide. The *N*-acetylmuramyl-L-alanine amidases cleave the amide bond between the stem peptide and sugar backbone and are the subject of this study (the role of PG remodeling enzymes is reviewed in Vollmer, 2008).

1.10 PG modifying hydrolases

During growth, PG is consistently remodeled by a plethora of hydrolases responsible for remodeling and stabilizing the PG layer (Uehera and Bernhardt, 2011). Cell wall hydrolases have a plethora of roles, these include sensing perturbations in the cell wall and triggering appropriate responses and thus ensuring the maintenance of the bacterial cell wall integrity (Uehera and Bernhardt, 2011). These enzymes also have a role in coordinating bacterial growth and division and are also implicated in host cell adhesion and invasion (Rico-Lastres *et al*., 2015). This diversity in function provides a strong rationale to further characterize and investigate the success of pathogenic bacteria in relation to hydrolases content.

1.10.1 Glucosidases. Glucosidases are classified as enzymes that breakdown polymerized carbohydrates. As previously mentioned, in PG glucosidases are involved in the cleavage of the bond between Glc*NA*c and Mur*NA*c. This group of enzymes can be further divided into three classes which are briefly reviewed below.

1.10.1.1 *N*-acetyl-β-D-glucosaminidases

Endo-*N*-acetyl-β-D-glucosaminidases (known as *N*-acetylglucosaminidases) catalyze the cleavage of Glc*NA*c residue from the attached sugar residues. A variety of glucosidases have been identified and characterized, in particular that of *E. coli*, otherwise referred to as NagZ. This is a cytoplasmic glucosaminidase utilizing Glc*NA*c-1, 6-anhydroMur*NA*c (muropeptide) produced during cell wall turnover and later used for recycling and induction of the β-lactam degrading β-lactamases (Votsch and Templin, 2000). As NagZ was shown to contribute to antibiotic resistance, Stubbs *et al* (2008) crystalized *Vibro cholerae* NagZ and designed an inhibitor mimicking the transition state of the catalytic reaction. Further characterization of bacterial glucosaminidases include studies assessing the function of *Enterococcus faecalis* AtlA.

Deletion of AtlA in *E. faecalis* led to the formation of long chains during the exponential phase of growth, implicating AtlA in the hydrolysis of the septum to facilitate cell separation after cytokinesis. However, the phenotype was abrogated in stationary phase, pointing to the possible involvement of additional hydrolases in cell division (Mesnage *et al*, 2008). Also, the crystal structure of NagZ from *Vibrio cholerae* has been solved, with a bound small-molecule inhibitor mimicking the putative transition state of the catalytic reaction (Stubbs *et al*., 2008).

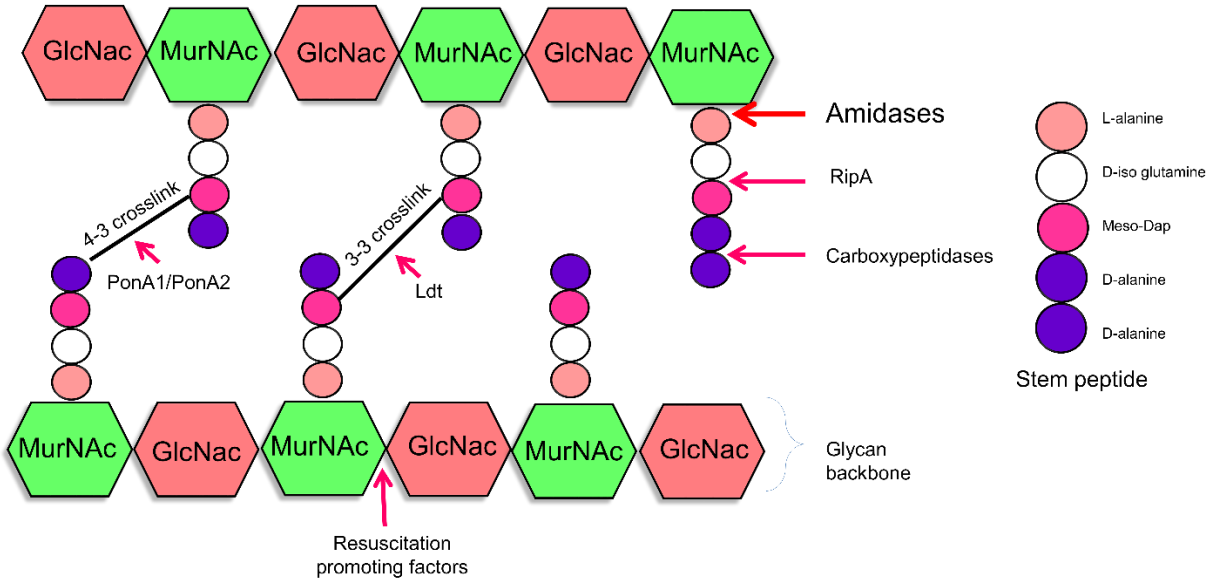

Figure 1.5: Diagrammatic representation of peptidoglycan (PG) structure and hydrolases responsible for remodeling during bacterial growth. The PG backbone is composed of Glc*NA*c (Pink) and Mur*NA*c (Green) sugars to which the stem peptide is attached and connects the two adjacent sugar backbone strands. Remodeling of bacterial PG is carried out by a plethora of hydrolases, which include the lytic transglycosylases, carboxypeptidases, endopeptidases and amidases. The amidases are the subject of this dissertation. Adapted from Machowski *et al* (2014). Figure drawn by student.

1.10.1.2 *N*-acetyl β-D-muramidases (Lysozymes)

N-acetyl β-D-muramidases, also termed *N*-acetylmuramidases, are responsible for cleaving the β-1,4-glycosidic bond between Mur*NA*c and Glc*NA*c resulting in the generation of a terminal Mur*NA*c residue. Compared to other cell wall hydrolases, these haven't been thoroughly investigated and therefore a significant gap still exists in the extrapolation of their biological roles. Two such muramidases have been characterized in *E. faecalis*, AtlB and AtlC. Loss of

AtlA (glucosamidase) impeded septum cleavage in *E. faecalis* forming long chains with attenuated cell division, however, AtlB is capable of compensating for the loss of function, albeit poorly. These data point to a role for AltA in septum cleavage (Mesnage *et al*, 2008). In addition to this, the combinatorial function of AtlA and AtlB is needed to ensure efficient PG turnover with AtlB and AtlC believed to contribute principally to PG metabolism (Mesnage *et al*, 2008)

1.10.1.3 Lytic transglycosylases

Lytic transglycosylases (LTs) also cleave the β-1,4-glycosidic bond between Mur*NA*c and Glc*NA*c. However, these enzymes differ from other hydrolases from the perspective that they use an intramolecular transglycosylation reaction, which results in the formation of 1,6-anhydromuropeptides (Engel, *et al*., 1992). LTs exist as a diverse group, with four distinct families (Family 1 – Family 4) classified in accordance by consensus motifs and sequence similarities, and bacteria usually carry a representative from each family. An investigation of Family 1 LTs showed a role in conjugation and secretion systems in *Agrobacterium tumefaciens* (VirB) and *Shigella flexneri* (IpgF) (Bayer *et al*., 2001). Family 2 LTs in *Neisseria gonorrhoeae* have been shown to play a role in septation (Schaub *et al*., 2016) and those of Family 3 in *Caulobacter crescentus* (PleA) have a role in flagella and pili formation (Viollier and Shapiro, 2003). In *B. subtilis*, the SleB LT plays a role in sporulation (Heffron, Orsburn and Popham, 2009). Furthermore, *N. gonorrhoeae* AtlA releases muropeptides similar to tracheal cytotoxins, which kill ciliated fallopian tube cells in organ culture, thus contributing to Gonococcal pathogenicity (Cloud and Dillard, 2002).

1.10.1.4 Resuscitation promoting factors

Resuscitation promoting factors (Rpfs) are structurally similar to soluble LTs with the ability to resuscitate non-replicating bacteria (Kana and Mizrahi, 2010). This family of proteins was initially identified in *Micrococcus luteus* (Mukamolova *et al*., 2002) and later in *Mtb*, which possesses five of these *rpf*-like genes (*rpfA, rpfB, rpfC, rpfD* and *rpfE*) (Mukamolova *et al*., 2002). There is growing evidence for the roles of Rpfs in cell wall remodeling, *Mtb* infection and resuscitation of chronic TB in mouse models (Rosser *et al*., 2017). A study conducted by Russel-Goldman *et al* (2008) investigated the ability of *rpf*-deficient (Δ*rpfAB*) *Mtb* strains to colonize

mononuclear phagocytes. This study demonstrated that combinatorial loss of RpfA and RpfB resulted in attenuated growth in murine macrophages (Russel-Goldman *et al*., 2008). In contrast, Kana *et al* (2008) demonstrated that the growth of the *Mtb rpf* quadruple gene knockout strain in human monocytes was not impaired when compared to the wild type strain. However, in the murine model of TB infection, virulence and the ability to cause disseminated disease was reduced in the *Mtb rpf* quadruple gene knockout strain. This was hypothesized to be due to changes in the cell wall that affected the ability of tubercle bacteria to resist stress (Russel-Goldman *et al*., 2008 and Kana *et al*., 2008).

1.10.2 Peptidases

Peptidases are responsible for cleaving a variety of bonds between amino acids in PG and or soluble fragments (Shockman and Holtje, 1994 and Holtje, 1995). However, the bonds are not considered traditional peptide bonds in that they involve the ɣ-carboxylic group of D-glu (bond between D-glu and *meso* Dap) instead of α-carboxylic group of one amino acid and that of the 3-3 cross bridge, which involves the ε-amino group of *meso*-Dap (Smith *et al*., 2000). Therefore, based on bond cleavage specificity, peptidases are divided into two classes, the Endopeptidases and the Carboxypeptidases (Vollmer *et al*., 2008). Both DD-endo and Carboxypeptidases have been implicated in prey rounding, which ensures efficient prey invasion and fitness of *Bdellovibrio* (Lerner *et al*., 2012). *Bdellovibrio* invade Gram negative bacteria within which they grow and divide using the host's macromolecules for energy and anabolism (Núñez *et al*, 2003). This invasion causes rounding up of the prey to ensure an osmotically stable environment for *Bdellovibrio*, preventing superinfection and allowing replication within its niche with limited competition (Lerner *et al*, 2012). Within the host, the bacterial pathogen then degrades the host's macromolecules, killing the prey and escaping with the aid of lytic enzymes (Lambert et al, 2011).

1.10.2.1 Endopeptidases

Endopeptidases are a class of peptidases that cleave within the stem peptide, these are further classified as DD-endopeptidases which cleave between D-ala and *meso*-Dap of the cross-bridge and LD- or DL- endopeptidases cleaving between the L and D-amino acids (Smith *et al*., 2000

and Sauvage *et al*., 2008). The NIpC/P60 peptidase family (Spr and YdhO) in *E. coli* were shown to cleave peptide cross bridges, which are essential for the coordination of bacterial growth and cell viability (Singh *et al*., 2012). Furthermore, *Haemophilus influenzae* EnvC and NIpD deletion mutants displayed cell membrane blebbing and altered cell morphology (Ercoli *et al*., 2015). In addition to this, a reduction in proteins such as the chaperones (HtrA and SurA) and increased β-barrel containing outer membrane proteins was noted, suggesting a role for EnvC in facilitating the transport of these proteins (Ercoli *et al*., 2015). EnvC was also implicated in *H. influenzae* biofilm formation and adherence to epithelial cells (Ercoli *et al*., 2015). In addition, the *Yersina pestis* peptidases, NIpD, has been characterized and shown to be involved in cell separation and bacterial pathogenesis as it is essential for the development of the bubonic plaque in model systems (Tidhar *et al*., 2009).

1.10.2.2 Carboxypeptidases

DD-Carboxypeptidases are responsible for cleaving the terminal D alanine amino acid of the stem peptide to regulate PG cross-linking and thus are important for PG integrity. *Streptomyces albus* D-ala D-ala carboxypeptidase and the *Enterococcus* VanX are involved in vancomycin resistance (Charlier *et al*., 2003 and Bussiere *et al*., 1998). *Campylobacter jejuni* (*C. jejuni*) LD-carboxypeptidase (Pgp2) is essential for maintaining the helical structure of *C. jejuni*, and its loss alters the muropeptide profile, with a complete lack of tripeptides and increased accumulation of tetrapeptides (Frirdich *et al*.,2014). Further analysis of cell motility, cell survival and pathogenicity indicated that loss of Pgp2 resulted in attenuated motility and a defect in *C. jejuni* biofilm formation and host colonization (Frirdich *et al*., 2014).

1.10.3 Amidases*: N*-acetylmuramyl-L-alanine amidases

The *N*-acetylmuramyl-L-alanine amidases (hereafter referred to as amidases for simplicity) comprise a class of Zn^{2+}-dependent PG hydrolases that can be divided into five families depending on the type of amidase domain present. These enzymes can include (major families according to Pfam database): The Amidase_2 (PF01510), Amidase_3 (PF01520), Amidase_02C, Amidase_5 and lastly Amidase_6 domains (Bateman *et al*., 2002 and Buttner *et a*l., 2015). Both the Amidase_2 and Amidase_3 domains assume a globular structure of mixed αβ- fold and are primarily found alongside AMIN and PGRP domains (Kerff *et al*., 2010). Amidases are

characterized by a conserved HXH motif (X- any amino acid), responsible for the coordination and binding of the Zn^{2+} ion at the catalytic site (Buttner *et al*., 2015). In the Amidase_2 domain proteins, the X amino acid is usually an aspartic acid but can also be substituted with a cysteine. In contrast, the Amidase_3 family coordinate the Zn^{2+} ion residue with a glutamate instead and have a binding groove bordered by loops instead of helices, the latter being typical of the Amidase_2 family (Rocaboy *et al*., 2013 and Buttner *et al*., 2015). In addition to this, the active site stabilizing the Zn^{2+} ion and binding of the muropeptide is broader compared to that of the Amidase_2 family of proteins (Buttner *et al*., 2015).

1.10.3.1 Role of amidases in bacterial cell differentiation

There is now growing evidence showing that bacteria undergo differentiation, generating specialized cells aiding in survival under hostile environments (Smith and Brun, 2005). Bacterial differentiation can be either inherent to bacterial growth mechanisms or triggered by adverse environmental stimuli, this involves complex regulatory pathways that trigger the expression of different genes involved in these processes (Smith and Brun, 2005). Bacterial differentiation has been extensively investigated in *B. subtilis*, where at the onset of starvation, dormancy is triggered in the form of forespore formation via a process called sporulation (Tan and Ramamuthi, 2014). The initial event is the formation of a polar septum that separates the sporulating cell into a larger mother cell (which coats the forespore in a series of PG layers forming the spore cortex and provides the proteins necessary for spore maturation) and a smaller forespore (Meador-Parton and Popham, 2000). Following maturation of the forespore, the mother cell undergoes lysis, releasing the dormant spore. This process enables *B. subitlis* to survive under extreme conditions. As mentioned before, differentiation triggers the expression of multiple genes involved in sporulation, including the amidases, namely CwlB, CwlC, CwlD and CwlH (Gilmore *et al*., 2004). Gilmore *et al* (2004) demonstrated a role for the amidase CwlD in *B. subtilis* spore heat resistance and hydrogen peroxide resistance, both of which requires the dehydration of the spore cytoplasm. This resistance is also mediated by the spore PG, i.e. the spore cortex, through the formation of δ-*N* acetylmuramic acid, which serves as a signal for autolytic enzymes responsible for spore core dehydration and spore heat resistance (Chen, Fukuoka and Makino, 2000). The autolytic enzymes act by removing the peptide side chain, through CwlD activity (Gilmore *et al*., 2004). In addition to this, CwlD was unexpectedly

expressed in both the mother cell and forespore compartments and was shown to facilitate PdaA function, involving deacetylation of the PG muramic acid and muramic δ-lactam formation (Gilmore *et al*., 2004). In addition to this, CwlD has been implicated in the degradation of the spore cortex during spore germination, facilitating the rehydration of the spore protoplast, release of solutes and resumption of metabolic activity. Therefore, loss of CwlD inhibits spore germination and thus initiation of bacterial growth (Popham *et al*., 1996).

The formation of biofilms is one of the most advantageous forms of bacterial differentiation. This process has been investigated in several organisms such as the commensal *Staphylococcus epidermis* (*S. epidermis*), which regulates the colonizing ability of *Staphylococcus aureus* (*S. aureus*) (Otto, 2009) by secreting proteases preventing the release of AtlE, which retains both amidase and glucosaminidase domains. This limits cleavage of the cell wall and DNA release, which in turn reduces biofilm formation capabilities under adverse conditions when these bacteria can switch to an invasive lifestyle (Iwase *et al*., 2010; Sugimoto *et al*., 2013; Buttner *et al*., 2015). *S. epidermis* biofilm formation occurs via two steps including the attachment of cells to the surface, followed by aggregation and formation of a multilayered structure (Buttner, Mack and Rohde, 2015). This cell-cell attachment is facilitated by polysaccharide intercellular adhesion and extracellular DNA, which has been shown to be paramount in *S. aureus* biofilm formation (Witchurch *et al*, 2002). Qin *et al* (2007) investigated biofilm-promoting factors in *S. epidermis*, particularly the role AtlE has in ensuring *S. epidermis* cell-cell communication, bacterial attachment to surfaces and consequent biofilm formation. This group demonstrated that the abrogation of AtlE function led to a decline in the amount of extracellular DNA in cultures, leading to defective biofilm formation (Qin *et al*., 2007). These results validated the work by Allesen-Holm *et al*., 2006, wherein it was demonstrated that extracellular DNA functions as a structural component and a cell communication compound in biofilms. Buttner *et al* (2015) also demonstrated that AtlE is needed for DNA release as its inactivation resulted in attenuated cell lysis and a corresponding reduction in DNA release, thus giving rise to a deficiency in *S. epidermis* biofilm formation.

Heterocyst formation in filamentous cyanobacteria, *Anabaena* species, is yet another elegant illustration of how bacteria can form functional multicellular communities (Zheng *et al*., 2017).

Heterocysts allow for intercellular exchange of material by creating an environment to facilitate nitrogen fixation, thus supplying nitrogenous compounds to the vegetative cells, which perform oxygenic photosynthesis and supply heterocysts with sugars for energy (Zheng *et al*., 2017). This entire process is dependent on intercellular communication, an example of this is the movement of proteins involved in heterocyst formation such as PatS, which moves through channels (nano pores) penetrating PG (Zheng *et al*., 2017). These nanopores enable communication and rapid movement of proteins and are created by amidases in both *Anabaena* and *Nostoc punctiforme* (Zheng *et al*., 2017). As evidence of this, an *amiC*1 mutant of Anabaena, when exposed to nitrogen as the only nutrient source, was deficient in heterocyst formation (Berendt *et al*., 2012). In addition, cell-cell communication in the mutant strain was investigated using fluorophore calcein as a tracer to monitor the transfer of molecules between adjacent cells (Berendt *et al*., 2012). The AmiC1 deficient strain failed to transfer calcein, further confirming that abrogating AmiC1 abolishes cell-cell communication (Berendt *et al*., 2012). Deletion of a second amidase in this organism, *amiC*2, did not entirely abrogate heterocyst formation and instead resulted in a semi-regular pattern of heterocysts along the filament, which were capable of growth on nitrogen as the sole nutrient source (Berendt *et al*., 2012). However, Zhu *et al* (2001) contradicted these findings and reported that an AmiC2 deficient mutant was defective in heterocyst formation. Furthermore, Zheng *et a*l (2017) identified another *Anabaena* amidase, designated as *all*1140 (amidase-C), which was also shown to aid in the exchange of intercellular material and the differentiation of heterocysts for nitrogen fixation by forming nanopore/channels connecting neighboring cells.

1.10.3.2 The role of amidases in bacterial pathogenesis

Streptococcus pneumoniae infection has been implicated in bacterial sepsis and meningitis, inevitably leading to high rates of mortality worldwide (O'Brien *et al*., 2009). As outlined by Kadioglu *et al* (2008) and van der Poll *et al* (2009), effective clearance of pneumococcal disease requires the activation of three complement system cascades (classical, alternative and lectin pathway; C3b), which ensures efficient opsonization and clearance by professional phagocytes. The classical pathway (CP) ensures recognition of pneumococci through antigen-antibody complexes and the alternative pathway (AP) triggers the amplification of C3b deposition, through hydrolysis of the C3b component (Walport, 2001; Lambris, Ricklin and Geisbrecht,

2008). However, pneumococci have evolved mechanisms to evade complement recognition through the binding of cholesterol-dependent cytolysin pneumolysin (Ply) to the CP component (C1q), thus decreasing C3b deposition (Fernández-Tornero et *al.*, 2001). For this mechanism to be effective, the pneumolysin has to be released into the extracellular space, this is facilitated by the major pneumococcal autolysin, LytA involved in cell lysis (Fernández-Tornero et *al.*, 2001). Ramos-Sevillano *et al*., 2015 demonstrated that LytA is involved in minimizing immune recognition by aiding in Ply activity and C3b evasion via inhibition of both the AP and CP complement pathways, which ultimately results in reduced complement activation. Furthermore, LytA was shown to bind C4BP and FH regulators, which inhibit damage of stander cells from continuous complement activation (Ramos-Sevillano *et al*., 2015). These mechanisms are used to successfully avoid the complement response and degrade the secreted C3b component, counteracting the effects of complement activation (Ramos-Sevillano *et al*., 2015). Further investigation also showed LytA involvement in the enhancement of active and invasive disease establishment in mice models and altered phagocytosis (Ramos-Sevillano *et al*., 2015). An investigation by Terrasse *et al*., 2015 revealed that pneumococcal LytA is needed for GAPDH release, which promotes bacterial adhesion and invasion of host cells.

The role of amidases in bacterial virulence and pathogenesis is further highlighted by the *Neisseria gonorrhoeae* AtlA, which releases PG fragments (PG derived cytotoxins) identical to the tracheal cytotoxin (TCT) previously shown to kill ciliated fallopian tube cells (Cloud and Dillard, 2002). The role of amidases in bacterial pathology has also been investigated in *Salmonella typhimurium.* Folkesson *et al* (2005) demonstrated that the loss of the AmpD amidase in *S. typhimurium* compromises the organism during infection by inducing higher levels of reactive nitrogen intermediates (RNI), which are essential in microbial host defense. The group also monitored invasion using the gentamicin survival assay and found that the invasion of *ampD* mutants was lower than wild-type. They predicted that the accumulation of muropeptides affects the invasion capacity of *S. typhimurium*. In J774-A.1 cells, which were used to investigate the ability of the mutant to grow intracellularly, *ampD* mutants displayed a decreased ability to colonize these cells, evidenced by lower colony forming units compared to wild-type (Folkesson *et al*., 2005). Muropeptide accumulation may also interfere with the normal regulation of essential virulence determinants, thus reducing the ability of the bacteria to limit the

inflammatory response (Collier-Hyams *et al*, 2002). In addition to these host-derived effects, accumulation of muropeptides may also have signaling effects on the pathogen (Folkesson *et al*., 2005).

The importance of amidases on bacterial fitness and pathogenicity has also been recorded in investigations with the pathogen *H. pylori*. Abrogation of *H. pylori* AmiA resulted in alterations in the morphological transition from spiral to coccoid forms upon entry into stationary phase, led to the formation of chains and affected cellular motility (Chaput *et al*., 2016). As a result of these defects, *H. pylori* displayed attenuated bacterial fitness, as observed by the failure to colonize the stomach of C57/BL6J mice (Chaput *et al*., 2016). Similarly, a *P. aeruginosa* AmpDh knockout required a considerably higher Lethal Dose (LD_{50}), indicative of reduced pathogenicity in comparison to wild-type PAO1 and PA14 strains (Perez-Gallego *et al*., 2016). Furthermore, invasion capacity of the amidase mutant was analyzed by challenging human type II alveolar epithelial cells with PAO1 and the mutant strain however, no difference in intracellular bacterial numbers was found between these strains (Perez-Gallego et *al.*, 2016). When cytotoxicity was analyzed by quantifying lactate dehydrogenase (LDH) released in culture, the mutant was defective in mediating cytotoxicity due to the repression of key virulence factors such as LasA, phospholipase C, and TTSS components (Perez-Gallego *et al*., 2016). The authors postulate that down-regulating or abrogating amidase expression in *P. aeruginosa* results in de-repression of the beta lactamase *ampC*, leading to extremely high *ampC* expression. This consumes a major energetic burden, which compromises cell physiology, fitness and virulence (Perez-Gallego *et al*., 2016).

The importance of amidase activity has also been extensively documented in *Listeria monocytogenes*, which recently made newspaper headlines having caused more than 80 deaths in the South Africa. Amidase denoted as Ami, in *L. monocytogenes* has been shown to mediate hepatocyte colonization through the promotion of adhesion and entry into cells, which is required for increased bacterial load. Deletion of this amidase resulted in reduced liver colonization following infection of mice with the Ami deficient strain (Asano *et al*., 2012). This study also demonstrated that Ami is involved in the hyperstimulation of the immune response, thereby enhancing cytokine production in response to Listeria infection. Whilst this might seem counter-

productive, the group demonstrated that this contributes to the pathogenesis and inflammation associuated with Listerial infection (Asano *et al*., 2012).

1.10.3.3 Use of amidases as biomarkers, antibacterial agents and vaccine candidates

Identifying biomarkers for sepsis aids in the differentiation between infected and uninfected patients, thus serving as a useful diagnostic tool as the use of blood cultures is inefficient, with frequent false negatives (Bloos and Reinhart, 2014). Pinheiro Da Silva *et al* (2016) investigated multiple bacterial proteins as possible sepsis biomarkers and showed that the amidase PGLYRP2 has the potential to be used as a sepsis biomarker in critically ill patients as significant PGLYRP2 shedding can be detected in the plasma. In addition to the use of amidases as biomarkers of disease, Tillman *et al* (2013) demonstrated the utility of amidases as antimicrobials for controlling the growth of the spore forming pathogenic bacterium, *Clostridium perfringens*. In this case, exposure of the bacteria to the lytic amidase Slei resulted in reduced bacterial growth and a change in morphology with the cells being vacuolated (Tillman *et al*., 2013). The use of amidases as antibacterial agents is also exploited by eukaryotic cells. Insect Peptidoglycan Recognition Proteins (PGRPs) (which have an *N*-acetylmuramoyl-L-alanine amidase domain) have been shown to initiate the activation of prophenoloxidase cascades that generate antimicrobial melanin and reactive oxygen species. They are also involved in activation of Toll and Imd pathways and facilitate bacterial phagocytosis (Wang *et al*., 2005). Mammals also have PGRPs however, they function more like effector molecules instead of receptors and are referred to as PGLYRPs (Liu *et al*., 2000). Mammalian PGLYRP1 is present in granulocytes granules and has antibacterial properties, PGLYRP2 is constitutively expressed in the liver and gets secreted in the blood stream, its expression correlates with differentiation of keratinocytes and the induction of stress responses mediated through the activation of p38 MAPK pathway (Wang *et al*., 2005). Wang *et al* (2005) showed that upon exposure to bacteria, MKK6 and p38 MAPK, become phosphorylated. These proteins are involved in keratinocyte responses to proinflammatory signals and stresses required for the induction of PGLYRP2 transcription. This enables the digestion of bacterial PG, which reduces or eliminates the ability of polymeric PG to activate proinflammatory activity. The mechanism in this case involves either the abrogation of the Nod2-activating capacity of PG, which requires muramyl-dipeptides, or the generation of

Nod1 activating peptides (tripeptides, generated through amidase activity), both of which ultimately enhance antimicrobial defenses (Dziarski and Gupta, 2006; Wang *et al*., 2005).

Nair *et al* (2015), investigated the ability of the peptidoglycan amidase, Atl-AM, to serve as an efficient vaccine candidate for *S. aureus* and *S. epidermis*. Splenocyte proliferation assays and BALB/c mouse infections were used to determine the immunogenicity and antigenicity of Atl-AM respectively (Nair *et al*., 2015). Immunized BALB/c mice produced elevated levels of antibodies against Atl-AM, and splenocytes stimulated with Atl-AM multiplied significantly, thus validating Atl-AM as a good antigen and possibly a vaccine candidate (Nair *et al*., 2015). Further work demonstrated that vaccination with Atl-AM increased $CD4^+$ T cell differentiation with increased levels of Th1 (3.78%) and Th2 (1.96%), which skewed the immune response towards Th1. This was coupled with the production of interferon gamma (IFN-γ) and tumor necrosis factor- (TNF), which among other signatures has been shown to be essential for *S. aureus* vaccine success (Nair *et al*., 2015). Vaccination with Atl-AM also resulted in production of high titers of IgG2a and IGg2b antibodies, which are essential for increased opsonophagocytic killing. Significantly increased IgG1 titers were observed, which confirm the activation of the Th2 cell mediated immune response (Nair *et al*., 2015). This group also investigated the clearance of *S. aureus* in Atl-AM immunized mice by polymorphonuclear neutrophils (hPMNs). High association of the bacteria and neutrophils was observed, 40 % of which survived in the Atl-AM immunized mice compared to 85 % in the mock immunized control mice sera (Nair *et al*., 2015). In addition to the clearance of *S. aureus*, the efficacy of the Atl-AM vaccine was demonstrated by challenging the immunized mice with a lethal dose of *S. aureus*, this resulted in the survival of 7 out of 8 vaccinated mice compared to 1 out of 8 mock immunized mice, along with consistent expression of the Atl-AM antigen during growth of *S. aureus* (Nair *et al*., 2015).

1.10.3.4 The role of amidases in cell wall recycling and antibiotic resistance

Antibiotic resistant *H. pylori*, causing duodenal and gastric ulcers of the mucosa and gastric adenocarcinoma, possess an amidase AmiA (Chaput *et al*., 2016). Knockout of the *amiA* gene pointed to a role in ensuring β-lactam resistance, as exposure of the mutant strain to amoxicillin resulted in an MIC of >256 mg/ml, which was substantively higher than the wild type, an effect possibly mediated through an altered PG structure (Perez-Gallego *et al*., 2016). Antibiotic

resistance attributed to amidases was also reported in *P. aeruginosa*, with AmpD, AmpDh2 and AmpDh3 triple mutants in PAO1 and PA14 strains displaying a >1000-fold increase in AmpC expression and resultant increased resistance towards β-lactams (Perez-Gallego *et al*., 2016). The simultaneous inactivation of the three amidases also increased the doubling time of both strains, this is believed to be as a result of AmpC overexpression (β-lactamase) (Perez-Gallego *et al*., 2016).

1.10.3.5 The role of amidases in symbiosis

Burkholderia is a widely known endosymbiont of the insect *Riportus clavatus,* residing in its posterior midgut and contributing to the insect's fitness and development (Kikuchi, Hosokawa and Fukatsu, 2007). To investigate this, the effects of cell division defects and the role of the amidase, AmiC, in *Burkholderia* were assessed (Lee *et al*., 2015). Deletion of AmiC resulted in abrogated colonization post oral infection and a concomitant defect in cell motility and colonization of the insect's midgut (Lee *et al*., 2015). In addition to this, long-chained cells were seen, suggesting AmiC directs cell separation in *Burkholderia* (Lee *et al*., 2015). Considering this, it was hypothesized that the alteration in cell morphology is responsible for the abrogation in cell motility, which is needed to ensure symbiotic association with the *Riportus* host insect (Lee *et al*., 2015). Another symbiont, the gram negative *Wolbachia endobacteria* resides in host derived vacuoles, particularly those of arthropods and filarial nematodes, which can cause lymphatic filariasis and onchocerciasis (Specht *et al*., 2013). In these organisms, the endobacteria are required for fertility, survival, oogenesis and resistance to different pathogens. In addition to responding to changes in nutrient availability, they also play parasitic roles by manipulating the host's reproduction (Zug and Hammerstein, 2015). The *Drosophial Wolbachia* genome is extremely reduced to aid adaptation to the host (Stepkowski and Legocki, 2001) and has retained only one of the cell wall amidases, the periplasmic amidase AmiD (highest homology, 27 % sequence identity). Wilmes *et al* (2017), demonstrated that Wolbachial AmiD has enzymatic activity dependent on Zn^{2+}, which is essential for cleavage of PG like structures and might play a crucial role in PG turnover, thus precluding the host's immune receptors from detecting cell wall fragments and eliciting an immune response (Wilmes *et al*., 2017). The functional conservation of AmiD is an indicator of the essentiality of digesting anhydromuropeptides and the role the nolecules play in the lifestyle of the insect (Wilmes *et al*., 2017).

1.11 Cell division and division site placement in mycobacteria

Cell division processes are essential for bacterial multiplication and pathogenesis and are therefore considered vulnerable therapeutic targets in pathogenic bacterial infections. Bacterial cell division is coordinated by a multi-protein complex referred to as the "divisome", wherein specific protein- protein interactions determine whether cell division takes place or is arrested (Sureka *et al*., 2010). The mycobacterial divisome consists of cytoskeletal proteins (FtsZ), structural elements (FhaB, FtsW, FtsQ, CrgA and CwsA), PG synthases (PBPs and PonA1) and hydrolases (RipA and possibly amidases) (Kieser and Rubin, 2014).

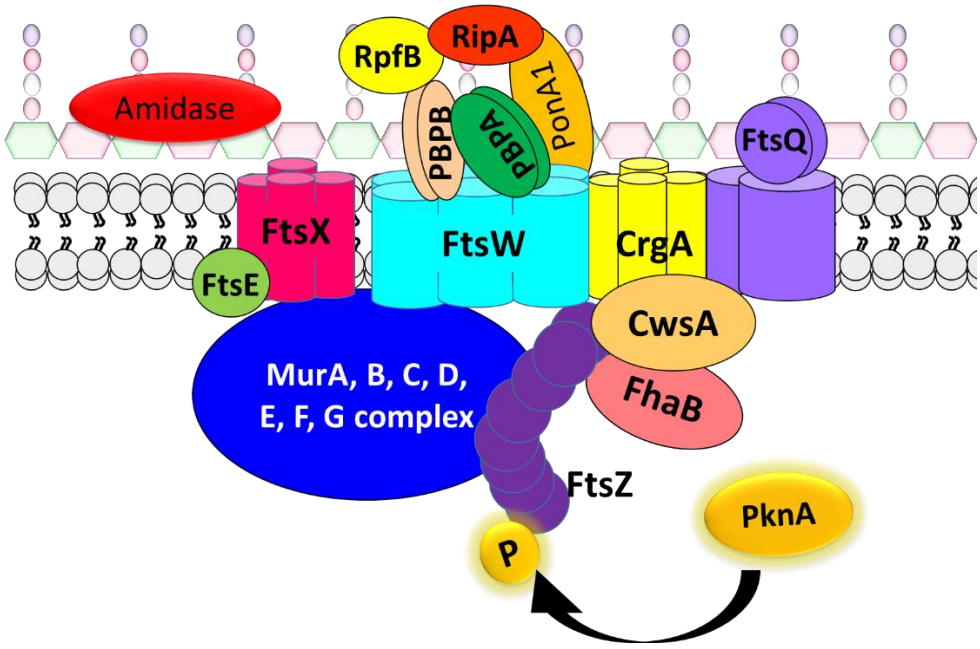

Figure 1.6: Representation of the multiprotein complex known as the divisome which responsible for coordinating bacterial cell division. Bacterial cell division is initiated by the polymerization of FtsZ, placement of the Z-ring at the respective site, with the aid of phosphorylation by PknA and other factors. The recruitment of FtsZ causes localization of other divisome proteins such as FhaB, which stabilizes the ring. These include factors such as FtsW, FtsQ, CrgA and CwsA, which are recruited to the site of division thus forming the divisome. Furthermore, PG synthases and hydrolases are recruited to the septum along with FtsE and FtsX. Together, these facilitate septum synthesis and septal hydrolysis. Adapted from Kieser and Rubin (2014). Figure drawn by student.

The divisome functions in synchrony to ensure efficient cell wall synthesis, division and maintenance of cell wall integrity. A schematic illustration of the divisome is given in Figure 1.6. Formation of septa is initiated through the polymerization of the FtsZ into a ring like structure (Z-ring) which determines the site of cell division and provides the contractile force necessary for ensuring membrane constriction (Adams and Errington, 2009; Li *et al*., 2013). Alterations in FtsZ expression levels in *M. smegmatis* interferes with cell division resulting in the formation of filamentous cells, buds, branch like structures and decreased cell viability (Dziadek *et al*., 2003). Z-ring formation is subsequently stabilized by interactions between FtsZ and FhaB, which forms a link between FtsZ and FtsQ, ensuring accurate Z ring placement (Kieser and Rubin, 2014). Previous investigation into the function of FhaB highlight that deletion of this protein disturbs cell division, resulting in elongated *Mtb* cells grown in macrophages, with reduced intramacrophage multiplication (Sureka *et al*., 2010). Through interaction with FhaB, FtsQ is able to interact with CrgA (cell division protein), aiding in FtsZ PBPA/B interaction (Plocinski *et al*., 2011; Kieser and Rubin, 2014). As seen with the loss of FtsZ and FhaB individually, depletion of CrgA also results in the formation of elongated cells, it was hypothesized that this phenotype maybe be linked to failure to recruit septum PG synthases such as PBPB (Plocinski *et al*., 2011). In addition to this, it is thought that PBP joins the complex through FtsW interaction and a FtsZ-FtsW-PBPB complex coordinates cell division cues with septum synthesis (Datta *et al*., 2006). Furthermore, cell division is coupled with cell elongation through CrgA- CwsA (elongation complex protein) interaction (Plocinski *et al*., 2012). Following the recruitment of cytoskeletal, structural proteins and PG synthases (PBPA, PBPB and PonA1), hydrolases are recruited to drive separation of the daughter cells (Kieser and Rubin, 2014). As mentioned in the sections above, these encompass a variety of proteins such as amidases, endopeptidases and glucosaminidases and others. The mycobacterial RipA (an endopeptidase) has been shown to play a crucial role in cell separation and cell wall integrity, as deletion of the peptidase leads to formation of chains and increased antibiotic susceptibility (Chao *et al*., 2013). Subsequent to this paper, a publication on an Amidase 1 (Ami1) in *M. smegmatis* reported involvement of this enzyme in the coordination of cell division as its loss not only resulted in chains and deregulated FtsZ bundling but also resulted in the mislocalization of DivIVA (Senzani *et al*., 2017). This led to the formation of ectopic branches, which ensured continued survival of the mutant strain (Senzani *et al*., 2017). With cell division being so crucial to bacterial survival, inhibitors of this

process have been previously screened/ developed for mycobacteria. These include analogs binding to the FtsZ polymer thus inhibiting FtsZ function (Kumar *et al*., 2010; Mathew *et al*., 2016). This is illustrative of the promise of inhibiting bacterial growth and cell division through targeting PG remodeling enzymes, a notion that should be confirmed in *Mtb*.

1.12 The elongation complex

Mycobacteria along with a great number of actinobacteria grow by polar extension, which is a departure from the canonical lateral wall growth model (Cameron *et al*., 2015). However, the mechanisms that underpin this modality of growth remain elusive, thus underscoring the need for further research in this area (Cameron *et al*., 2015). Subsequent to polar extension, mycobacteria adopt an asymmetric growth pattern which introduces morphogenic heterogeneity that is advantageous to bacteria under stressful conditions, particularly antibiotic stress (Keiser and Rubin, 2014). One of the proteins essential for polar growth is the coiled coil protein Wag31/DivIVA, which anchors a multiprotein complex to the site of active PG synthesis (Typas *et al*., 2012; Meniche *et al*., 2014). DivIVA localization to the poles is followed by recruitment of the cell wall synthesis protein A (CwsA), which then stimulates the activities of the Lipid II synthesis proteins (MraY and MurG) through phosphorylation (Jani *et al*., 2010; Plocinski *et al*., 2012). The multi-protein complex required for cell elongation is referred to as the elongasome complex (Szwedziak and Löwe, 2013). A schematic representation of the elongasome is given in Figure 1.7. Kang *et al* (2008) showed that Wag31 is an essential protein, which when depleted causes the rounding of one pole instead of forming a rod-shape, this is thought to be caused by abrogation in polar PG synthesis. In addition to this, Wag31 controls cell shape and cell wall synthesis in response to environmental stimuli (Kang *et al*., 2008). Further investigation into the elongasome complex involved deletion of the LD-transpeptidases (Ldts) (Figure 1.7), which resulted in alterations in cell morphology as evidenced by the formation of short cells and cell bulging (Schoonmaker, Bishai and Lamichhane, 2014). Loss of CwsA in mycobacteria led to the formation of swollen/ bulging cells. Investigation of the role of CwsA in cell wall synthesis using fluorescent vancomycin (Van-FL, which localizes to areas of new cell wall synthesis) showed that Δ*cswA* cells had ~50% reduction in Van-FL staining and the bulged regions of the mutant strain had faint to no staining, suggesting defective polar growth (Plocinski *et al*., 2012).

Interestingly, the essential mycobacterial amidase CwlM was shown to be required for cell elongation as depletion resulted in elongation defects and a significant reduction in growth (Boutte *et al*., 2016). The role of CwlM in cell elongation is through association and activation of the first protein in the PG biosynthesis pathway MurA, this is facilitated by CwlM phosphorylation (Boutte *et al*., 2016). Furthermore, CwlM dephosphorylation during starvation inevitably resulted in lower MurA activity, a decline in cell wall turnover and thus increased tolerance of multiple antibiotics (Boutte *et al*., 2016).

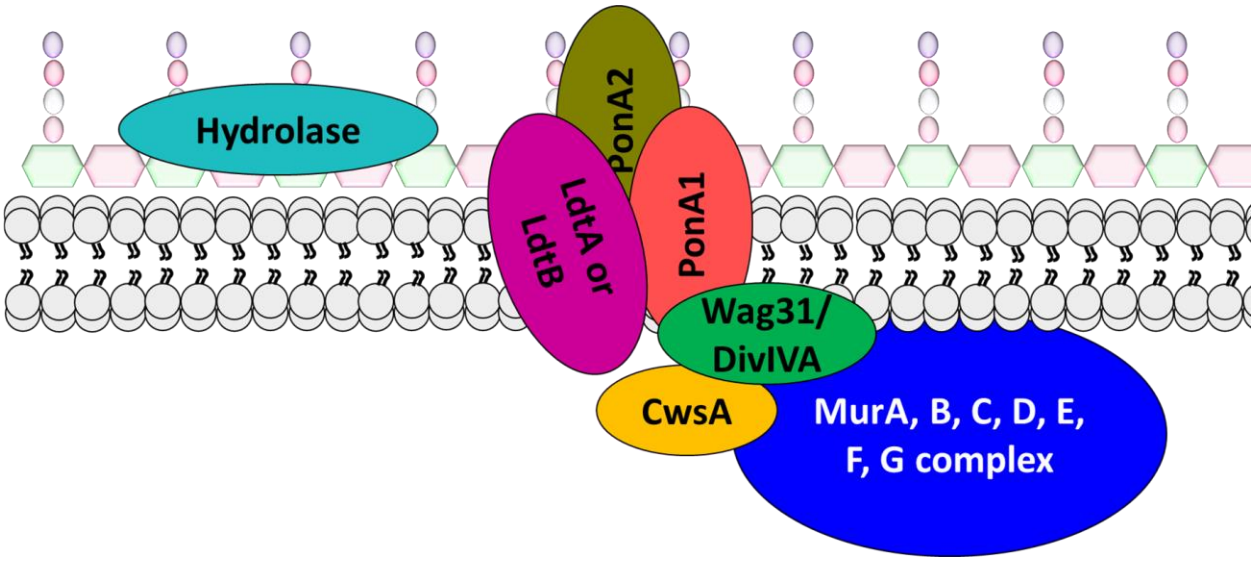

Figure 1.7: Schematic representation of the mycobacterial cell elongation complex. The protein machinery directing cell growth at the poles is comprised of PG synthases and hydrolases, along with structural and regulatory proteins. This multi-protein complex responsible for polar elongation is anchored by Wag31/DivIVA, which localizes at the poles. Wag31 localization at the poles recruits CwsA, stabilizing cell wall synthesis proteins. Further recruitment of PG synthases and hydrolases takes place to ensure a coordinated synthesis: degradation ratio. Adapted from Kieser and Rubin (2014). Figure drawn by student.

The research in mycobacterial cell division and polar growth outlined thus far highlights the need for careful coordination of cell elongation through intricate control of the elongasome protein-protein interactions. This MSc dissertation was focused on advancing the knowledge on mycobacterial cell division by assessing the function of amidases. As mentioned before, TB remains a global threat regardless of the widespread use of chemotherapy for treating infected and diseased individuals (Boshoff, 2017). The current chemotherapeutic regimen entails 2

months of treatment with the first line drugs INH, rifampicin (RIF), pyrazinamide (PZA) and ETH for drug sensitive TB, this is subsequently followed by a 4-month treatment with INH and RIF (WHO, 2015 and Boshoff, 2017). However, with the resurgence of drug resistance strains there is an imminent need to discover and screen for novel anti-TB drugs. Development of drugs that shorten treatment duration with the least side effects may lead to lead to higher patient compliance and aid in eradicating TB. Considering the background review presented on amidases, explicitly highlighting their diverse role in pathogenesis, it is possible that these enzymes could serve as new TB drug targets. To validate this, three distinct amidases_2 domain containing Amidases were studied in this MSc research in the non-pathogenic fast-growing *Mycobacterium smegmatis*, a model organism used for TB research.

1.13 Hypothesis:

Amidase_2 domain containing amidases play important roles in cell division and PG remodeling and deletion thereof will result in notable cell growth/division defects.

1.14 Aims and objectives

Using comparative genomics, 3 putative amidases in *M. smegmatis* were identified for further study, these were designated as Ami3, Ami4 and Ami5.

Preliminary work: I, Nombeko Sikhosana, undertook an Honours project (Sikhosana, 2015*) to assess the function of Ami3 and Ami4. During the course of this work, deletion mutants were generated, followed by a very preliminary characterization. This research was then advanced in my MSc work. As a result, at the beginning of the MSc, two mutants defective either in Ami3 or Ami4 were available. The MSc research started with rigorous genotypic characterization of these existing strains, together with construction of genetically complemented derivatives. An Ami5 mutant did not exist at this stage and was constructed during the course of this MSc. Considering this, specific objectives were as follows:

1. To conduct a detailed bioinformatics analysis of these three amidases
2. To genotypically confirm knockout mutants for Ami3 and Ami4
3. To construct an Ami5 deletion mutant

4. To phenotypically characterize the above-mentioned mutant strains using in vitro growth experiments and various forms of microscopy
5. To create reporter strain derivatives of the mutants that carry markers for cell elongation and division.
6. To study mutant and reporter strains using single-cell time-lapse microscopy
7. To search for interacting partners for mycobacterial amidases as this may provide further insight into their biological functions.

Nombeko Sikhosana. 2015. Characterization of Amidase_2 domain proteins in *Mycobacterium smegmatis*. Honours project conducted at the CBTBR, Department of Molecular Medicine and Haematology, School of Pathology, Wits University. Unpublished.

2. Materials and Methods

2.0 Bacterial strains, plasmids, chemicals and growth conditions

A detailed list of reagents used in this study and their recipes is shown in Appendix A (Table 1)

2.0.1 Bacterial strains and culture conditions

E. coli and *M. smegmatis* strains, as well as plasmids used in this work, are listed in Table 1 and Table 2. Bacterial strains were grown aerobically at 37°C with constant agitation in media with the appropriate antibiotic where necessary. Bacterial stocks were preserved in 33% glycerol and stored at -80°C. The following sections detail growth conditions for respective bacterial strains and their derivatives.

Table 1: List of plasmids used and generated in this study

Plasmid names	Description	Reference/ Source
pBluescript	*E. coli* cloning vector, Amp^r, *lacZ-alpha*, OriE	Promega
p2NIL	*E. coli* cloning vector, Kan^r	Parish and Stoker, 2000
pGOAL17	Plasmid carrying *lacZ-sacB*-Kan^r markers as a *Pac*I *cassette*; Kan^r	This study
p2NIL_ PAC_ *ami3*	Knockout vector for creating the Δ*ami3* mutant using the p2NIL vector and *Pac*I cassette (from pGOAL17); Kan^r	This study
p2NIL_ PAC_ *ami4*	Knockout vector for creating the Δ*ami4* mutant using the p2NIL vector and *Pac*I cassette (from pGOAL17); Kan^r	This study
p2NIL_ PAC_ *ami5*	Knockout vector for creating the Δ*ami5* mutant using the p2NIL vector and *Pac*I cassette (from pGOAL17); Kan^r	This study
pMV306H	*E. coli*-*Mycobacterium* integrating shuttle vector. Integrates at the L5 *attB* site in mycobacteria. Hyg^r	H. Boshoff
pMV306H::*ami3*	Derivative of pMV306H carrying a full length copy of *ami3* plus 300 bp upstream of start codon representative of native promoter sequence; Hyg^r	This study

pMV306H::*ami5*	Derivative of pMV306H carrying a full length copy of *ami5* plus 500 bp upstream of start codon representative of native promoter sequence; Hyg^r	This study
pTweety	*E. coli-Mycobacterium* integrating shuttle vector. Has an L5 *attP* site for integration at a locus containing the tRNA^{Lys} on the mycobacterial chromosome. Kan^r	This study
pTweety::*ami4*	Derivative of pTweety carrying a full-length copy of *ami4* plus 300 bp upstream of start codon representative of native promoter sequence; Kan^r	This study
pMV306H::*divIVA*-rseGFP	Derivative of pMV306H carrying a wild-type *divIVA* allele (along with the promoter region) tagged at the C-terminus with GFP. Therefore, the vector expresses a GFP fusion protein; Hyg^r	CBTBR M. Maphatsoe M.Sc. (Unpublished)
pMV306H::*ftsZ*-rseGFP	Derivative of pMV306H carrying a wild-type *ftsZ* allele plus promoter region tagged with GFP. This vector expresses a GFP recombinant protein; Hyg	CBTBR Senzani *et al*., 2017
pUAB300	*E. coli-Mycobacterium* shuttle plasmid carrying the mDHFR fragment 1 and 2, together with a glycine linker; Hyg^r	Singh *et al*., (2006)
pUAB300_ *ami3*	Derivative of pUAB300 carrying a full length copy of MSMEG_6406: Hyg^r	This study
pUAB400	*E. coli-Mycobacterium* shuttle plasmid carrying mDHFR fragment 3; Kan^r	Singh *et al*., (2006)
pUAB400_*Mmpl*	Derivative of pUAB400 carrying a full-length copy of *mmpL* wild-type gene; Kan^r	This study
pUAB400_ *pap2*	Derivative of pUAB400 carrying a full-length copy of the *pap2* wild-type gene; Kan^r	This study
pUAB400_*glft*	Derivative of pUAB400 carrying a full-length copy of *glft* wild-type gene; Kan^r	This study
pUAB400_*erp*	Derivative of pUAB400 carrying a full-length copy of *erp*; Kan^r	This study
pUAB400_*ponA1*	Derivative of pUAB400 carrying a full-length copy of *ponA*; Kan^r	This study

Table 2: List of strains generated and used in this study

Strains	Description	Reference/ Source
	***E. coli* Strains**	
E. coli (DH5α)	Cloning strain with high transformation efficiency	Promega, Madison, WI
E. coli (BL21(DE3) pLysS)	Protein expression strain with IPTG-inducible promoter region for T7 RNA polymerase	Promega
	***Mycobacterium* Strains**	
Parental strains: *Mycobacterium smegmatis* (mc^2155)	High frequency transformation mutant of *M. smegmatis* ATCC 607	Snapper *et al*., 1990
Δ*ami3*	Derivative of mc^2155 carrying an unmarked, in-frame deletion in *ami3* where 99 bp from the 5' end and 99 bp 3' end remain, with 1413 bp deleted.	This study
Δ*ami4*	Derivative of mc^2155 carrying an unmarked, in-frame deletion in *ami4* in which 99 bp from 5' end and 99 bp from the 3'end was retained, with 630 bp were deleted.	This study
Δ*ami5*	Derivative of mc^2155 carrying an unmarked, in-frame deletion in *ami5* whereby 99 bp from the 5' end and 99 bp from the 3' end was retained, with in 342 bp deleted.	This study
Δ*ami3*::*ami3*pMV306H	Derivative of *M. smegmatis* Δ*ami3* with an integrating plasmid pMV306H expressing *ami3* from its own promoter; Hyg^r	This study
Δ*ami4*::*ami4*pTweety	Derivative of *M. smegmatis* Δ*ami4* with an integrating plasmid pTweety expressing *ami4* from its own promoter; Kan^r	This study
Δ*ami5*::*ami5*pMV306H	Derivative of *M. smegmatis* Δ*ami5* with an integrating plasmid pMV306H expressing *ami5* from its own promoter; Hyg^r	This study
mc^2155::DivIVA-rseGFP	Derivative of *M. smegmatis* expressing a GFP tagged wild-type allele of *divIVA* at the tRNA glycine site. Constructed by electroporation of -	This study

mc^{2}155::DivIVA-rseGFP	- plasmid pTweety::*divIVA*-GFP into *M. smegmatis* wild-type. Kan^r	This study
Δ*ami3*::*divIVA*-rseGFP	Derivative of *M. smegmatis* Δ*ami3* with integrating plasmid pTweety expressing a C-terminal rseGFP-tagged derivative of DivIVA from its own promoter; Kan^r	This study
Δ*ami4*:: *divIVA*-rseGFP	Derivative of *M. smegmatis* Δ*ami4* with integrating plasmid pTweety expressing a C-terminal rseGFP-tagged derivative of DivIVA from its own promoter; Kan^r	This study
Δ*ami5*::*divIVA*-rseGFP	Derivative of *M. smegmatis* Δ*ami5* with integrating plasmid pTweety expressing a C-terminal rseGFP-tagged derivative of DivIVA from its own promoter; Kan^r	This study
mc^{2}155::FtsZ-rseGFP	Derivative of *M. smegmatis* expressing a GFP tagged wild-type allele of *ftsZ* at the tRNA Lysine site. Constructed by electroporation of plasmid pMV306H::*ftsZ*-GFP into wild-type *M.smegmatis*. Hyg^r	This study
Δ*ami3*::*ftsZ*rseGFP	Derivative of *M. smegmatis* Δ*ami3* with integrating plasmid pTweety expressing a C-terminal rseGFP-tagged derivative of FtsZ from its own promoter; Kan^r	This study
Δ*ami4*:: *ftsZ*rseGFP	Derivative of *M. smegmatis* Δ*ami4* with integrating plasmid pTweety expressing a C-terminal rseGFP-tagged derivative of FtsZ from its own promoter; Kan^r	This study
Δ*ami5*::*ftsZ*rseGFP	Derivative of *M. smegmatis* Δ*ami5* with integrating plasmid pTweety expressing a C-terminal rseGFP-tagged derivative of FtsZ from its own promoter; Kan^r	This study
mc^2 155 (pUAB300/pUAB400)	Derivative of *M. smegmatis* carrying shuttle plasmids pUAB300 and pUAB400; Kan^r	This study
mc^2 155 (RipA-DHFR [F1,2]/RpfB [F3])	Derivative of *M. smegmatis* carrying recombinant proteins RipA DHFR [F1,2] and RpfB [F3] co-expressed to confirm interaction of RipA with RpfB; Hyg^r, Kan^r. Used as a positive control.	D. Ralefeta
mc^2 155 (Ami3-DHFR [F1,2]/PAP2 [F3])	Derivative of *M. smegmatis* carrying recombinant proteins Ami3-DHFR [F1,2 domain] and PAP2 [F3 domain] co-electroporated in *M. smegmatis* to -	This study

mc^2 155 (Ami3-DHFR [F1,2]/PAP2 [F3])	create a dual recombinant strain for the investigation of protein-protein interaction; Kan^r and Hyg^r	This study
mc^2 155 (Ami3-DHFR [F1,2]/Glft [F3])	Derivative of *M. smegmatis* carrying recombinant proteins Ami3-DHFR [F1,2 domains] and Glft [F3 domain] co-electroporated in *M. smegmatis* to create a dual recombinant strain for the investigation of protein-protein interaction; Kan^r and Hyg^r	This study
mc^2 155 (Ami3-DHFR [F1,2]/Erp [F3])	Derivative of *M. smegmatis* carrying recombinant proteins Ami3-DHFR domain [F1,2] and Erp [F3] recombinant proteins co-expressed in the *M. smegmatis* to investigate potential interaction; Kan^r and Hyg^r	This study
mc^2 155 (Ami3-DHFR [F1,2]/ PonA1 [F3])	Derivative of *M. smegmatis* carrying recombinant proteins Ami3-DHFR [F1,2] and PonA1 [F3] co-expressed in *M. smegmatis* background to investigate possible interaction between the two proteins; Kan^r, Hyg^r	This study
mc^2 155 (Ami3-DHFR [F1,2]/MmpL[F3])	Derivative of *M. smegmatis* carrying recombinant proteins Ami3-DHFR [F1,2] and MmpL [F3] co-expressed in the *M. smegmatis* background to investigate protein-protein interaction; Kan^r and Hyg^r	This study
$mc^2$155 (pSE100)	Derivative of $mc^2$155 expressing the empty pSE100 vector, Hyg^r	This study
$mc^2$155 (pSE6406)	Derivative of $mc^2$155 ectopically expressing MSMEG_6406 from pSE100 vector, Hyg^r	This study
$mc^2$155 (pSE5315)	Derivative of $mc^2$155 ectopically expressing MSMEG_5315 from pSE100 vector, Hyg^r	This study

2.0.2 Growth conditions of *E. coli* DH5α strain

E. coli (DH5α) was cultured aerobically in Lysogeny Broth (LB) (Reagents in Appendix A, Table 1A) at 37°C with continuous shaking at 250 rpm or on solid Luria Bertani agar medium (LA) (Reagents in Appendix) overnight. Transformants with plasmids greater than 8000 bp were grown at 30°C to avoid rearrangement. When appropriate, drug resistant markers in *E. coli* cells

carrying plasmids were selected with the appropriate antibiotic. Antibiotic concentrations were as follows: Ampicillin (Amp) 100 µg/ml, Kanamycin (Kan) 50 µg/ml and Hygromycin (Hyg) 200 µg/ml. In addition to antibiotic resistance for selection, 2 % Xgal and 5% sucrose were used to select for specific *E. coli* clones.

2.0.3 Growth conditions of *M. smegmatis* strains

M. smegmatis strains were grown at 37°C. Bacteria were cultured in either 7H9 Middlebrook medium (Appendix A) or Sauton's medium (Appendix A), unless or otherwise stated. *M. smegmatis* liquid cultures were shaken at 115 rpm and grown overnight. Mycobacterial colony forming units (CFU) were assessed by plating ten-fold serial dilutions on 7H10 Middlebrook agar with appropriate antibiotic where necessary (Appendix A; Table 1). For the maintenance of plasmids electroporated into mycobacterial strains, media was supplemented with appropriate antibiotics at final concentrations of 50 µg/ml for Hyg and 25 µg/ml for Kan. Further selections markers used include 2 % Xgal, 2% sucrose and 7.5 µg /ml or 15 µg /ml TRIM.

2.1 DNA manipulation

2.1.1 Mycobacterial DNA extraction

2.1.1.1 Cetyltrimethylammonium bromide DNA extraction (CTAB) protocol

The mycobacterial waxy cell wall necessitates the use of protocols with special consideration for these factors to lyse the cells and isolate good quality genomic DNA. For this, the cetyltrimethylammonium bromide DNA extraction (CTAB) protocol is routinely used. Mycobacterial cells were grown on 7H10 Middlebrook agar to obtain a lawn of cells, which was scraped off from the plates, resuspended in water and heat killed at 65°C for 1 hour. This was subsequently followed by centrifugation for 10 minutes at 13000 rpm, the pellet was then resuspended in TE buffer pH 8.0 (Appendix A, Table A2) with 50 µl of Lysozyme (10 mg/ml) and incubated at 37°C for 1 hour. Following the digestion of the bacterial cell wall with lysozyme, proteins were digested with 6 µl of the broad spectrum serine protease, Proteinase K (10 mg/ml) in 70 µl of SDS (10%), which activates the function of the former, and incubated at

65°C for 2 hours. To ensure the DNA stays in solution, 100 µl of 5 M NaCl was added. Subsequently, 80 µl of CTAB/NaCl was also added and incubated at 65°C for 10 minutes, to facilitate DNA precipitation. To enable the separation of proteins and polysaccharides from nucleic acid, an equal volume of $CHCl_3$/isoamyl alcohol (24:1) was added, mixed and centrifuged for 5 minutes at 13000 rpm. The aqueous layer was transferred to a clean tube to which 0.6 volume of isopropanol was added, placed on ice for 30 minutes and centrifuged for 20 minutes at 13000 rpm. The resulting DNA pellet was washed with 70% ethanol to remove salts, centrifuged for 5 minutes and dried. The lyophilised DNA was resuspended in an appropriate volume of TE buffer or nuclease free water. The DNA was quantified using the Nanodrop ND-1000 Spectrophotometer (NanoDrop technologies). To assess the quality of the DNA, an aliquot of the DNA was electrophoresed on 0.8% agarose gel with an appropriate high molecular weight marker (Appendix C). The extracted DNA was stored at -20°C for subsequent use.

2.1.1.2 Small scale mycobacterial DNA extraction

For initial genotypic confirmation or screening of strains, direct PCR was performed on individual colonies, where the DNA was isolated by boiling. For the colony boil method, an entire colony was picked and resuspended in 100 µl of nuclease free water and boiled at 95°C for 10 minutes to denature proteins and break open the cell wall to release the genomic DNA. Following this, an equal volume of chloroform was added, followed by centrifugation at 13000 rpm for 10 minutes. The supernatant was then aliquoted into a clean tube and 2 µl used for each PCR reaction.

2.1.2 *E. coli* plasmid DNA extraction

2.1.2.1 Plasmid bulk DNA extraction

The Qiagen Spin Miniprep kit (Whitehead Scientific, South Africa) is a silica gel membrane-based method which was used for bulk plasmid DNA extraction from derivatives of *E. coli* DH5α harbouring the required constructs or plasmids. For this, 5 ml of culture was grown in LB medium overnight with shaking, supplemented with the appropriate antibiotic and plasmid DNA extracted as per the manufacturer's guidelines. Briefly, the cell pellet was resuspended in 250 µl of buffer P1, which has a colour indicator for cell lysis, and RNase for the digestion of RNA

during the extraction process. Subsequently, 250 µl of buffer P2 (Lysis buffer) was added, followed by the addition of 350 µl of buffer N3, which contains chaotropic agents (guanidinium hydrochloride and potassium acetate) that act to neutralise cell lysis and facilitate DNA binding to the column. The mixture was transferred into a clean Eppendorf tube and centrifuged at 13000 rpm for 10 minutes, the supernatant was applied to the QIAprep 2.0 spin column, and centrifuged at 13000 rpm for 1 minute, the flow through was discarded. The QIAprep 2.0 spin column was washed with the ethanol containing buffer PE to remove contaminants and following this, residual buffer PE was removed by further centrifugation at 13000 rpm to ensure no interference with subsequent enzymatic reactions. Following this, DNA was eluted using 1× TBE Buffer and measure as outlines in Section 2.1.4.

2.1.2.2 Small scale plasmid extraction

For small scale plasmid extractions, the alkaline lysis mini prep protocol was used. Prior to extraction, *E. coli* cultures transformed with plasmids of interest were grown overnight in 2ml LB media supplemented with the appropriate antibiotics. The cells were harvested at 13000 rpm and resuspended in 100 µl resuspension buffer (solution I, Appendix A, Table 2). Subsequently, 200 µl of lysis buffer (solution II, Appendix A, Table 2) was added and mixture was inverted and incubated at room temperature for 10 minutes. Finally, 150 µl of neutralizing solution (solution III, Appendix A, Table 2) was added followed by incubation of the mixture on ice for 10 minutes. This was followed by centrifugation at 13000 rpm for 5 minutes to separate proteins from the DNA following which, the supernatant was decanted to a clean tube and precipitated with 600 µl of isopropanol. The pellet was washed using 70% ethanol, dried, and resuspended in the appropriate volume of nuclease free water. DNA was stored at -20°C until further use.

2.1.3 DNA purification and removal of contaminating proteins

2.1.3.1 Sodium Acetate precipitation

Following the extraction of chromosomal DNA or plasmid DNA, purification of DNA by the sodium acetate precipitation protocol was carried out to remove contaminating proteins, salts and other impurities. To the DNA, 1/10 volume of 3 M sodium acetate (pH 5.2, Appendix A, Table 2) and 2× 100% EtOH was added, this was subsequently incubated on ice for 1 hour. Following this, the mixture was centrifuged at 13000 rpm for 30 minutes, the supernatant was discarded and

the pellet washed with 70% EtOH and dried using the Eppendorf 5301 concentrator centrifugal reporter. The DNA was then resuspended in an appropriate volume of nuclease free water and stored at -20°C for subsequent use.

2.1.4 Nucleic acid quantification and visualization

Quantification of DNA was performed using the Nanodrop ND-1000 (Nanodrop Technologies) which quantifies DNA as a measure of absorbance at 260 nm. In addition to quantification, it allowed for analysis of nucleic acid purity as measured by the 260/280 nm and 230/260 nm ratio, representing contamination by proteins and organic solvents. Further to this, agarose gel electrophoresis was used to quantify and visualize DNA based on the intensity of the DNA bands in comparison to the molecular weight marker (Appendix C) bands of known concentrations.

2.1.5 DNA amplification-Polymerase chain reaction and PCR Fragment purification

Primers were designed using the bioinformatics tool, Primer3 (http://frodo.wi.mit.edu/), which gives the most optimal primer sequences based on the selection criteria in the table below

Table 3: Primer3 parameters for primer design

	Size	Tm (°C)	%GC
Minimum	**20**	55	55
Maximum	**25**	65	62
Optimum	**23**	60	60

Minimum size should read 18, optimum 21 and maximum 24

2.1.5.1 Roche FastStart Taq PCR

The low fidelity Taq polymerase (Thermofisher) was used for the screening and/ confirmation of mutants and complemented derivatives generated in this study. PCR reactions were set up according to the manufacturer's instructions with the use of appropriate primers (Appendix A, Table 3 and Table 4). A 25 µl reaction was used, consisting of 0.2 mM dNTPs each, DNA template between 10-100 ng/µl, forward and reverse primers to a final concentration of 1 µM each, 1× GC Rich buffer, 1× PCR buffer, 2 U Taq polymerase and nuclease free water (Sigma-Aldrich) to make up the volume of the final reaction. The reactions were subsequently incubated in a thermocycler using the following conditions: an initial cycle of denaturation at 95 °C for 4

minutes, 30-35 cycles of 30 seconds denaturation at 95 °C, 1 minute annealing time at a temperature specific for the set of primers, elongation for 30 seconds at 72 °C, followed by a final elongation step at 72 °C for 10 minutes.

2.1.5.2 Q5 High-Fidelity DNA polymerase PCR

For the synthesis of PCR products used for cloning, the proof reading High Fidelity polymerase, Q5 was used as per manufacturer's instructions. The PCR reactions were set up as follows: 1× Q5 Reaction buffer, 200 µM dNTPs, 0.5 µM forward and reverse primer each, < 1000 ng template DNA, 0.02 U/µl Q5 High Fidelity DNA polymerase and 1× Q5 High GC Enhancer, the reaction was made to 50 µl with nuclease free water. Thermocycling conditions used were: an initial denaturation of 98 °C for 30 seconds, 25-35 cycles of second denaturation for 5-10 seconds at 98 °C, 1 minute annealing at 50-72 °C, initial elongation at 72 °C for 20-30 seconds and final extension at 72 °C for 2 minutes.

2.1.6 PCR Fragment Purification

Following DNA amplification using High Fidelity DNA polymerase Q5, the templates were purified using the Macherey-Nagel (Germany) silica membrane PCR clean up and gel extraction kit. Purification was carried out as per manufacturer's instructions. Binding of the DNA fragment to the silica membrane column was facilitated by adding NTI buffer to the DNA, followed by adding the mixture to the column. This was centrifuged at 12 210 rpm for 30 seconds. The silica membrane column was then washed twice with NT3 buffer, which was supplemented with ethanol and both times, centrifuged at 12 210 rpm for 30 seconds. An extra spin was performed to dry the column and elute any ethanol that might hinder enzyme activity downstream. DNA was eluted using buffer NE and by centrifugation at 12 210 rpm.

2.1.7 DNA Manipulation

2.1.7.1 Restriction digestion of plasmid DNA and PCR products

Restriction digest reactions were carried out as per the manufacturer's instructions, with 1 µg DNA digested with 1 U enzyme (Roche Applied Science, United States) in 10× appropriate buffer and nuclease free water to make up the reaction to the desired volume. The reaction was incubated for 1 hour at 37 °C, followed by inactivation of the enzyme at the appropriate

temperature as specified by manufacturer. Following this, the restriction digests were visualized using agarose gel electrophoresis (Section 2.1.1.1). Where the restriction digests were for cloning, the DNA was purified as outlined in Section 2.1.6 and procedure followed as stated in section 2.1.7.3 to 2.1.8.

2.1.7.2 Phosphorylation and Dephosphorylation of DNA fragments

PCR fragments have 5'-hydroxyl termini that were phosphorylated using T4 PNK (polynucleotide kinase, New England Biolabs, United States), which transfers a phosphate group to the phosphate deficient terminus for efficient ligations. The reaction was carried out as per manufacturer's instructions using 1 µg template DNA, 1 U enzyme and 10 × PNK buffer, with the reaction made up to appropriate volume with nuclease free water and incubated at 37 °C for 1 hour. The enzyme was de-activated at 65 ºC for 10 minutes. Linearized plasmid DNA was dephosphorylated using Antarctic Phosphatase (APP) (New England Biolabs, United States) which removes the 5' phosphate group, preventing vector re-ligation and thus reducing vector only background colonies after transformation. The reaction was carried out as per manufacturer's instructions using 1 µg of plasmid DNA, 1 U of Antarctic Phosphatase (New England Biolabs, United States), 1/10 of 10 × Antarctic Phosphatase Reaction Buffer (New England Biolabs, United States) and nuclease free water to make up the reaction to desired volume. The reaction was then incubated at 37 ºC for 1 hour, following which the enzyme was de-activated at 80 ºC for 2 minutes.

2.1.7.3 DNA ligations

DNA ligations were carried out using T4 Ligase (New England Biolabs, United States), with reaction ratios calculated using a constant concentration of vector DNA, with the following equation used to determine insert amount:

$$\text{Amount of insert DNA needed (ng)} = \frac{50\ ng\ Vector\ DNA\ x\ Insert\ size\ (bp)}{Vector\ size\ (bp)}$$

For efficient ligations, different ratios of vector DNA: insert DNA were used, these were 1:1, 1:2 and lastly 2:1 ratios, with ligation reactions carried out according to the manufacturer's

instructions. A reaction was carried out with 1 U enzyme and 1/10 volume of T4 ligation buffer at room temperature for 1 hour, followed by heat inactivation of the ligase at 80 °C for 2 minutes.

2.1.8 Bacterial transformation

2.1.8.1 Preparation of *E. coli* chemically competent cells for transformation

E. coli DH5 α or BL21 chemical competent cells were prepared using calcium chloride method. This method makes use of $CaCl_2$, which optimizes the ability of bacteria to incorporate plasmid DNA, by facilitating the binding of the negatively charged DNA to the charged lipopolysaccharides of the cell, thus expediting genetic transformation. Fresh LB medium was inoculated with a single *E. coli* colony and grown at 37 °C overnight. The following day, 100 ml of LB was inoculated with 1 ml of the preculture and incubated at 37 °C for 3-5 hours. Following this, the cells were chilled on ice for 20 minutes and collected by centrifugation at a speed of 4000 rpm for 10 minutes (4 °C). The cell pellet was resuspended in $CaCl_2$ (Appendix A, Table 2) and incubated on ice for 20 minutes again. Following this, the cells were harvested by centrifugation at 4000 rpm for 10 minutes and again, the cell pellet was resuspended in 5 ml of $CaCl_2$ and kept on ice until use. For transformation, 100 µl of competent cells was added to the DNA ligation and incubated on ice for 15 minutes. A no DNA control was included (negative control). Subsequently, the cells were heat shocked at 42 °C for 90 seconds to allow them to take up the plasmid and at the same time, depolarizing the cell membrane of the treated cells. The reduction of membrane potential decreases the cytoplasmic negative charge, allowing the movement of negatively charged DNA into the cell. The cells were then cooled on ice for two minutes, which aids in increasing the membrane potential of cells to their prior state. Subsequently, recovery with 800 µl of warm LB was carried out and following this, the cells were incubated at 37 °C for 1 hour. Cells were plated on LA containing appropriate antibiotic and incubated overnight to allow for selection of positive transformants.

2.1.9 Preparation and Transformation of *M. smegmatis* competent cells for electroporation

A pre-culture (OD_{600}>1) was inoculated into 50-100 ml of fresh 7H9 medium and grown at 37 °C to mid log phase (OD_{600} = 0.6-0.8). Cells were then harvested by centrifugation (4000 rpm, 10 minutes, 4°C) followed by three washes (to remove salts and cell debris) with gentle resuspension in cold 10% glycerol. Finally, cells were resuspended in 3 ml of 10% cold glycerol. For transformation, 300 µl of electro-competent cells were used to which DNA (1-3 µg) was added and aliquoted into cold 0.2 cm GenePulser cuvettes (Biorad). The parameters for the BioRad GenePulserX-Cell™ used were as follows: Voltage 2500 V, Resistance 1000 Ω, distance 2 mm and capacitance 25 µF. Following pulsing, the time constant was recorded, and the cells were rescued with 800 µl of LB an incubated at 37 °C for 3-16 hours. Following incubation, the transformation was plated on 7H10 containing the appropriate antibiotics and/or supplements and grown for 2-7 days at 37 °C.

2.2 Generation of *M. smegmatis* strains used in the study

2.2.1. Two-step allelic exchange homologous recombination for construction of knockout deletion mutants

Disruption of putative amidase genes, MSMEG_6406 (*ami3*), MSMEG_5315 (*ami4*) and MSMEG_0533 (*ami5*) was carried out using gene replacement by homologous recombination, with plasmid p2NIL (Table 1). As mentioned previously, *ami3* and *ami4* were deleted in an Honours project. The *ami5* deletion was made in this MSc and the process, which was similar to that adopted for *ami3* and *ami4*, is described hereafter. Briefly, upstream and downstream regions flanking the gene of interest were amplified taking into consideration the frame of the gene to eliminate polar effects (Figure 2.1). The primers used to create the knockout constructs were designed using the bioinformatics tool, Primer 3 with gene sequences obtained from Smegmalist (http://mycobrowser.epfl.ch/smegmalist.html). The resulting PCR fragments were purified and combined with p2NIL plasmid as outlined in Section 2.1.7.3 to generate a suicide vector carrying a truncated version of the allele. This was used to transform *E. coli* DH5 α competent cells (Section 2.2.1.5.1), followed by the selection of transformants on LA plates supplemented with Kan (50 µg/ml), after which a small-scale plasmid extraction was carried out on the possible positive clones (Section 2.1.2). Possible clones were subsequently screened with the appropriate restriction enzymes (Section 2.1.7.1) to determine if they carried the PCR

fragments. Subsequently, the *PacI* cassette of pGOAL 17, which carries the *sacB* gene (encodes for the counter-selectable marker levan sucrase) and *lacZ* gene (encodes β galactosidase) was introduced into the *PacI* site of the p2NIL plasmid carrying the truncated gene of interest. The resulting construct was used to transform wild-type *M. smegmatis* strain by electroporation to obtain single crossovers. The transformants were selected on 7H10 Kan (25 µg/ml) and 2 % X-gal plates and incubated for 3-5 days at 37 °C. Positive transformants were expected to yield a blue colour indicative of the presence of the *lacZ* gene (and hence the construct) on media supplemented with X- gal. The *lacZ* gene encodes the protein β-galactosidase, which cleaves X-gal yielding galactose and 5-bromo-4-clhoro-3-hydroxyindole, which is subsequently dimerized and oxidized into a blue product.

The single cross over (SCO) strain was grown overnight in 7H9 media supplemented with Kan (25 µg/ml), thereafter, this was used to inoculate fresh 7H9 broth grown overnight in the absence of antibiotic to facilitate the double crossover (DCO) event. For counter selection (induction of the loss of the *sacB*, *lacZ* and antibiotic markers together with the wild type gene), a serial dilution (10^{0}-10^{-8}) of the culture was plated on 7H10 agar plates, supplemented with 2 % sucrose and 2 % X-gal. The expression of *sacB*, in the presence of sucrose, results in the formation of levan (6-β-D-fructosyl), which disrupts normal growth and metabolism of the cell resulting in death. Thus, during the second crossover, the loss of the vector backbone and its markers, with concomitant retention of either the wildtype gene or mutant gene, results in the formation of white colonies (loss of *lacZ*). These colonies are also sensitive to antibiotics (loss of Kan^{r}) and are able to grow in the presence of sucrose (loss of *sacB*). Following counter selection, the resulting colonies were picked and screened using colony boil and PCR (Section 2.1.1.2 and 2.1.5) to determine whether they contained the wild-type or truncated version of the gene of interest. Further confirmation was carried out using Southern blot (Section 2.2.3.1) to ensure loss of the gene and qPCR (Section 2.4.3) with primers directed at the gene of interest.

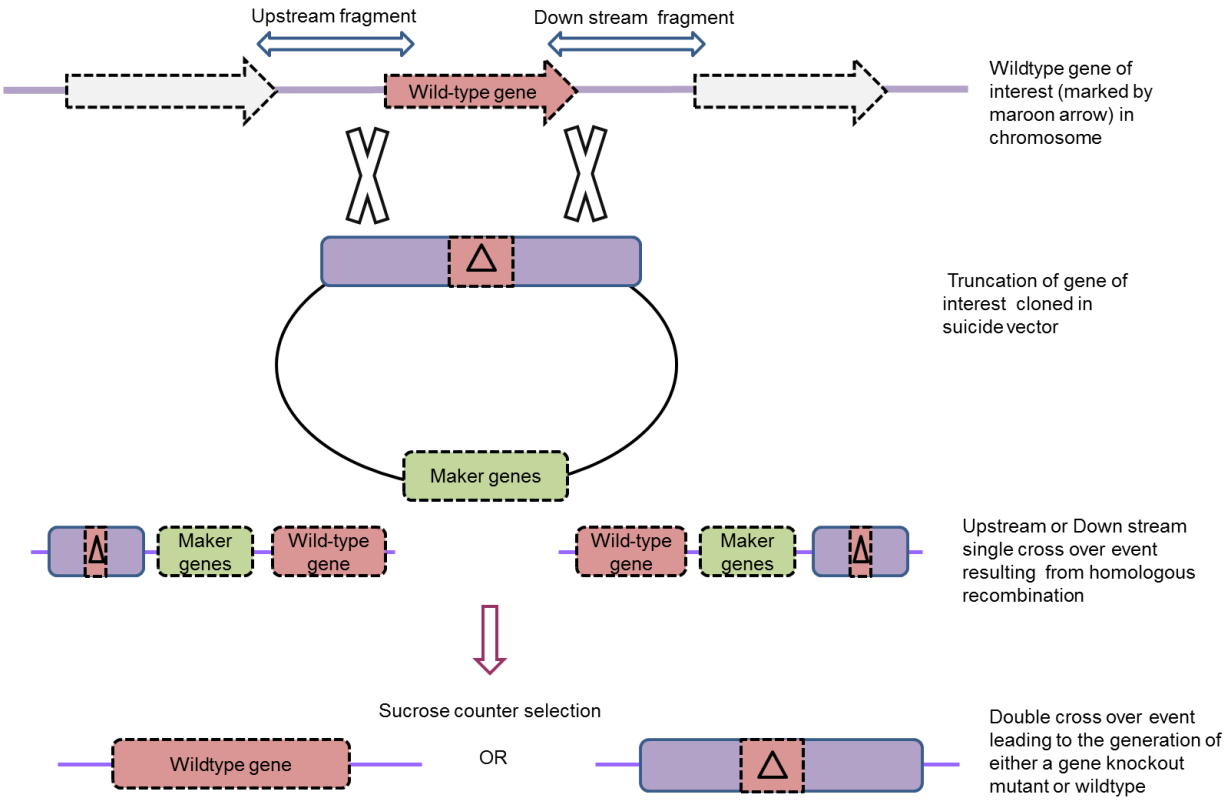

Figure 2.1: Diagrammatic representation of two-step allelic exchange homologous recombination. Shown is the process carried out for the construction of deletion mutants using PCR based gene truncation. Upstream and downstream regions of the gene of interest were inserted into a suicide vector with appropriate selection and counter selection markers. Two processes are allowed to take place, the first is the formation of a single crossover event and the second is a double crossover event to generate gene mutation. Figure drawn by student.

2.2.2 Generation of *M. smegmatis* complementation strains

To ensure that phenotypic differences obtained with the mutant strains were due to the loss of function of the deleted gene, a complementation strain wherein the gene was reintroduced into the mutant strain background was created. This was accomplished by amplifying the respective *M. smegmatis* amidase genes (*ami3*, *ami4* and *ami5*), which were cloned under the control of their native promoters (300 bp upstream region) into the integrating vector, pTweety for *ami4* and pMV306H for *ami3* and *ami5*. This allowed for the integration of the functional gene either into the $tRNA^{GLY}$ locus (pMV306H) or $tRNA^{LYS}$ locus (for pTweety), allowing native regulation

and expression by appropriate mechanisms in mycobacteria. Complementation vectors carrying the respective genes were electroporated into the appropriate *M. smegmatis* deletion strain and transformants were selected on 7H10 agar with the appropriate antibiotic after incubation at 37 °C for 3 days. Restoration of gene expression for each complement strain was confirmed by qRT PCR.

2.2.3 Genotypic verification of the parental and mutant strain

2.2.3.1 Southern blot analyses

Southern blotting is a technique that allows for the identification of a specific restriction fragment in a pool of many others. It involves the separation of digested DNA using agarose gel electrophoresis and its transfer and immobilization onto a nitrocellulose membrane. This is then followed by hybridization of chemiluminescently or radioactively labeled probes specific for a fragment of DNA. Detection of the hybridized fragments is done by autoradiography using X-ray film. Detailed steps are described below.

2.2.3.2 Probe synthesis and Electro blotting

The PCR DIG Probe Synthesis kit (Roche Applied Science, United States) was used to construct alkali-labile digoxigen (DIG)-dUTP probes as per manufacturer's instructions. Briefly, 50 µl reactions were set up separately for upstream and downstream probes, these contained 50 ng DNA, 2.5 µl 10 µM primers (forward and reverse), 0.3 µl Taq enzyme, 5 µl 1× PCR buffer and 10 µl 10× GC buffer. The labeling reaction was supplemented with 2.5 µl dNTPs and 2.5 µl DIG labeled dNTPs, whilst the control was supplemented with 5 µl dNTPs with no DIG. Reactions supplemented with DIG-labeled dNTPs were run on the same gel with a corresponding unlabeled PCR product to confirm the incorporation of the label. This is done as labeling leads to an increased molecular weight shift that can be visually detected on an agarose gel.

Prior to performing a Southern blot, it is essential to ensure minimal or no shearing of DNA during extraction so as to obtain specific restriction fragments. Purified genomic DNA from *M. smegmatis* (2 µg) was digested overnight with 1 U of the appropriate endonuclease at 37 °C and fragments separated on an agarose gel (run at 80 V for 2 hours). Following electrophoresis, the

gel was soaked in depurination solution (Appendix A, Table 2) for 15 minutes, a buffer that results in the decomposition of the sugar molecule. The depurination solution was discarded and followed by two washes with dH_2O with subsequent soaking in denaturation solution (Appendix A, Table 2) for 30 minutes with gentle shaking. The alkaline solution leads to the denaturation of double stranded DNA by breaking hydrogen bonds, hence aiding in transfer and binding to the membrane and for creating single stranded DNA for hybridization. This was followed by neutralization of the gel by soaking in 1× TBE (Appendix A, Table 2) for 5 minutes, as DNA will not bind to the nitrocellulose membrane unless the pH is greater than 9. Following the last wash, the gel was overlaid with Hybond™-N nitrocellulose membrane (Amersham), sandwiched between 2 Whatman filter papers and 2 porous sponges and finally enclosed in a plastic cassette. The sandwiched gel and membrane were transferred into an Omni PAGE electroblotting unit (Cleaver Scientific Ltd CS-300V) containing 1× TBE. The DNA was then transferred onto the nitrocellulose membrane at 600 A and 130 V for 2 hours at 4°C. Thereafter, the DNA was cross-linked to the membrane by UV irradiation (induces covalent attachment to the membrane) at 2500 mJ/cm^3 for 2 minutes in a UV Stratalinker 1800 (Stratagene).

2.2.3.3 DNA hybridization and detection

Following crosslinking, the membrane was prehybridized in 10 ml of DIG Easy Hybridization solution (Roche Applied Science, United States) at 60 °C for 30 minutes (this blocks the unused DNA binding sites on the membrane surface ensuring that the specific signal is easily detected). The hybridization temperature was calculated as per manufacturer's instructions using the calculation the formula below.

$$Tm = 49.82 + GC\ content - {}^{600}/_{L}$$

Table 4: Description of formula

Tm	Melting/ Hybridization Temperature
49.82 and 600	Constants
CG content	Relative to entire sequence
L	Length of gene being amplified

The labeled probe was denatured at 65°C for 10 minutes, added onto the membrane and hybridized overnight at 60 °C. The following day, the probe mixture was poured out and stored at -20 °C for future use. Afterwards, the membrane was washed several times to remove non-hybridzed probe. The first wash was done twice in solution I (Appendix A, Table 2) at room temperature for 5 minutes and the second wash with solution II (Appendix A, Table 2) at 68 °C for 15 minutes. The membrane was rinsed in wash buffer (Appendix A, Table 2) for 5 minutes at room temperature and incubated in 1× blocking buffer (Appendix A, Table 2) for 30 minutes. For immunological detection of the DIG-labelled DNA probes, the membrane was incubated in 20 ml of 1× antibody buffer (Appendix A, Table 2) for 30 minutes and followed by two washes in wash buffer (Appendix A, Table 2) for 15 minutes. After this, the membrane was placed in a hybridization bag and 1 ml CSPD substrate gently spread onto the DNA side of the membrane, followed by incubation at 37°C for 10 minutes. The alkaline phosphatase attached to the antibody dephosphorylates the CSPD substrate, which leads to chemiluminescence at a wavelength of 477 nm that can be detected on the X- ray film. The membrane was exposed to X-ray film (CL-XposureTM Film Thermo Scientific) for 30 minutes - 1 hour and developed manually in the dark. For developing, the X-ray film was placed in developer solution (Thermo Scientific Fischer) for 30 seconds, rinsed in sterile dH_20 for 30 seconds, placed in fixative solution (Thermo Scientific Fischer) for 30 seconds, rinsed again in sterile dH_20 for 30 seconds and hung to dry.

2.3 Generation of amidase overexpressing strains

To overexpress the mycobacterial amidase genes, the *E. coli-Mycobacterium* shuttle vector pSE100 was used which continuously drives gene expression in an unregulated, constitutive manner. The amidase genes were amplified from the *M. smegmatis* genome by PCR using gene specific primers, with the native promoter included. The PCR templates were cloned into respective sites of pSE100, followed by electroporation into the parental strain. The transformants were selected on 7H10 media supplemented with Hyg (50 µg/ml) and incubated at 37 °C. A plasmid only carrying strain was also created as a control.

2. 4 Analysis of gene expression

2.4.1 RNA extraction

RNA extraction was carried out using the Nucleospin RNA II Kit (Macherey whiteGermany) as per manufacturer's instructions. *M. smegmatis* strains were grown in 7H9 broth at 37 °C overnight to an OD_{600nm} of 0.3 and the cells collected at 4000 rpm for 10 minutes at 4 °C. This was followed by resuspension of the pellet in 500 µl of TE buffer (Appendix A, Table 2), 350 µl RA1 lysis buffer (Macherey Nagel, Germany) and 3.5 µl β-mercaptoethanol, which is responsible for denaturing RNases through the reduction of disulfide bonds, thus altering enzyme conformation needed for function. Subsequently, cell disruption was carried out by aliquoting the cell suspension into MagNA lyser Green Beads (Roche Applied Science, United States) lysing matrix tubes, followed by 3× 60 seconds of bead beating using the MagNA Lyser (Roche Applied Science, United States). This was carried out at a speed of 6000 rpm, with cooling on ice for 2 minutes between each lysis step. Lysates were then transferred to nucleospin filter columns and centrifuged at 12 210 rpm. To adjust RNA binding conditions, 350 µl of 70% ethanol was mixed with the flow through, which was transferred into a nucleospin RNA column and centrifuged for 60 seconds at 12 210 rpm. The flow through was discarded and the column was desalted with 350 µl of Membrane Desalting Buffer (MDB) and centrifuged at 12 210 rpm to dry the membrane. The column was then treated with 100 µl DNAse I, followed by incubation at room temperature to digest any DNA in present. Subsequently, 200 µl of RAW2 buffer was used to wash the column, followed by centrifugation at 11 000 ×g for 1 minute. This was then followed by two washes with 600 µl buffer RA3 and then 250 µl of the same buffer with centrifugations carried out as mentioned before. The column was then placed into a clean Eppendorf tube and the RNA was eluted with RNase free water by centrifugation at 12 210 rpm for 1 minute.

2.4.2 Reverse Transcriptase PCR (RT-PCR)/ first strand cDNA synthesis

Following RNA extraction with the kit, residual genomic DNA was removed with a second DNase I treatment. Briefly, an aliquot of the sample was treated with Turbo DNase I (Life Technologies) for 30 minutes at 37 °C. This was then followed by the inactivation of DNase I by the addition of 2 µl of inactivator (Macherey Nagel, Germany) and incubating at room temperature for 2 minutes, followed by centrifugation for 5 minutes at 12 000 rpm. The upper

phase was aliquoted into a new tube and the RNA was quantified using the Nanodrop (Nanodrop Technologies). For cDNA synthesis, a 10 µl reaction containing 1 µg RNA, 10 mM dNTP (1 µl) mix and 50 ng/µl random hexamers (1 µl) was incubated at 65 °C for 5 minutes, followed by incubation on ice for 1 minute. Subsequently, RT reactions were carried out using SuperScript™ III reverse transcriptase (Invitrogen) as per manufacturer's instructions. Briefly, a 20 µl RT+ reaction was set up using 10 µl of the RNA/primer mix, 4 µl 25 mM $MgCl_2$, 2 µl of 10 × RT Buffer, 2 µl 0.1 M DTT, 1 µl nuclease free water and 0.5 µl SuperScript III. cDNA synthesis was carried out using the following parameters in a Biorad thermocycler: 25 °C for 10 minutes 50 °C for 50 minutes and 85 °C for 5 minutes and thereafter chilled on ice. The resulting cDNA was used for quantitative PCR (qPCR).

2.4.3 Quantitative real time PCR

qPCR was performed using Sso Fast Evagreen Supermix (Biorad) as per manufacturer's instructions. Briefly, 20 µl reactions were set up, each containing 10 µl Evagreen Supermix, 0.125 µl forward primer (10 µM), 0.125 µl reverse primer (10 µM), 2 µl cDNA/ DNA template and nuclease free water. Primers used for gene expression analysis are listed in Table B4. All reactions were incubated in the CFX96 Real-Time PCR detection system (Biorad), using the following parameters: denaturation 95 °C for 3 min, annealing was at 60°C for 30 min, and the extension was set at 72 °C for 30 min. Amplification cycles were 40 cycles for both genes. Melt curve analysis was conducted from 65 °C with a gradual increase in 0.5 °C increments every 0.05 sec to 95 °C, with SYBR Green quantification conducted continuously throughout this stage. The raw data was analyzed using the Biorad CFX Manager 3.0 Software (Biorad) and compared against the standard curve of 10^7 to 10^0 genomes. The housekeeping gene, *sigA* was used as a standard for normalization as it is expressed at a consistent level throughout all growth phases.

2.5 Sequencing of gene fragments

All fragments generated by PCR were sequenced in their respective vectors by the central DNA Sequencing Facility of Stellenbosch University, to confirm the absence of mutations. This was done by using the Big Dye terminator v3.1 Cycle Sequencing kit and Bioline Half Dye Mix.

Finch TV version 1.4 was used to analyse the sequencing quality by visually checking the chromatograms. The Clone Manager Sequence analysis tool was used to further analyse the sequences.

2.6 Phenotypic analysis of *M. smegmatis* knockout strains

2.6.1 Growth kinetic analysis of *M. smegmatis* knockout strains

Growth analysis was carried out in either 7H9 or Sauton's media supplemented with the appropriate antibiotics when necessary using a shaking incubator set at 100 rpm at 37 °C. Cultures from late logarithmic phase were inoculated in 7H9 or Sauton's medium to a final OD_{600nm}=0.02. The growth rate was determined by recording optical density (OD) at three-hour intervals. Three replicates were used per sample and each experiment was performed at least three times. The number of inoculated bacteria was confirmed by CFU counts, a 10-fold dilution series was performed for each phase of growth. Dilutions were plated on 7H10 media and incubated at 37 °C for 2 days, following which, the number of colonies formed were enumerated. As before, three replicates were conducted.

2.6.2 Biofilm formation

Analysis of *M. smegmatis* biofilm formation was carried out by growing cells in 7H9 media to stationary phase. The cells were then harvested at 4000 rpm and washed three times in Sauton's media, following which, the OD_{600nm} was adjusted to 1.0 in Sauton's media. Afterwards, a 10-fold serial dilution ranging from 10^0 to 10^6 was prepared and 20 µl of each dilution was added into 2 ml of Sauton's media in 24 well flat bottom Nunc plates. Plates were incubated at 37 °C for 7-14 days without disturbance. Thereafter, images were captured using the Zeiss Stereo Microscope (1.25× magnification).

2.6.3 Crystal violet biomass estimation assay

To each biofilm well, 0.1% crystal violet (Sigma-Aldrich) was added and the stain was incubated at room temperature for 10 minutes. Planktonic bacteria were pipetted out and the plates were allowed to dry for 15 minutes. Subsequently, 1 ml of 99% ethanol was added to each well and

incubated at room temperature for 10 minutes. Following this, the contents in each well was mixed. A 1:100 dilution was prepared using ethanol and OD_{600nm} measurements were taken.

2.6.4 Minimum inhibitory concentration determination

M. smegmatis from logarithmic growth phase was inoculated in 10 ml of 7H9 supplemented with antibiotic, where necessary, and grown to an OD_{600nm}=0.3-0.4 by shaking at 37 °C. These cultures were diluted 1:100 and used for inoculation into microtitre plates containing a 2-fold antibiotic dilution series. Antimicrobial starting concentrations were as follows: INH (250 µg/ml), imipenem (100 µg/ml), EMB (100 µg/ml), teicoplanin (100 µg/ml). The broth microdilution method was used in clear 96 well round bottom plates (Domenech *et al*., 2005). The plates were then incubated at 37 °C for 7 days and growth was assessed in the presence of antimicrobial agents with MIC measured as the minimum drug concentration needed to inhibit growth. A schematic representation is given in Figure 2.2.

2.6.5 The ethidium bromide assay

M. smegmatis strains were grown in 15 ml of 7H9/glucose salt medium at 37 °C to an OD_{600} of 0.8. Cultures were centrifuged at 4500 rpm for 10 minutes, the supernatant discarded and the pelleted cells washed in PBS (pH 7.4) three times. The OD_{600} was then adjusted to 0.4 with PBS and glucose (0.4%). Ethidium bromide (10 µg/ml) was added to 7H9/glucose medium in 96 well plates and diluted two-fold. Following this, 50 µl of bacterial cell culture (OD_{600} 0.4) was added and the plate incubated at 37 °C for 1 hour with shaking in a plate reader. Fluorescence was measured in the plate reader using 530 nm band pass and 585 nm high pass filters as the excitation and detection wavelengths respectively. Fluorescence was recorded every 60 seconds for 60 minutes at 37 °C. A schematic representation is given in Figure 2.2.

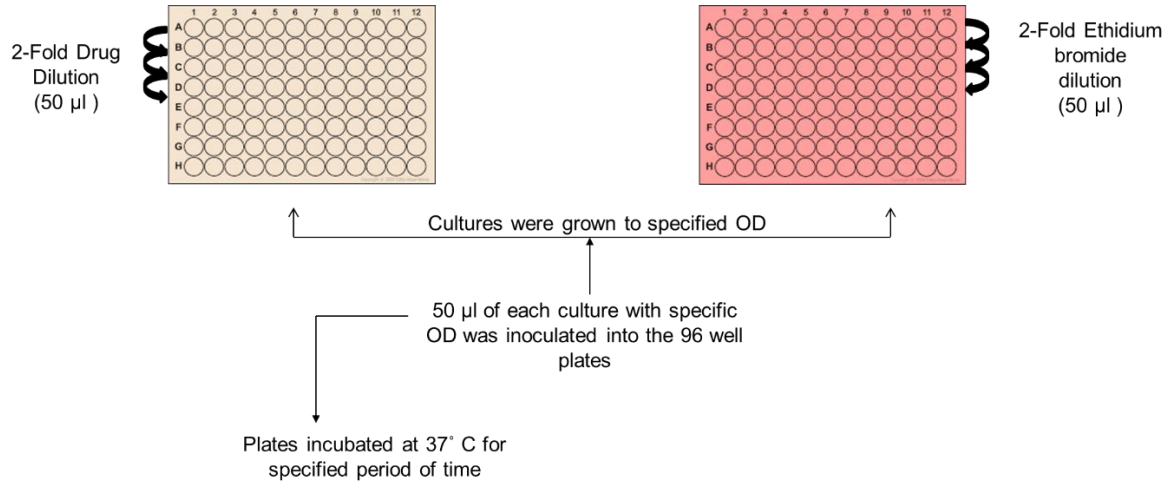

Figure 2.2: Flow chart depicting the process involved in the analysis of cell wall stability using antibiotic (MIC) susceptibility and ethidium bromide accumulation in the cytosplasmic space.

2.7 Identification of amidase interacting partners using a bacterial 2-hybrid system (M-PFC assay)

To identify possible amidase interacting proteins, all three amidase genes and possible interacting partners derived computationally from STRING were amplified from the *M. smegmatis* genome by PCR using gene specific primers. The PCR fragments were cloned into the respective plasmids (pUAB300 and pUAB400) and co-electroporated into *M. smegmatis*. The resulting recombinant *M. smegmatis* strains are listed in Table 2. The transformants were selected on 7H10 media supplemented with Hyg (50 µg/ml) and Kan (25 µg/ml) and were grown at 37 °C for 2 days. Positive clones were sub cultured in 7H9 media supplemented with the appropriate antibiotics and cultures were plated on 7H10 supplemented with antibiotics and various Trimethoprim (TRIM) concentrations to investigate the strength of the interactions. Growth on TRIM plates indicated interaction between proteins. Controls for MFC-assays included known interacting partners as the positive control (RpfB and RipA) (Hett, Chao and Rubin, 2010) and empty vectors were co-electroporated in the *M. smegmatis* parental strain background as the negative controls.

2.7.1 Plasmid construction for the M-PFC assay

The plasmids pUAB300 and pUAB400 contain DHFR (fragments 1 and 2 [F1, 2]) and DHFR (fragment 3[F3]) respectively. These are fused to putative interacting partners and if the proteins interact, fragments 1-3 are reconstituted to create a functional DHFR, which confers resistance to TRIM. Putative interacting partners are identified by the ability to grow on TRIM containing plates, Figure 2.3. In-frame fusions of MSMEG_6402 (*pap2*), MSMEG_6403 (*glft*), MSMEG_6405 (*erp*), MSMEG_6900 (*ponA1*) and MSMEG_0250 (*mmpl*) with pUAB400 were generated. To facilitate cloning, restriction sites *PvuI* and *BamHI* were added on the primer sequences. The PCR fragments and pUAB400 plasmids were digested with these enzymes to facilitate insertion of the PCR product to the plasmid. These constructs contain the respective protein domains fused to the DHFR[F3] domains.

2.7.2 Mycobacterial protein fragment complementation assay

Recombinant *M. smegmatis* expressing *ami3-dhfr* [1, 2]/ *pap2-dhfr* [3], *ami3-dhfr* [1, 2]/ *glft-dhfr* [3], *ami3-dhfr* [1, 2]/ *erp-dhfr* [3], *ami3-dhfr* [1, 2]/ *mmpl-dhfr* [3], and *ami3-dhfr* [1, 2]/ *ponA1-dhfr* [3] were selected on 7H10 agar plates containing Kan (25) and Hyg (50) (Figure 2.3). The parenthesis in this case illustrate the fragment of the DHFRF that the protein of interest was fused to. This was followed by growth of the recombinant strains on 7H10 agar with the appropriate antibiotics and varying concentrations of TRIM (Figure 2.3).

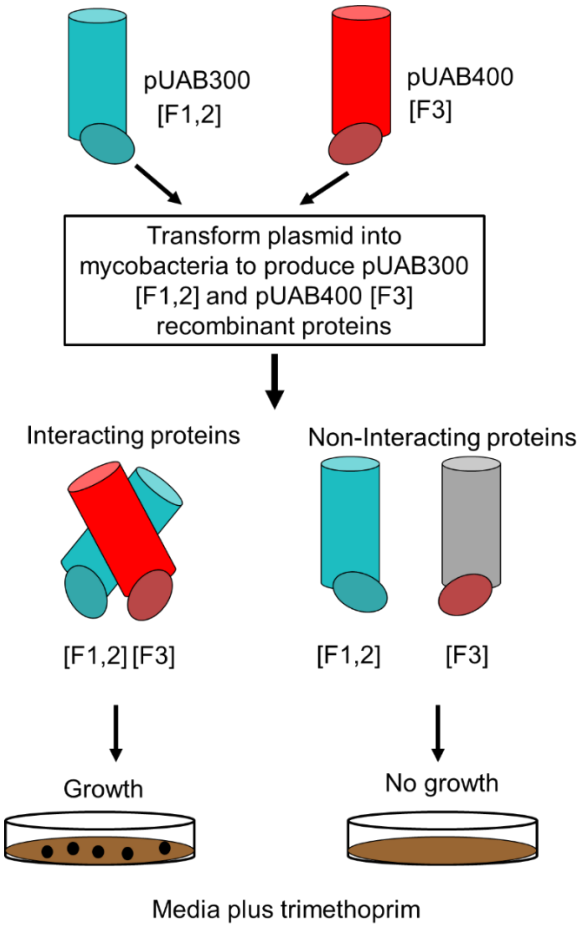

Figure 2.3: Schematic representation of the M-PFC assay for protein-protein interaction screening. *M. smegmatis ami3* PCR fragments cloned into pUAB300 and the possible interaction partner cloned into pUAB400 are co-electroporated into *M. smegmatis* mc^2155 and plated on 7H10 media supplemented with appropriate antibiotics and trimethoprim (TRIM). Interaction is indicated by growth in the presence of TRIM and no interaction results failure to grow in the presence of TRIM.

2.8 Microscopy

2.8.1 Copper Click reaction with a D-alanine analogue

Cells were grown to exponential phase (OD_{600nm} 0.6) overnight, following which, they were harvested at 13000 rpm and the pellet washed in PBS three times. The pellet was later in 7H9 Middlebrook media resuspended with a click chemistry D-alanine analog at a final concentration of 1 mM. The cells were allowed to grow for 3 hours at 37°C. Following incubation, the cells were washed three times with PBSTB (Appendix A, Table 3), followed by the addition of 1 mM $CuSO_4$ (Appendix A, Table 3), 128 µM TBTA (Appendix A, Table 3), freshly prepared 1.2 mM

sodium ascorbate (Appendix A, Table 3) and 20 µM azido probe (Appendix A, Table 3). The reaction was allowed to proceed for 60 minutes at room temperature with shaking, following which the cells were once again washed three times in PBS, spotted onto 2 % agarose pad on a glass slide and imaged with the Ziess Observer Z1 inverted microscope, following which the images were analyzed with the ZEN lite software (Zeiss). A schematic representation of this PG labeling process is shown in Figure 2.4.

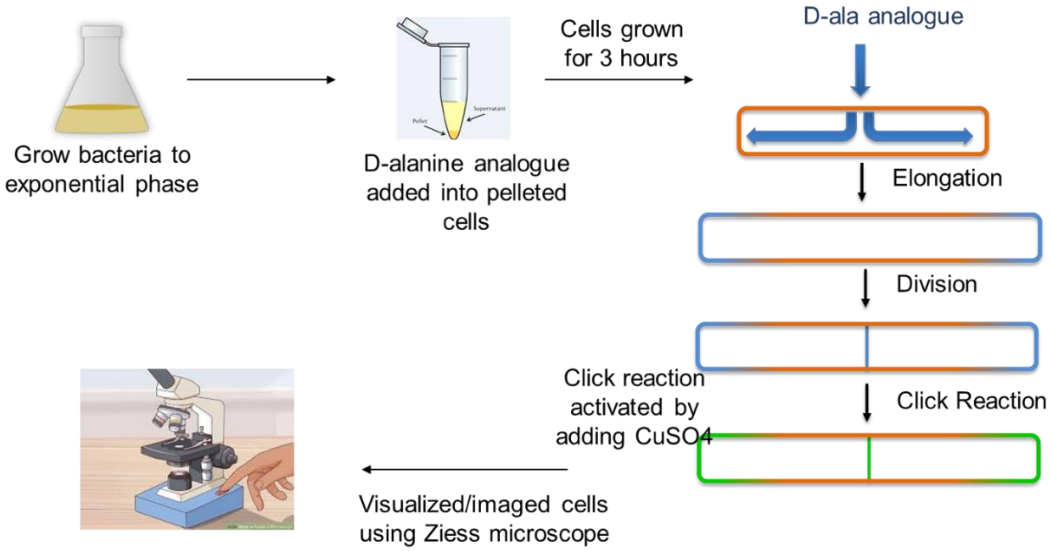

Figure: 2.4: Flow diagram depicting the process involved in spatially identifying areas of new PG growth. For this, click chemistry D-alanine analogue was used as it will get inserted into new PG. After insertion a copper-dependent click reaction is carried out, which results in fluorescence.

2.8.2 DMN-Trehalose staining

The DMN-Trehalose stain was used for the analysis of in vivo labeling of mycolic acids in the mycobacterial cell wall. The stain makes use of the mycobacterial cell wall component, trehalose which is attached to a solvatochomic dye. When incorporated into the cell wall, the dye produces green fluorescence (Figure 2.5). The analysis of mycobacterial growth was therefore performed by growing cell cultures at 37°C with shaking to an OD_{600} of 0.6. The cells were harvested by centrifugation at 12470 × g for five minutes, the cells were washed with PBS (three times) and thereafter, resuspended in 100M DMN-Trehalose in 1 ml Middlebrook 7H9. This was followed by incubation at 37°C for one hour with shaking (100 rpm). Cells were pelleted by centrifugation at 12470 × g for 5 minutes and resuspended in 50 µl water. Cells (10 µl) were then spotted onto

glass slides and visualized with the Zeiss Observer Z1 inverted fluorescence microscope, with the images analysed using ZEN lite software (Zeiss).

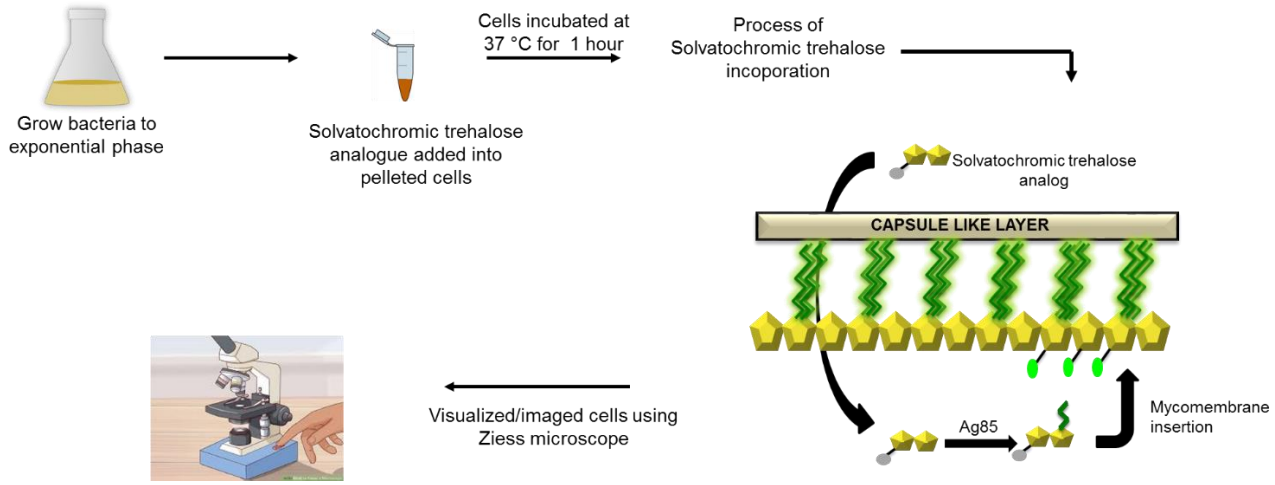

Figure 2.5: Schematic representation of the mycobacterial cell wall DMN-Trehalose staining process and the incorporation of the trehalose analog. DMN Tre labelling is a no wash visualization of live mycobacterial cells. Cells cultured to exponential phase (OD_{600}), harvested, resuspended in 7H9 with solvatochromic trehalose and incubated for 1 hour at 37 ºC. Prior to incorporation into the mycobacterial membrane, DMN-Tre is metabolically converted into trehalose monomycolate via the Ag85 complex. Upon incorporation into the mycomembrane it undergoes an increase in fluorescence as the fluorescence is triggered by hydrophobicity of this layer, enabling the detection of mycobacterial cells with the aid of a microscope.

2.8.3 Scanning Electron Microscopy

To view the cell surface of the various *M. smegmatis* strains created, cells were grown in 50 ml 7H9 media to an OD_{600nm} ~ 0.5. This was followed by harvesting of the cells by centrifugation (4500 rpm; 10 min) and a single wash in 0.01 M PBS (pH7.4). The cells were then re-suspended and fixed in 2.5% gluteraldehyde (SIGMA) in 0.01 M PBS overnight at room temperature. Thereafter, cells were pelleted and rinsed in PBS three times followed by re-suspension in 100 µl of 2% osmium tetraoxide for 1 hr at room temperature. Cells were then washed in PBS three times and dehydrated by washing in increasing concentrations of ethanol; 30 %, 70 %, 90 %, and twice in 100 %. Cells were spotted onto a filter, coated twice with carbon and viewed using a FEI Nova NenoSEM 230 (University of Cape Town).

2.8.4 Time-lapse microscopy

Mycobacterial strains generated in this study were grown in microfluidic devices with time-lapse microscopic analysis carried out as outlined before (Dhar and Manina, 2015). Briefly, the different bacterial cultures were grown to exponential phase in ink-well bottles at 37°C. The presence of clumps was removed by filtering the cells through a 5 µm filter. The bacteria were seeded onto microfluidic devices and imaged using a Delta vision personal DV imaging system (GE HealthCare Life Sciences) utilizing a 100 × objective (Olympus Plan Semi Apochromat, 1.3 NA). To acquire the images, 10 to 15 minutes intervals were chosen using a CoolSnap HQ2 camera. Middlebrook 7H9 medium was circulated through the microfluidic device at a flow rate of 25 µl/min. The analysis was carried out by a collaborator, Dr. N Dhar at EPFL in Switzerland. The student analyzed all the resulting videos in extensive detail. The resulting images were processed using ImageJ v 1.47 (Rasband, W.S., ImageJ, U.S. National Institute of Health, Bethesda, Maryland, USA, http://imagej.nih.gov/ij/,1997-2015).

2.9 A description of the bioinformatics analyses tools used in this investigation

2.9.1 The BioCyc Pathway/ Genome database collection (http://biocyc.org): This is a pool of databases and pathways that facilitate the analyses of different metabolic pathways, genomes and possible protein functions. BioCyc was used to identify the *E. coli* amidase protein sequences and investigate homologs in closely related species.

2.9.2 Protein family database (pFAM) (http://pfam.xfam.org): The pFAM database encompasses protein family domains, sequence alignments and provides protein annotations. This database was used to identify the amidase_2 and amidase_3 domain in the amidase proteins, which are the focus of this investigation.

2.9.3 KEGG: Kyoto Encyclopaedia of Genes and Genomes (http://www.genome.jp/kegg/): This database encompasses various databases aiding in understanding gene function, biological systems and pathways. This tool was used to identify amidase homologs of both the amidase_2 and amidase_3 domain families in different species.

2.9.4 Uniprot (http://www.uniprot.org): This is an online bioinformatics tool that makes available information from different tools, providing protein sequences, previous work undertaken on the protein of interest and the appropriate references. Uniprot was used to obtain protein sequences of the amidase domain containing proteins whose function and role in cell wall biogenesis has been extensively investigated.

2.9.5 National Centre for Biotechnology Information (NCBI) Basic Local Alignment Search (BLAST) Tool (http://www.ncbi.nlm.nih.gov/): This bioinformatics tool is an algorithm used for identifying DNA/protein sequences curated from multiple databases, identifying sequences homologous to the query by comparing the query to all sequences in the database. NCBI/BLAST was used to identify and compare query sequences of interest with a library of sequences sharing homology and to understand protein function through text mining.

2.9.6 SMEGMALIST (http://mycobrowser.epfl.ch/smegmalist.html): This is a curated database of *M. smegmatis* genome. This database makes available the gene sequences and their annotations, also allows for sequence alignments and identification of query proteins. This database was used to search for the genes of interest in *M. smegmatis* and analyze the operon that they are found in.

2.9.7 TUBERCULIST (http://tuberculist.epfl.ch/): This is a repository of *M. tuberculosis* genome sequences and allows for the analysis of gene sequences and their operons. This tool was used to search for *M. tuberculosis* genes of interest and aid in the analysis of their neighbouring genes.

2.9.8 CLUSTAL Omega (http://www.ebi.ac.uk/Tools/msa/clustalo/): This is a multiple sequence alignment tool that utilizes guide trees, which aid in constructing the order of the alignment. In addition to this, the program uses Hidden Markov Models which aid in dealing with gaps within protein families. This program was used to align the family of proteins identified with the tools outlined above to assess sequence homology and conservation of amino acids shown to be critical for protein function.

2.9.9 Interactive Tree of life (ITOL) (http://itol.embl.de/): ITOL is an algorithm tool used for visualizing, annotating and constructing phylogenetic trees. This program was used to visualize/ investigate the relationships between the amidase proteins from different species, previously aligned using Clustal Omega. This tool gives information on functional relationships between the protein under investigation and those previously studied.

2.9.10 Search Tool for the Retrieval of Interacting Genes/Proteins (STRING) (http://string-db.org/): This is a database that predicts protein associations by importing the knowledge from databases of physical and curated knowledge, text mining by searching for statistically relevant gene co-occurrences in different species and analyzing proximity of gene within a genome. Also included is co-expression of proteins and possible protein fusion events which may be functionally linked. This tool was used to determine possible proteins that the query proteins might associate with and broaden the understanding of the functionality of the selected proteins by getting a glimpse in the associated pathways.

2.9.11SignalP4.1 Server (http://www.cbs.dtu.dk/services/SignalP): This is a bioinformatics tool useful for the identification of signal peptides presence within a protein sequence, this tool also gives the location of the signal peptide and the cleavage site from different organisms. It is based on information obtained from various neutral networks. SignalP was used to predict the presence/absence of signal peptides in the proteins under investigation and determine whether the proteins are exported or remain in the cytoplasmic compartment of the cell.

2.9.12 Iterative Threading Assembly Refinement (I-TASSER) (http://zhanglab.ccmb.med.umich.ede/I-TASEER): I-TASSER is a protein structure prediction tool basing its predictions on previously crystallized or identified protein structures. This tool makes use of a collection of databases to aid in the modeling of the query 3D protein structure, the residues involved in protein function or binding of certain metals that aid in function. This tool was used to predict 3D structure of mycobacterial amidase_2 domain family of proteins and compare them with those whose structures have been solved.

2.9.13 PyMOL (http://www.pymol.org): Is a computer program which runs with the help of the python program. This tool is useful for monitoring and visualizing molecular structure of the protein. The database was used to visualize the protein structures predicted using I-TASSER.

3. Results

Schematic representation of this MSc study

An outline of the work undertaken in this MSc is given below

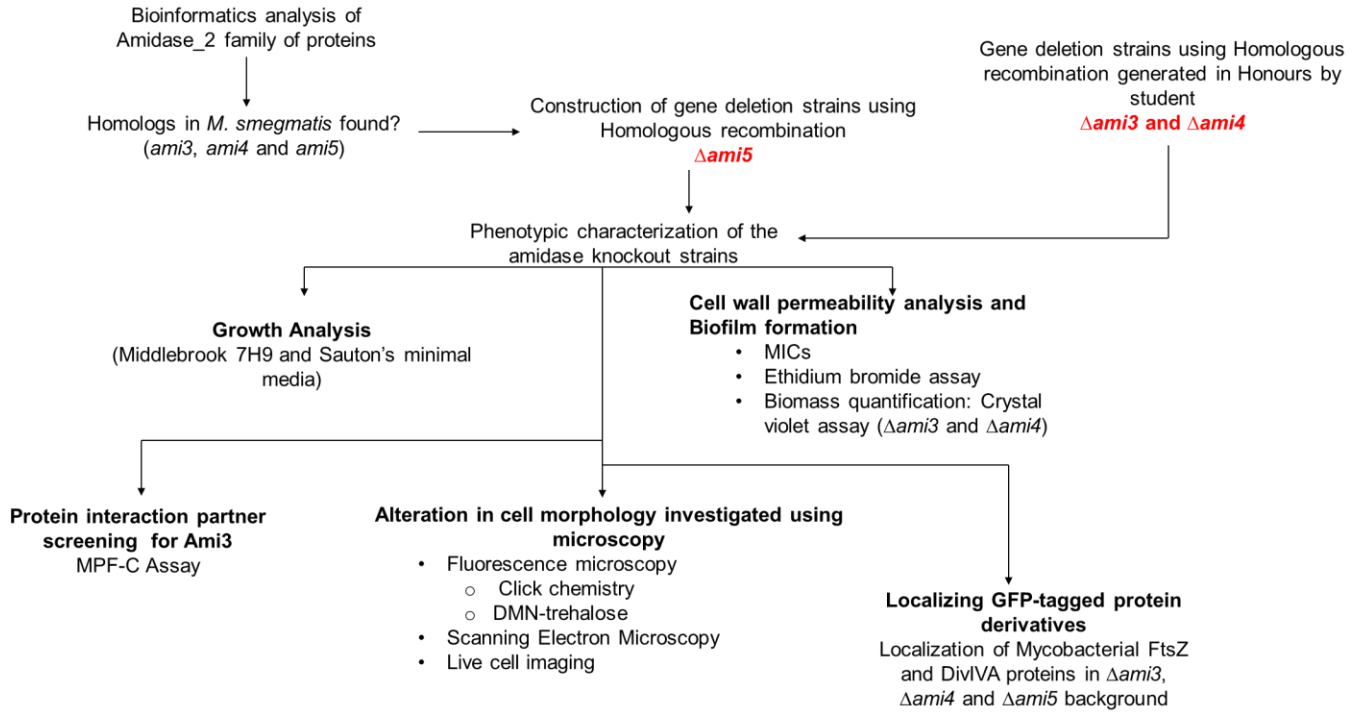

Flow Diagram of the study of Amidase_2 family of proteins in *M. smegmatis*.

3.1.1 Identification of *M. smegmatis* amidase_2 domain containing proteins

The amidase_2 domain proteins have been well characterized both structurally and functionally in *E. coli* (Kerff *et al*., 2010), yet very limited information is available on these proteins in mycobacterial species. However, with the vast availability of computational tools (Section 2.9), we were able to identify and investigate the function of this family of proteins in *M. smegmatis*, a model organism used for *Mtb* research. The NCBI/BLAST protein database was used to search for mycobacterial amidase_2 family protein homologs using *E. coli* AmiD and AmpD sequences as a reference. However, owing to the high divergence of the mycobacterial amidase terminal regions, no matches were obtained. Consequently, the amidase_2 domain region only was used to identify possible homologs, shown in Figure 3.1, from the PFAM, BLAST and KEGG

databases. Using this approach three amidase_2 domain containing proteins were identified in the *M. smegmatis* genome namely MSMEG_6406 and MSMEG_5315, both with homologs in *Mtb*, annotated as Rv3811 and Rv3594 respectively. The third, MSMEG_0533 had no identifiable homolog in *Mtb* but the close sequence identity to MSMEG_5315 is suggestive of a duplication event. Furthermore, MSMEG_6406 carries a signal peptide (Figure 3.3, Supplementary Figure 2), which indicates possible translocation to the periplasm and the lack of this in the two other amidases suggests that they are cytoplasmic proteins. A multiple sequence alignment of the amidase_2 type sequences from different species was carried out to assess the conservation of residues essential for amidase function (Figure 3.1). The alignments in Figure 3.1 indicated that the histidines (H^{35} and H^{151}), and aspartic acid (D^{161}) or cysteine (C^{161}) residues responsible for the coordination of Zn^{2+} are highly conserved across the different organisms and in mycobacteria. *E. coli* numbering is used for amino acids. The cysteine residue which has replaced aspartic acid in mycobacteria has been shown to be essential for the activity of several amidases as the thiol group can function as a nucleophile (Rigden, Jedrzejas and Galperin, 2003). Additional amino acids known to be important in amidase_2 class function are also highly conserved, particularly in MSMEG_5315 (*Mtb* homolog Rv3594). These include threonine (T^{37}), located in the carbohydrate binding site, tryptophan (W^{83}) which coordinates the stem peptide, asparagine (N^{100}) involved in tertiary structure stabilization, glutamine (Q^{4}) which coordinates with a proton acceptor in catalysis, lysine (K^{159}) involved in the stabilization of the tetrahedral state during catalysis and lastly, proline (P^{162}) which positions the aspartic acid (D^{161}) binding the Zn^{2+} in the active site (Figure 3.1 and Supplementary Figure 1 showing the rest of the alignment).

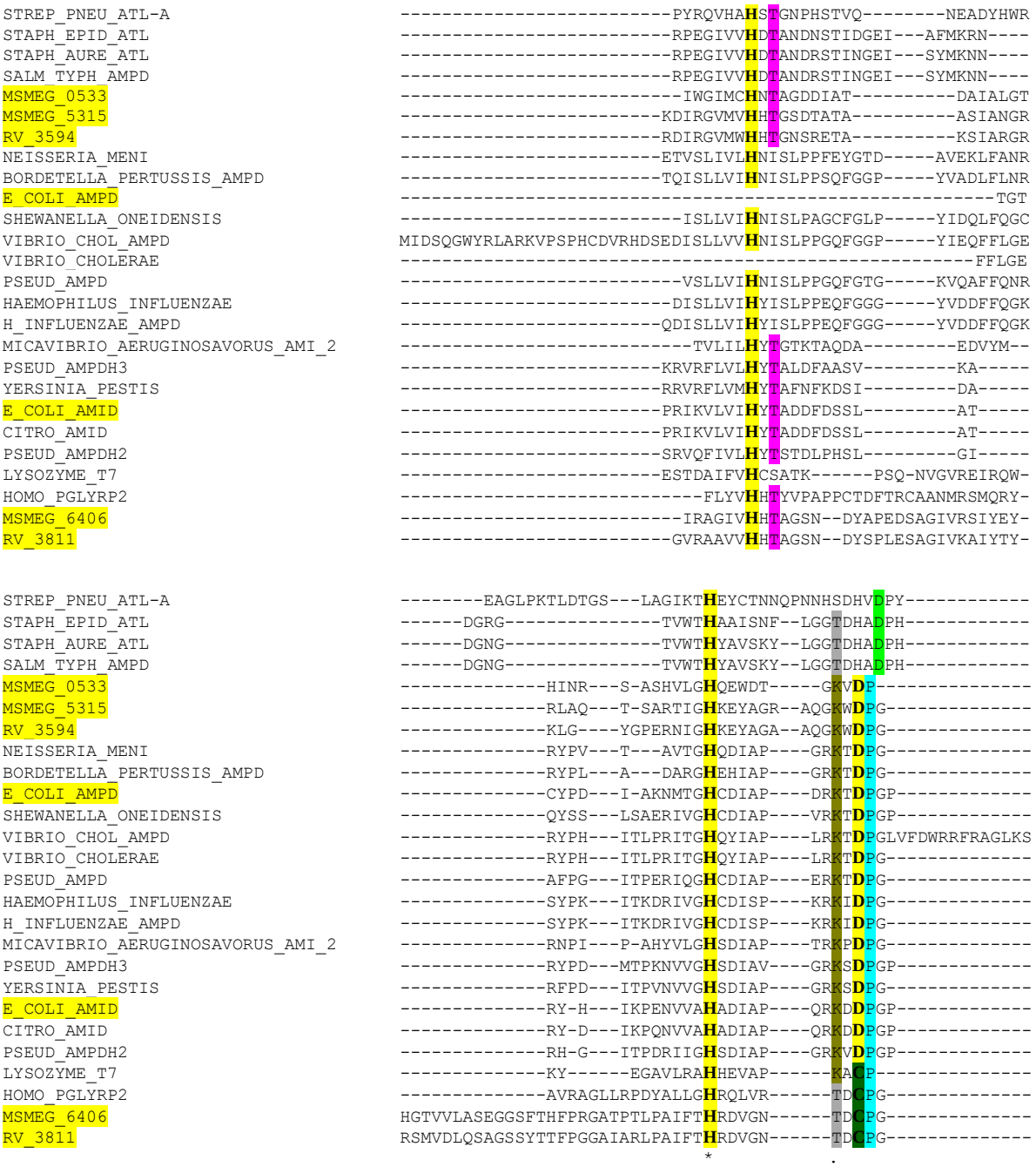

Figure 3.1 Multiple sequence alignment of Amidase_2 domain family of proteins using Clustal Omega analysis. Shown are *E. coli* AmiD homologous protein sequences from different species with the conservation of the amidase catalytic triad highlighted (HXH). The residues responsible for forming a tetrahedral coordination with the Zn^{2+} include histidine (H) and the highly conserved aspartate (D) are highlighted in yellow. Divergence from the traditional HDH to HCH was observed for some of the amidases. Residues involved in the catalysis of PG cleavage are also highlighted. Species highlighted in yellow are under investigation in this study. C - cysteine (Dark green) substituted-aspartic acid in Ami3, P – proline (Cyan), K- lysine (Brown) and T- threonine (Grey) are residues aiding in the function of the amidase protein.

Overall, the bioinformatics analyses revealed that these mycobacterial proteins are candidate *N*-acetylmuramyl-L-alanine amidases and based on the divergence from other characterized amidases, instead of the classic *ampD* and *amiD* annotations, we proposed naming these mycobacterial genes *ami3* (MSMEG_6406), *ami4* (MSMEG_5315) and *ami5* (MSMEG_0533). This nomenclature is used throughout this dissertation.

3.1.2 Phylogenetic analysis and domain conservation

Following the detection of amidase_2 family members and corresponding protein sequence analyses in various species, further *in silico* analysis was performed to elucidate the potential roles of these amidases in *M. smegmatis* with respect to their evolutionary relationship amongst the different species. The phylogenetic tree indicated a clear separation of the Ami3 clade from Ami4 and Ami5. Interestingly, the analyses indicated close homology of Ami3 (*Mtb* homolog Rv3811) to the *Homo sapien* PGLYRP2 protein, involved in host defense against foreign bacterial pathogens and plays an important role in the innate immune response. It also shares homology with the bacteriophage T7 lysozyme and the amidase of *Synechococcus elongates* amongst others. The mycobacterial Ami4 (*Mtb* homolog Rv3594) and Ami5 proteins, which are closely related, clustered with a large group of proteins including the *E. coli* and *P. aeruginosa* amidase_2 family proteins amongst others. These enzymes have been previously shown to function in cell wall hydrolysis, peptidoglycan recycling and antibiotic resistance (Rivera *et al*., 2016).

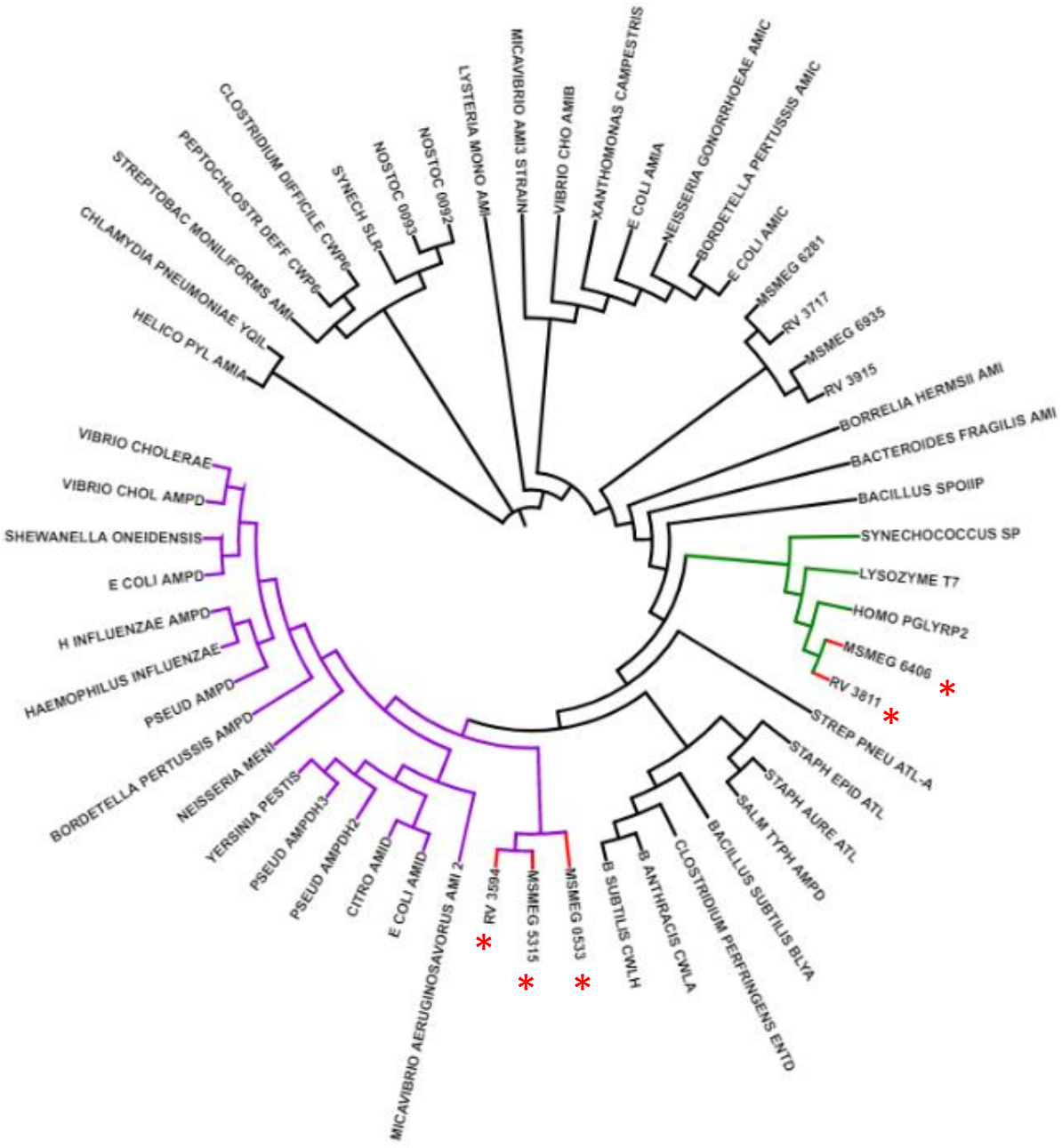

Figure 3.2: Phylogenetic analysis of the amidase_2 family of proteins. Phylogenetic analysis of mycobacterial amidases Ami3, Ami4 and Ami5. The tree is based on the identifiable *E. coli* AmiD and AmpD homologs for each species. Those species indicated in purple share homology with the mycobacterial Ami4 and Ami5, whilst those indicated in green were closely related to the Ami3 protein.

3.1.3 Domain organization of the amidase_2 and amidase_3 domain containing proteins

The two main families of amidases include the amidase_2 and amidase_3 domain containing proteins. Although both domains catalyze cleavage of PG by releasing L-ala from MurNAc, the size of their active sites and folds differ; amidase_3 enzymes cleave muropeptides whilst amidase_2 proteins cleave anhydromuropeptides, with AmiD having dual specificity for both types of PG moieties (Uehara and Park, 2007). However, despite these differences the catalytic activities of these amidases are similar in that the active site Zn^{2+} ion bound to the water molecule is pushed toward the glutamic acid in the amidase_3 domain or histidine in amidase_2, activating and triggering the nucleophilic attack on the amide bond between L-ala and MurNAc (Kerff et al., 2010). The result is a tetrahedral conformation of the amide carbon and a –

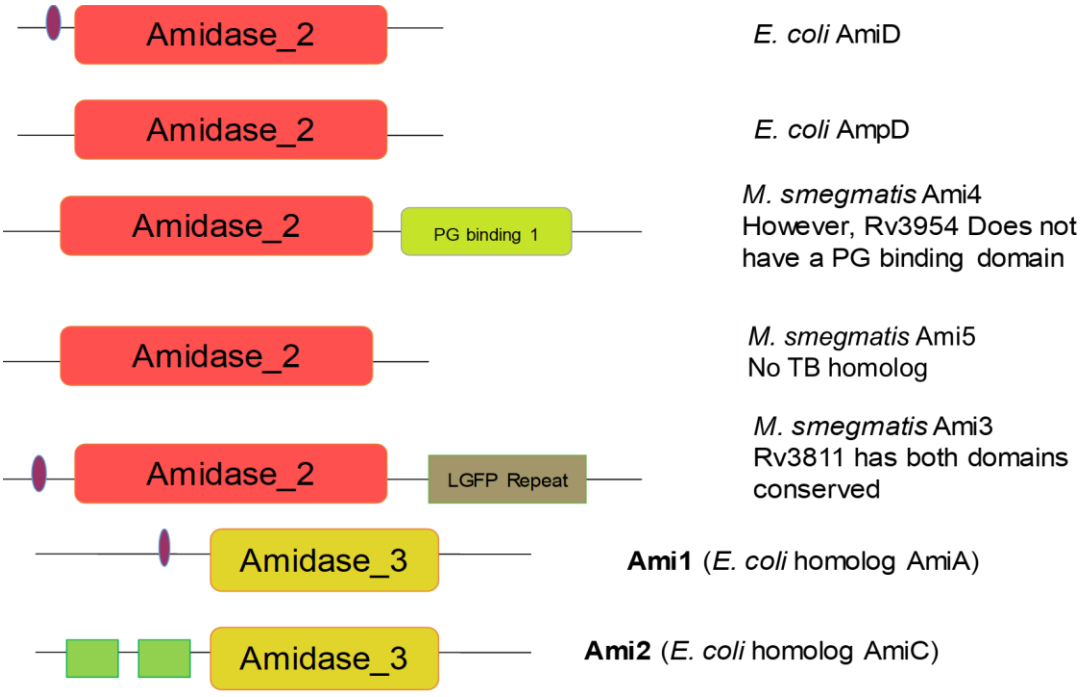

Figure 3.3: Domain organization of PG *N*-acetylmuramoyl-L-alanine amidases (Amidases) in *E. coli*, *M. smegmatis* and *M. tuberculosis*. The amidase_3 domain (mustard) found in combination with the signal peptide (purple) in the case of the cell division Ami1 proteins and with a PG binding domain in green (PG synthesis regulating Ami 2).The amidase_2 domain (pink) is also found along with signal peptide (purple) and an LGFP repeat (Ami3) in grey and is accompanied by a PG binding domain (green blocks) for Ami4.

- pentameric coordination of the catalytic Zn^{2+}. This tetrahedral intermediate is stabilized by hydrogen bonds involving the carbonyl oxygen of the scissile bond and carbonyl oxygen from L-ala, and an oxygen from MurNAc (Kerff *et al*., 2010). Domain content of mycobacterial amidases is given in Figure 3.3. Amidase domains are normally found in association with other protein motifs, which commonly include the transmembrane peptidoglycan recognition protein domain or the PG binding domain found in the amidase_2 (Ami4) and amidase_3 (Ami2) domain-containing proteins. These domains are responsible for the recognition and binding of the PG substrate. In addition to this, amidases can also possess a signal peptide, as observed in Ami1 and Ami3, which facilitates the transportation of the protein to the periplasmic region. Ami3 contains a LGFP repeat domain, which is a 54 amino acid repeat thought to be involved in the maintenance of cell wall integrity and cell shape (Adindla *et al*., 2004).

3.1.3.1 Amidase_2 domain proteins: Tertiary structure predictions

To extrapolate the biological function of the amidase_2 family of proteins and their conformational characteristics, the overall three-dimensional structures were analyzed using the bioinformatics tools I-TASSER and Phyre^2 to determine the conservation of protein folds amongst different species. The results are shown in Figure 3.4. The *E. coli* AmiD protein has been crystallized and was used as the basis for determining structural conservations in the mycobacterial amidase homologs. According to Kerff et al (2010), AmiD is composed of eight α-helices and nine β-strands. The zinc ion critical for amidase activity is bound to the active site and coordinated by the side chain residues His^{35}, His^{151} and Asp^{161} (Kerff *et al*., 2010). In the protein, the Asp^{161} side chain of the catalytic triad sits in the random coil, whereas His^{151} is found on the helix and His^{35} in the β-sheet. A similar pattern is also depicted with the Ami3 predicted tertiary structure, despite the Cys^{270} replacement of Asp, and in Ami4, demonstrating that a metal ion can be accommodated, Figure 3.4. However, the Ami5 His side chains are dissimilar and are positioned outside the α-helix and β-strand, whether this affects the strength of Zn^{2+} binding is unknown, Figure 3.4. The conservation of protein structure may reflect similar protein functions. Furthermore, amidase domain containing proteins are important surface antigens in pathogenic bacteria and represent possible drug and/or vaccine targets, suggesting that they may have been under positive selection during evolution. This would explain the high degree of conservation in divergent bacterial species.

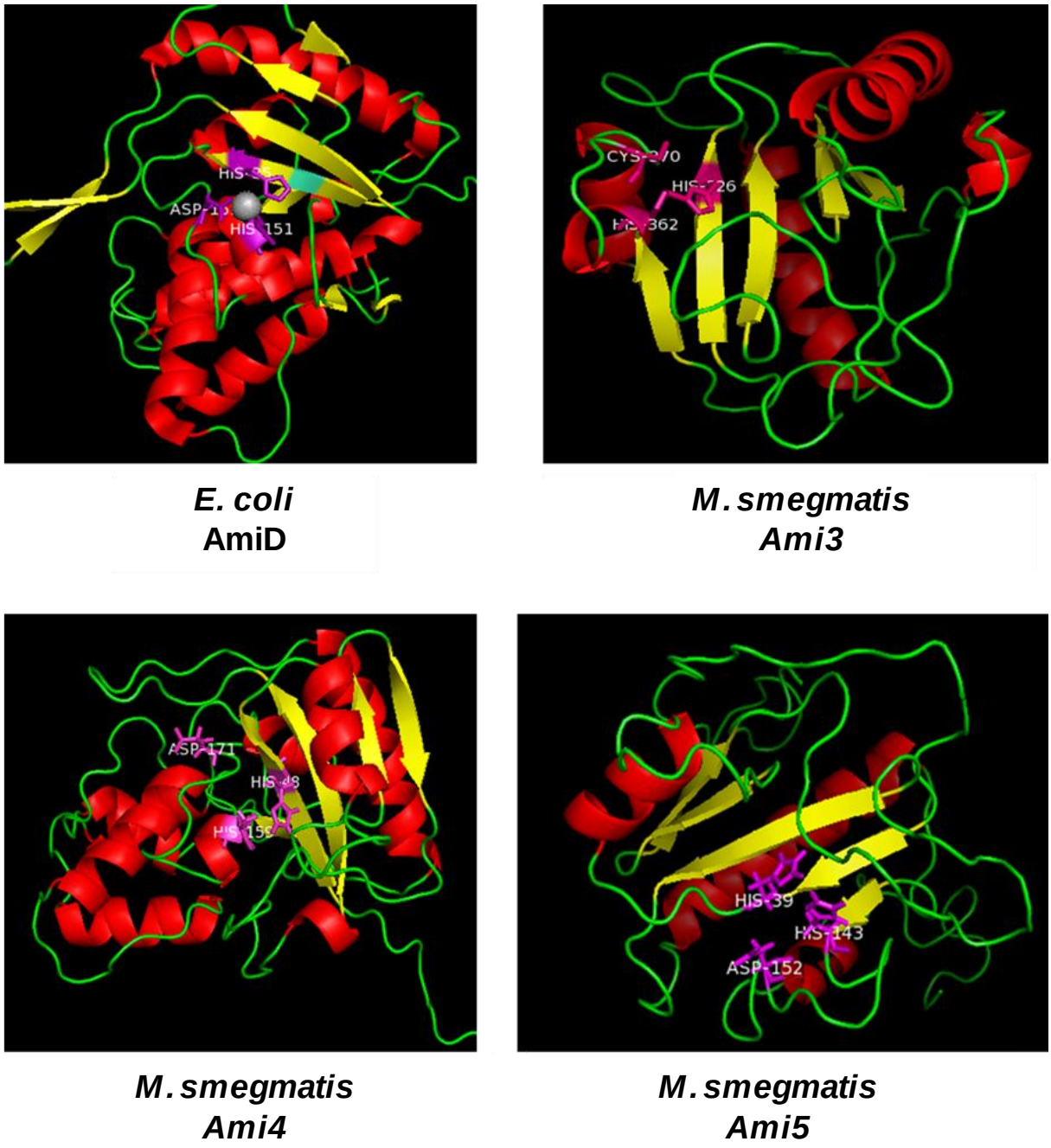

Figure 3.4: Tertiary structure of the amidase_2 domain family of proteins in *E. coli* and *M. smegmatis*. Shown are 3D ribbon representatives of AmiD (*E. coli*), Ami3, Ami4 and Ami5 (*M. smegmatis*). Helices are shown in red, beta sheets in yellow and coils in green. In magenta is the conserved catalytic triad (His-His-Asp/Cys) with the zinc ion represented by a grey sphere. For the mycobacterial amidases, i-Tasser models do not reflect the zinc but the overall structure to coordinate this metal is present.

3.2 Strategy used for the generation of *M. smegmatis* amidase gene deletions

To investigate the potential role of amidases, the established two step allelic exchange system (Parish and Stoker, 2000) was used to generate deletion mutants of the putative amidase_2 family genes in *M. smegmatis*. Amidase knockout strains were created as detailed in Section 2.2. Briefly, amidase genes were targeted for deletion by creating a suicide construct which carries a truncated version of the gene of interest. The strategy is further detailed in Figure 3.5

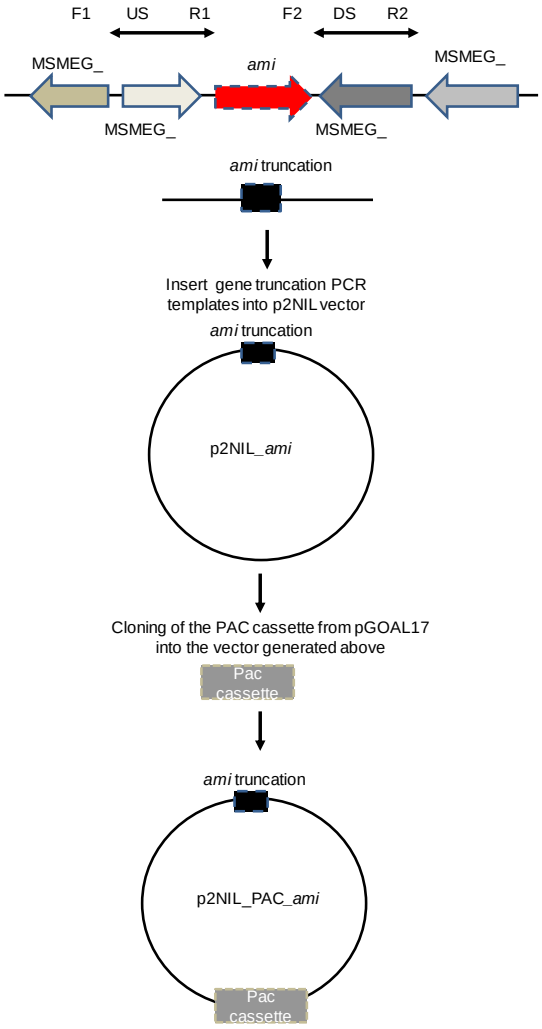

Figure 3.5: Generation of amidase deletion suicide constructs. Primers specific to the region (F1, R1 and F2, R2) depicted in the figure were designed to construct an in frame truncated version of the gene of interest by fusing the upstream (US) and downstream (DS) regions. The two fragments are ligated together to the p2NIL plasmid by three-way cloning. A suicide construct is then created by ligating the *Pac*I cassette, which contains *sacB* and *lacZ* gene, to the p2NIL_*ami* construct.

As previously mentioned, the *ami3* and *ami4* mutants were constructed in an Honours project by myself (Sikhosana, 2015) and for context, brief details of the construction and characterization are given below.

3.2.1 Construction of the *M. smegmatis ami3* deletion construct

The *ami3* suicide construct was generated and profiled in an Honours project by the student (Sikhosana, 2015) through restriction mapping as depicted in Supplementary Figure 3. The restriction digest profile yielded all the expected sizes, hence the vector integrity was maintained. An exception was *SalI* which was mapped to the vector backbone and not in the region of interest. Also, the 3169 bp fragment generated from the *HindIII* digestion yielded a higher than expected size (Supplementary Figure 3) but this modification was found to be present in the original pGOAL17 vector. Further analysis of vector integrity was performed by sequencing the amplified product which showed no mutations in the regions cloned (data not shown, conducted in Honours).

3.2.2 Construction of the *M. smegmatis ami4* deletion construct

The *ami4* suicide construct was generated and profiled by the student in an Honours project (Sikhosana, 2015) through restriction mapping as outlined in section 2.1.7.1 (Supplementary Figure 4). The suicide vector integrity was maintained as digests yielded the expected sizes (Supplementary Figure 4) and plasmid DNA sequencing verified no mutations in the construct (data not shown, conducted in Honours). As above, the *HindIII* restriction yielded a DNA band slightly higher than the expected, which again mapped to the vector backbone.

3.2.3 Construction of the *M. smegmatis ami5* deletion construct

The *ami5* suicide construct was profiled by restriction mapping as depicted in Figure 3.6. The suicide vector integrity was maintained as most restriction digests yielded the expected fragment sizes. The *MluI* restriction revealed additional bands due to partial digestion and *EcoRI* also showed non-specific cutting due to star activity from prolonged incubation with the enzyme. Again, the region of interest was sequenced and no mutations were found (data not shown).

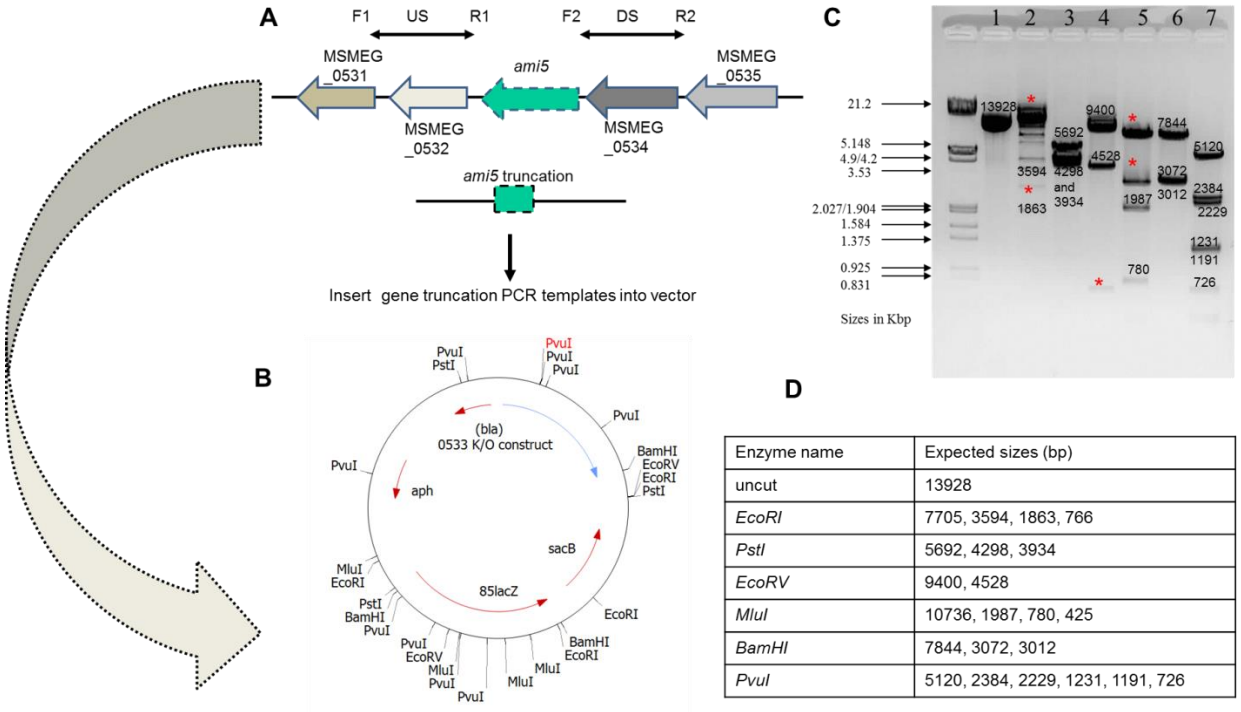

Enzyme name	Expected sizes (bp)
uncut	13928
EcoRI	7705, 3594, 1863, 766
PstI	5692, 4298, 3934
EcoRV	9400, 4528
MluI	10736, 1987, 780, 425
BamHI	7844, 3072, 3012
PvuI	5120, 2384, 2229, 1231, 1191, 726

Figure 3.6: Restriction profile of p2NIL_pG17_*ami5*. (A) *M. smegmatis* genomic map and the position of the gene within the genome. The allelic exchange strategy for the generation of the deletion strains is also depicted, with the site of primer binding. (B) Final *ami5* knockout construct used to transform the *M. smegmatis* wild-type parental strain. (C) Agarose gel (0.8%) of digested fragments: Roche marker IV [Lane 1] uncut construct control (13928 bp), *EcoRI* [Lane 2], *PstI* [Lane 3], *EcoRV* [Lane 4], *MluI* [Lane 5], *BamHI* [Lane 6], *PvuI* [Lane 7]. The red Asterix depict unexpected bands as a result of incomplete digestion or sequencing errors on the plasmid backbone (D) Table depicting the specific enzymes used and the expected fragment sizes (bp).

3.3 Strategy for the generation of the *M. smegmatis* amidase gene deletion strain

From the aforementioned results, the vectors were suitable to generate unmarked in-frame deletions of the respective amidase genes (*ami3*, *ami4* and *ami5*) in *M. smegmatis* were created. This was done by transforming the *M. smegmatis* parental strain with the respective suicide construct generated as indicated in Sections 2.2. The suicide construct integrates into the parental strain genome via homologous recombination resulting in the generation of a single crossover (SCO) strain, which harbors both the wild-type and truncated version of the amidase gene (Figure 2.2). Following the generation of the SCO strain, a DCO strain was generated and identified by a counter selection screen as described in Section 2.2. The selected colonies were screened using

PCR to determine whether the mutant gene was present within the genome and confirmed further by Southern blot and real time qPCR.

3.3.1 Generation of *M. smegmatis* Δ*ami3* strain

Genetic disruption of the *ami3* gene in *M. smegmatis* using two step exchange homologous recombination was confirmed during Honours with PCR (Sikhosana, 2015) using the strategy outlined in Section 2.1.5.1. The results of this analysis confirmed the deletion mutant, generating an amplicon of 350 bp for the mutated version of the gene and 100 bp for the wild-type gene in the parental strain (Figure 3.7 D).

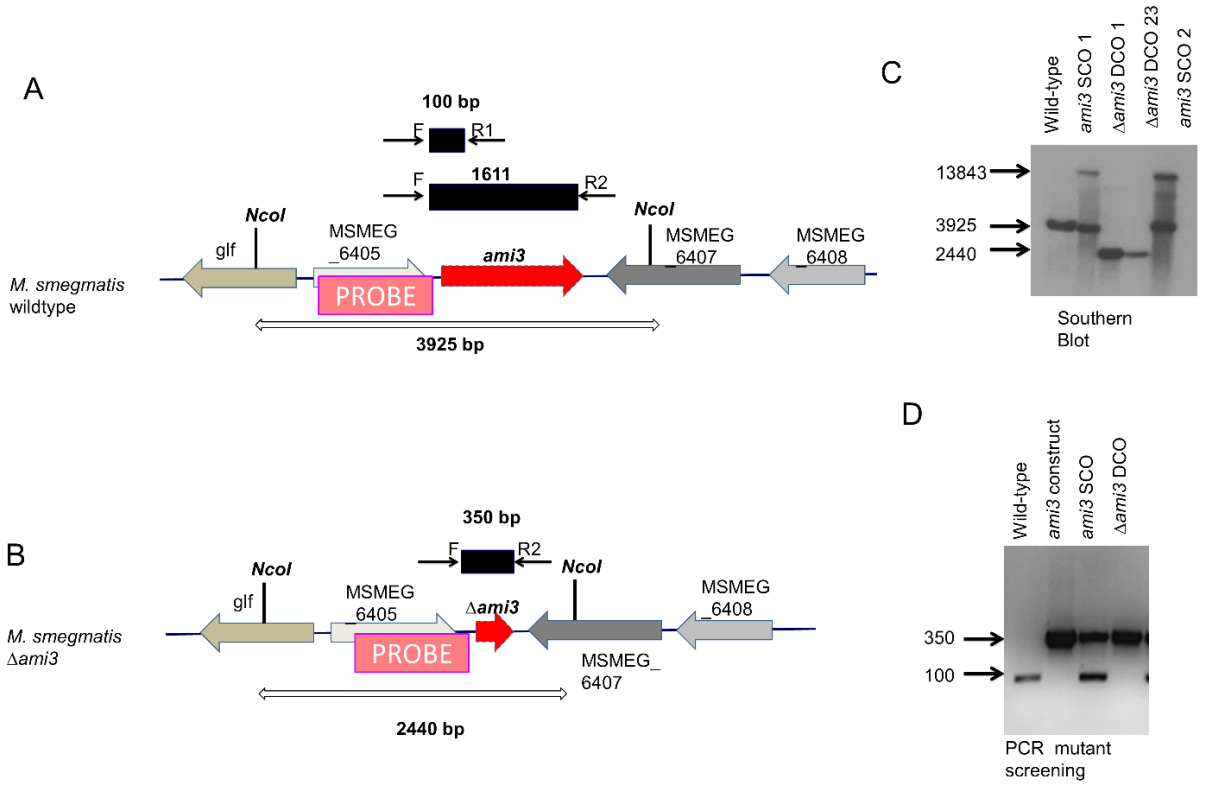

Figure 3.7: Genotypic characterization of *M. smegmatis* Δ*ami3.* (A and B) In all cases, genomic maps are shown for both the wild-type (mc^2 155) and mutant along with relevant sizes expected for PCR (shown with inward arrows) and Southern Blot analysis (shown with outward arrows). (C) Southern blot analysis results where DNA was digested with *Nco*I (D) PCR (conducted in Honours, and shown here for completeness, Sikhosana, 2015) confirmed gene deletions. Black boxes show the PCR amplicons. The 1611 bp amplicon was not seen as primer R1 probably displaced extension from Primer R2. The map for the SCO is not shown.

However, as a PCR screen for genetic mutants is inadequate, further confirmation was performed using Southern blotting in this MSc. Prior to this, genomic extractions from the wild-type, DCO mutant, Δ*ami3* and SCO strain were carried out as outlined in Section 2.2. As expected, the strains confirmed the genotypic characteristics that were anticipated when genomic DNA was digested with *Nco*I. When probed with a fragment of DNA corresponding to the upstream region, the wild-type strain displayed the expected 3925 bp fragment, the mutant Δ*ami3* yielded 2440 bp fragment and the SCO strain exhibited a 13843 bp and 3925 bp bands, thus verifying the PCR results previously obtained (Figure 3.7 C).

3.3.2 Generation of Δ*ami4 M. smegmatis* strain

Following the disruption of the *M. smegmatis ami4* gene using the two-step allelic exchange system, the mutants were confirmed using PCR and Southern blotting as mentioned in the previous section. The mutant strain produced an expected 370 bp fragment with the wild-type producing a PCR fragment size of 135 bp, Figure 3.8. This was followed by further confirmation using Southern blotting in this MSc. DNA extracted from the Δ*ami4*, SCO and wild-type strain was digested with *Nco*I and Southern blotting was carried out as per Section 2.2.3.1. Southern blotting results confirmed the successful construction of an *ami4* deficient strain. When digested DNA was probed with a fragment of DNA corresponding to the downstream region, the wild-type strain displayed the expected 3865 bp fragment, Δ*ami4* generated a 4705 bp fragment and the SCO strain exhibited 6943 bp and 4705 bp bands (Figure 3.8).

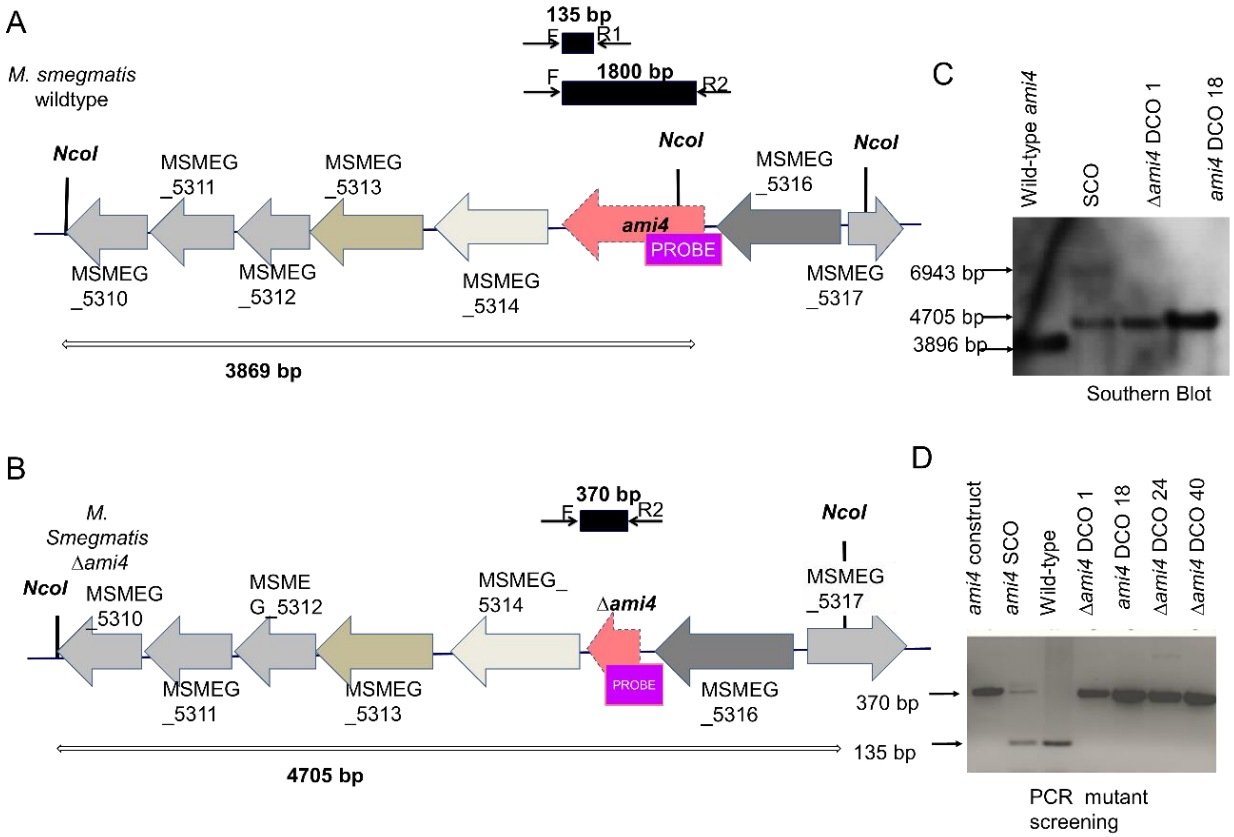

Figure 3.8: Genotypic characterization of *M. smegmatis* Δ*ami4*. (A and B) In all cases, genomic maps are shown for both the wild-type and mutant along with relevant sizes expected for PCR (shown with inward arrows) and Southern blot analysis (shown with outward arrows). Probe binding region is depicted by the purple block (C) Southern blot analysis results, DNA was digested with *Nco*I (D) PCR confirmation of gene deletions (conducted in Honours, and shown here for completeness, Sikhosana, 2015). Black boxes show the PCR amplicons. The 1800 bp amplicon was not seen as primer R1 probably displaced extension from Primer R2. The map for the SCO is not shown.

3.3.3 Generation of the Δ*ami5 M. smegmatis* strain

Genetic disruption of the *ami5* gene in *M. smegmatis* was also confirmed with PCR and Southern blot. Using PCR, the truncation of the *ami5* gene generated an amplicon of 1375 bp and 1444 bp for the wild-type gene (Figure 3.9). Genomic extractions from the wild-type, mutant and SCO strains were carried out in preparation for Southern blotting, the results of which confirmed the successful deletion of *ami5*. Genomic DNA was digested with *PvuI*, ran on 0.8% agarose gel and probed with fragment of DNA corresponding to the upstream region. The wild-type strain displayed the expected 1851 bp and 1590 bp fragments, Δ*ami5* generated 1851 bp and 1181 bp

bands and the SCO strain exhibited 1851 bp, 1590 bp and 1181 bp bands (Figure 3.9). Following confirmation of successful *ami5* gene deletion, the strain (together with the Ami4 and Ami4 deletion mutants) was then further investigated by phenotypic characterization.

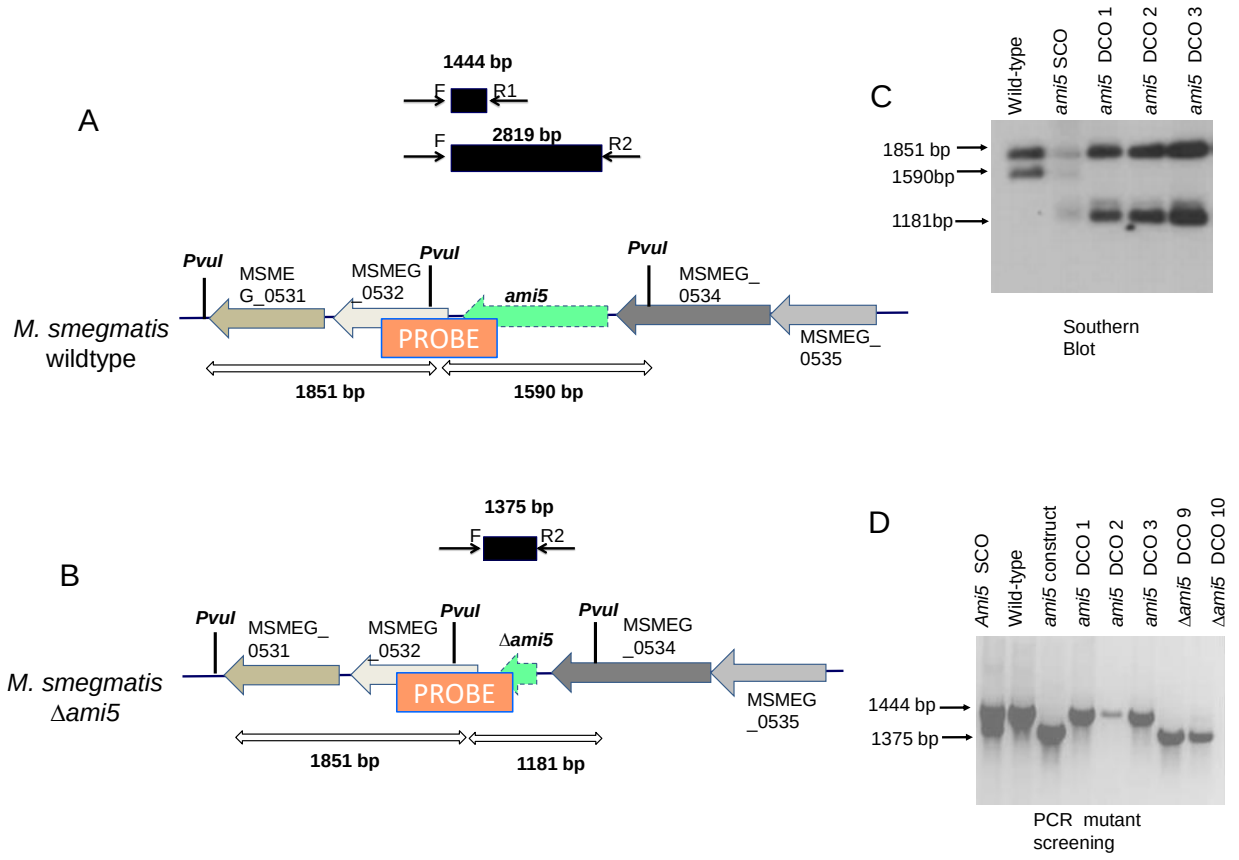

Figure 3.9: Genotypic characterization of *M. smegmatis* Δ*ami5*. (A and B) In all cases, genomic maps are shown for both the wild-type and mutant, along with relevant sizes expected for PCR (shown with inward arrows) and Southern blot analysis (shown with outward arrows). (C) Southern blot analysis results, DNA was digested with *Nco*I (D) PCR confirmation of gene deletions. Black boxes show the PCR amplicons. The 2819 bp amplicon was not seen as primer R1 probably displaced extension from Primer R2. The map for the SCO is not shown.

3.4.1 Generation of *M. smegmatis* Δ*ami3* complementation strains

Genetic complementation is achieved through the re-introduction of a functional copy of the deleted gene on a recombinant plasmid and transformation into the gene knockout mutant strain to revert the phenotype back to wild-type. To achieve this, the full length *ami3* gene with the

promoter region was cloned into the integration vector pMV306H. This vector integrates at tRNA ^{Gly} gene site in the mycobacterial genome. Construction and restriction mapping of the plamid construct used for genetic complementation is given in Figure 3.10.

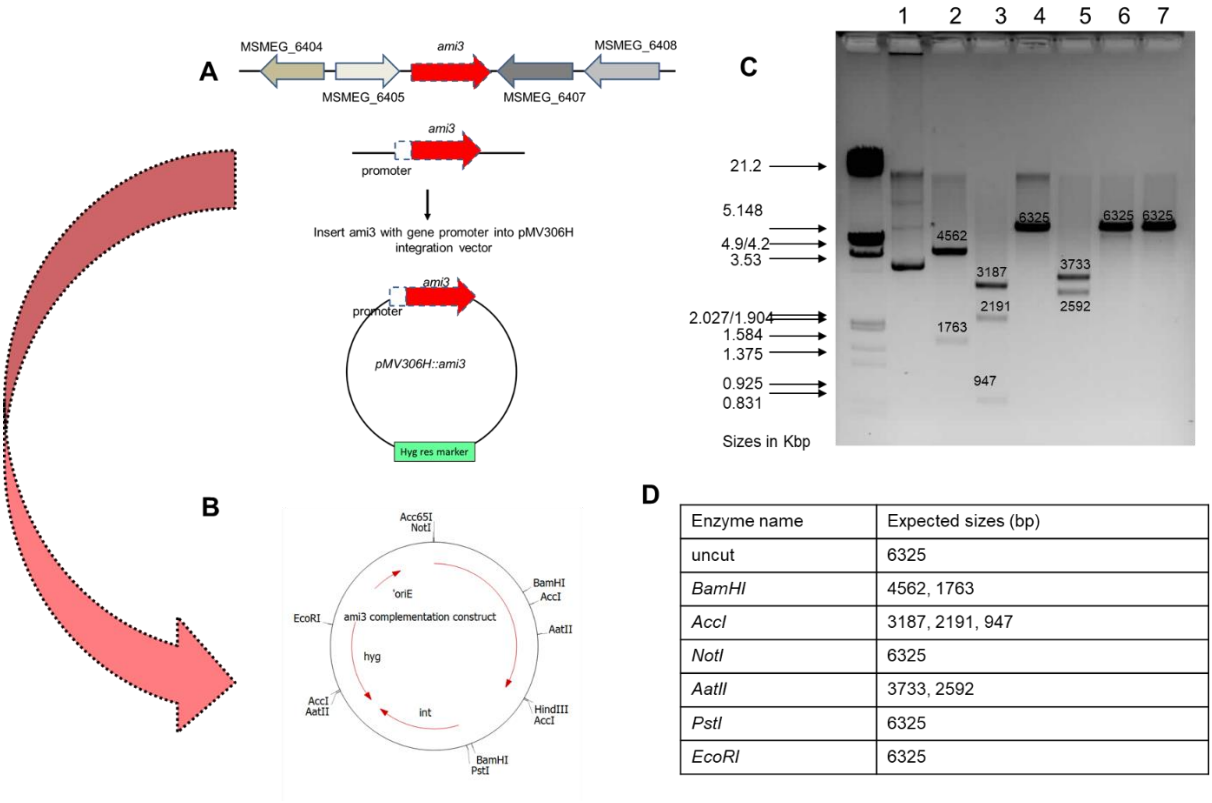

Enzyme name	Expected sizes (bp)
uncut	6325
BamHI	4562, 1763
AccI	3187, 2191, 947
NotI	6325
AatII	3733, 2592
PstI	6325
EcoRI	6325

Figure 3.10: Restriction profile of pMV306H::*ami3*. (A) *M. smegmatis* genome map and the position of *ami3* within the genome. The coding region of *ami3* gene with the promoter region was cloned into the integration vector pMV306H. (B) Final pMV306H::*ami3* construct used to transform *M. smegmatis* Δ*ami3*. (C) Agarose gel (0.8%) of digested fragments: Roche marker IV [Lane 1] uncut construct control (13928 bp), *Bam*HI [Lane 2], *Acc*I [Lane 3], *Not*I [Lane 4], *Aat*II [Lane 5], *Pst*I [Lane 6], *Eco*RI [Lane 7]. (D) Table depicting the specific enzymes used and the expected fragment sizes (bp).

To confirm the genetic complementation of the *ami3* gene, RT-PCR was performed as described in Section 2.4.3. As shown in Figure 3.11, the Δ*ami3* mutant did not display any *ami3* gene expression as expected. Expression was regained upon re-introduction of the wild-type gene in the mutant background in the complemented strain (Δ*ami3::ami3)*. Expression levels in the genetically complemented strain were comparable to that seen in the wild type.

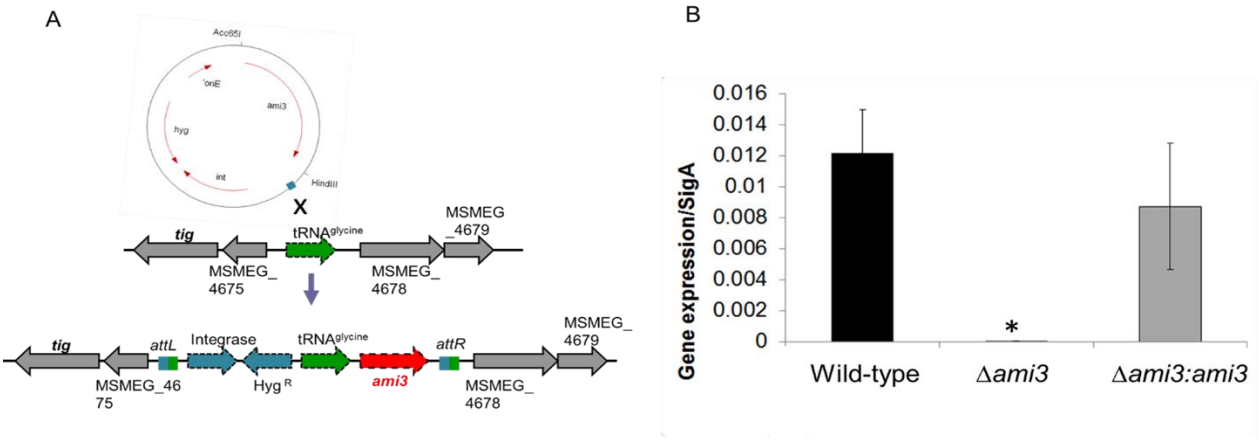

Figure 3.11 Genetic complementation of the *M. smegmatis* Δ*ami3* mutant with pMV306H*::ami3*. (A) Diagrammatic representation of pMV306H*::ami3* integration into the *M. smegmatis* chromosome. The plasmid makes use of the L5 integration system, the site of attachment (blue block) integrated at the $tRNA^{Gly}$ locus of the chromosome (green arrow) resulting in the incorporation of this locus on either the right (*attL*) or left (*attR*) of the plasmid. (B) Analysis of *ami3* expression in relation to *sigA* expression in wild type, Δ*ami3* and the complemented strain Δ*ami3::ami3*. Shown is the average expression of *ami3* mRNA in each background. Error bars are representative of standard error of the mean (SEM) of three independent replicates, with significant difference considered as $p < 0.05$ (*) using the Student's *t*-test (non-parametric test).

3.4.2 Construction of Δ*ami4* genetic complementation strain

To create a complement for the *ami4* deficient strain, the *ami4* gene together with the promoter region was amplified and cloned into the pTweety integrating vector (Figure 3.12). This vector possesses an integrase and putative *attP-int* site, allowing it to integrate at the $tRNA^{Lys}$ site in the mycobacterial genome. This vector is maintained well, even in the absence of a selective antibiotic (Pham *et al*., 2007). RT-PCR was also performed to determine the level of *ami4* expression in the wild-type and complemented strains, and to confirm the absence of expression in the mutant strain. Marginal expression of *ami4* was detected in the mutant strain due to non-specific primer binding (confirmed by melt curve analysis [data not shown]) and complementation fully restored expression of the gene (Figure 3.13).

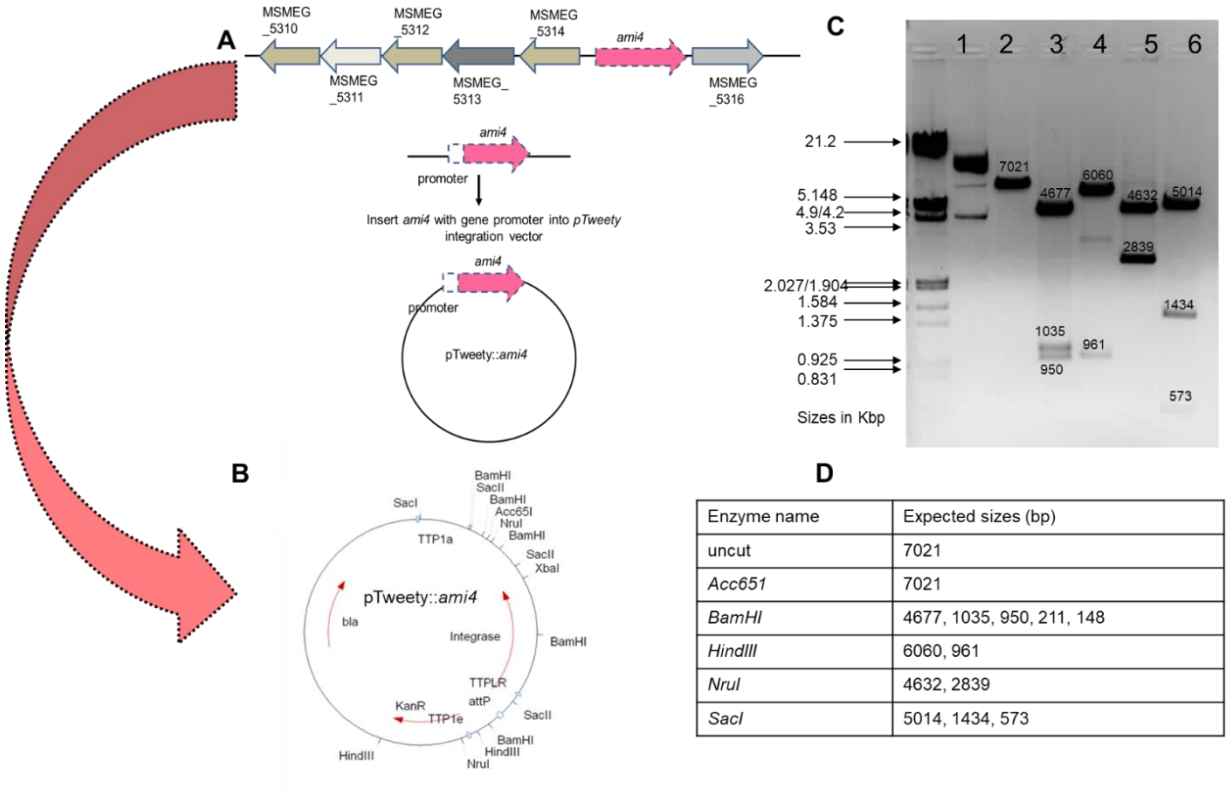

Enzyme name	Expected sizes (bp)
uncut	7021
Acc651	7021
BamHI	4677, 1035, 950, 211, 148
HindIII	6060, 961
NruI	4632, 2839
SacI	5014, 1434, 573

Figure 3.12: Restriction profile of pTweety::*ami4*. (A) *M. smegmatis* genome map and the position of the gene within the genome. The coding region of *ami4* gene, the promoter region was cloned into the integration vector pTweety. (B) Final pTweety::*ami4* construct used to transform *M. smegmatis* Δ*ami4*. (C) Agarose gel (0.8%) of digested fragments: Roche marker IV, [Lane 1] uncut construct control (13928 bp), *Acc*651 [Lane 2], *Bam*HI [Lane 3], *Hin*DIII [Lane 4], *Nru*I [Lane 5], *Sac*I [Lane 6]. (D) Table depicting the specific enzymes used and the expected fragment sizes (bp).

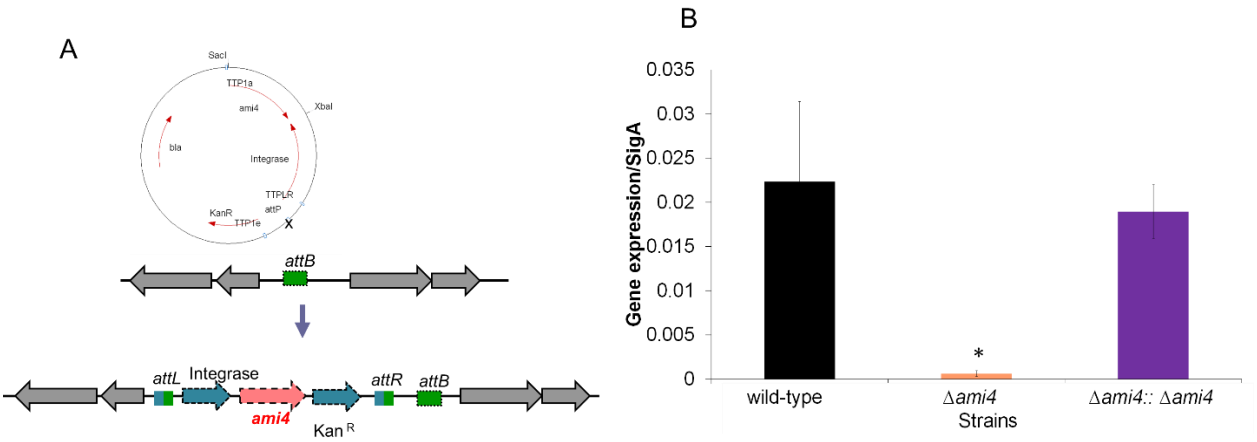

Figure 3.13: Genetic complementation of the *M. smegmatis* Δ*ami4* mutant with pTweety::*ami4*. (A) Diagrammatic representation of pTweety::*ami4* integration into *M. smegmatis* chromosome. The plasmid makes use of the L5 integration system, the site of attachment (blue block) integrates at the $tRNA^{Lys}$ locus of the chromosome (green arrow) resulting in the incorporation of this locus on either the right (attL) or left (attR) of the plasmid. (B) Analysis of *ami4* expression (mRNA) in relation to *sigA* in the gene deficient, Δ*ami4* and complemented strain, *Δami4::ami4*. Shown is the average expression of *ami4* mRNA in each background conducted as three independent replicates, with significant difference considered as $p < 0.05$ (*) using the Student's *t*-test (non-parametric).

3.4.3 Genetic Complementation of *M. smegmatis* Δ*ami5* strain

The full length *ami5* gene with the promoter region was cloned into the integration vector pMV306H. Gene specific primers with *Acc*651 engineered in the 5' of the forward primer and *HindIII* in the 3' end of the reverse primer (Table A1 Appendix A) were used to amplify the gene allowing for directional insertion into the integration vector. Following transformation of *E. coli* DH5α cells, clones were screened by restriction mapping (Figure 3.14). As shown in the Figure 3.14, fragments obtained following digestion with specific enzymes corresponded with the expected sizes. This was then followed by electroporation of the construct into the *M. smegmatis* Δ*ami5* strain. As pMV306H is an L5 integration vector, it integrates into the $tRNA^{Glycine}$ site in the genome allowing the gene to be expressed from a different location. Growth of the transformants in the presence of Hygromycin was used as a selection screen for positive clones. Time limitations precluded a qRT-PCR analysis of gene expression.

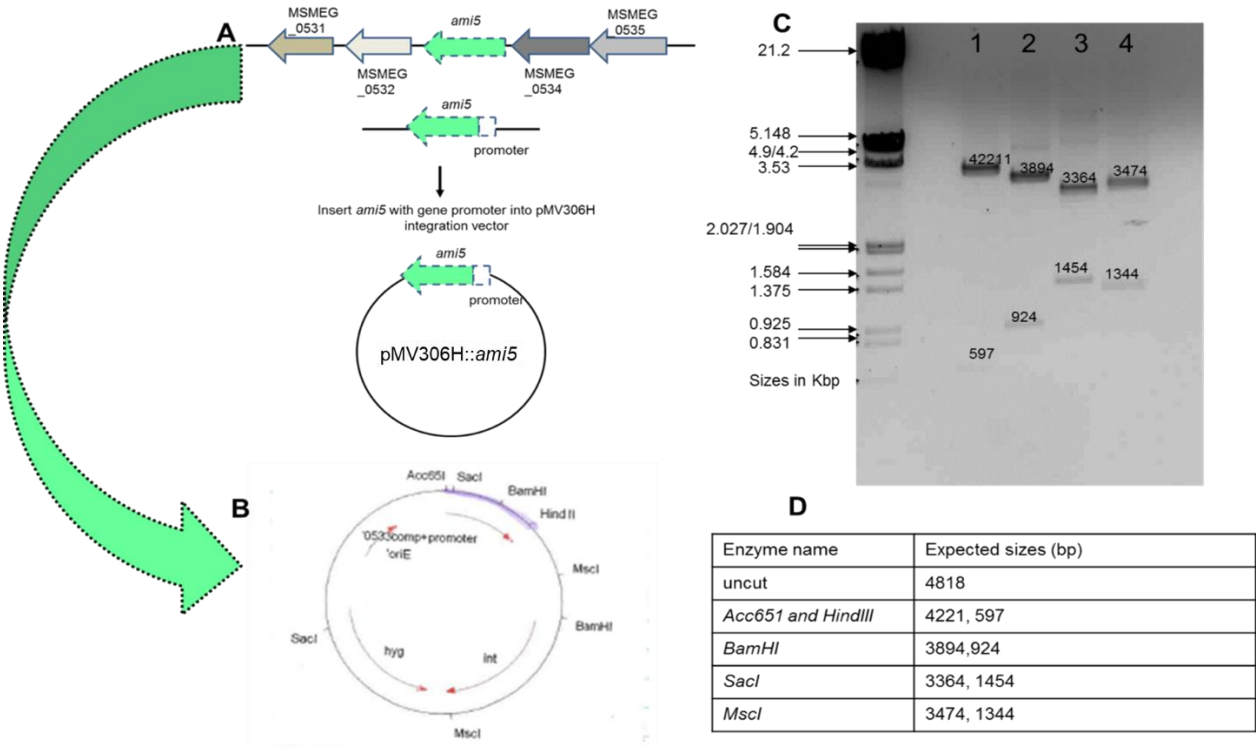

Enzyme name	Expected sizes (bp)
uncut	4818
Acc651 and HindIII	4221, 597
BamHI	3894,924
SacI	3364, 1454
MscI	3474, 1344

Figure 3.14: Restriction profiling of pMV306H::*ami5* (A) *M. smegmatis* genome map and the position of the gene within the genome. The coding region of *ami5* gene with the promoter region was cloned into the integration vector pMV306H (B) Final pMV306H::*ami5* construct used to transform *M. smegmatis* Δ*ami5*. (C) Agarose gel (0.8%) of digested fragments: Roche marker IV, [Lane 1] uncut construct control (4818 bp), *Acc*651 and *Hin*DIII [Lane 2], *Bam*HI [Lane 3], *Sac*I [Lane 4], *Msc*I [Lane 5]. (D) Table depicting the specific enzymes used and the expected fragment sizes (bp).

3.5 Phenotypic characterization of the Amidase_2 domain mutant *M. smegmatis* strains

The redundancy of bacterial amidases makes it difficult to dissect specialist versus combinatorial function in mycobacteria. To study mycobacterial amidases, three distinct knockout mutants were generated as described above. These mutants were then further studied by probing cell growth patterns, peptidoglycan remodeling/incorporation, susceptibility towards antibiotics, biofilm formation and measuring cell length, all of which point to critical functions in cell elongation or division.

First, the growth kinetics of *M. smegmatis* strains, with truncated versions of the amidase gene of interest in this study, were assessed. Growth analysis was carried out on the wild-type parental strain, deletion mutants and their respective complementation strains using two distinct media,

namely Middlebrook 7H9 and Sauton's minimal media. Middlebrook 7H10 agar plates were used to assess the ability to form colonies. The two media conditions were used to simulate a carbon replete environment (7H9) and stress/starvation conditions (Sauton's media). Three independent biological repeats were conducted for each strain. The data are given below.

3.6 *M. smegmatis* Δ*ami3* phenotypic characterization

3.6.1 Mycobacterial Ami3 is dispensable for growth

Following the identification of *M. smegmatis ami3* with closest homology to the well characterized *E. coli amiD*, its involvement in mycobacterial growth kinetics was assessed. It was hypothesized that *ami3* may not be essential for bacterial growth as previously observed in studies investigating *E. coli amiD* (Uehara and Park, 2007). As expected, the absence of Ami3 did not lead to a significant growth defect in either rich or minimal media however, negligible delayed growth at the exponential phase was seen, but bacteria soon recovered and grew similarly to wild-type. Also, the loss of Δ*ami3* did not affect *M. smegmatis* colony forming ability, confirming that *ami3* is dispensable for *in vitro* growth, Figure 3.15

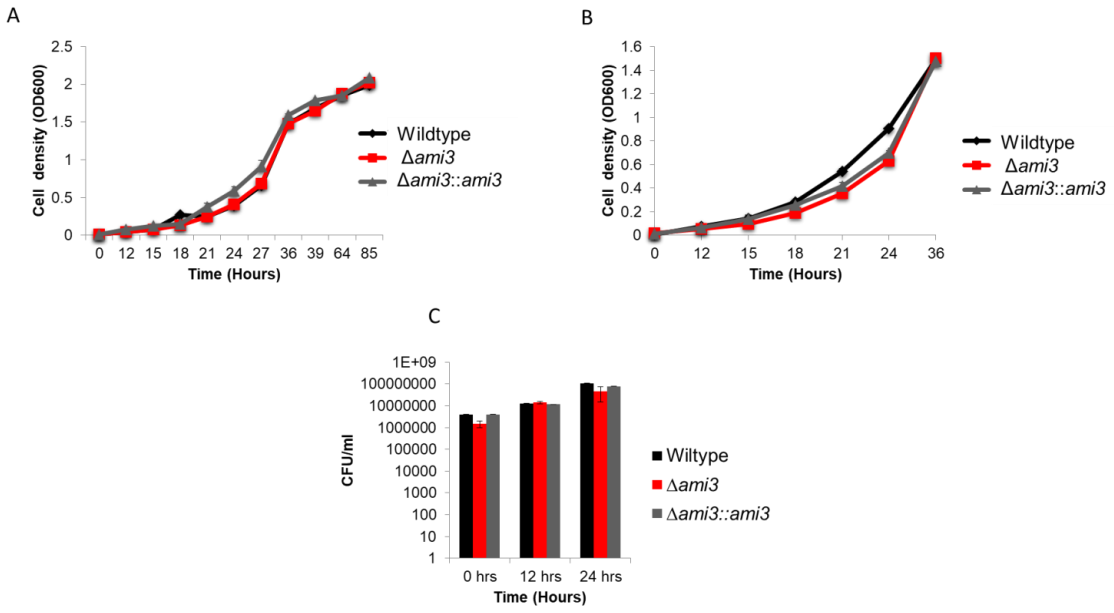

Figure 3.15: Growth kinetic analysis of the Δ*ami3* strain in relation to wild-type and the complement strain. -

Growth curves of the parental strain *M. smegmatis* wild-type (black), *M. smegmatis* Δ*ami3* (red) and *M. smegmatis*-Δ*ami3*::*ami3* (grey) in Middlebrook 7H9 (A) and Sauton's minimal media (B) monitored by measurement of OD600 at three hour intervals, represented as line scatter plots. Growth of the Δ*ami3* strain in Sauton's media was marginally delayed at the exponential phase compared to the wild-type and complement strains (C) Strains were plated on 7H10 media and incubated at 37 °C for 2 days. Growth analysis of viable bacteria was measured by CFU counts represented as a histogram. The values shown are the averages of three independent replicates, there were no significant growth differences between strains. Error bars are representative of standard error of the mean (SEM), Student's t-test (non-parametric) statistical analysis was used with (*) $p < 0.05$ considered as significant.

3.6.2 *M. smegmatis* Ami3 plays a role in biofilm formation and cell wall permeability

A biofilm consists of bacteria that secrete an extracellular matrix to surround the community and coordinate their gene expression as a survival strategy when encountering stressful conditions (Steinberg and Kolodkin-Gal, 2015). To determine whether deletion of the mycobacterial amidase_2 family of proteins had an effect on biofilm formation, the cells were diluted and inoculated in Sauton's minimal media, grown for a for a week and stained with crystal violet to determine biomass formation. Although a significant reduction in biomass for the gene knockout mutant was observed, there was no difference in surface cording of the biofilm when compared to the wild-type, Figure 3.16. Genetic complementation reversed this defect.

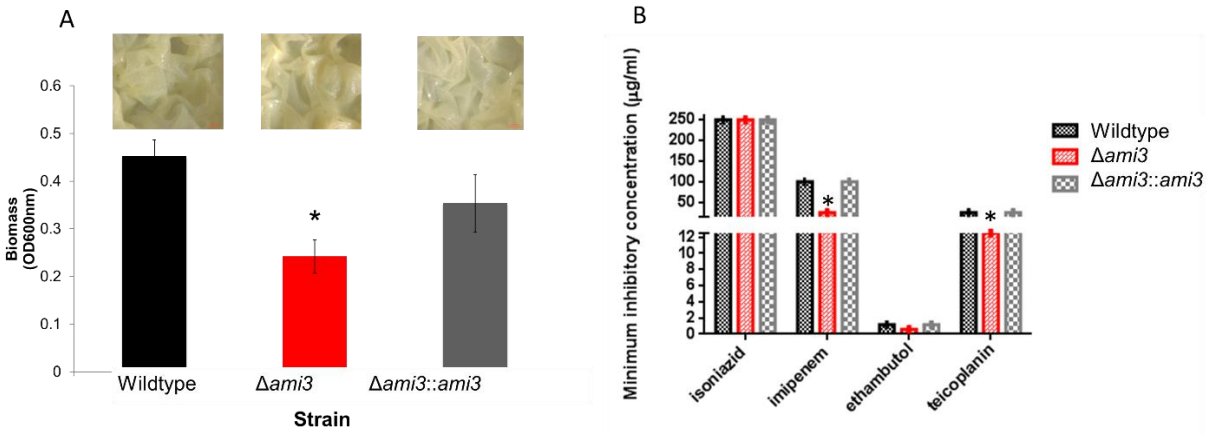

Figure 3.16: Biofilm formation after 7 days in Sauton's minimal media. Shown are the biofilms that formed at the 10^2 dilution. Biomass was determined by crystal violet staining following a 10 minutes incubation of the samples with the dye, the experiments were performed in triplicate. (A) Shown above is the biofilm and amount of biomass (histogram) in the wild-type, Δ*ami3* and the Δ*ami3*::*ami3* strain. The Δ*ami3* strain is capable of forming biofilms however, as measured by crystal violet, the biomass of this strain is significantly lower than that of the parental and complemented derivative. Although only the 10^2 dilution is shown for the biofilm, the same results were observed for

all dilutions (data not shown) (B) The minimum inhibitory concentrations (MIC) of the wild-type (black), - Δ*ami3* strain (red) and Δ*ami3*::*ami3* strain (grey) to isoniazid, imipenem, ethambutol and teicoplanin are depicted in the bar graph. Fold-change in MIC's is calculated compared to the wild-type strain. The Δ*ami3* strain is more sensitive to imipenem, teicoplanin and ethambutol when compared to the wild-type. The statistical differences between wild-type and mutants were determined by using a Student's t-test (non-parametric) with (*) $p < 0.05$ considered significant.

As biofilm biomass was reduced in the Δ*ami3* strain, suggestive of a defective cell wall, it was hypothesized that the strain would be sensitive to cell wall targeting antibiotics. To investigate this, the susceptibility of theΔ*ami3* strain to various antibiotics was assessed. The results are reported as minimal inhibitory concentrations (MIC's), which is the lowest concentration of drug inhibiting bacterial growth. Indeed, a 4-fold downshift in imipenem MIC was observed in the *M. smegmatis* Δ*ami3* strain (Figure 3.16 B). This was also observed when the strain was exposed to teicoplanin, with a 2-fold reduction compared to the wild type and complemented strains. The increased susceptibility to imipenem suggests a cell wall defect in the mutant as this antibiotic compromises cell wall synthesis through PBP inhibition, resulting in the formation of spheroblasts that lead to rapid lysis and eventually cell death (Trautmann *et al*., 1998). Teicoplanin, a glycopeptide, inhibits cell wall synthesis by preventing PG polymerization, which also results in cell death (Somma, Gastaldo and Corti., 1984). Overall, these results suggested that the loss of Ami3 led to an imbalance in PG homeostasis. Also, exposure of the mutant strain to isoniazid, which inhibits the synthesis of mycolic acids, an essential component of the cell wall and ethambutol, which inhibits arabinosyl transferase had no impact on bacterial viability. This indicated that defects, if present, were only located in the PG layer and not in other components in the cell wall.

3.6.3 Increased ethidium bromide transport across the cell wall correlates with increased antibiotic susceptibility

The inherent ability of mycobacteria to exclude certain molecules due to active efflux systems and the relatively impermeable cell wall are considered the main causes of antibiotic tolerance in these organisms. To assess if the cell wall was changed in the *ami3* mutant, ethidium bromide transportation was investigated in the wild-type and amidase knockout strain. The accumulation of ethidium bromide was monitored under conditions conducive to maximum efflux (i.e. in the presence of glucose with shaking incubation at 37 °C). The *ami3* mutant demonstrated

accumulation of ethidium bromide across all dilutions tested. Marginal ethidium bromide influx was seen in both the wild-type and complement strain when exposed to 0.6 µg/ml-10 µg/ml of the compound (Figure 3.17). The increase in ethidium bromide influx observed may attributed to changes in cell wall rigidity and possibly, efflux pumps.

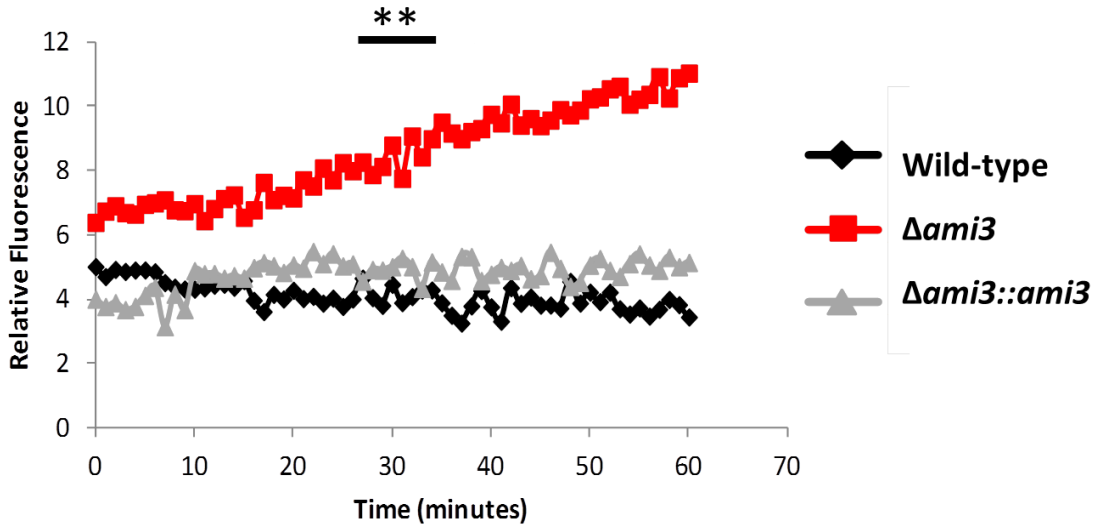

Figure 3.17: Analysis of cell wall permeability of the Δ*ami3* strain. Permeability of the mycobacterial cell wall was assessed by quantifying ethidium bromide diffusion into the cells through monitoring fluorescence for an hour. The Δ*ami3* strain displays an increased fluorescence demonstrating enhanced ethidium bromide uptake. Data represents three independent experiments with (**) $p < 0.01$, non-parametric student *t*-test

3.6.4 Maintenance of cell length is dependent on *ami3* activity

To assess if there were changes in the incorporation of new PG at the cell poles, click chemistry labeling was carried out as per Section2.8.1 and the cells were imaged using fluorescence microscopy. For this a click chemistry D-Ala analogue was used. D-Ala is inserted into new PG units and as these units get incorporated into nascent PG, the label can be used to trace sites of new PG synthesis. Mycobacteria incorporate new cell wall material at the poles and as a result, the wild-type strain displays strong polar staining with this analogue, Figure 3.18 A. The Δ*ami3* strain maintained the canonical PG staining pattern, however, the cells were longer than those of the wild-type and polar synthesis was outwardly extended as seen with the staining pattern in

Figure 3.18A and B with cells adopting more of diffused staining pattern compared to the wildtype. This defect was reversed in the genetically complemented strain. As yet, it is unclear what diffused staining points to in terms of mycobacterial growth and no further conclusions can be drawn in this regard. Following this, the disparities in cells length were quantified by measuring the distance between the two poles within the cells. We found that Δ*ami3* cells, ranged from 5 µm to 14 µm and were thus longer than the wild-type cells, which ranged from 2.5 µm to 8 µm (Figure 3.18C). From these data, *ami3* may also have a role in maintaining normal cell length, facilitating cell division and spatially controlling PG turnover.

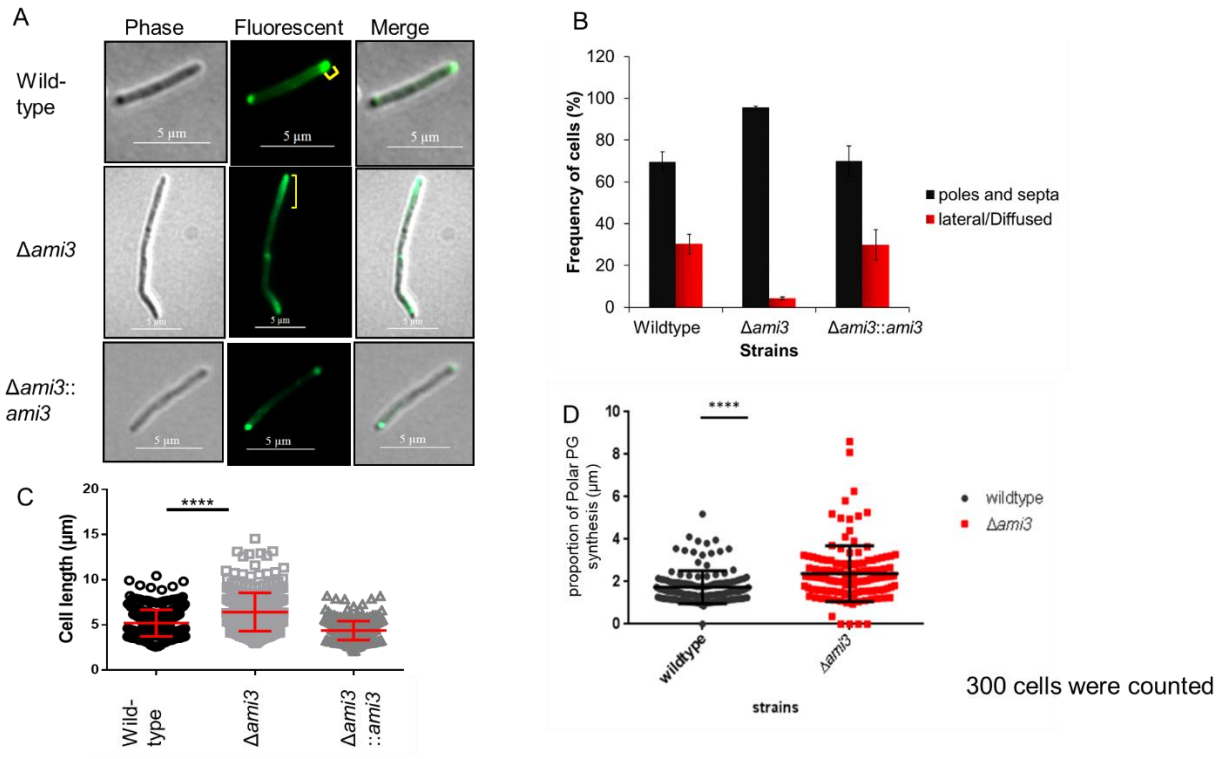

Figure 3.18: *M. smegmatis ami3* modulates cell shape and division. (A) Fluorescence microscopy carried out to determine spatial alterations in PG synthesis using D-alanine analog and click chemistry. Staining of new PG at the poles on the Δ*ami3* is longer when compared to wild-type, yellow bracket. (B) Deletion of *ami3* in *M. smegmatis* resulted in altered staining patterns for new PG. (C) Measurements of cell length in *ami3* defective mutant. Cell length quantification of Δ*ami3* strain appears to be different from the parental strain; wild-type (black circles) and Δ*ami3::ami3* strain (dark gray triangles), with Δ*ami3* strain forming abnormally long cells. (D) Proportion of cells with altered nascent PG incorporation in the mutant strain is significantly higher than that of the parental strain. Statistical analysis was carried out using the Student's *t*-test (non-parametric) with (****) p <0.0001 considered significant.

In addition to this, staining of the mycolic acid layer using DMN-tre confirmed the presence of multiple septa in the Δ*ami3* strain thus highlighting a role for this amidase in cell division (Supplementary Figure 6). Furthermore, polar elongation/growth in mycobacteria is thought to be asymmetrical thus giving rise to heterogeneity within a generation (Singh et al., 2013). Therefore, we sought to investigate this in the Δ*ami3* strain as incorporation of new PG cell length seem to be affected. We calculated the ratio of PG incorporation at both poles by calculating the difference in polar fluorescence thus translating to the pattern rate or pattern of mycobacterial growth. As expected, wild-type incorporated new PG asymmetrically as seen with different sizes in polar fluorescence, whilst the pattern for the Δ*ami3* strain was somewhat similar, however at this was at different ratios as the cells are longer than those of the wild-type (Figure 3.18 D).

3.6.5 Defective septal placement and cell division is evident in an *ami3* mutant

The cell division defects observed thus far prompted further investigation of cell division processes in the *ami3* mutant strain by focusing on the cytoskeletal element FtsZ, which is responsible for recruiting cell division proteins, required for coordinating cell division, to the septum (Kieser and Rubin, 2014). A FtsZ-GFP tagged derivative (Senzani *et al*., 2017) was introduced into the mutant strain and localization was investigated using fluorescence microscopy. Under normal conditions, FtsZ localizes to the site of cell division, forming single foci or two prior septal placement. Loss of *ami3* resulted in deregulated FtsZ localization (Figure 3.19). This is evident with the long cells having more than one FtsZ loci, however, two loci are also normally found in wild type although at differing proportions from the Δ*ami3* strain. We further investigated the surface of the bacterial mutant strain to determine any alterations in cell morphology using scanning electron microscopy. Loss of *ami3* not only led to elongated cells that failed to divide but also resulted in cells forming Z-rings/ division scars at random intervals pointing to defect in FtsZ-ring placement and or septal PG synthesis (Figure 3.19 B).

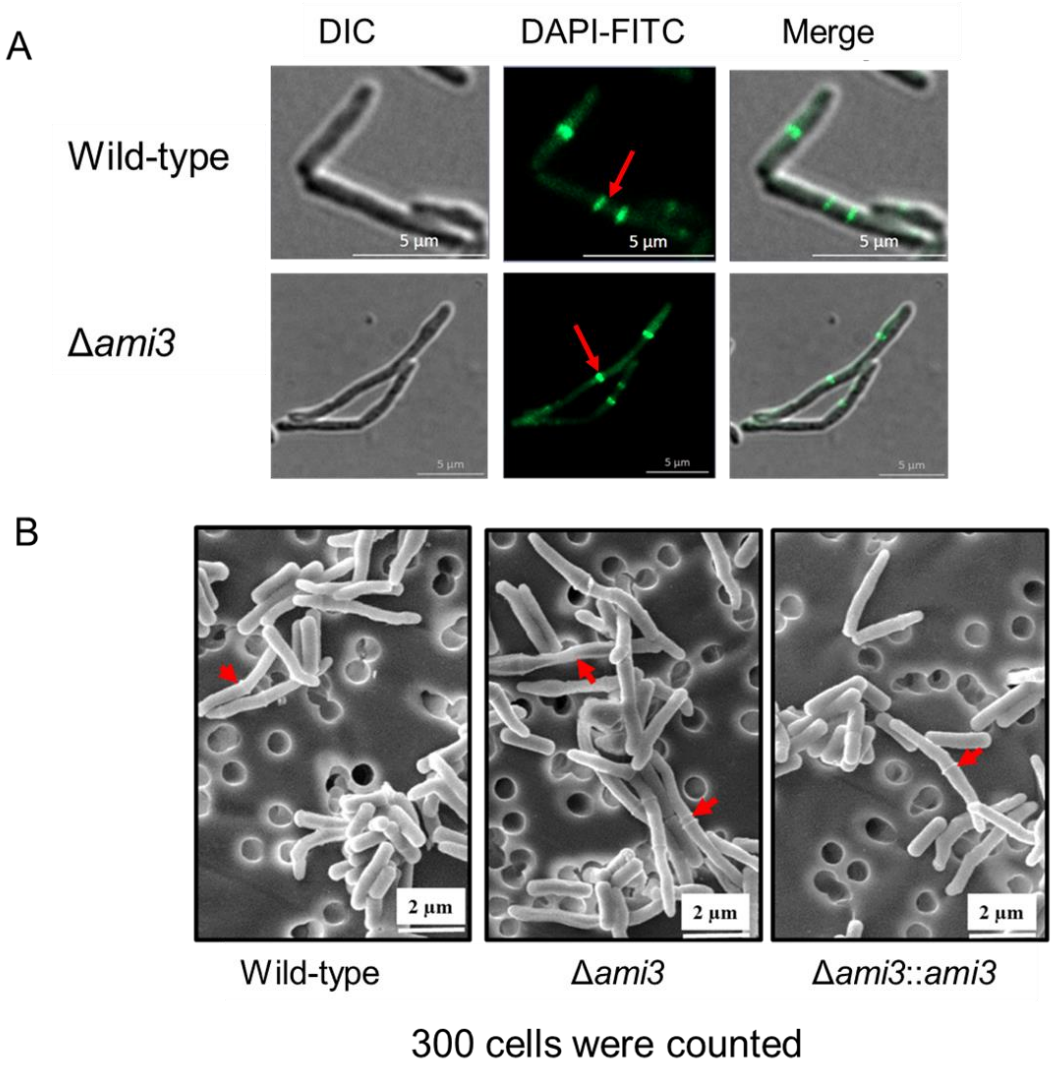

Figure 3.19: Scanning electron micrographs of Δ*ami3* and fluorescence microscopy of mycobacterial FtsZ in the Δ*ami3* background. A) Localization of GFP tagged derivative of FtsZ in the wild-type, Δ*ami3* and Δ*ami3*::*ami3* strains respectively to investigate possible altered localization pattern and function. Deletion of *ami3* leads to punctate pattern of FtsZ localization. Scale bar = 5 µm, the merge images show the localization of the respective cytoskeletal proteins in the fluorescent channel and cell shape is seen using phase contrast simultaneously. B) Exponential phase cultures fixed in glutaraldehyde and washed/ dried in varying ethanol concentrations were viewed under a scanning electron microscope to analyse bacterial cell surface. Wild-type (first panel) shows normal mycobacterial bacilli with single septa and normal length ~5 µm, the Δ*ami3* strain displayed unusually long cells with some bulging at the poles and some having irregular multiple division scars (middle panel, defects indicated by red arrows). The genetically complemented strain (Δ*ami3*::*ami3*) depicting normal cells, similar to those of the wild-type strain (normal cells in both panels indicated by red arrow).

3.6.6 Ectopic polar growth in the Δ*ami3* strain as a result of DivIVA mislocalization

Following the observations on altered cell elongation, division, morphology and PG synthesis, we hypothesized that DivIVA (Wag31), which is involved in coordination of mycobacterial cell wall elongation, is aberrantly localized in the *ami3* mutant, leading to defects in the processes of PG synthesis. To prove this, a DivIVA-GFP derivative (Maphatsoe, MSc. Unpublished, 2016) was used to determine whether DivIVA localization was affected in the Δ*ami3* strain. In wild type, DivIVA is localized to the cell poles and septa, Figure 3.20. Due to failed cell division, cells with branches were seen in the *ami3* mutant, this is discussed later. Multiple DivIVA foci were detected in the mutant strain, particularly in branching cells, suggesting that deletion of *ami3* altered cell growth, division and elongation therefore promoting DivIVA mislocalization, leading to growth at ectopic sites, (Figure 3.20)

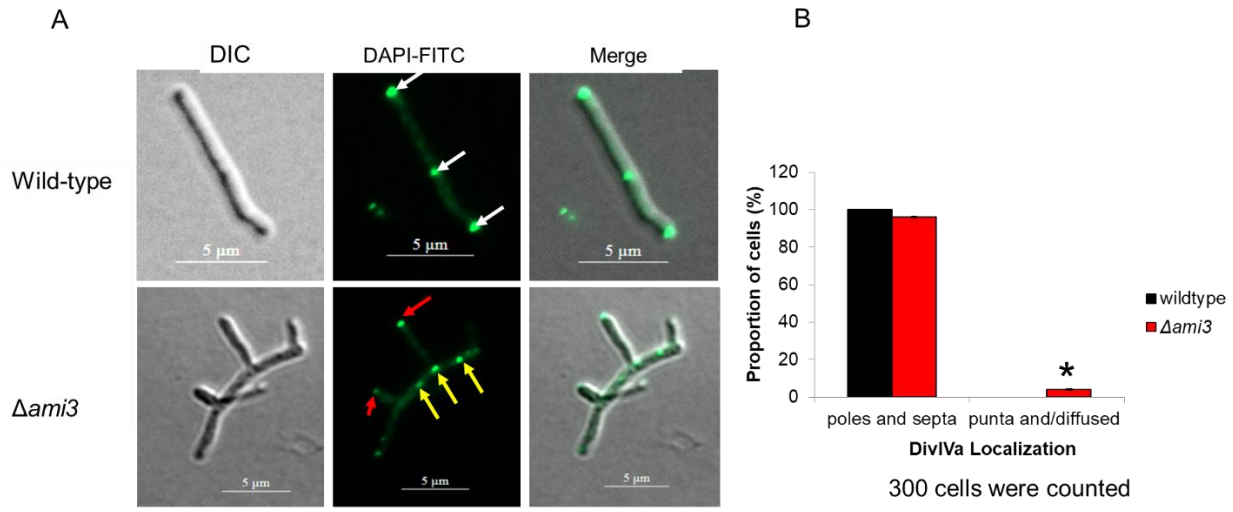

Figure 3.20: Mycobacterial DivIVA localization in Δ*ami3* background. The Δ*ami3* strain was transformed with a DivIVA-GFP derivative. Thereafter fluorescence microscopic images of DivIVA were taken to visualize localization pattern in the *ami3* mutant, with the pattern of localization quantified by calculation of the proportion of cells adopting a specific pattern. A) GFP-DivIVA localization. In the wild type, GFP-DivIVA localized to the poles and septa (shown by white arrow in first panel) whilst in the Δ*ami3* mutant, DivIVA localization adopted punctate localization (indicated by yellow arrows), landing at ectopic sites resulting in the formation of lateral branches and budding along mid-cell (indicated by red arrows). Some diffused DivIVA was noted also. B) Graphical representation of microscopic results showing the observed patterns of DivIVA localization in the wild-type and Δ*ami3* strain with 300 cells counted for each strain. The experiment was performed in triplicate to validate results. Statistical analysis was carried out using the Student's *t*-test (non-parametric) with (*) $p < 0.05$ considered significant.

To further investigate the defects seen with fluorescent microscopy, time lapse microscopy was used which allows real-time observation of bacterial growth with the use of agarose pads or customized microfluidic devices. This technique was used to compare the different strains, evaluate differences in growth, study phenotypic differences in bacterial populations and track the movement of tagged proteins. Growth of mycobacteria in 7H9 Middlebrook medium was analyzed in real time, the parental strain (wild-type) grew normally under these condition, extending at the poles and dividing at a single septa to form two daughter cells (Figure 3.21). This was evidenced by the presence of morphologically normal, rod-shaped bacteria that divided by binary fission. The loss of *ami3* led to aberrant growth characteristics with cells not only failing to divide following elongation, but also forming branches at the lateral axis (Figure 3.21), forming flat poles where new cells emerged, and forming coiled cells instead of the characteristic rods (Supplementary Figure 9). The formation of lateral and polar brunches necessitated further investigation. We therefore assessed movement of the PG synthesis directing protein DivIVA in real-time using live cell microscopy.

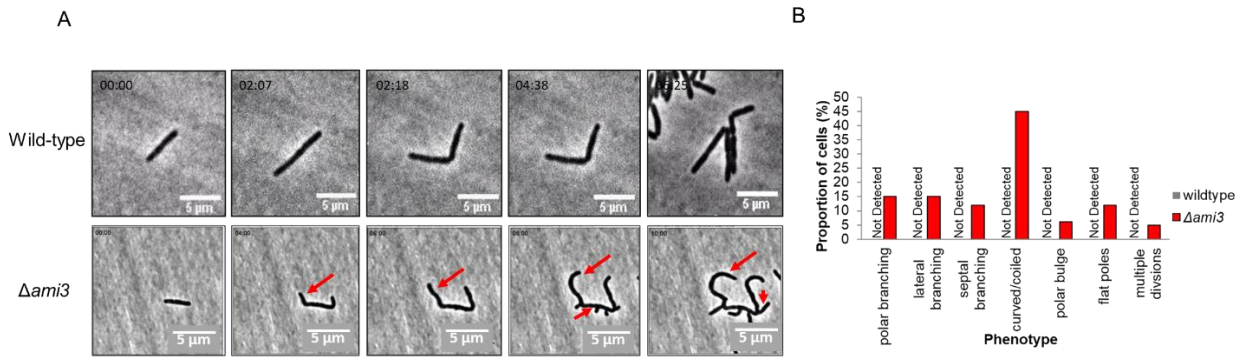

Figure 3.21: Time-lapse microscopy analysis of mycobacterial cell branching and coiling in the *ami3* mutant. A) Cells were grown and imaged in Middlebrook 7H9 media. The videos show growth of wild-type (top panel) displaying a typical growth pattern (polar extension) and cell division (single septa at mid-cell) of mycobacteria resulting in the formation of two daughter cells. The panels below depict the Δ*ami3* strain, which displays branching and coiling of cells (indicated by red arrows) suggestive of deregulated PG synthesis and cell division. Scale = 5 µm. Time frame is in hours. B) Multiple phenotypes were noted in the ami3 mutant, shown in the histogram, with the most prominent being curved/ coiled cells. None of these defects were seen with the wild type. Total micro-colonies assessed = 100 cells.

As mentioned before, DivIVA localizes at the poles and septa (sites of nascent cell wall synthesis) driving cell elongation and cell wall synthesis at the new poles following cell division. As previously demonstrated, DivIVA localizes to the cell poles and septum in wild type, Figure 3.23. However, consistent with our previous results in the *ami3* mutant, DivIVA mislocalized across the lateral axis, possibly resulting in the aberrant growth modalities observed (Figure 3.22). One of the branches underwent septal constriction with DivIVA failing to localize at the site, however, the constriction did not result in cell division as the cells remained attached, suggesting a defect in cell separation failure (Figure 3.22). Some of the micro colonies in the *ami3* mutant seem to have maintained the ability to conduct classical bacterial growth and cell division (data not shown). We hypothesize that the generation of suppressor mutants or alternative mechanisms compensating for the loss of *ami3* allowed for this.

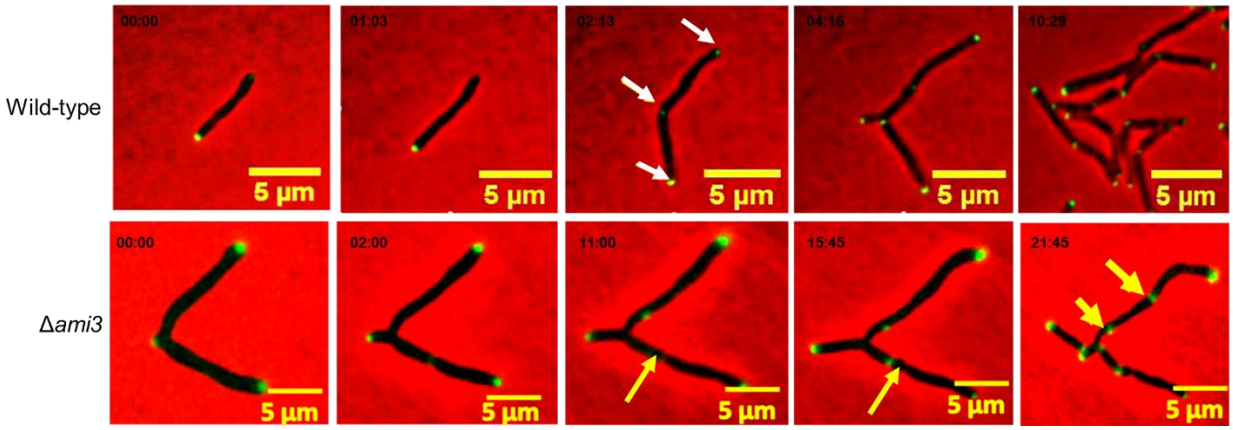

Figure 3.22: Time lapse microscopic images for DivIVA-rsEGFP localization. *M. smegmatis* wild-type and Δ*ami3* were grown in 7H9 Middlebrook medium were subjected to time lapse microscopy to assess the localization of DivIVA. In the wild type strain, DivIVA localizes at the site of active cell wall synthesis (i.e. pole and septa) indicated by the yellow arrows (first panel). However, in the Δ*ami3* strain (second panel), DivIVA localizes at ectopic sites (indicated by yellow arrows on bottom panel) in addition to the traditional sites of synthesis as indicated by the yellow arrows resulting in the formation of Y shaped cell with delayed elongation and division compared to wild-type as seen on the time stamps. **See Supplementary Video 1 in attached USB.**

3.6.7 Mycobacterial cell wall proteins potentially interact with Ami3 to coordinate bacterial cell wall synthesis and cell division

We screened for possible Ami3 interaction partners using the bioinformatics tool STRING (functional protein association networks [version 10.0]). Several possible interactions were

identified (Figure 3.23 and Supplementary Figure 5), of these, only genes whose function was known were taken further in the MPF-C assay to determine whether the hits indeed interact with mycobacterial Ami3. Plasmid constructs were designed using clone manager to ensure that the genes were in frame with the domains of mDHFR. The primers were designed by taking the gene coding sequence with the respective restriction sequences added at the 5' end. Following successful cloning, the constructs were electroporated into *M. smegmatis* parental strain (wild-type). The plasmids for the MPF-C assay were generated using the N-terminal tagging vectors pUAB300 and pUAB400. Following construction, each plasmid was restriction mapped to ensure the maintenance of the integrity of genes that were cloned (Supplementary Figure 11-16).

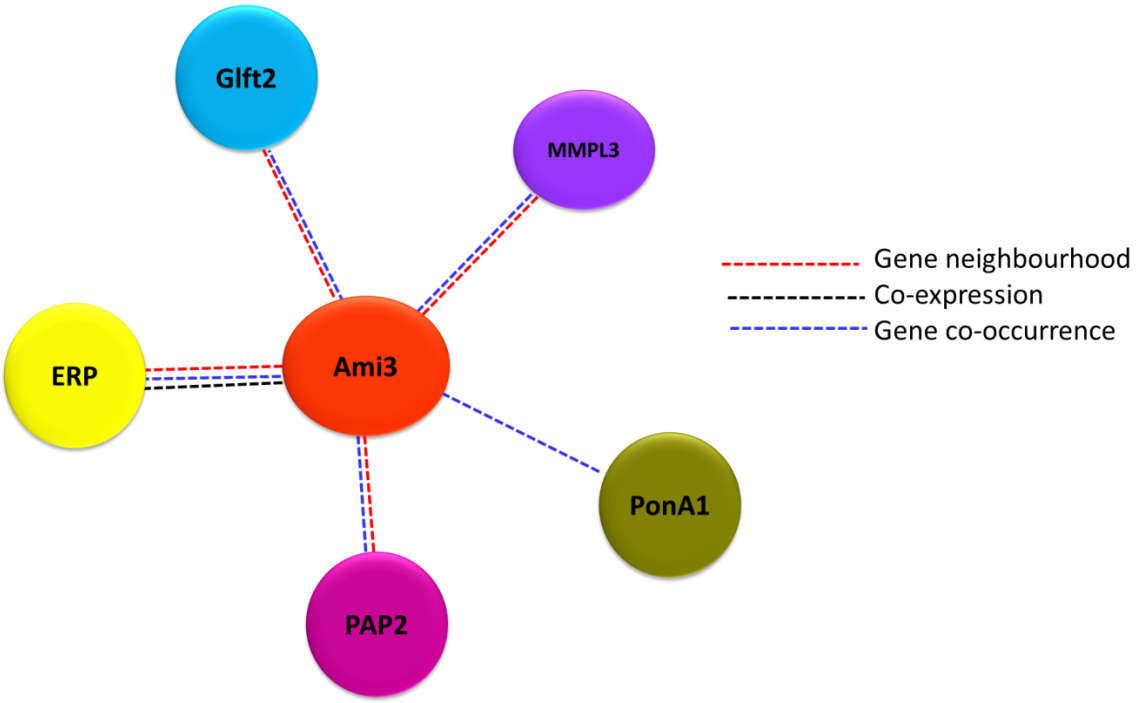

Figure 3.23: Schematic representation of possible Ami3 interacting partners as determined by the SRING database. From the STRING database results, Glft2, MMPL3, ERP, PAP2 and PonA1 emerge as possible Ami3 interacting partners and were chosen for further investigation. The dotted lines depict the types of interactions predicted by the database, i.e. red dotted lines are indicative of genes predicted to be in the same neighborhood, blue dotted lines are genes that have been shown to occur during similar processes and lastly black dotted lines indicate genes that are co-expressed.

Plasmids that were constructed to probe for interactions were co-electroporated into the *M. smegmatis* parental strain and plated on 7H10 Kan/Hyg plates. The transformants were selected

and subcultured onto 7H10 Kan/ Hyg/ 7.5 µg/ml TRIM and subsequently 15 µg/ml TRIM to assess the strength of the interaction (Figure 2.3). As expected, extensive growth in 7.5 µg/ml and 15 µg/ml TRIM was observed in the positive control, which was the RipA_RpfB strain where the interaction has been previously reported (Hett et al., 2008) and no growth was seen in the negative control (pUAB300_pUAB400). A screen of the chosen genes was performed to determine which of the possible partners interact with Ami3. From the proteins selected, the galactofuranosyltransferase (GlfT2), which catalyzes the polymerization of the galactan domain of AG, the Mycobacterial membrane protein Large (MmpL), whose role in *Mtb* has been linked to virulence in mice, and the penicillin binding protein (PonA1), responsible for ensuring coordinated cell growth and division through the synthesis of PG, displayed growth on low concentrations of Trim (Figure 3.24). However, with increasing TRIM concentration, the Gflt2-Ami3 pair displayed impaired growth, suggesting that the interaction between these proteins was weak, or possibly non-specific (Figure 3.24). The Phosphatidic acid phosphatase (PAP), which catalyzes the dephosphorylation of phosphatidic acid (PA) to yield diacylglycerol (DAG), a key precursor for TAG biosynthesis and the extracellular protein family (Erp) failed to grow in the presence of TRIM, suggesting the lack of physical interaction with the amidase Ami3 (Figure 3.24). Hence this analysis yielded PonA1 and MmpL as possible interacting partners for Ami3.

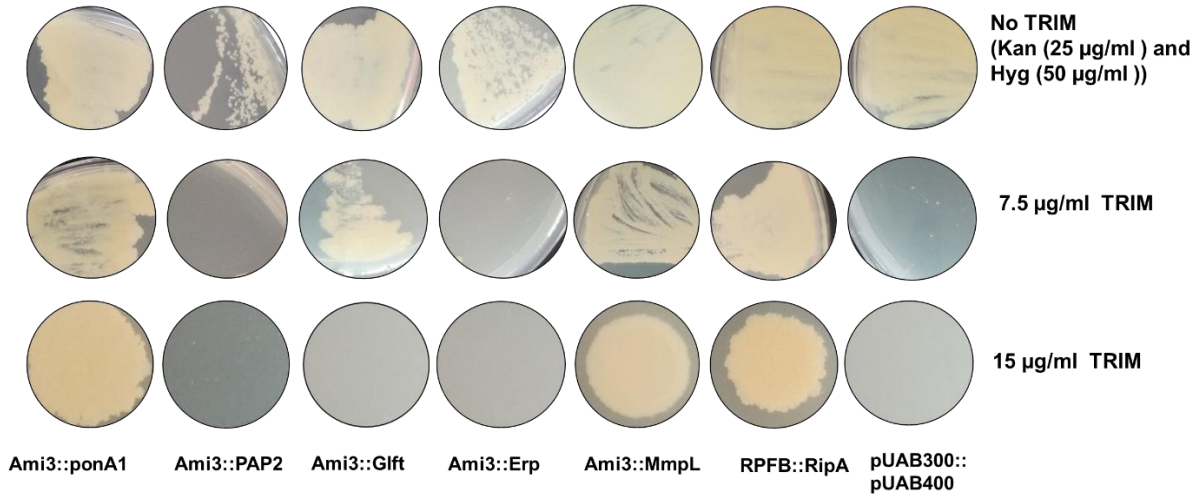

Figure 3.24: Ami3 interacting partner screening using the M-PFC assay. Shown is the growth of *M. smegmatis* on agar plates. *M. smegmatis* cells (mc^2155) were independently transformed with M-PFC plasmid pairs producing: Ami3[F1,2]_PonA1[F3], Ami3[F1,2]_PAP2[F3], Ami3[F1,2]_Glft2[F3], Ami3[F1,2]_Erp[F3] and Ami3[F1,2]_MmpL[F3], with RipA[F1,2]_RpfB[F3] and pUAB300_pUAB400 serving as the positive and negative control respectively. The text in parenthesis refers to the fragment of the mDHFR to which the gene of interest was

fused. See material and methods for further details. Transformants were subcultured in 7H10 medium with TRIM (7.5 µg/ml and 15 µg/ml), Kan (25 µg/ml) and Hyg (50 µg/ml) and incubated at 37 °C for 3-7 days. Growth is indicative-of protein-protein association, as seen in Ami3[F1,2]_PonA1[F3] and Ami3[F1,2]_MmpL[F3] at the highest concentration of TRIM.

3.7 Phenotypic characterization of Δ*ami4* strain

3.7.1 Loss of *ami4* has no effect on *M. smegmatis* growth in axenic culture

Growth analysis was performed to examine the effects of *ami4* deletion in *M. smegmatis*. Previous work has demonstrated no growth defects in an *E. coli ampD* deficient strain, closely related to the *M. smegmatis ami4*. Consistent with this, no growth defects were seen in the *M. smegmatis* Δ*ami4* strain, in contrast, the mutant strain grew slightly faster than its wild type counterpart and genentic complement, reaching exponential phase at an accelerated rate (Figure 3.25 A). However, this defect was not considered significant as CFU counts revealed no difference in the colony forming ability of the parental or complemented strains versus the mutant strain (Figure 3.25 B).

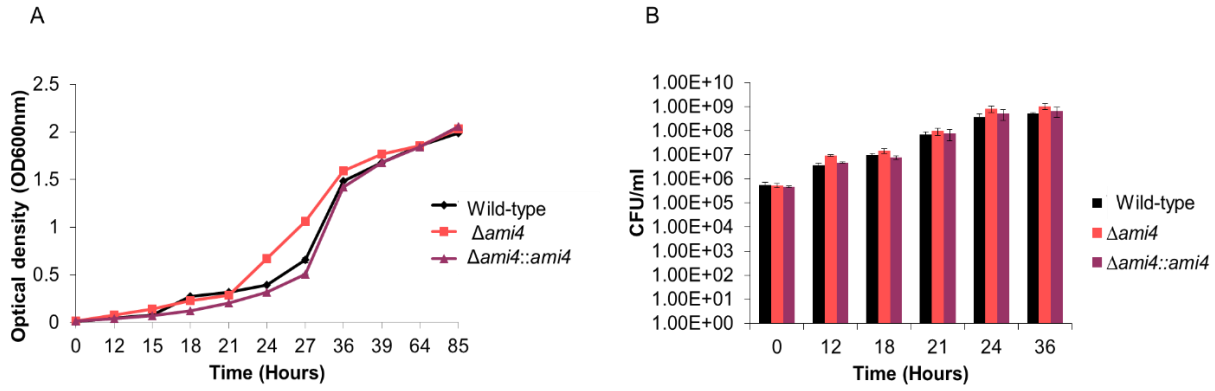

Figure 3.25: Growth kinetic analyses of Δ*ami4 M. smegmatis* strain. Growth was monitored by optical density (A) and by CFUs (B). Growth of the parental strain *M. smegmatis* wild-type (black), *M. smegmatis* Δ*ami4* (peach) and *M. smegmatis* Δ*ami4*::*ami4* (purple) was conducted in Middlebrook 7H9 media monitored at three hour intervals. The values shown are the average of three independent replicates. The Δ*ami4* strain in axenic culture reached exponential phase at a faster rate compared to the wild-type and Δ*ami4*::*ami4*. Although a difference in growth was seen in axenic culture, quantification of growth using CFU did not confirm the results seen in panel A. Error bars are representative of standard error of the mean (SEM), Student's *t*-test (non-parametric) with (*) $p < 0.05$ considered significant.

3.7.2 Loss of Ami4 affects biofilm formation and teicoplanin tolerance

We next assessed whether the disruption of Ami4 negatively impacted the ability of *M. smegmatis* to form stable biofilms as characterized by an intricate thick textured reticulation pattern on the surface of pellicle biofilms. The deletion of *ami4* had no impact on biofilm formation, similar to the loss of Ami3 as the strain was able to form a corded biofilm. However, quantification of biomass revealed a reduction in biomass implying that the total amount of organisms were affected (Figure 3.26A). This defect was not reverted in the genetically complemented strain, which also showed signs of reduced biomass. Inclusion of the vector only control (pTweety Δ*ami4)* confirmed this was a result of the addition of a Kanamycin harboring vector, which may have affected biofilm formation (Figure 3.26A).

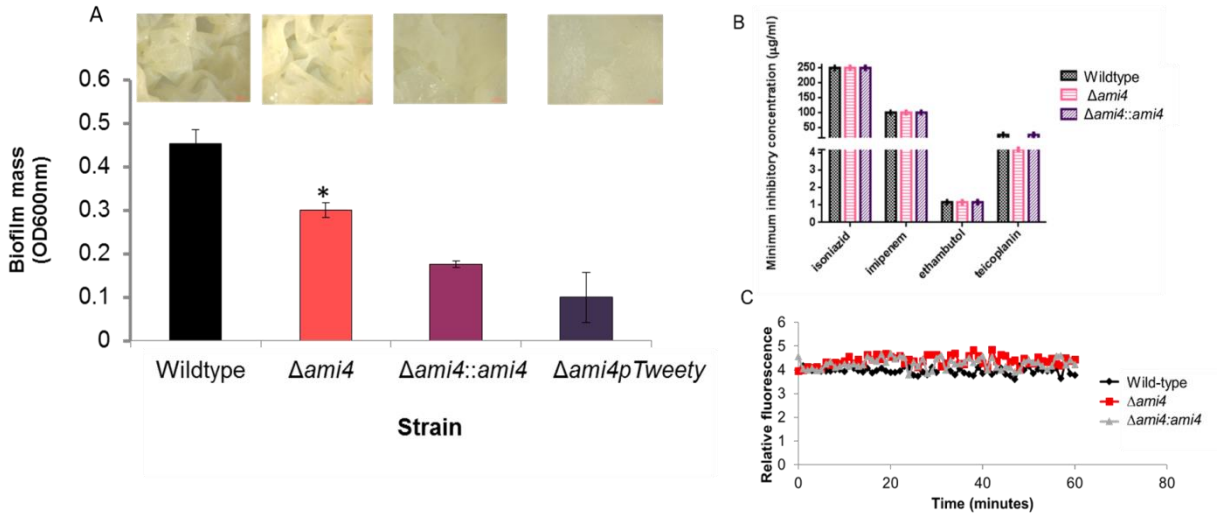

Figure 3.26: Biofilm formation, antibiotic susceptibility and ethidium bromide diffusion in the *ami4* mutant. Biomass was determined by crystal violet staining. Results show the means of three independent experiments with triplicate samples. (A) Shown is the biofilm and amount of biomass in the wild-type, Δ*ami4* and genetically complemented strain Δ*ami4::ami4*, a difference in biomass was seen in the Δ*ami4*, however, presence of kanamycin cassette seems to affect biofilm and biomass in the genetically complemented strain (B) Minimum inhibitory concentration with isoniazid, imipenem, ethambutol and teicoplanin was calculated as fold change using the wild-type as reference strain, Δ*ami4* showed sensitivity to teicoplanin only. (C) Ethidium bromide assay for analysis of cell wall permeability was performed, with no significant difference observed. The statistical differences between the wild-type and mutant was determined using the Student's *t*-test (non-parametric) with $p < 0.05$ considered significant

Following this, we investigated the effect of cell wall targeting antibiotics on the survival of the Δ*ami4* strain (Figure 3.26 B). Loss of Δ*ami4* did not render *M. smegmatis* more susceptible to isoniazid, imipenem or ethambutol however, reduced tolerance to teicoplanin was observed (Figure 3.26 B), suggesting impairment of cell wall remodeling and or permeability. To further investigate whether this susceptibility to teicoplanin could possibly be attributed to increased cell wall permeability or a disturbance in cell membrane pumps, we used the ethidium bromide diffusion assay outlined in Section 2.6.5. No difference in permeability was observed using the fluorescence intensity of ethidium bromide (Figure 3.26C).

3.7.3 Ami4 has a role in PG synthesis coordination

Peptidoglycan hydrolases have been implicated in cell wall homeostasis and loss of function has thus been shown to have detrimental effects on the maintenance of the mechanisms responsible for not only for PG synthesis but also bacterial shape (Frirdich and Gaynor, 2013). As stated in Section 3.7.1, deletion of *ami4* does not have obvious effects on growth either in liquid or on agar, however the marginal increase in susceptibility to teichoplanin led us to hypothesize that there must be defects in PG synthesis when *ami4* is deleted. Mycobacteria grow by incorporating PG at their poles and septa unlike their rod-shaped counterparts, *E. coli* (Kieser *et al*., 2015). Analysis of *M. smegmatis* wild type and genetically complemented strain indicated the expected pattern of PG synthesis (Figure 3.27). However, the ∆*ami4* strain incorporated D-Ala across the lateral axis of the cell resulting in the formation of short fat cells. This clearly indicates a defect in regulation of the PG synthesis machinery. To further elucidate these results, both the PG synthesis and cell length phenotype were quantified and as shown in the microscopy results, loss of *ami4* leads to distorted PG biosynthesis and thus alterations in cell shape (Figure 3.27)

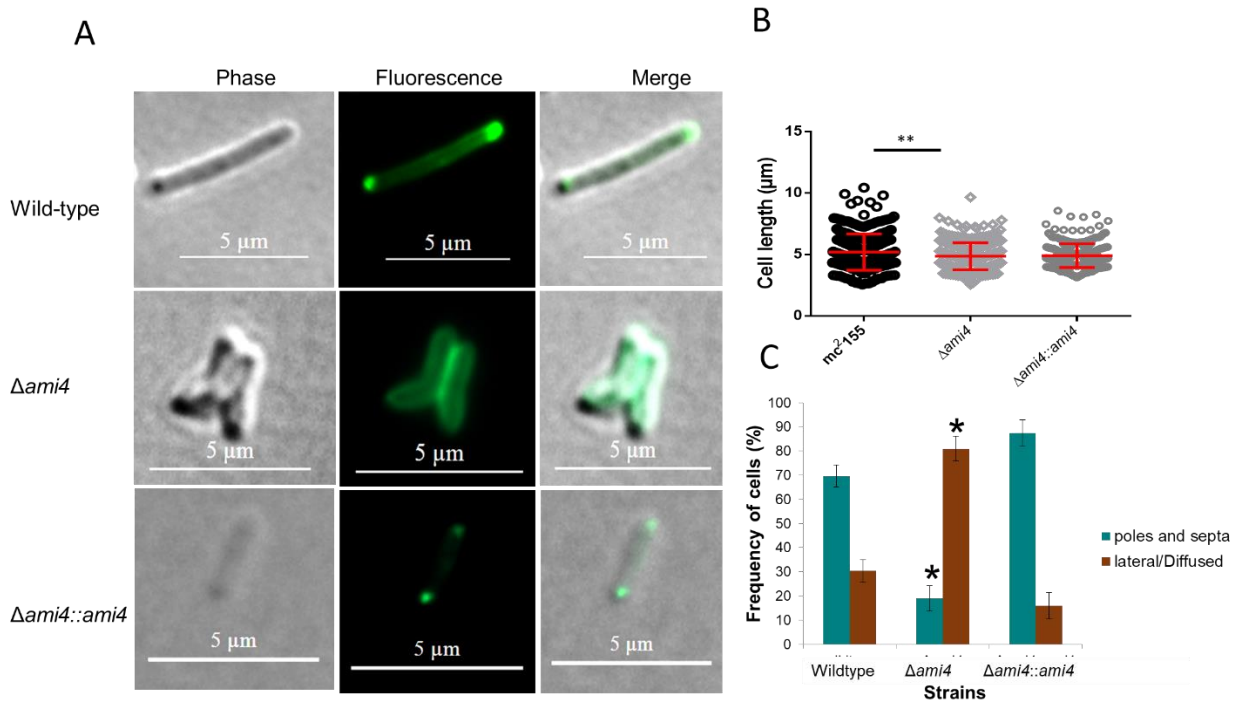

Figure 3.27: *M. smegmatis* Ami4 modulates cell length and shape. (A) Fluorescence microscopy carried out to study alterations in PG synthesis using D-ala and click chemistry. As expected, staining was observed at the cell poles for wild type, *ami4* mutant cells did not display this pattern of staining. Deletion of the *ami4* gene in *M. smegmatis* resulted in altered cell length and width, with cells appearing fatter and shorter than the parental strain. (B) Bacterial cell length quantification depicted in graphical form confirmed the results observed in the microscopic images, with Δ*ami4* cells being shorter than the wild-type. (C) Nascent PG staining patterns are shown (Histogram) with Δ*ami4* colonies appearing marginally different from those of the wild-type. Cells appear to be shorter as measured previously and incorporate new PG axially rather than at the poles, as seen with the staining pattern. Three independent experiments were conducted with 100 cells counted for each replica. Statistical analysis was carried out using the Student's *t*-test (non-parametric) with * indicative of $p < 0.05$ and ** indicative of $p < 0.01$, considered as significant.

3.7.4 Loss of Ami4 results in cell death

The maintenance of bacterial cell shape, septation and autolysis is primarily governed by PG hydrolases and the loss of Ami4 appears to impact some of these features. To further investigate this, live cell imaging was employed to gain a better understanding of the overall impact of this. The loss of Ami4 resulted in growth/division defects that were suggestive impaired PG synthesis/homeostasis. Loss of Ami4 also led to the formation of septal bulges, which later became polar bulges and rounding of poles resulting in the formation of short fat cells (Figure

3.28). Furthermore, this dysregulation in PG synthesis in the *ami4* deficient strain resulted in extrusion of cell wall material which is a sign of dysregulated PG synthesis and cell wall rigidity and later on, cell death (Supplementary Figure10).

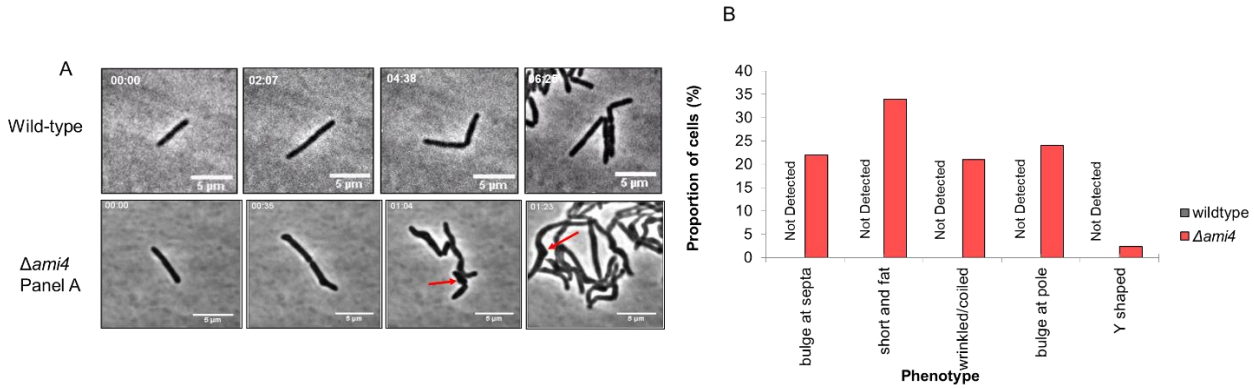

Figure 3.28: Time-lapse microscopy analysis of cell branching, bulging and bursting in the *ami4* mutant. Cells were grown and imaged in Middlebrook 7H9 media. (A) The videos show growth of wild-type (top panel) with the typical growth pattern (polar extension) and cell division (single septa at mid-cell) of mycobacteria. The bottom panel shows the Δ*ami4* strain, which forms branches, fat cells and Y-shaped cells suggestive of deregulated PG synthesis. Scale = 5 µm. Time frame is in hours. (B) Quantification of the multiple phenotypes noted in the time-lapse videos with the most prominent being short fat cells. Total micro-colonies assessed 100 cells.

3.7.5 Mislocalization of DivIVA alters mycobacterial growth dynamics

The previous observations demonstrated the emergence of lateral branches and ectopic polar growth indicative of misdirected cell wall synthesis, possibly through the mislocalization of elongasome enzymes recruited to the poles. In addition to this, strikingly altered morphology was seen, with cells forming bulges at the septa and release of cell wall material (Supplementary Figure 10). From previous work, it is known that DivIVA is responsible for maintaining bacterial cell morphology and determining the pattern of cell wall biogenesis at the poles, therefore DivIVA localization in the mutant and wild-type strain was monitored by creating a DivIVA-GFP tagged derivative (vector obtained from Maphatsoe MSc. 2016, unpublished), and localization patterns visualized using time lapse microscopy. Loss of *ami4* led to a “patchy” DivIVA fluorescence pattern, which was unlike that seen for wild type wherein fluorescence was seen at the poles and septa as expected (Supplementary Figure 7). Next, DivIVA localization was visualized using time lapse microscopy which enables real time visualization during bacterial growth. The videos (Figure 3.29) validated the results seen in Supplementary figure 7. In

addition, formation of ectopic sites of growth was either accompanied or preceded by DivIVA mislocalization along the lateral axis of the cell or subpolar region, resulting in the formation of branches (Figure 3.29). In addition to this, DivIVA was unstable leading to bacterial cell death in some instances (Figure 3.29).

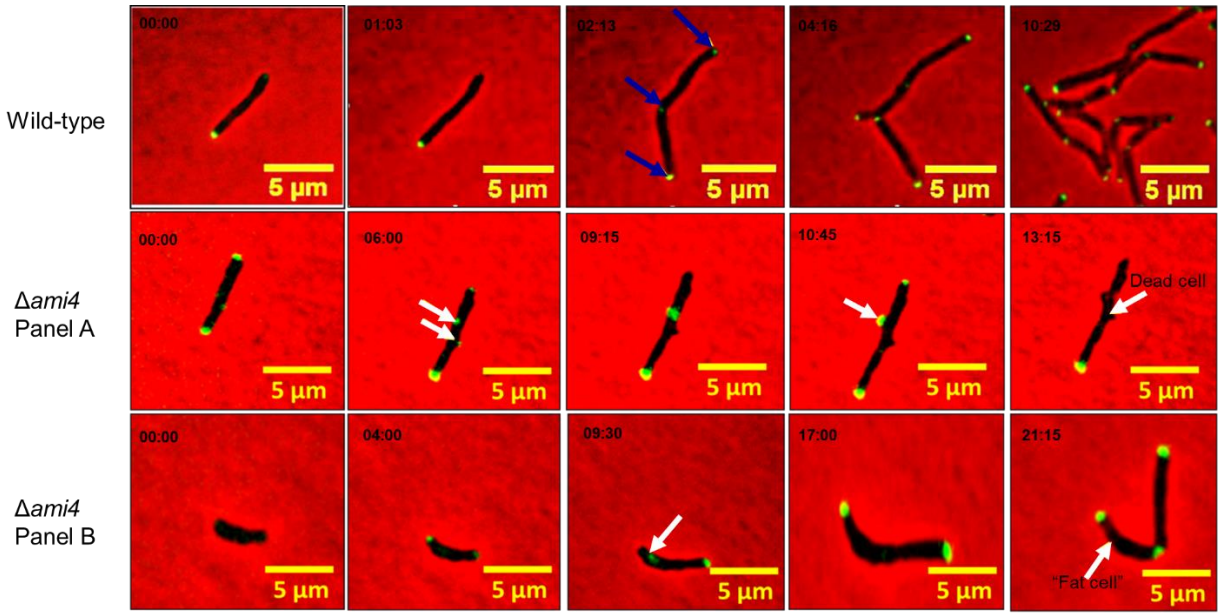

Figure 3.29: DivIVA fails to assemble properly in the Δ*ami4* strain. Time-lapse microscopy analysis of DivIVA-GFP localization in the *M. smegmatis* wildtype and Δ*ami4* strain. Strains were grown in 7H9 Middlebrook and subjected to time-lapse microscopy. (First panel) Wild-type DivIVA localization at the poles and septa (classical sites of active growth). (Panel A and B) In the Δ*ami4* DivIVA localizes at more than one site along the cell and seems unstable leading to the formation of branches, fat cells and death in some cells. **See Supplementary Video 2 in attached USB.**

3.8 Role of the amidase_2 domain containing protein, Ami5, in bacterial cell length maintenance and cell wall homeostasis

3.8.1 Loss of Ami5 has no effect on *M. smegmatis* growth in axenic media

As Ami5 shares high homology with Ami4, we initially hypothesized that these proteins could perform redundant functions. With that possibility in mind, we studied Ami5 further to determine whether it had evolved to perform a distinctive function or whether it functionally overlapped with Ami4. Growth kinetics analyses of wild-type, the *ami5* deficient mutant strain and genetically complementation strain Δ*ami5*::*ami5* were conducted by inoculation of strains in

7H9 Middlebrook/ Sauton's media. An increased growth rate was observed for the *ami5* knockout strain in both 7H9 and Sauton's minimal media (Figure 3.30 A and B). To some extent, these differences reflected in the CFU analysis, but they were not statistically significant (Figure 3.30 C).

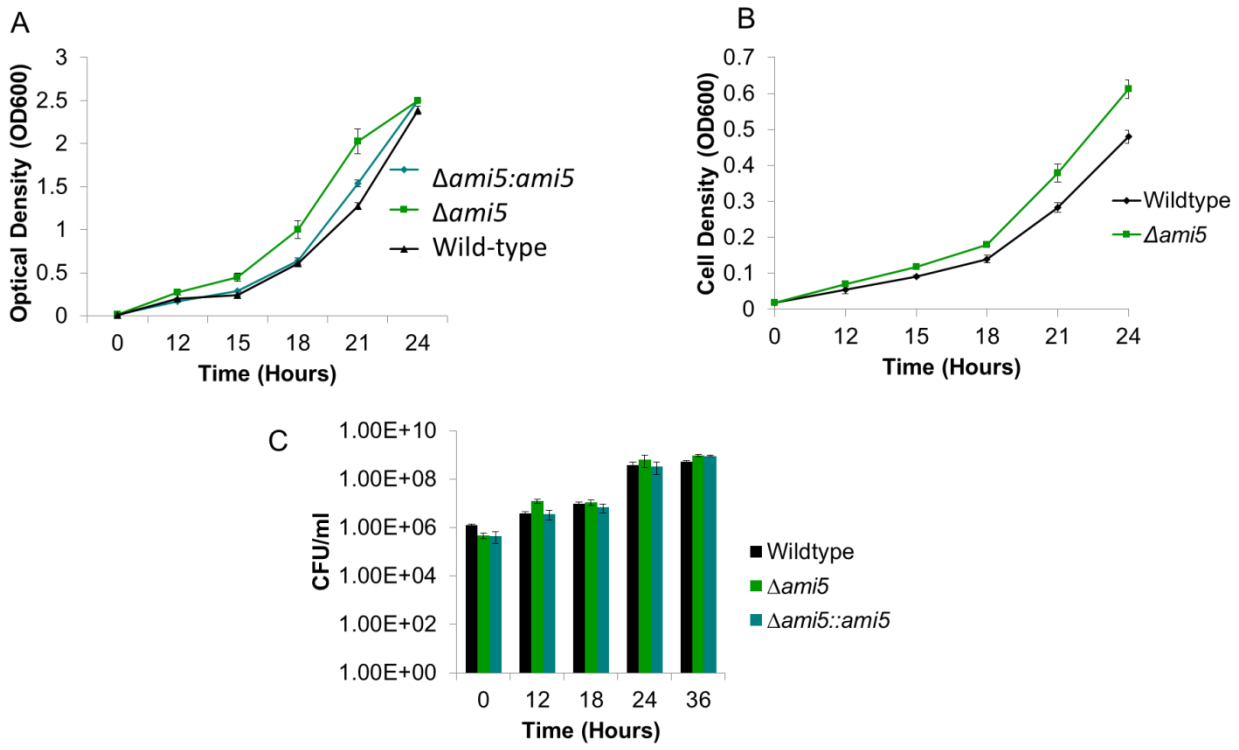

Figure 3.30: Growth kinetic analysis of Δ*ami5* strain in relation to wild-type and complement. (A and B) Growth of parental strain *M. smegmatis* mc^{2}155 wild-type (black), *M. smegmatis* Δ*ami5* (green) and *M. smegmatis* Δ*ami5*::*ami5* (blue) in Middlebrook 7H9 and Sauton's minimal media monitored by measurement of OD_{600} at three hour intervals. (C) Growth analysis of viable bacteria was measured by CFU counts. The values shown are the averages of three separate experiments. Error bars are representative of standard error of the mean (SEM), Student's *t*-test (non-parametric) with (*) $p > 0.05$ considered non-significant

3.8.2 Loss of Ami5 results in resistance to ethambutol and vancomycin

As with the other mutants generated in this study, we sought to investigate the inhibitory effect of cell wall targeting antibiotics on the Δ*ami5* strain. The β-lactam antibiotics imipenem and amoxicillin had no effect on the Δ*ami5* mutant when compared to the parental strain, this was also seen when the strain was exposed to cycloserine and teicoplanin (Figure 3.31).

Unexpectedly, exposure of Δ*ami5* to ethambutol resulted in an increase in resistance to the arabinosyl transferase inhibitor, possibly indicative of decreased permeability of the cell wall (Figure 3.31 A). In addition to this, a two-fold increase in resistance was observed with vancomycin. Overall, these results demonstrate that the defects seem to be distinct from those observed in the *ami3* and *ami4* deficient mutants, suggesting that Ami5 may have evolved distinct functions. Due to difficulties experienced in growing the complement strain as it was later contaminated and along with time constraints, the Δ*ami5*::*ami5* complementation strain was not included in the MIC experiment. Subsequently, the ethidium bromide assay was used as an indicator of cell wall permeability and the extent of cell membrane pump activity. No significant difference was observed between the wild-type and the Δ*ami5* mutant strain indicating that resistance cannot be attributed to a decrease in cell wall permeability (Figure 3.31 B).

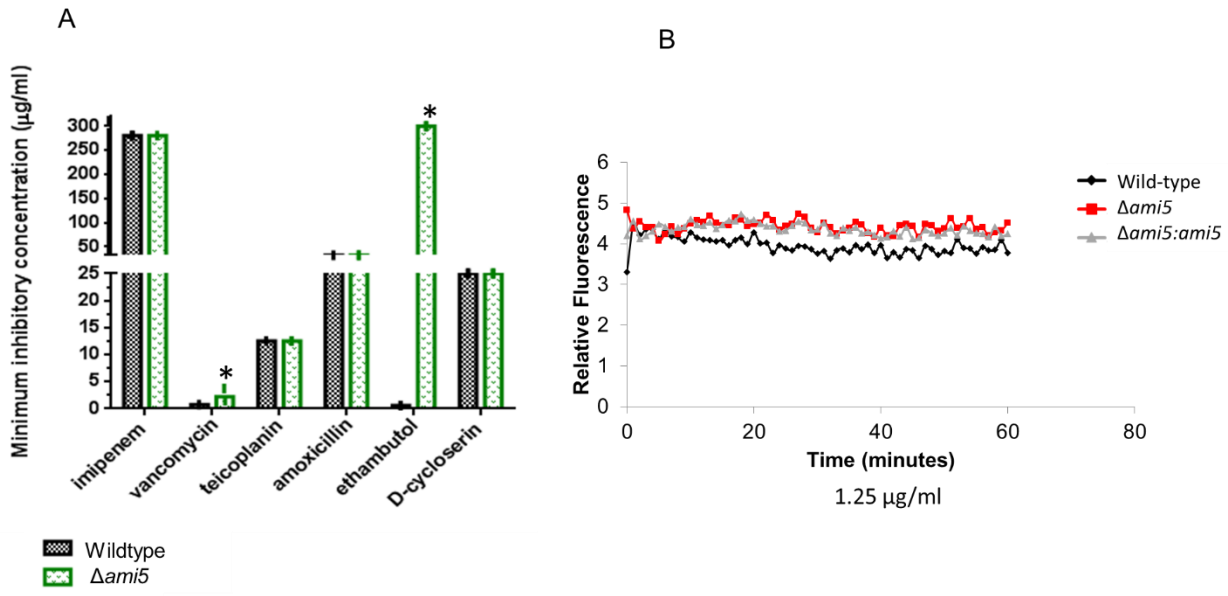

Figure 3.31: **Drug susceptibility assays and ethidium bromide diffusion in Δ*ami5* *M. smegmatis* strain**. Experiments were set up independently in triplicates. A) The Δ*ami5* strain was grown in the presence of different cell wall targeting antibiotics in a 96 well plate for 7 days. Bacterial survival was measured by the visible formation of a pellet at the bottom of the well. Exposure to ethambutol and vancomycin yielded an increased resistance to both antibiotics. B) Wild-type, Δ*ami5* and Δ*ami5*:: *ami5* strains were grown to OD_{600}=0.4, washed twice in PBS, exposed to 1.25 µg/ml of ethidium bromide and incubated at 37 °C for 1 hour, with absorbance taken every 60 seconds. Results show that loss of *ami5* does not affect the permeability of the cell wall. The statistical differences between wild-type and mutants were determined using the Student's *t*-test (non-parametric); with (*) $p < 0.05$ considered significant.

3.8.3 Loss of Ami5 results in the formation of mini cells

To determine whether deletion of Ami5 affects PG synthesis or sites of synthesis, biosynthesis of *M. smegmatis* PG was investigated as previously described for the other mutants. Loss of *ami5* resulted in the formation of mini-cells with an average length of 1 µm to 5 µm, shorter than wild-type, these cells incorporate nascent PG at the poles and future septa as in the parental strain (Figure 3.32 A). From this, it appears that although cell division was affected, the ability of the cells to grow via polar addition of new PG remained was maintained (Figure 3.32 A). Furthermore, quantification of stained cells confirmed our initial observations indicating a large number of cells in the Δ*ami5* strain were less than 2 µm in length and yet maintained the conventional PG staining pattern (Figure 3.32 B and C).

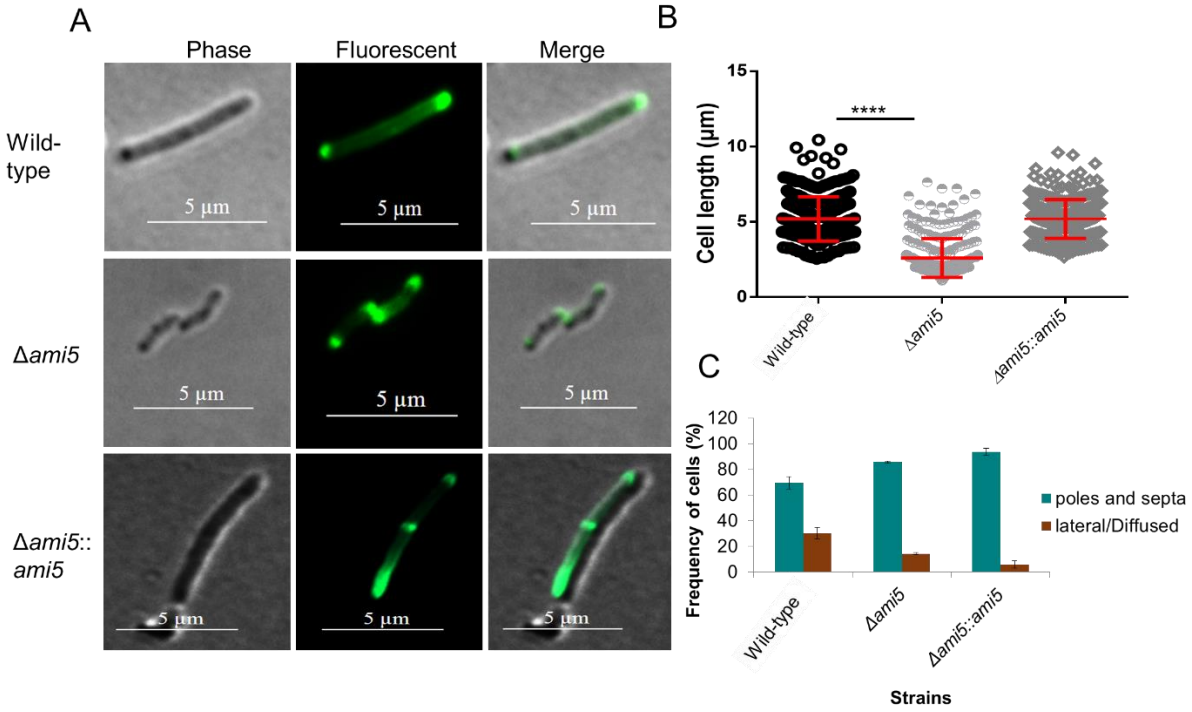

Figure 3.32: *M. smegmatis ami5* modulates cell shape. (A) Deletion of the *ami5* in *M. smegmatis* resulted in altered cell length with some of the cells appearing shorter than the parental strain, however maintaining the canonical nascent PG staining pattern seen in wild-type mycobacteria. (B) Cell length quantification of the wild-type, Δ*ami5* and Δ*ami5*::*ami5* indicate that the loss of *ami5* severely altered cell *M. smegmatis* cell length. (C) Quantitative analysis of staining patterns adopted by the wild-type, Δ*ami5* and Δ*ami5*::*ami5* strains. Loss of *ami5* did not have a significant effect on mycobacterial PG incorporation as the staining pattern was maintained throughout. Statistical analysis was carried out using the Student's *t*-test (non-parametric) with (****) $p < 0.001$ considered significant.

Scanning electron microscopy is an excellent tool for investigating ultrastructure of microorganisms as it reveals morphological features of isolated organisms. Nano-SEM was used to determine changes in bacterial cell architecture as a result of *ami5* deletion. Mycobacterial cells grown in Middlebrook 7H9 exhibited a smooth surface with cells forming rods of normal size. However, cells lacking the *ami5* gene formed short cells (Figure 3.33), validating the fluorescence microscopy results, Figure 3.32. However, it should be noted that this was a heterogeneous observation as the *ami5* deletion strain seemed capable of forming cells of normal length also. The phenotype was reverted back to wild-type levels with the complementation of the gene.

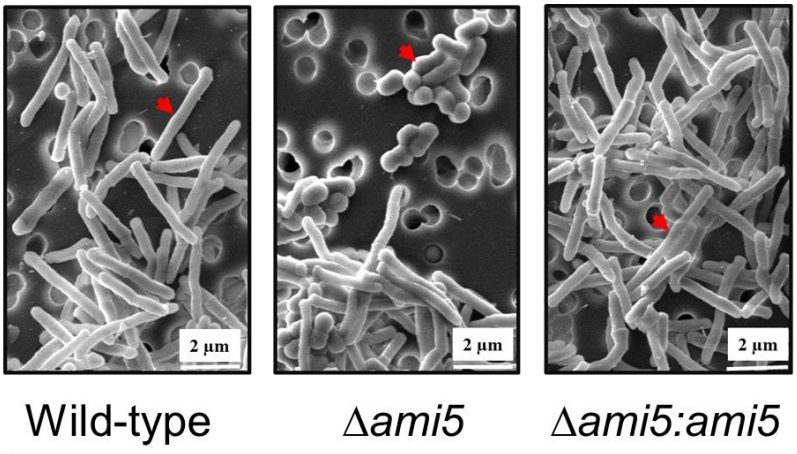

Figure 3.33: Scanning electron microscopy of wild-type, Δ*ami5* and Δ*ami5*::*ami5* strains. Cells were cultured in Middlebrook 7H9, followed by fixation in gluteraldehyde in preparation for viewing using SEM. Wild-type (far left) cells formed smooth rods and grew to normal size, the loss of *ami5* (middle) led to formation of short cells with some appearing normal. The phenotype was reverse by complementation, with cells forming expected sized bacilli (Panel-far right).

3.8.4 Loss of Ami5 leads to the formation of short cells

Confocal microscopy and SEM micrographs were confirmed by time lapse microscopy videos which enabled the monitoring of these strains in real time utilizing agarose pads or a customized microfluidic device. From this it was evident that the loss of Ami5 led to the formation of what appeared to be mini cells but strangely were incapable of propagating (Figure 3.34). We hypothesized that these could be membrane blebs, which result at the late stages of apoptosis

(Figure 3.34). As expected the cells with these extrusions lysed and died. In addition to this, the live cell imaging showed the development of bulging poles in the Δ*ami5* strain, resulting in unipolar growth.

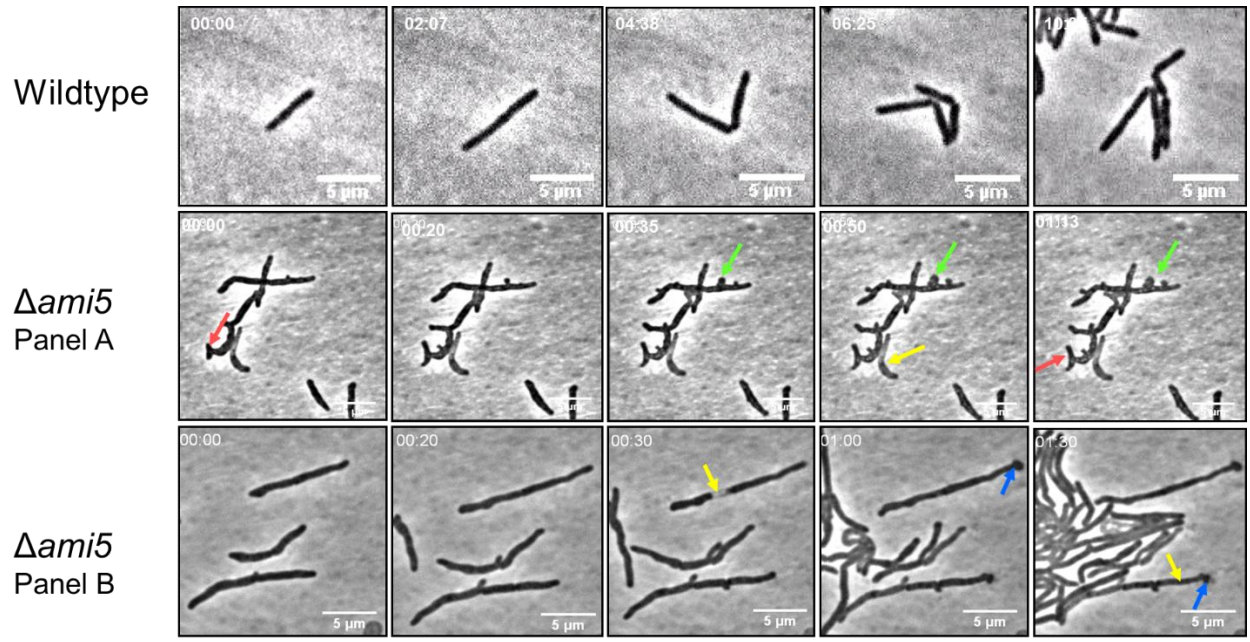

Figure 3.34: Time-lapse microscopy analysis of Δ*ami5* pole rounding and cell death Cells were grown and imaged in Middlebrook 7H9 media. The videos show growth of wild-type (top panel) showing typical growth pattern (polar extension) and cell division (single septa at mid-cell) of mycobacteria, resulting in the formation of two daughter cells. Panel A: *M. smegmatis* Δ*ami5* time lapse microscopy images showing formation of membrane blebs (green arrow), formation of flat poles which eventually form new cells (indicated by red arrows) and cell death (shown by yellow arrow), suggestive of dysregulated PG synthesis and cell division. Panel B: *M. smegmatis* Δ*ami5* strain time lapse microscopy images showing deregulated PG synthesis seen through the formation of rounding poles (indicated by blue arrows) and eventual loss of cell wall material followed by a speedy recovery (indicated by yellow arrow). Scale = 5µm; Time frame is in hours

3.8.5 Loss of Ami5 leads to formation of viable short cells

A plethora of hydrolases are involved in the maintenance of normal mycobacterial cell length and size, in addition to this, the placement of the division septum and timing of cytokinesis is coordinated with chromosomal replication and segregation (Männik and Bailey, 2015). Following our observations with SEM and Click chemistry, we decided to investigate whether

the formation of short cells might be a result of FtsZ mislocalization. A GFP tagged derivative of FtsZ was created (Senzani *et al*., 2017) and used to transform the wild-type and Δ*ami5* strain. Both strains were cultured in Middlebrook 7H9 supplemented with the appropriate antibiotics and grown to early exponential phase. Strains were viewed under DIC and FITC to investigate possible changes in phenotype as a result of *ami5* deletion. As mentioned before, mycobacteria grow asymmetrically along their poles with 80 % of mid log phase cells dividing symmetrically and around 5-10 % adopting an asymmetric cell division pattern (Vijay *et al*., 2014). Therefore, we sought to investigate cell division in Δ*ami5* strain so as to investigate the resulting "mini cells". A GFP-tagged derivative of FtsZ (Senzani et al., 2017) was used to transform wild-type and Δ*ami5* strain. As expected, FtsZ in the wild-type strain formed two foci which eventually coalesced to form one focus at the septum resulting in cell division and the formation of two daughter cells (Figure 3.35). Loss of *ami5* surprisingly had no obvious effect on FtsZ localization when compared to the wild type strain despite the formation of "mini cells" in this strain (Figure 3.35).

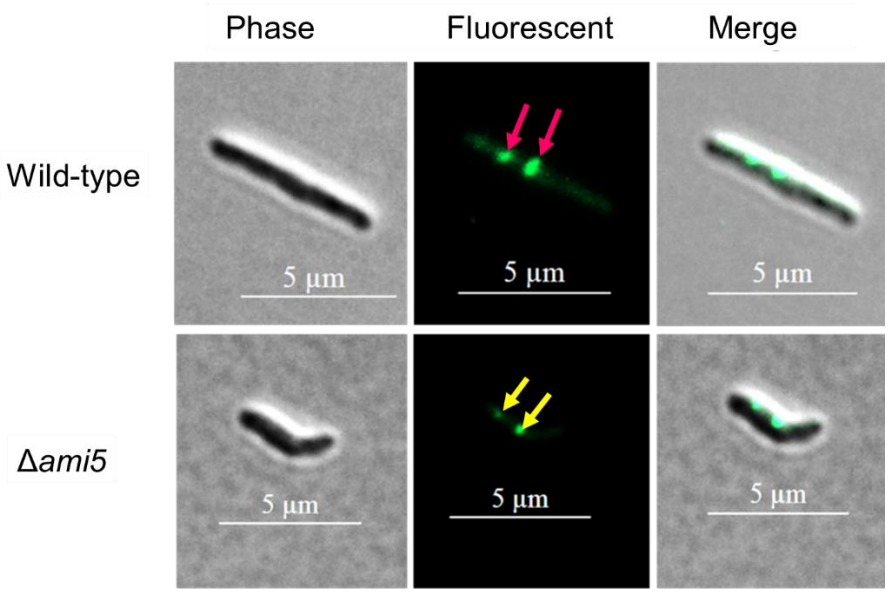

Figure 3.35: Confocal microscopy showing FtsZ localization in wild-type and Δ*ami5* strains. A GFP tagged derivative of FtsZ generated was used to transform wild-type and Δ*ami5* strains. The wild-type strain displays normal mid-cell localization of FtsZ with cells showing two FtsZ foci that later bundle together to form a single focus (pink arrows). The Δ*ami5* strain displays the same pattern of localization in the short cell, showing that loss of this amidase does not affect FtsZ polymerization (yellow arrows).

4. Discussion

Tuberculosis continues to be a thorn in the health system with its relentless onslaught being fueled by inherent tolerance to lethal concentrations of antibiotics. In addition, tubercle bacteria have developed strategies to circumvent host immune detection and killing thus enabling growth within the toxic environment of host macrophages. Furthermore, the prolonged multi-drug regimen needed to achieve bacterial clearance is difficult for health care systems and is thought to drive *Mtb* dormancy (Zumla *et al*., 2013; Prideaux *et al*., 2015). The rapid emergence of drug resistant strains, and the challenges faced in the development of novel drugs due to issues surrounding the permeability of the cell wall layer has hindered the development of novel effective drugs (Sacks and Behrman, 2009). The PG layer plays an important role in bacterial survival as highlighted in previous sections and makes for an attractive target, especially when combined with the fact that PG has no counterpart in mammalian cells (Silver, 2006; Bugg et al., 2011). Therefore, understanding the mechanisms directing PG synthesis and identifying the pathways associated with its remodeling may yield useful information for TB drug development.

As such, this Masters project focused on the remodeling of the mycobacterial PG layer by a group of enzymes denoted as amidases, which have been implicated in the maintenance of PG homeostasis and cell wall permeability by regulating cleavage of the amide bond between *N*-acetylmuramoyl moiety and L-amino acids in bacterial cell walls (Hett and Rubin, 2008). Previous research in other organisms implicates this family of proteins in bacterial cell division, pathogenicity, invasion and immune evasion through inhibiting detection by NOD receptors amongst other processes (Johnson, Fisher, and Mobashery, 2013). Hence the role of mycobacterial cell wall amidases with regards to cell growth, elongation and division was investigated. As previously mentioned, two super-families of amidases exist, these are the amidase_2 and the amidase_3 domain containing family of proteins. The latter have been implicated in bacterial cell division, however for the purposes of this study, we focused on the amidase_2 family of proteins in *M. smegmatis*. The identification of the amidase_2 family of proteins in mycobacteria proved complicated with initial nucleotide and protein BLAST analysis identifying no counterpart for the *E. coli* amidases in mycobacteria. However, use of the amidase_2 domain with PFAM and CDD, which uses both sequence and structural information,

yielded two proteins with characteristic peptidoglycan recognition protein domains (distant domain homologs). Further investigations using the KEGG pathway database allowed for the detection of a third amidase. Canonical *E. coli* amidase_2 family proteins have the typical HDH motif responsible for ensuring tetrahedral coordination of the catalytic Zn^{2+} (Kerff *et al*, 2015), this order of residues is maintained by the amidase Ami4 (*M. smegmatis* and *Mtb*) and Ami5 (*M. smegmatis*). In contrast, Ami3 (*M. smegmatis* and *Mtb*) has acquired a substitution of the aspartic acid with a cysteine residue, notably also found in the eukaryotic PGLYRP proteins. This cysteine was shown to be essential for activity of amidases, with the thiol groups functioning as the nucleophiles (Rigden, Jedrzejas and Galperin, 2003). In contrast to the amidase_3 family of proteins, amidase_2 domain containing proteins from literature seemingly have no role in cell division or elongation in other organisms, however, were implicated in immune evasion, triggering of β lactam resistance and PG recycling (Torrens *et al*., 2017). As previously seen, biological roles of PG hydrolytic enzymes maybe divergent in different organisms, therefore with this in mind this project investigated the role of amidase_2 domain family of proteins in *M. smegmatis*.

4.1 Bioinformatics, in silico analysis and drug susceptibility

The presence of a functional catalytic triad capable of binding the Zn^{2+} residue as identified by *in silico* analysis of Ami3, Ami4 and Ami5 indicated that these proteins were potentially catalytically active. Ami4 and Ami5 are devoid of a signal peptide, suggesting that they play a vital role in cytosolic compartment, whilst Ami3 harbors a signal peptide and might be actively involved in PG remodeling in the periplasmic space. In addition to this, Ami3 has an LGFP repeat, which is thought to be involved in the maintenance of cell wall integrity, explaining why the loss of Ami3 results in the formation of cells with altered cell shape. Ami4 possesses a PG binding domain, which could facilitate bacterial cell wall degradation during growth. As previously reported, amidase_2 family of proteins *P. aeruginosa* AmpD and AmpDh2/3 single and double mutants were disposable for growth in axenic culture (Moya *et al*., 2008). Similarly, the AmiD protein in *E. coli* is dispensable for growth (Uehera and Park, 2007). In this study, the mycobacterial amidases assessed were individually dispensable for growth in axenic culture and on agar, showing no significant different in growth from the wild-type with the Δ*ami3* strain

growing marginally slower than the wild type. This prompted an assessment of possible defects in cell wall permeability and antimicrobial sensitivity.

Previous studies have demonstrated a role for the cell wall amidase_2 family of proteins in cell wall recycling and resistance to β-lactams (Lee *et al*, 2009). The amidase AmpD, which is exclusive for the cleaving of anhydromuropeptides is a negative regulator of β-lactamase expression (Höltje *et al*., 1994). Upon inactivation of the amidase, the substrate (anhydromuropeptide) accumulates in the cytosol and acts as a positive effector for β-lactamase expression, thus yielding β-lactam resistance (Höltje *et al*., 1994). This mechanism highlights an interesting communication network between the chromosome and the cell wall (Jacobs *et al*., 1995; Lee *et al*., 2009). Considering this, we wanted to determine whether deletion of mycobacterial amidases confers resistance to β-lactam and other cell wall targeting antibiotics. Exposure to antimicrobials showed that both Δ*ami3* and Δ*ami4* were strains susceptible to some β-lactams. In the case of Δ*ami3* this was explained by increased cell wall permeability as determined by the ethidium bromide assay. However, loss of *ami5* resulted in resistance to specific β-lactams, which was not associated with changes in cell wall permeability (ethidium bromide assay), suggesting that this strain developed resistance through unknown mechanisms.

4.2 Role of mycobacterial Ami3 in coordinating cell elongation and division

Previous studies on the amidase_2 family of proteins reported no cell growth or division defects (Uehara and Park, 2007), however, morphological defects were screened for in this study as biological roles of conserved hydrolytic enzymes are known to diverge from species to species. In *M. smegmatis*, the deletion of *ami3* led to the formation of elongated cells with aberrant FtsZ ring structures however, this defect was not lethal as the strain continued to grow. Labeling of the cell wall using the D-ala click method and DMN-tre showed altered incorporation of cell wall material with PG synthesis extending the length of the pole and both stains showing the existence of more than a single FtsZ ring foci within a cell. Furthermore, Scanning Electron and Time-lapse Microscopy demonstrated continued cell growth in the mutant strain. However, cell extension/ elongation occurred at unusual sites such as the lateral axis, septa and polar branching, resulting in the formation of Y-formed cells. In addition to this, certain micro colonies of the mutant strain formed extremely elongated cells, which eventually divided, forming multiple

daughter cells. Surprisingly, the branches eventually led to the formation of viable cells which could also grow and divide on their own. The results obtained for the mycobacterial Δ*ami3* strain are similar to those observed in the Δ*ami1* mutant of *M. smegmatis* (Senzani *et* al., 2017) suggesting possible redundancy between these the two amidases. However slight differences in morphology were seen, the mechanistic reasons underpinning this remain to be unraveled.

We further sought to understand these aberrant growth patterns by investigating the localization of DivIVA in the *ami3* mutant strain. DivIVA is known as a polymer-forming protein/tropomyosin like protein that assembles at sites of high negative curvature, thus providing a platform to recruit cell elongation proteins at the poles, driving cell growth (Kang *et al*., 2008; Meniche *et al*., 2014;). Depletion of DivIVA in *M. smegmatis* was originally shown to result in rounding of one pole thus implicating it in polar PG synthesis and maintenance of the mycobacterial rod shape (Scherr and Nguyen, 2009). In addition to this, it also depends on phosphorylation in response to environmental stimuli (Kang *et al*., 2008; Meniche *et al*., 2014). Alterations of *Streptococcus coelicolor* DivIVA phosphorylation and expression levels causes fragmentation of DivIVA foci, leading to branching and altered cell curvature (Flärdh, 2003; Hempel *et a*l.,2012). Live cell imaging of the Δ*ami3* strain revealed a similar fragmented and mislocalized DivIVA, wherein the random foci along the lateral axis of the cell wall resulted in further DivIVA recruitment, triggering branch formation. Septal branch formation as a result of *ami3* deletion is hypothesized to be as a result of the newly formed curvature of the septa recruiting more DivIVA to the septa. In this case, failure of division results in the formation of a bud. The failure of the division process to complete in the *ami3* mutant highlights a role for this enzyme in the late stages of cell division, possibly through degrading septal PG.

FtsZ is a bacterial tubulin homolog responsible for the contractile force that drives membrane invagination during cytokinesis by assembling at the mid-cell into a ring like structure known as the Z-ring (Lutkenhaus, 1991; Osawa and Erickson, 2013). The Z-ring is guided by cellular arrangement of genomic DNA, the cell shape and composition of its lipids and PG envelope (Galli, Paly and Barre, 2017). Research conducted in other organisms has shown that the overproduction of FtsZ, or removal of its interacting partner FtsA or antagonist Min, leads to multiple Z-rings at both mid-cell and the poles, or between nucleoids in long cells (Lutkenhaus,

Pichoff and Du, 2012; Yu and Margolin, 1999). Therefore, we investigated FtsZ localization using a GFP tagged derivative of the protein. Microscopy showed coordinated FtsZ localization with two Z-rings in the wild-type that would eventually form a bundled Z-ring polymer, forming the basis of the divisome. FtsZ localization was unaffected in the *ami3* mutant, unlike reports in the literature with regards to the amidase_3 class deleted strains; *E. coli* triple Δ*amiA* Δ*amiB* Δ*amiC* mutant (Bernhardt and Boer, 2003) and the *M. smegmatis* Δ*ami1* mutant (Senzani *et al*., 2017), where additional Z-rings were localized within chaining cells. However, in a fraction of the Δ*ami3* cells, division scars were seen in the SEM micrographs, likely from the instabilities in PG synthesis-cell division coordination. The formation of multiple Z rings/ division scars at ectopic sites may also be associated with a disturbance in chromosome segregation (Santi *et al*., 2013), however further investigations have to be conducted to establish this.

Extensive research in bacterial cell division has emphasized the need for coordinating septum PG synthesis and hydrolysis with chromosome segregation during division (Plocinski *et al*., 2012; Hett and Rubin, 2008). Accordingly, coordination of the function of PBPs function is linked to FtsZ activity and expression levels (Wells and Margolin, 2012). Upon the removal of PBPs, rod shaped *E. coli* formed branches, implicating these proteins in prevention of ectopic poles formation (Potluri, de Pedro and Young, 2012). The same results were seen when FstZ levels were increased in the deletion mutant, with Z-rings slanted at an angle rather than forming perpendicular to the lateral axis (Potluri, de Pedro and Young, 2012). To explain this, Wells and Margolin (2012) suggested that distortions in Z-ring orientation (i.e. slanting) briefly drove pre-septal PG synthesis off-center, however, reorientation of these rings during synthesis left the aberrantly localized pre-septal PG inert, thus resulting in a division scar. These later formed false poles causing synthesis of PG around them, driving formation of lateral branches (Wells and Margolin, 2012). These results illustrated that the PBPs help to maintain the perpendicular orientation of the Z-ring and ultimately ensure correct septum placement in relation to the chromosome. We observed some overlapping defects in this regard, however, further investigation is needed to fully explain the division defects in the *ami3* mutant.

4.3 Ami3 interactions reveal a link between the elongasome and divisome complexes and PG Lipid layer biosynthesis

Protein-protein interactions are essential to ensure coordinated bacterial cell growth, division and virulence. As mentioned before, protein-protein interaction complexes are essential for a plethora of functions, therefore the identification and disruption of key interactions between protein partners could provide a broader understanding of their mechanisms under physiological and pathological conditions. These studies may also yield mechanistic information on how to block bacterial cell growth, leading to the development of novel antimicrobial agents. Considering this, we sought investigate possible protein interactions involved in septum cleavage using the M-PFC assay. The screen for Ami3 interacting partners produced PonA1 which is a penicillin binding protein (PBP1) with transpeptidase and transglycosidase domains (Keiser et al., 2015). This protein has been implicated in mycobacterium septal degradation, interacting with RipA an endopeptidase, which also interacts with RpfB a lytic transglycosylase (Hett, Chao and Rubin, 2010). PonA1 has been shown to play a crucial role in both cell elongation and septation, with alteration in either PonA1 domains leading to the formation of ectopic poles and an altered cell length (Kieser et al., 2015). Furthermore, PonA1 is thought to transiently interact with DivIVA, which coordinates bacterial growth by recruiting enzymes involved cell elongation (Meniche et al., 2014; Keiser et al., 2015).

There are startling similarities in phenotypes between a *ponA1* knockdown (reported by Keiser *et al*., 2015) and the Δ*ami3* strain generated in this study. According to Keiser *et al* (2015), abrogation in transglycosylase activity in PonA1 leads to the formation of ectopic poles, hypothesized to be as a result of imbalances in glycan polymerization to cross-linking ratio, resulting in increased cross-link formation. They suggested that the number of cross-links might have distorted PG architecture, thus possibly changing membrane curvature enough to misdirect recruitment of the elongation complex to aberrant foci (Keiser et al., 2015). The authors also outlined that to maintain polar growth and cell shape, regulation of PonA1 activity through protein-protein interactions was vital. Furthermore, they showed the need for PonA1 phosphorylation to ensure maintenance of cell length, as a lack thereof leads to transglycosylase hyperactivity and the formation of elongated cells (Keiser et al., 2015). In this case,

phosphorylation acts as a negative regulator of elongation, because transglycosylase phosphorylation (thought to drive elongation), correlates with the stages of the cell cycle. This is illustrated by the observation that phosphorylation of PonA1 occurs during the switch from elongation to septation (Keiser et al., 2015). Lastly, the disruption of the transpeptidase domain of PonA1 enhanced susceptibility to teicoplain, much like the loss of Ami3. What is interesting about this finding is that PonA1 has been found to be part of the mycobacterial divisome and elongosome whilst amidases are thought to be strictly part of the divisome. The similarity in phenotypes supports the hypothesis that these proteins possibly interact to regulate PG biosynthesis and degradation at the cell pole.

Another interaction partner of Ami3 is the *Mycobacterium* membrane protein Large (MmpL) that belongs to the RND (resistance, nodulation and cell division proteins) group of transporters, which are multidrug resistance pumps recognizing and mediating the transport of substances across the cytoplasmic membrane (Domenech, Reed and Barry, 2005). Previous studies on this transporter have shown that MmpL3 transports trehalose-monomycolate, a component of the mycolic acid lipid layer and imports heme (Viljoen *et al*., 2017). Furthermore, studies on MmpL7 have shown that this protein is involved in the transport of pthiocerol dimycocerosate (PDIM) and that MmpL8 is required for the synthesis of Sulfolipid 1, through transportation of its precursor in *Mtb* (Domenech, Reed and Barry, 2005). PDIM has been shown to participate in receptor dependent phagocytosis of *Mtb* bacilli by controlling invasion of macrophages through targeting lipid organization in the host membrane and preventing phagosomal acidification, thereby driving the bacilli into a protective niche (Astarie-Dequeker et al., 2009). In addition to this, Sulfolipid 1 in culture models has been shown to be involved in altering phagosome-lysosome fusion, disruption of mitochondrial oxidative phosphorylation, activation and suppression of cytokines and modulating reactive oxygen species (Goren et al., 1976; Kato and Goren, 1974; Brodin et al., 2010). However, loss of Sulfolipid 1 in *Mtb* results in varying phenotypes, probably owing to differences in laboratory strains and techniques (Gilmore et al., 2012). Although the role of Ami3 in *M. smegmatis* virulence could not be investigated due to the non-infectious/ pathogenic nature of this soil dwelling bacterium, we propose to advance this work in future studies in *Mtb* and investigate whether there is any association between Ami3-MmpL interaction and *Mtb* pathogenesis.

4.4 Mycobacterial biomass and biofilm formation possibly depend on Ami3 function

Biofilms provide reservoirs of cells that can repopulate colonized sites upon treatment with antimicrobials and thus promote bacterial persistence and drug tolerance conditions (Richards and Ojha, 2014). This form of bacterial differentiation is characterized by the release polysaccharides, proteins and DNA (Limoli, Jones and Wozniak, 2015), which has been linked to the action of amidases, therefore allowing microbes to stick to their surface (Qin *et al*., 2007). Unlike most bacteria, mycobacteria do not excrete exopolysaccharides as an extracellular matrix to develop and maintain biofilms, instead short chain fatty acids are secreted (Ojha *et al*., 2005).

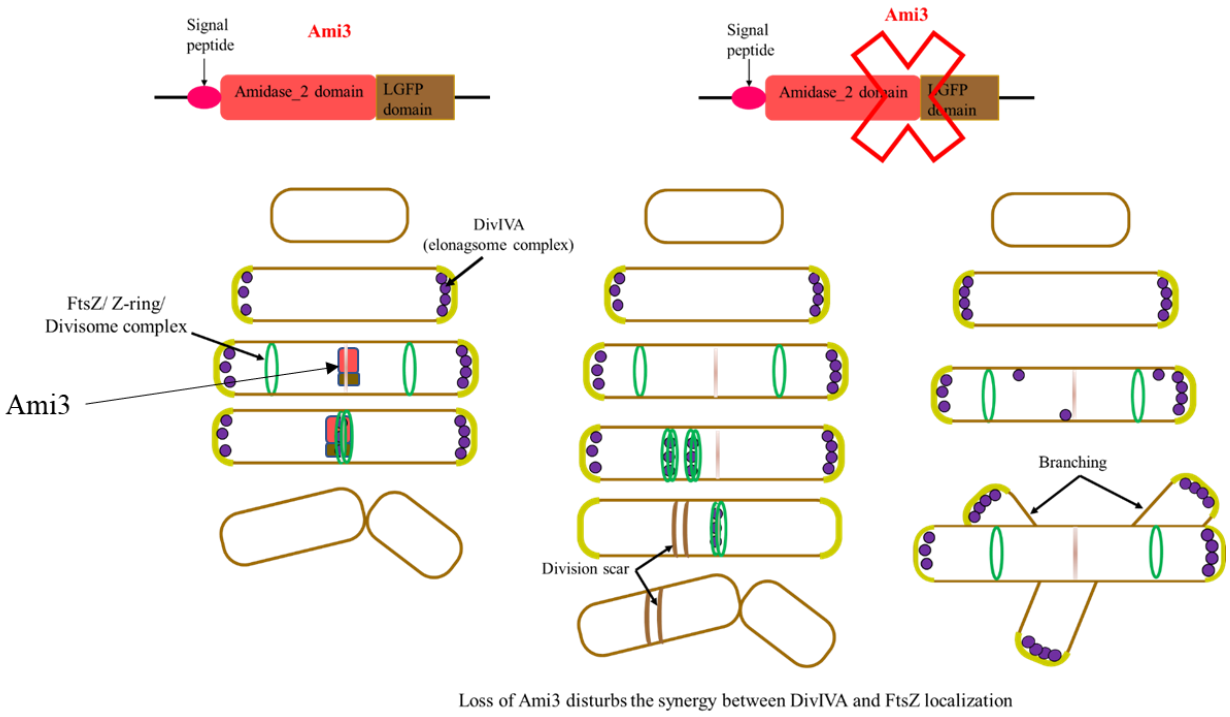

Figure 4.1: Model for the role of Ami3 in cell elongation and division. A model wherein Ami3 is involved in driving cell elongation and division during mycobacterial growth is proposed. Normally, mycobacteria remodel cell wall at the polar ends of the cell and the septum. This is aided by a variety of proteins, some of them indicated in the diagram. DivIVA localizes at the poles driving cell growth, thereafter the Z-ring assembles, resulting in the formation of two daughter cells. However, the two systems get distorted in the event of Ami3 deletion. This includes the failure to correctly place the Z-ring, resulting in the formation of multiples division scars. The other is the mislocalization of DivIVA which results in ectopic pole elongation along the lateral axis of the cell, leading to branching. Ami3 is a possible interacting partner of PonA1, this interaction may facilitate some of the above-mentioned functions.

Although the loss of *ami3* did not severely affect the ability of the bacteria to form the traditional textured surface of mycobacterial biofilms, the biomass was significantly less than that of the wild type. This suggests that loss of *ami3* resulted in attenuated production and/or release of the above mentioned polymers, possibly affecting adhesion between bacteria and to the surface, which would ultimately reduce biofilm biomass. A model for the role of Ami3 in mycobacteria is given in Figure 4.1

4.5 The deletion of Ami4 causes dysregulated cell wall remodeling and the release of cell wall material, accompanied by cell death

The deletion of Ami4, a homolog of *E. coli* AmpD led to the formation of bulging septa and the formation of wide and branching Y-shaped cells, with defects in polar localization of DivIVA. This suggests that the cytoplasmic amidase, Ami4 is needed to ensure regulated cell wall synthesis and the maintenance of cell shape through synchronized actions with DivIVA and FtsZ. Absence of Ami4 caused ectopic DivIVA localization, which eventually led to cell lysis. How Ami4 influences this remains to be discovered. The formation of bulging cell poles has been reported previously with enzymes involved in cell wall hydrolysis. The deletion of *Mtb* CwsA, shown to be involved in cell wall synthesis and division, resulted in the formation of polar bulges and defects in DivIVA localization, resulting in altered cell wall synthesis (Plocinski *et al*., 2012). Based on this, it was concluded that CwsA plays a crucial role in septal and polar PG synthesis coordination and cell shape maintenance through the concerted action of other cell wall synthesis and division proteins (FtsI, DivIVA, CrgA and indirectly FtsZ) (Plocinski *et al*., 2012). In *B. subtilis*, the loss of the division proteins EzrA and GpsB results in defects in both cell elongation and division, along with failure to complete cell pole maturation, leading to the formation of bulging poles (Claessen *et al*., 2008). These phenotypes have also been associated with the loss of PonA1 in mycobacteria, from disturbances in transglycosylase and transpeptidase activities (Claessen *et al*., 2008; Keiser *et al*., 2015). The imbalance in PG synthesis and degradation in the absence of Ami4 subsequently led to cell death, likely due to destabilization of the ability to maintain osmotic pressure. A model for the role of Ami4 is given in Figure 4.2.

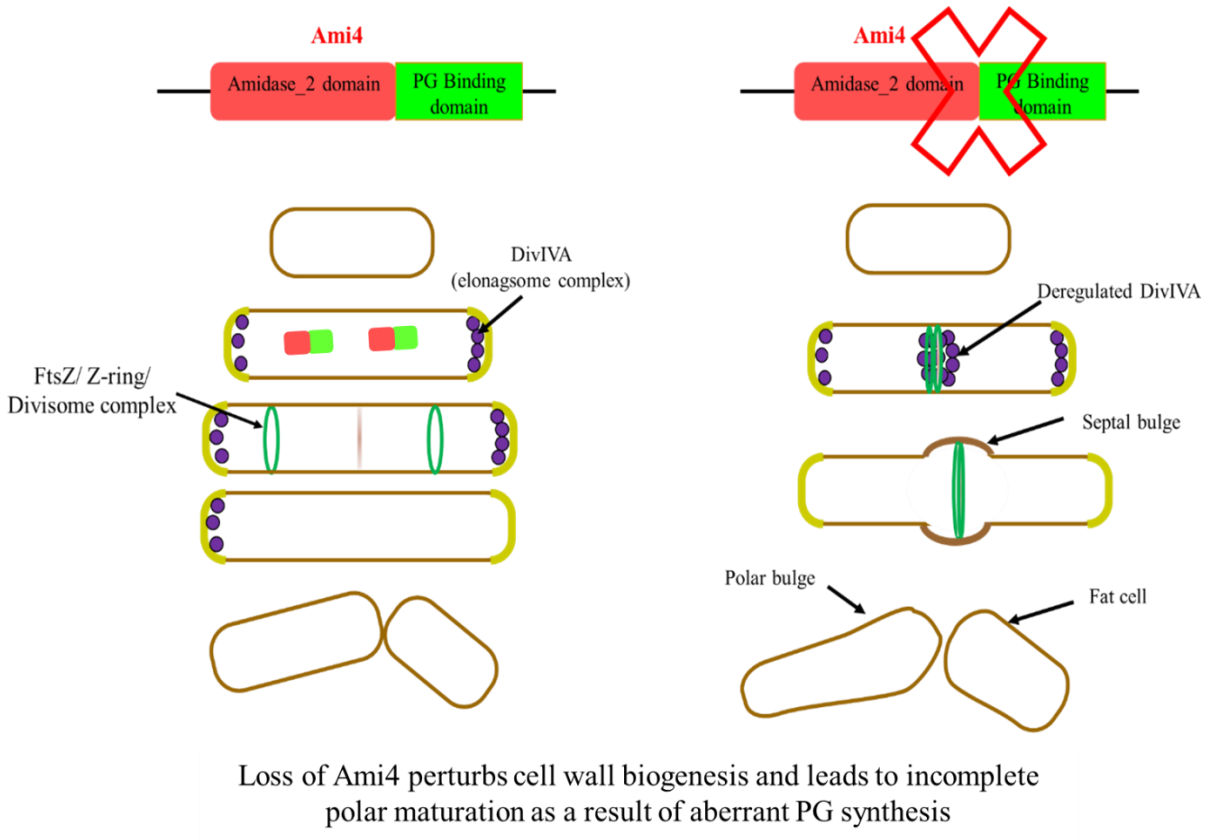

Figure 4.2: Proposed model for the role of Ami4 in mycobacterial cell size homeostasis. *M. smegmatis* maintains cell width by ensuring constant cell wall remodeling and thus extension at the poles, with Ami4 coordinating PG insertion and cell growth homeostasis by acting in conjunction with cell elongation complex, i.e. DivIVA. This investigation demonstrated that the loss of Ami4 results in the deregulation of PG remodeling and cell size homeostasis, leading to the formation of septal and polar bulges, which inevitably led to the formation of fat cells with variable width and eventual bacterial lysis.

4.6 The role of *M. smegmatis* Ami5 in cell wall homeostasis and cell death

The loss of Ami5, also thought to be an AmpD, homolog led to the formation of dumb-bell shaped cells with the release of mini-cells, which incorporated the D-alanine analogue, indicating they retained enough metabolic ability to maintain their cell wall. Further investigation with live cell microscopy demonstrated that a large number of these cells were defective in their ability to grow and replicate. This could be explained by a disproportionate segregation of genetic material, limiting these cells in their ability to independently propagate. In addition to this, the loss of Ami5 led to defective polar formation, the rounding of poles, curving and wrinkled cells. A GFP tagged FtsZ strain was generated, however, the strain did not shown any visible

difference in FtsZ localization, when compared to the wild-type. Further analysis demonstrated an accumulation of the D-alanine analog at the poles. Rounding of the polar ends was prominent in a large number of the micro-colonies depicting a defect in the control of polar PG synthesis, some of these grew through elongation at a single pole. Lastly, micro-colonies of the Ami5 mutant strain also produced membrane blebs, which are synonymous with cells undergoing late apoptosis (Bayles, 2014). To summarize, the loss of Ami5 led to dramatic phenotypes including mini-cells, membrane blebbing, elongated cells bulging at a single pole and cell death.

Previous work has demonstrated the presence of bacterial Program Cell Death (PCD) with bacterial strategies synonymous to those of the eukaryotic Bcl-2 being investigated (Bayles, 2003). The above observations along with the resulting cell death results observed in the Ami4 deletion strain suggest a role for amidases in the programmed cell death pathway (PCD) (Bayle, 2014). Processes characteristic of PCD such as membrane blebbing and cell shrinkage are as a result of cysteine protease activation (caspases) (Thornberry and Lazebnik, 1998). Mycobacteria possess the cysteine protease, RipA whose overexpression leads to the loss of the mycobacterial rod shape and formation of spherical cells, which eventually lyse (Chao *et al*., 2013). Chao et al (2013) proposed that RipA overexpression might be stimulating other endogenous proteins which facilitate coordinated cell death. This change in cell morphology was also observed in the Ami5 deletion strain SEM micrographs, depicting that deletion of this amidase has a ripple effect in the ability of the strain to properly control hydrolase expression and thus PCD activation. However, further analysis of these results is needed to validate the presence of apoptotic processes in mycobacteria and the role of amidases in coordinating cell death. A model for Ami5 activity in mycobacteria is given in Figure 4.3.

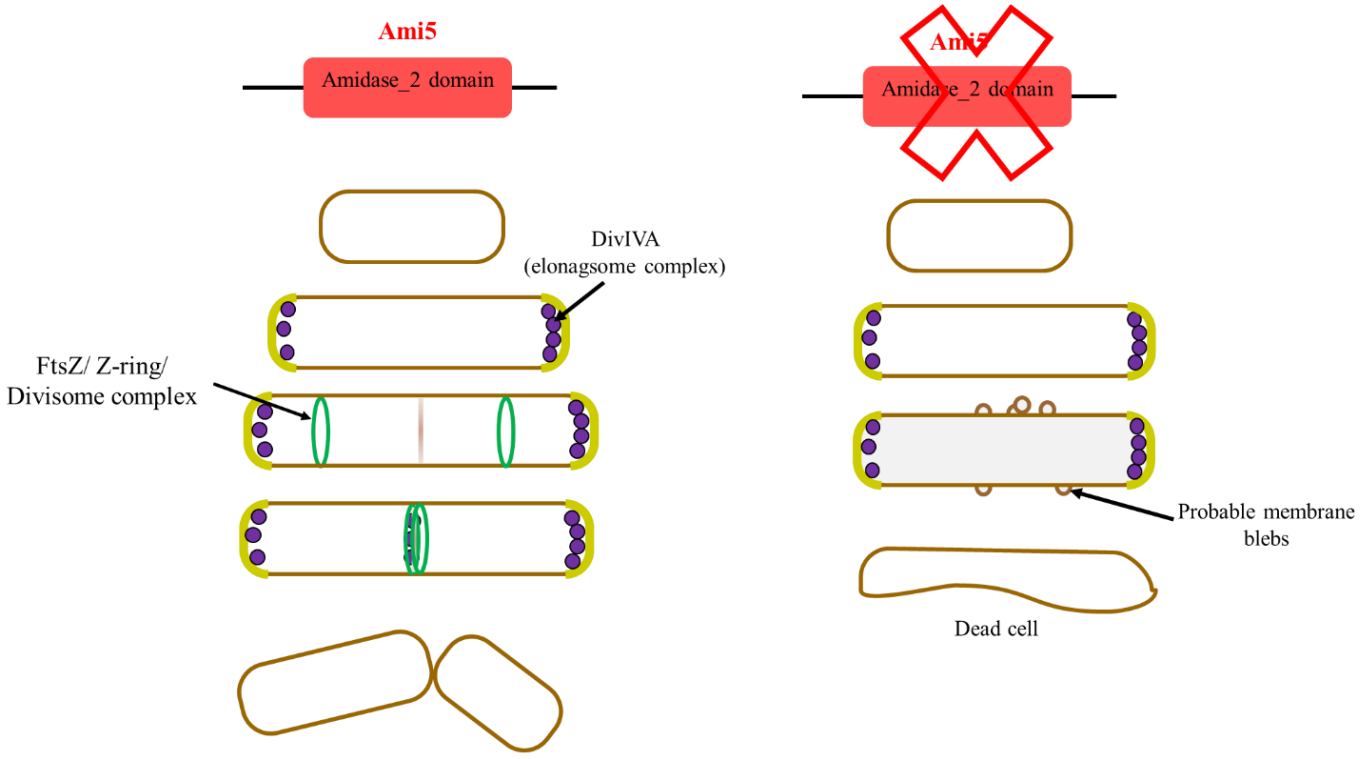

Figure 4.3: Model for the role of Ami5 in programmed cell death and cell size homeostasis. Wild-type mycobacterial growth processes are optimally coordinated to ensure regular cell growth at the poles and division at the septa as depicted in the illustration above. However, the loss of Ami5 resulted in the formation of short cells (that maintained ability to incorporate PG) and what seemed to be membrane blebs on the surface of the cell, suggestive of dysregulated bacterial programmed cell death.

5. Conclusion

Tight regulation of mycobacterial cell wall remodeling is essential for ensuring the maintenance of cell wall integrity and for bacterial proliferation/survival. Mycobacterial amidases have been implicated in a number of pathways that play a central role in cell elongation/division. In this study, we demonstrated a role of the amidase_2 family of proteins in coordinating cell wall synthesis and division and possibly in the control of PCD pathway. In addition to this, we demonstrated a role for Ami3 as a putative interacting partner for PonA1, thereby reinforcing its involvement in cell elongation and division. Another possible partner that emerged for Ami3 was the MmpL transporter, which indirectly implicated this amidase in antibiotic resistance through

the modulation of the lipid layer and biofilm formation. If these interactions are maintained in *Mtb*, they could also point to a role for Ami3 in *Mtb* host immune evasion. The other cytoplasmic amidases Ami4 and Ami5 have vital roles in maintaining cell wall homeostasis and controlling bacterial growth and division. Collectively, this work has demonstrated non-redundant, essential roles for amidases in mycobacteria and creates a strong case to study these enzymes in *Mtb* as possible new drug targets.

6. Future work

The M-PFC assay revealed important interaction of the Ami3 protein with MmpL shown to have a role in the inhibition of phagosome-lysosome fusion and in driving antibiotic resistance, hence future prospects include the determination of whether these results can be extrapolated into *Mtb.* Also, we propose that a detailed analysis of mycobacterial programmed cell death is necessary and that understanding these hydrolytic triggers could be of great use in eradicating TB.

Supplementary data

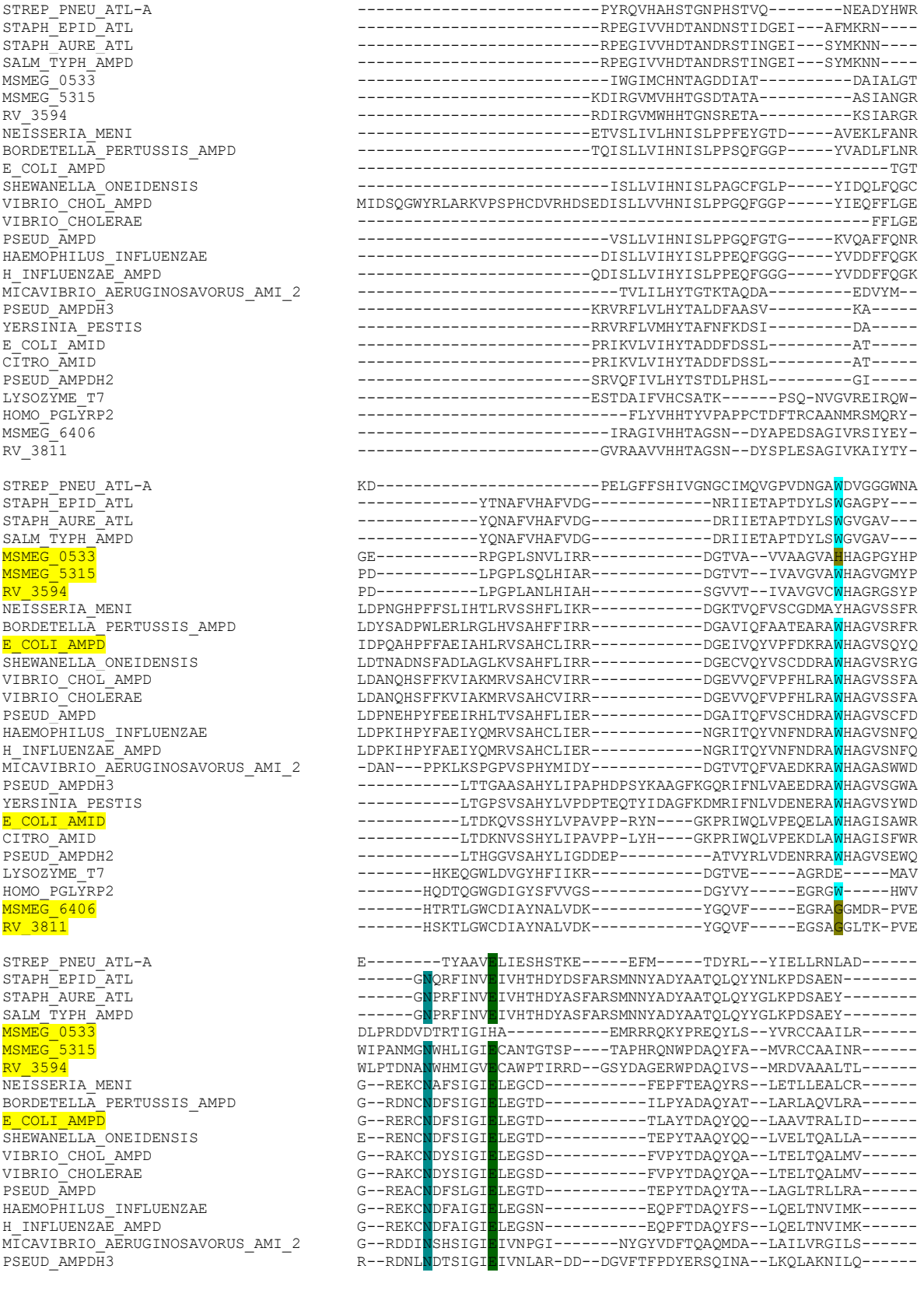

```
YERSINIA_PESTIS                  G--RNNLNDTAIGIETVNLAT-DN--DGVFTFPPYNVTQIAA--IKALASNILY------
E_COLI_AMID                      G--ATRLNDTSIGIELENRGWQKS--AGVKYFAPFEPAQIQA--LIPLAKDIIA------
CITRO_AMID                       G--ATRINDTSIGIELENRGWQKS--AGIKYFAPFEPAQIQA--LIPLAKDIIA------
PSEUD_AMPDH2                     G--RTWLNATSIGIEIVNQGYRDT--PQGRVWYPFSEAQIQA--LIPLLKDIAK------
LYSOZYME_T7                      GSHAKGYNHNSIGVCLVGGID-----DKGKFDANFTPAQMQS--LRSLLVTLLA------
HOMO_PGLYRP2                     GAHTLGHNSRGFGVAIVGNYT-----AALP-----TEAALRT--VRDTLPSC--------
MSMEG_6406                       GAHTGGFNRDTWGVAMMGNFD-----AVPP-----TPIQLRT--TGRLLGWRLGLDRIDP
RV_3811                          GFHTGGFNRNTWGVAMIGNFD-----DVAP-----TPIQIRT--VGRLLGWRLGMDDVDP
                                                 :

STREP_PNEU_ATL-A                 --------EAGLPKTLDTGS---LAGIKTHEYCTNNQPNNHSDHVDPY------------
STAPH_EPID_ATL                   ------DGRG---------------TVWTHAAISNF--LGGTDHADPH------------
STAPH_AURE_ATL                   ------DGNG---------------TVWTHYAVSKY--LGGTDHADPH------------
SALM_TYPH_AMPD                   ------DGNG---------------TVWTHYAVSKY--LGGTDHADPH------------
MSMEG_0533                       --------------HINR---S-ASHVLGHQEWDT-----GKVDP---------------
MSMEG_5315                       --------------RLAQ---T-SARTIGHKEYAGR--AQGKWDPG--------------
RV_3594                          --------------KLG----YGPERNIGHKEYAGA--AQGKWDPG--------------
NEISSERIA_MENI                   --------------RYPV---T---AVTGHQDIAP----GRKTDPG--------------
BORDETELLA_PERTUSSIS_AMPD        --------------RYPL---A---DARGHEHIAP----GRKTDPG--------------
E_COLI_AMPD                      --------------CYPD---I-AKNMTGHCDIAP----DRKTDPGP-------------
SHEWANELLA_ONEIDENSIS            --------------QYSS---LSAERIVGHCDIAP----VRKTDPGP-------------
VIBRIO_CHOL_AMPD                 --------------RYPH---ITLPRITGHQYIAP----LRKTDPGLVFDWRRFRAGLKS
VIBRIO_CHOLERAE                  --------------RYPH---ITLPRITGHQYIAP----LRKTDPG--------------
PSEUD_AMPD                       --------------AFPG---ITPERIQGHCDIAP----ERKTDPG--------------
HAEMOPHILUS_INFLUENZAE           --------------SYPK---ITKDRIVGHCDISP----KRKIDPG--------------
H_influenzae_ampD                --------------SYPK---ITKDRIVGHCDISP----KRKIDPG--------------
MICAVIBRIO_AERUGINOSAVORUS_AMI_2 ---------------RNPI---P-AHYVLGHSDIAP----TRKPDPG--------------
PSEUD_AMPDH3                     --------------RYPD---MTPKNVVGHSDIAV----GRKSDPGP-------------
YERSINIA_PESTIS                  --------------RFPD---ITPVNVVGHSDIAP----GRKSDPG--------------
E_COLI_AMID                      --------------RY-H---IKPENVVAHADIAP----QRKDDPGP-------------
CITRO_AMID                       --------------RY-D---IKPQNVVAHADIAP----QRKDDPGP-------------
PSEUD_AMPDH2                     ---------------RH-G---ITPDRIIGHSDIAP----GRKVDPGP-------------
LYSOZYME_T7                      --------------KY------EGAVLRAHHEVAP------KACP---------------
HOMO_PGLYRP2                     --------------AVRAGLLRPDYALLGHRQLVR------TDCPG--------------
MSMEG_6406                       HGTVVLASEGGSFTHFPRGATPTLPAIFTHRDVGN------TDCPG--------------
RV_3811                          RSMVDLQSAGSSYTTFPGGAIARLPAIFTHRDVGN------TDCPG--------------
                                                                 *           .
```

Supplementary Figure 1: Multiple sequence alignment of the amidase_2 domain family of proteins in different organisms. Shown is the rest of the alignment indicating the various Amidase residues that are conserved throughout the Amidase_2 domain family

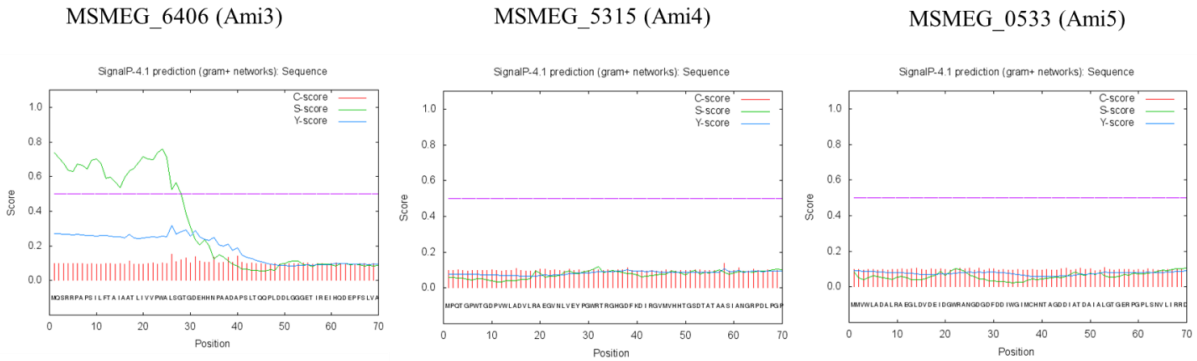

Signal peptide present-position 1-25 (Cleavage site between amino acid 25 and 26)

Signal peptide absent

Signal peptide absent

Supplementary Figure 2: SignalP analysis of Amidase_2 family of proteins in *M. smegmatis* (Ami3, Ami4 and Ami5) to determine presence of a signal peptide

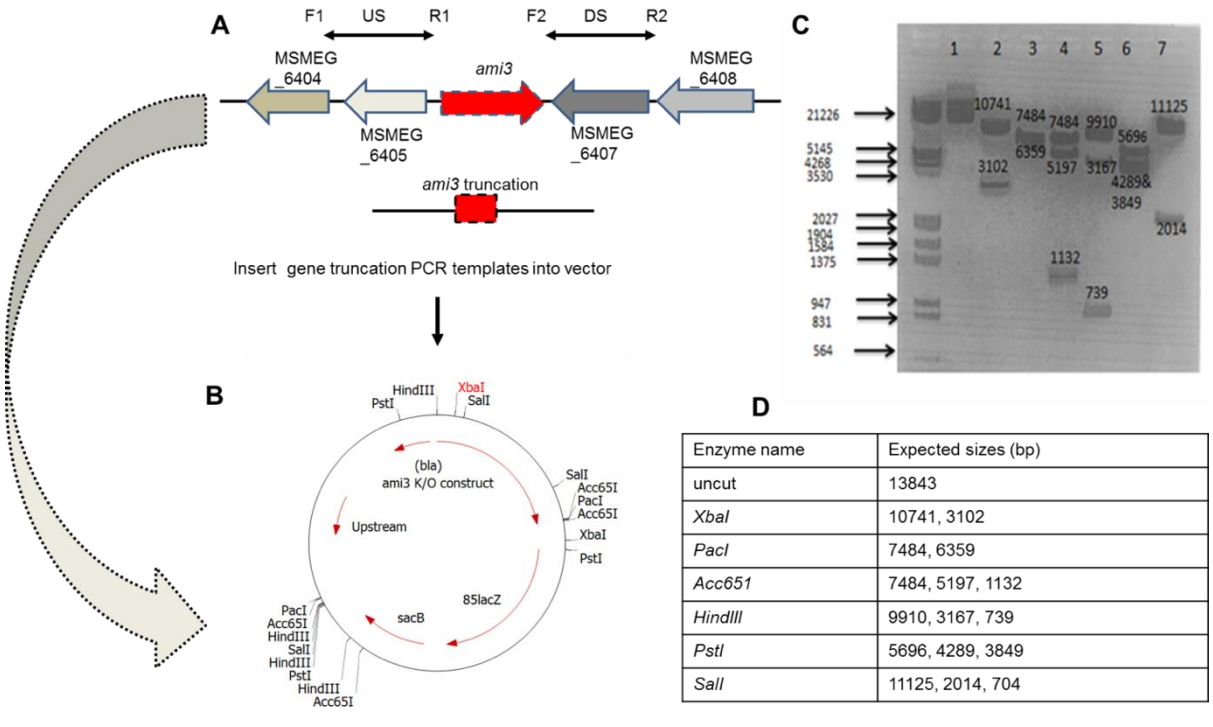

Enzyme name	Expected sizes (bp)
uncut	13843
XbaI	10741, 3102
PacI	7484, 6359
Acc651	7484, 5197, 1132
HindIII	9910, 3167, 739
PstI	5696, 4289, 3849
SalI	11125, 2014, 704

Supplementary Figure 3: Restriction profile of p2NIL_pG17_*ami3*. (A) *M. smegmatis* genomic map and the position of *ami3* within the genome. The two step allelic strategy for the generation of the deletion strains is also depicted with the sites of primer binding. (B) Final *ami3* knockout construct used to transform *M. smegmatis* wild-type parental strain. (C) Agarose gel (0.8%) of digested fragments: Roche marker IV, uncut construct control (143843 bp) [Lane 1], *Xba*I [Lane 2], *Pac*I [Lane 3], *Acc*651 [Lane 4], *Hind*III [Lane 5], *Pst*I [Lane 6], *Sal*I [Lane 7]. (D) Table depicting the specific enzymes used and the expected fragment sizes (bp).

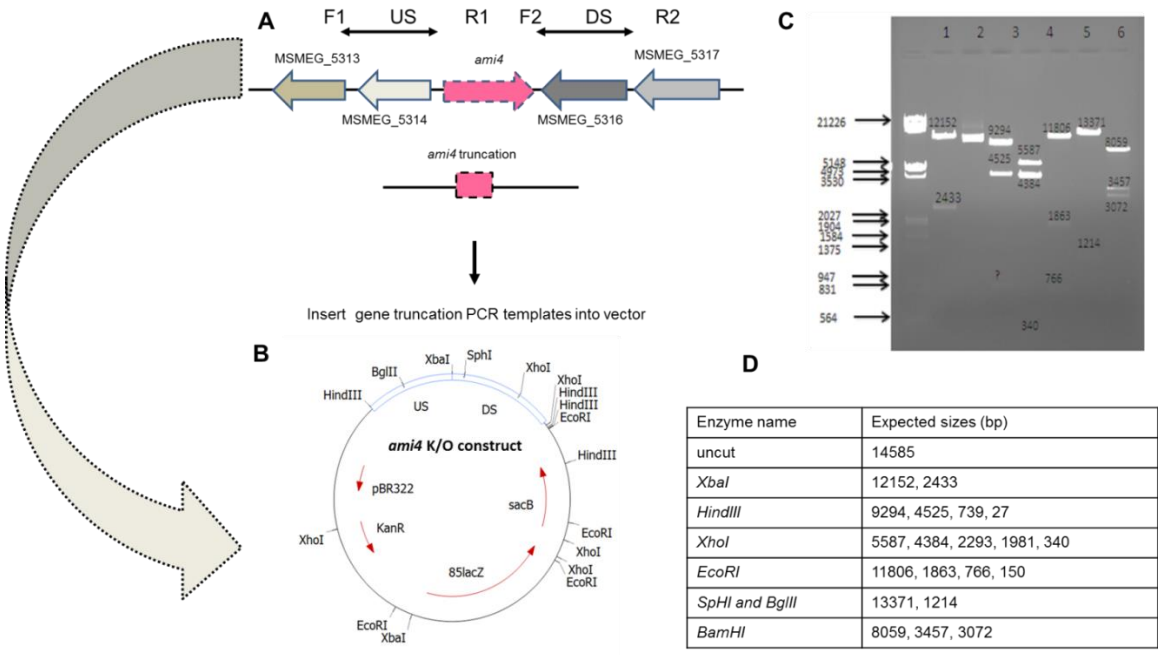

Enzyme name	Expected sizes (bp)
uncut	14585
XbaI	12152, 2433
HindIII	9294, 4525, 739, 27
XhoI	5587, 4384, 2293, 1981, 340
EcoRI	11806, 1863, 766, 150
SpHI and BglII	13371, 1214
BamHI	8059, 3457, 3072

Supplementary Figure 4: Restriction profile of *ami4p2NILpG17*. (A) *M. smegmatis* genomic map and the position of the gene within the genome. The two step allelic strategy for the generation of the deletion strains is also depicted with the sites of primer binding. (B) Final *ami4* knockout construct used to transform *M. smegmatis* wild-type parental strain. (C) Agarose gel (0.8%) of digested fragments: Roche marker IV, *Xba*I [Lane 1], uncut construct control (14 585 bp) [Lane 2], *Hind*III [Lane 3], *Xho*I [Lane 4], *Eco*RI [Lane 5], *Sph*I and *Bgl*II [Lane 6] and *Bam*HI [Lane 7]. (D) Table depicting the specific enzymes used and the expected fragment sizes (bp).

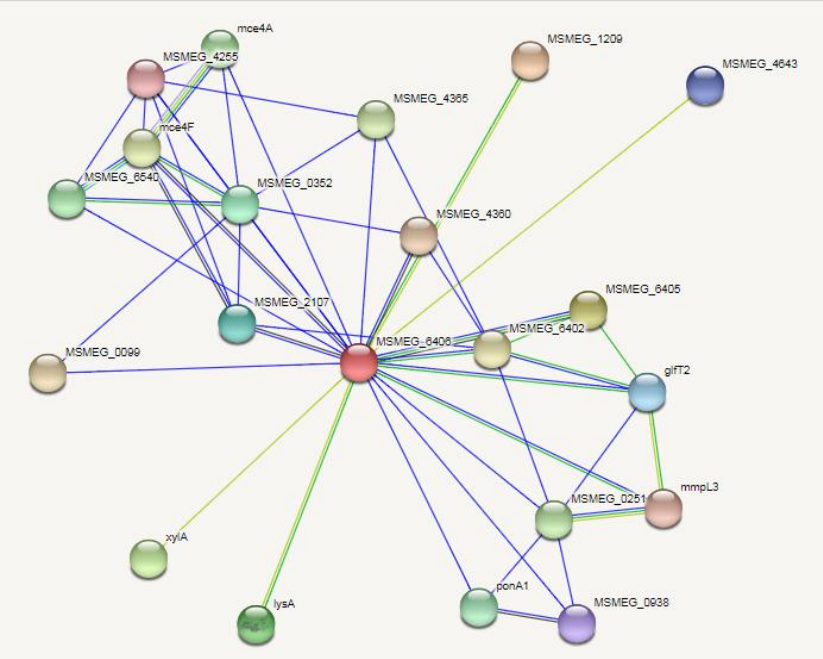

Supplementary Figure 5: Predicted Ami3 interacting partners using bioinformatics tool SPRING. From this analysis, PonA1, MmpL3, Glft2, MSMEG_6402 and MSMEG_6405 were further studied.

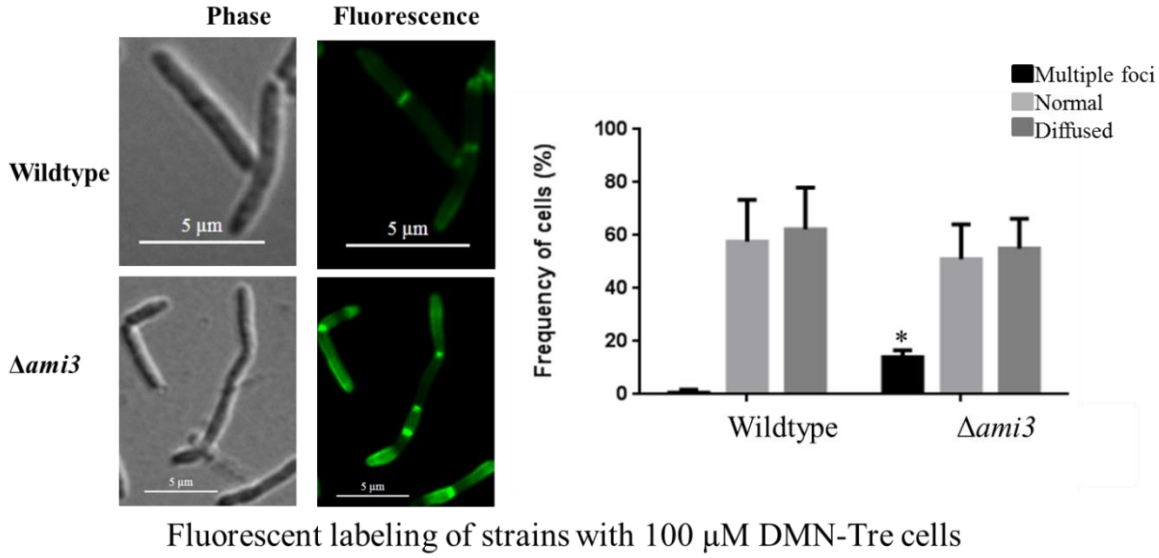

Fluorescent labeling of strains with 100 µM DMN-Tre cells

Supplementary Figure 6: *M. smegmatis ami3* modulates cell shape. Fluorescence microscopy carried out to determine alterations in cell wall synthesis using DMN-tre. (First panel) Wild-type strain showing characteristic cell growth and thus DMN-tre incorporation, (Second panel) Δ*ami3* strain showing DMN-tre fluorescence at multiple sites which seem to be the septa. Bar graph on right shows the quantity of cells with the respective fluorescence. Wildtype also has multiple fluorescence foci however not as significant as Δ*ami3* strain.

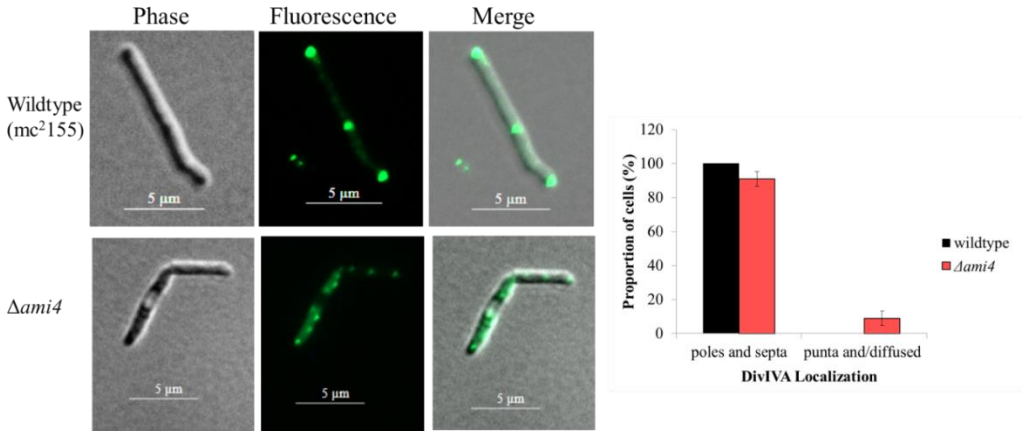

Supplementary Figure 7: Fluorescence microscopy of mycobacterial DivIVA localization in Δ*ami4* background. The Δ*ami4* strain was transformed separately with a DivIVA-GFP derivative, fluorescence microscopic images of DivIVA were taken to visualize localization pattern in the *ami4* mutant, with pattern of localization quantified by calculation of the proportion of cells adopting the specific pattern (Bar graph on right). GFP-DivIVA localization in Δ*ami4* was distorted and unfocused with Δ*ami4* cells showing puncta or diffused DivIVA which was not seen in wild-type cells.

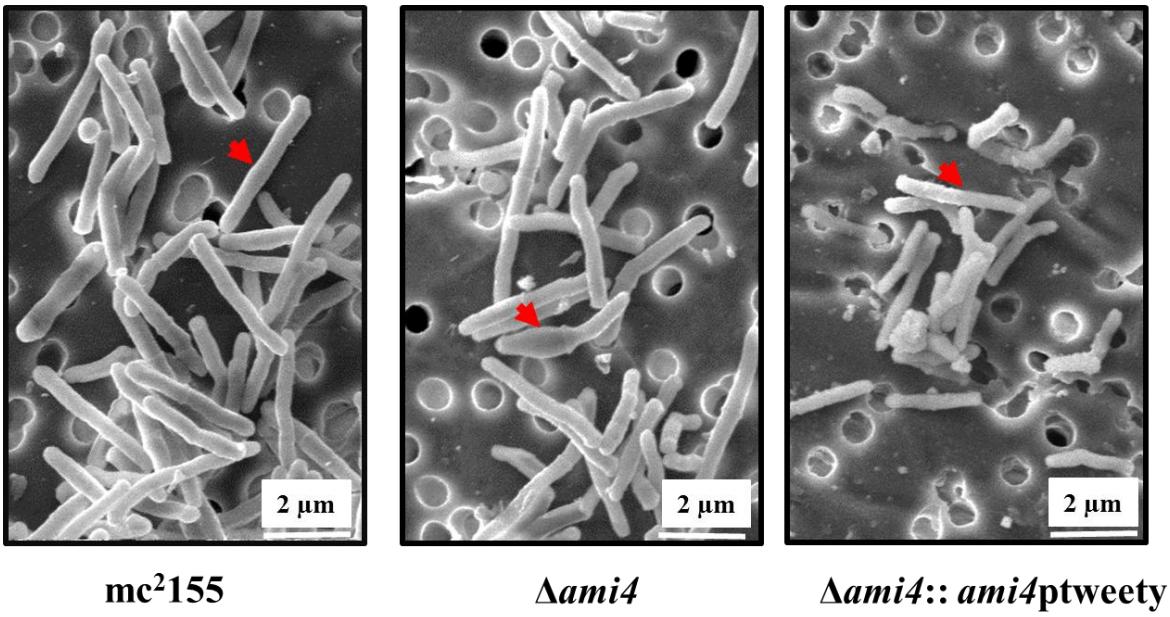

Supplementary Figure 8: Scanning electron microscopy of mc²155 (Wild-type), Δ*ami4* and Δ*ami4*:: *ami4* strains. Cells were cultured in Middlebrook 7H9, followed by fixation in gluteraldehyde in prepation for viewing using SEM. Wild-type (far left) cells formed smooth rods and grew to normal size, the loss of *ami4* (middle) led to formation of short/fat cells with polar/septal bulges. This phenotype was reversed by complementation, with cells forming normal mycobacterium bacilli (far right).

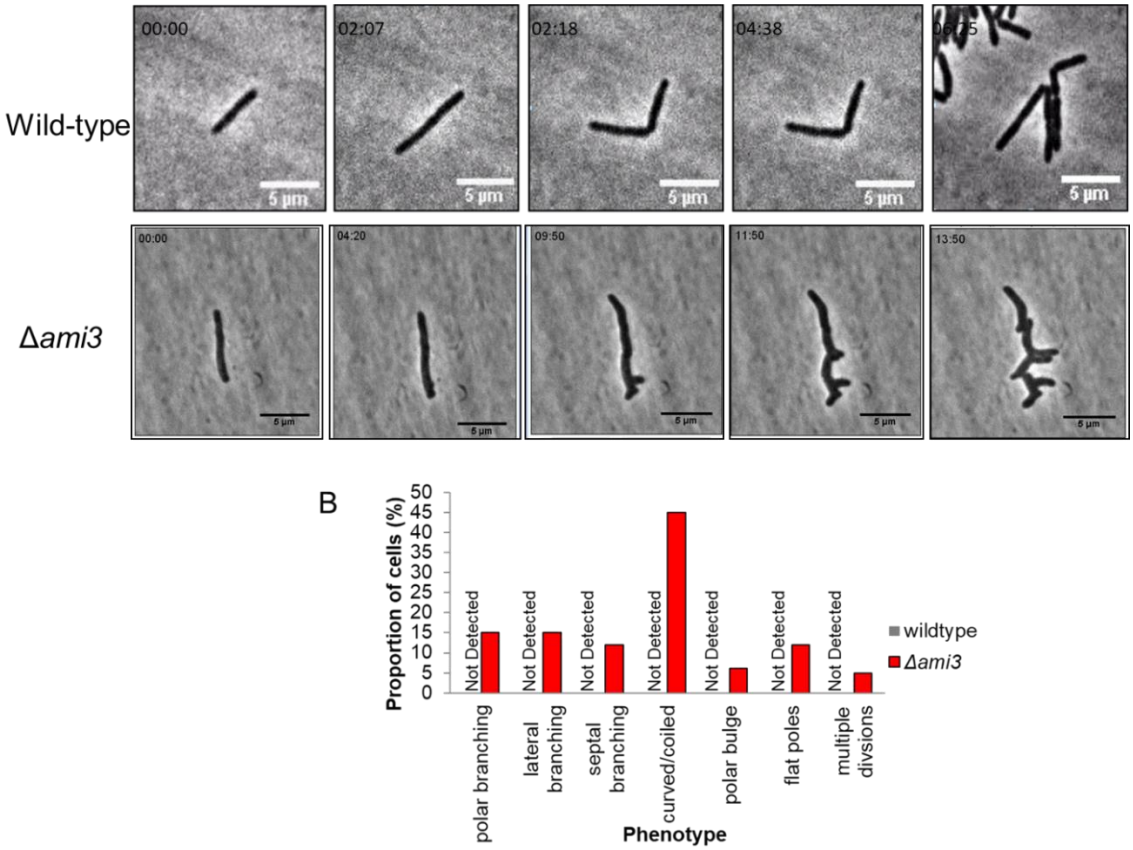

Supplementary Figure 9: Time-lapse microscopy of *M. smegmatis ami3* deficient strain and the resulting flat poles. A) Growth patterns of wild-type M. smegmatis in Middlebrook 7H9 media with different time stamps showing pattern of mycobacterial growth and division. Wild-type adopts simple pattern of growth, extending via poles and diving at the septa to produce two daughter cells (time stamp 04:38). The *ami3* deficient strain failed to adopt the same pattern, instead producing cells with flat poles (indicated by red arrow) and delayed division (time stamp 11:56). B) Graphical representation of phenotypes seen in both the wild-type and *ami3* deficient strains; total amount of cells counted= 100 micro-colonies.

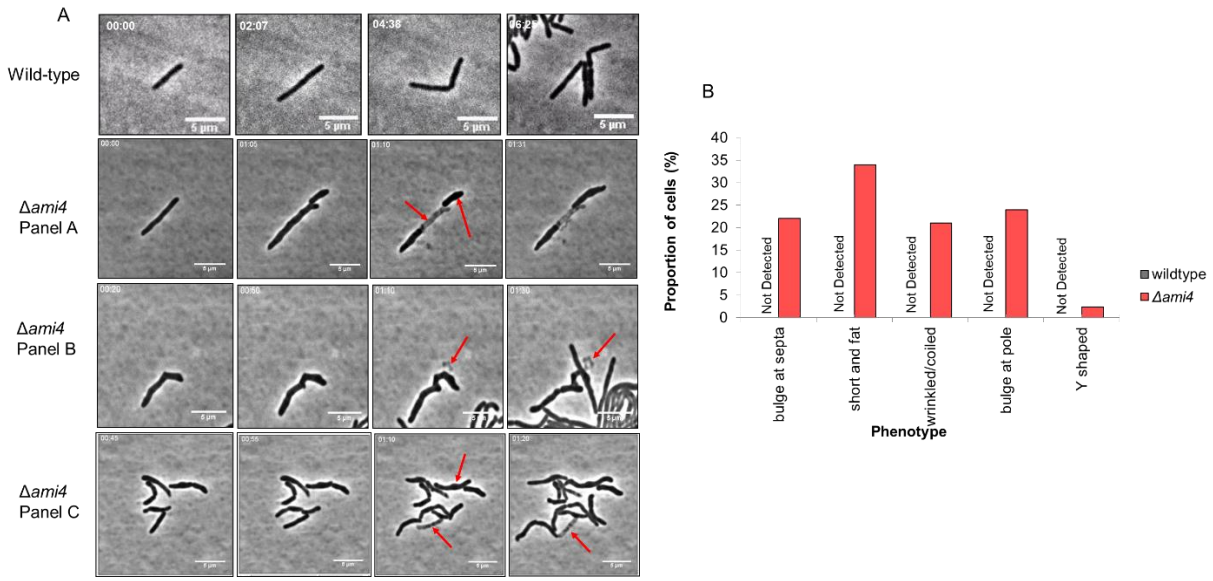

Supplementary Figure 10: Time-lapse microscopy of *M. smegmatis ami4* deficient strain and dysregulated cell wall synthesis. A) Growth patterns of wild-type *M. smegmatis* in Middlebrook 7H9 media with different time stamps showing pattern of mycobacterial growth and division. Wild-type adopts simple pattern of growth, extending via poles and diving at the septa to produce two daughter cells (time stamp 04:38). The *ami4* deficient strain failed to adopt the same pattern, instead producing fat cells which extruded cell wall material and later died (shown in red arrows throughout Δ*ami4* panels). B) Graphical representation of phenotypes seen in both the wild-type and *ami4* deficient strains; total amount of cells counted= 100 micro-colonies.

A

Enzyme	Fragment size (bp)
BamHI	2988, 2241, 1908, 624
NcoI	4924, 2837
NruI	3889, 2626, 1246
PstI	5413, 1866, 482
PvuI	4796, 1875, 649, 441
pvuII	6487, 1247
SmaI	5177, 1605, 979

B

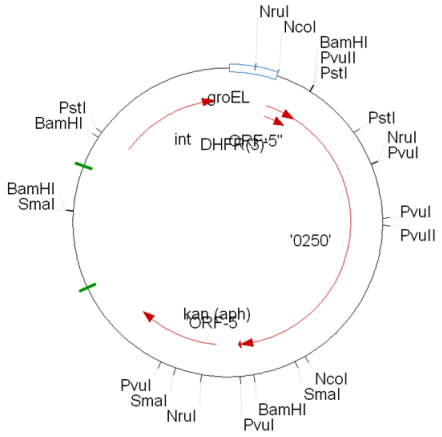

C

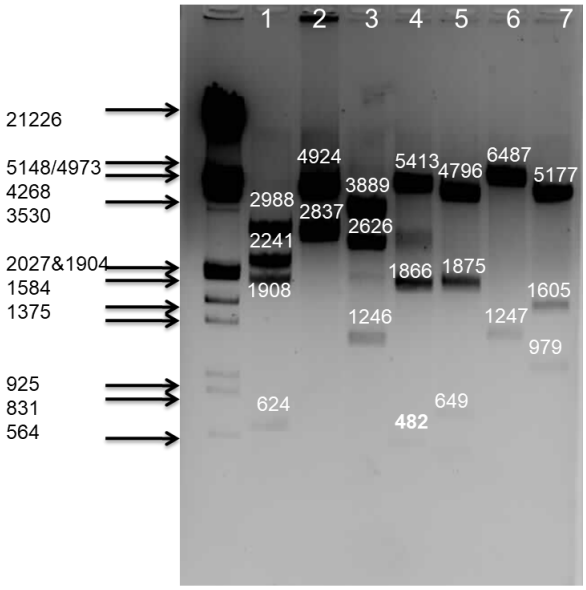

Supplementary Figure 11: Restriction profile of pUAB400_*mmpl*. A) The table displays the different restriction endonucleases used and the expected fragment sizes. B) 0250 pUAB400 final construct map with restriction endonuclease positions shown. C) 0.8% Agarose gel showing the fragment sizes following plasmid digestion with corresponding enzymes. Agarose gel of digested fragments: Roche marker III [Lane 1], *BamHI* [Lane 2], [Lane 3], *NruI* [Lane 4], *PstI* [Lane 5], *pvuI* [Lane 6], *pvuII* [Lane 7] and *SmaI* [Lane 8].

A

Enzyme	Fragment size (bp)
BamHI	2722, 1908, 624
MscI	3348, 1342, 562
NruI	3889, 1365
PvuI	4605, 649
SmaI	3649, 1605
XbaI	3401, 1853

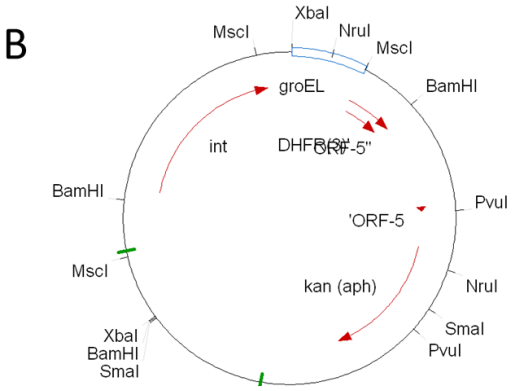

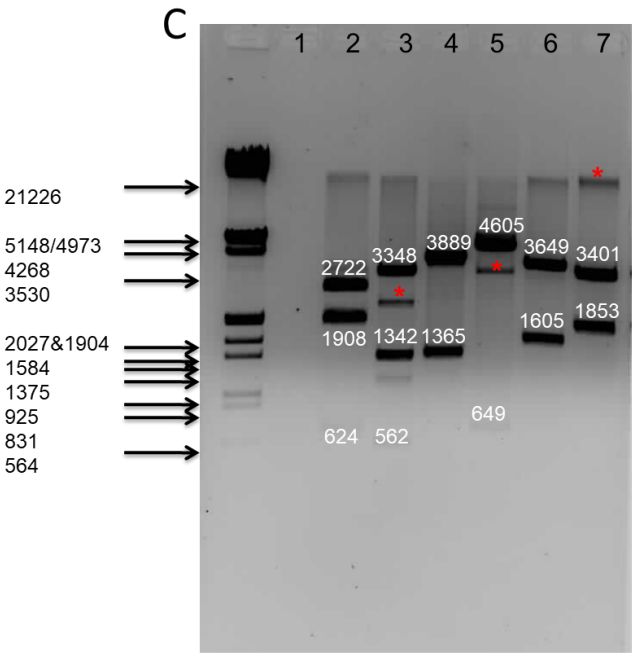

Supplementary Figure 12: Restriction profile of pUAB400_*pap2* A) The table displays the different restriction endonucleases used and the expected fragment sizes. B) 6402 pUAB400 final construct map with restriction endonuclease positions shown. C) 0.8% Agarose gel showing the fragment sizes following plasmid digestion with corresponding enzyme. Agarose gel of digested fragments: Roche marker III [Lane 1], *BamHI* [Lane 2], *MScI* [Lane 3], *NruI* [Lane 4], *pvuI* [Lane 5], *SmaI* [Lane 6] and *XbaI* [Lane 7]. The red asterix shows unexpected DNA fragments due to incomplete DNA digestion.

A

Enzyme	Fragment size (bp)
AatII	4951, 1701
BamHI	4120, 1908, 624
MscI	4746, 1342, 564
PstI	3776, 2766
PvuI	6003, 649
SmaI	2609, 2438, 1605

B

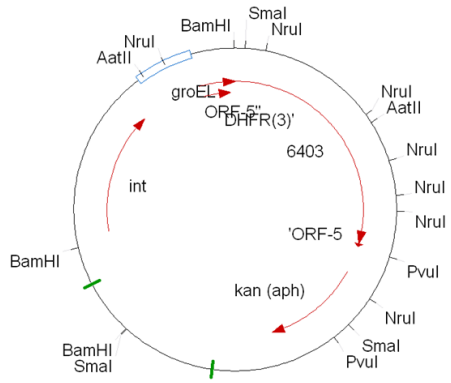

C

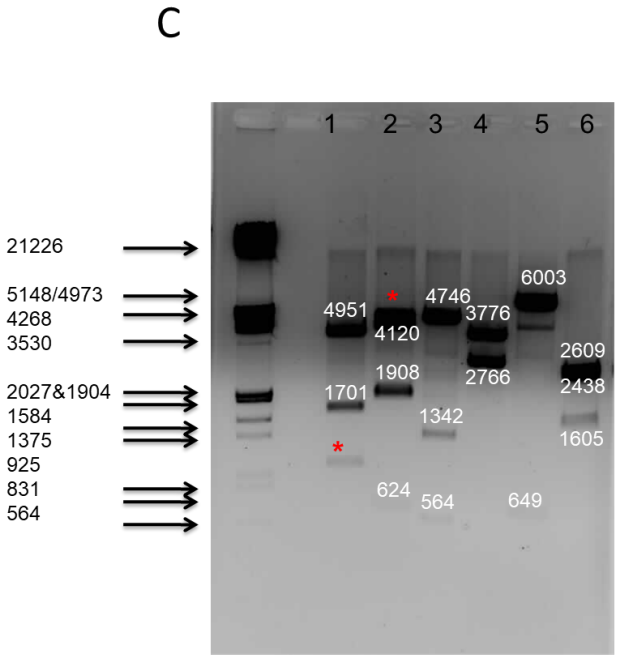

Supplementary Figure 13: Restriction profile of pUAB400_*glft*. A) The table displays the different restriction endonucleases used and the expected fragment sizes. B) 6403 pUAB400 final construct map with restriction endonuclease positions shown. C) 0.8% Agarose gel showing the fragment sizes following plasmid digestion with corresponding enzyme. Agarose gel of digested fragments: Roche marker III [Lane 1], *AatII* [Lane 2], *BamHI I* [Lane 3], *MscI* [Lane 4], *PstI* [Lane 5] *pvuII* [Lane 6], and *SmaI* [Lane 7]. The red asterix shows unexpected DNA fragments due to incomplete DNA digestion.

A

Enzyme	Fragment size (bp)
BamHI	2409, 1908, 624, 522, 93, 81
MscI	2862, 1342, 869, 564
NruI	3889, 1210, 538
PvuII	4834, 803
SmaI	2861, 1605, 1024, 147
XbaI	3784, 1853

B

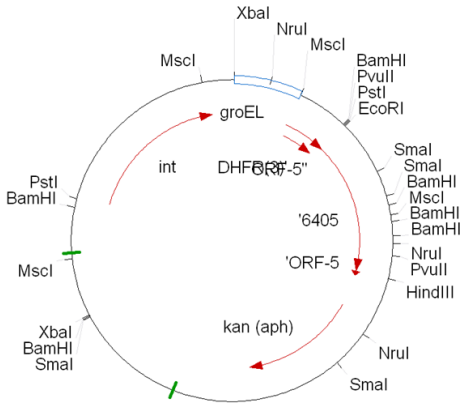

C

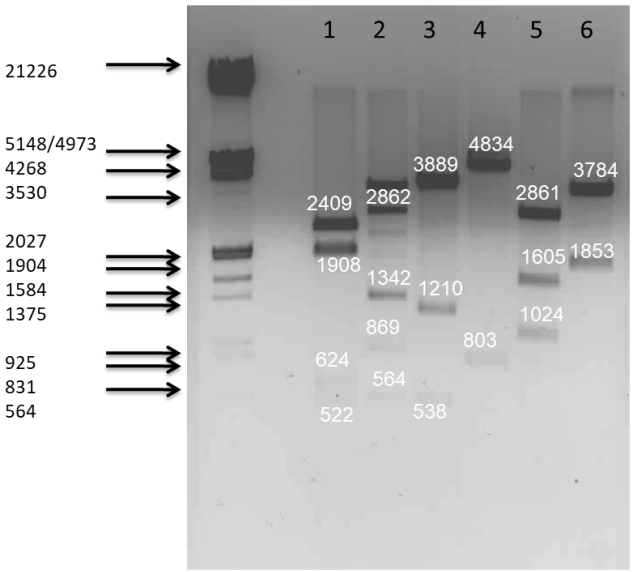

Supplementary Figure 14: Restriction profile of pUAB400_*erp*. A) The table displays the different restriction endonucleases used and the expected fragment sizes. B) 6405 pUAB400 final construct map with restriction endonuclease positions shown. C) 0.8% Agarose gel showing the fragment sizes following plasmid digestion with corresponding enzyme. Agarose gel of digested fragments: Roche marker III [Lane 1], *BamHI* [Lane 2], *MScI* [Lane 3], *NruI* [Lane 4], *pVUII* [Lane 5] *SmaI* [Lane 6] and *XbaI* [Lane 7]. The red asterix indicates failure to completely digest the DNA possibly as a result of too much DNA in the reaction.

A

Enzyme	Fragment size (bp)
AatII	3786, 1805, 927
BamHI	5849, 669
NruI	3159, 2428, 931
Negative control	No DNA expected
SacI	2752, 1476, 1019, 746, 525
SmaI	3260, 2472, 786

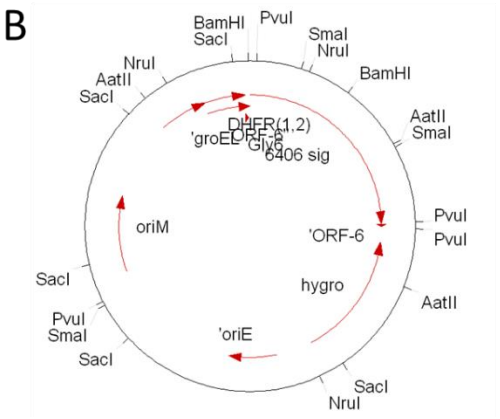

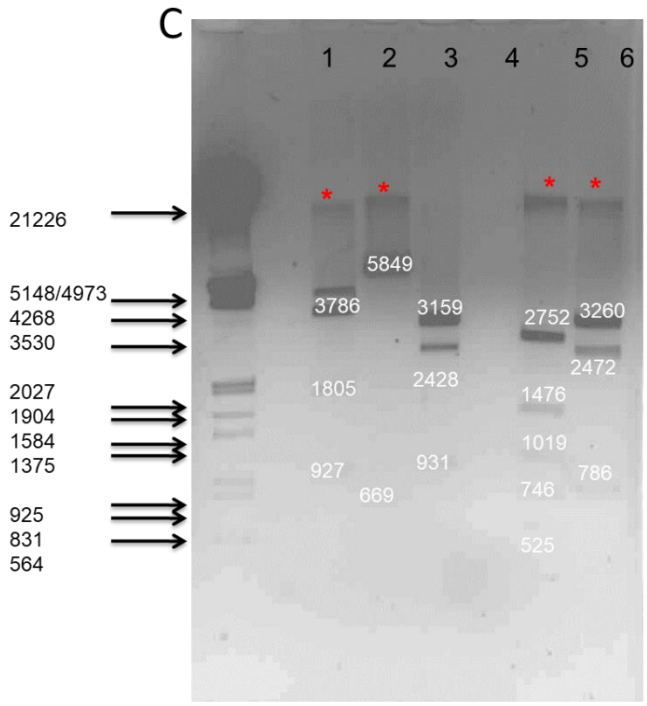

Supplementary Figure 15: Restriction profile of pUAB300_*ami3*. A) The table displays the different restriction endonucleases used and the expected fragment sizes. B) 6406 pUAB300 final construct map with restriction endonuclease positions shown. C) 0.8% Agarose gel showing the fragment sizes following plasmid digestion with corresponding enzyme. Agarose gel of digested fragments: Roche marker III [Lane 1], *AatII* [Lane 2], *BamHI* [Lane 3], *NruI* [Lane 4], Negative control [Lane 5] *SacI* [Lane 6], and *SmaI* [Lane 7]. The red asterix shows unexpected DNA fragments due to incomplete DNA digestion.

A

Enzyme	Fragment size (bp)
Acc651 and HindIII	2159, 4910
BamHI	3681, 1908, 844, 624, 12
MscI	5163, 1342, 564
NruI	3889, 2271, 821, 88
SmaI	5464, 1605
XbaI	5216, 1853

B

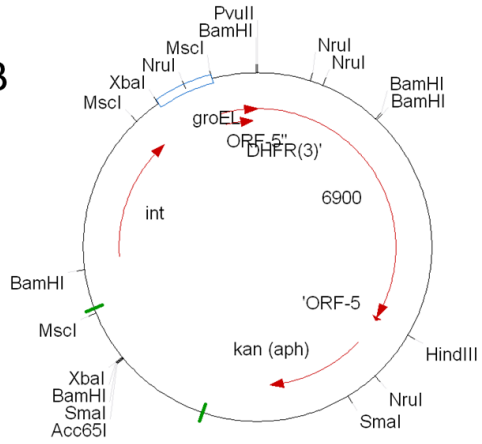

C

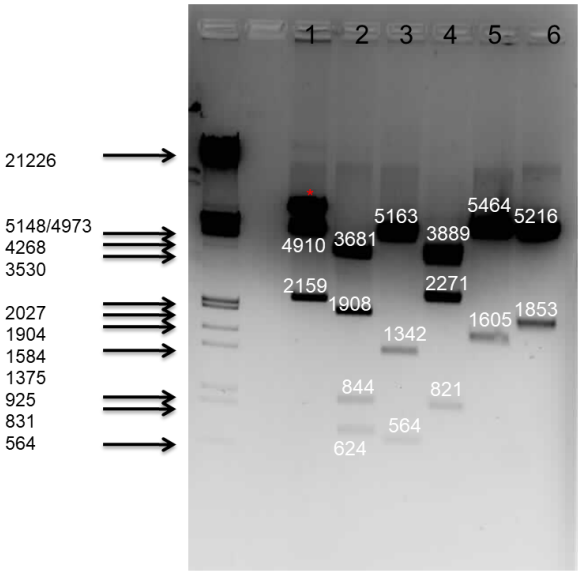

Supplementary Figure 16: Restriction profile of pUAB400_*ponA1*. A) The table displays the different restriction endonucleases used and the expected fragment sizes. B) 6900 Puab400 final construct map with restriction endonuclease positions shown. C) 0.8% Agarose gel showing the fragment sizes following plasmid digestion with corresponding enzyme. Agarose gel of digested fragments: Roche marker III [Lane 1], *Acc651* and *HindIII* [Lane 2], *BamHI* [Lane 3], *MscI* [Lane 4], *NruI* [Lane 5] *SmaI* [Lane 6], and *XbaI* [Lane 7]. The red asterix shows unexpected DNA fragments due to incomplete DNA digestion.

Appendix A

Table 1: Media and recipes used in this study

Following preparation, media was autoclaved…

Middlebrook 7H9 minimal media	4.7 g 7H9 powder 2 ml glycerol 0.2% glucose 0.85% sodium chloride
Middlebrook 7H10 minimal media plates	19 g 7H10 powder 5 ml glycerol 0.2% glucose 0.85% sodium chloride 0.05% Tween 80
Luria-Bertani broth (LB)	10 g sodium chloride 10 g tryptone 5 g yeast
Luria-Bertani agar plates (LA)	10 g tryptone 10 g sodium chloride 5 g yeast extract 15 g agar
Sauton's Minimal media	0.05% (w/v) KH_2PO_4 0.05% (w/v) $FeSO_2$ 0.2% (w/v) citric acid 0.005% (w/v) ferric citrate 0.2% (v/v) glycerol 0.0001% (v/v) $ZnSO_4$ 0.01% (v/v) Tyloxapol

Table 2: Reagents used in this study

Solutions for plasmid extraction	Reagents
Solution I	50 mM glucose, 25 mM Tris-HCL (pH 8), 10 mM EDTA in DH2O
Solution II	1 % SDS, 0.2 M NaOH dissolved in sdH2O
Solution III	3 M potassium acetate, 11.5 % acetic acid dissolved in sdH2O
Solutions for genomic DNA extraction	Reagents
CTAB	4.1 % NaCl, 10 % N-acetyl-N,N,N-trimethyl ammonium bromide dissolved in dH2O
TE Buffer	10 mM Tris-HCl (pH 8), 10 mM EDTA dissolved in Dh2o
Chloroform	Chloroform
Phenol:chloroform	Chloroform 24 ml, 1 ml isoamyl alcohol
Sodium acetate	3 M sodium acetate dissolved in dH2O, pH 5.2
Solutions for E. coli transformation	Reagents
Calcium chloride	0.1 M calcium chloride in dH2O, autoclaved
Southern Blot	Reagents
Denaturation solution	0.5 M NaOH, 1.5 M NaCl in dH2O
Depurination solution	0.25 M HCl in dH2O
TBE (5 ×)	Tris-Borate-EDTA powder (Sigma) dissolved in 2l Dh2o
SSC (20 ×)	3M NaCl, 0.3M sodium citrate in dH2O
Soln I	10 ml 20X SSC, 1 ml 10 % SDS, 89 ml dH2O
Soln II	2.5 ml 20X SSC, 1 ml 10 % SDS, 96.5 ml 10 % SDS 10 g powder, 100 ml sdH20
Maleic acid buffer	116.1 g maleic acid powder, 87. 66 g NaCl, pH 7.5 withNaOH pellets, make 1000 ml final volume with dH2O
Wash buffer	0.1M Maleic acid buffer, 0.3 % Tween20
Blocking solution	1 × blocking solution in maleic acid buffer
Detection buffer	0.1M Tris-HCl, 0.1M NaCl in dH2O (pH 9.5)
Antibody solution (Roche)	Dilute 1 in 10 000 in blocking solution
CSPD (Roche)	Disodium 2-chloro-5-(4-methoxyspiro (2-dioxetane-3,2 (2- dioxetane-3,2'-(5'-chloro)-tricyclo[3.3.1.1. 3, 7.]decan)-. 4- yl)-1-phenyl phosphate

Table 3: All primers used in the study

Table : Primer sequences used in the construction of amidase knockout strains

Primer	Sequence (5'- 3')	Annealing temperature for DNA polymerase	Expected (bp)
amidase3 (MSMEG_6406) Upstream region			
*ami3*UF	GTGAAGCTTCCGTACTTGTGGACCTCGAT	60°C	1500 bp
*ami3*UR	GTGAGATCTGTGACTGCACGGACTGATGT		
amidase3 (MSMEG_6406) Downstream region			
*ami3*UF	GTGAGATCTGTGAGAAGCACACCGTGGTC	60°C	1500 bp
*ami3*UR	GTGGGTACCCCGCTACCTGATCAGACACA		
amidase4 (MSMEG_5315) Upstream region			
*ami4*UF	GTGAAGCTTGTCGGACCGAGTTGAAAAGA	62°C	1700 bp
*ami3*UR	GTGTCTAGAGGGATACTCGACGAGGTTGA		
amidase4 (MSMEG_5315) Downstream region			
*ami4*UF	GTGTCTAGAGCGACTTCCAGCGTCGTA	65°C	2000 bp
*ami4*UR	GTGGGTACCACTCGTCCAAGCCCACCT		
amidase5 (MSMEG_0533) Upstream region			
*ami5*UF	GTGAAGCTTCAACACCATCCGAAACACAG	60°C	
*ami5*UR	GTGAGATCTGTCGAAGTCGCCGTCACCGTT	68°C	1500 bp
amidase5 (MSMEG_0533) Downstream region			
*ami5*DF	GTGAGATCTCTCAGTTCACACGCGCATTCT	63.80°C	
*ami5*DR	GTGGGATCCATGCCGTGCTTCTTGAACTT	59.88°C	1500 bp

Table 4 : Primers for *ami3*, *ami4* and *ami5* complementation

Primer	Sequence (5'- 3')	Annealing temperature for DNA polymerase	Expected (bp)
	amidase3 (MSMEG_6406)		
*ami3*F	GTGGGTACCACCTATCCGATCCTGGGTGAT	57°C	2098 bp
*ami3*R	GTGAAGCTTGTCACCACCACCAACGCC	59°C	
	amidase4 (MSMEG_5315)		
*ami4*F	GTGGAGCTCGAAGTCCTCGGCGTACC	62°C	1200 bp
*ami4*R	GTGTCTAGACGACCTCATACGCCATCTGC	55°C	
	amidase 5 (MSMEG_0533)		
*ami5*F	GTGTCTAGATCTCAGGGCTGTTGGAAGTC	64.41°C	
*ami5*R	GTGAAGCTTGGCCTGCTGCTGAATCTC	63.63°C	937 bp

Table 5: Primers for the MPF-C assay

Primer	Sequence (5'- 3')	Tm (˚C)
ami3 F (No SigP puab300)	GTGCTGCAGCTCAGCGGGACCGGCGACGAAC	65°C
ami3 R (puab300)	GTGAAGCTT TCAGGCGATCGGCGTGAAGCGCT	60°C
ami3 F(Signal puab300):	GTGCTGCAGGTGCAGTCACGTCGTCCCGCGC	62°C
pap2 F (PUAB400):	GTGCAGCTGATGAGCGACGCCCCGCGCGGCGA	67°C
*pap*2 R (PUAB400):	GTGAAGCTT TCATCTGTCTCCTTCGGCACCGAC	65°C
glft F (PUAB400):	GTGCAGCTGATGAGTGACATCCCTTCCGGCGC	60°C
gflt R(PUAB400):	GTGAAGCTTTCATCGTCCGACTTTCTCCGGTG	60.5°C
erp F(SIGP PUAB400):	GTGGAATTCGTGCCGAACCGCCGTCGACGCAAG	62.4°C
erp F(NO SIGP PUAB400):	GTGGAATTCGCACCCGTGCCGCCGCCTGCCTGA	63°C
erp R(PUAB400):	GTGAAGCTTGCAACTCAGCATTCCCCCGCAC	66°C
mmpl F (PUAB400):	GTGGAATTCGTGTTCGCCTGGTGGGGTCGGACC	66°C
mmpl R (PUAB400):	GTGAAGCTT CTACAGCCTGCCTTCGCGGCGC	65.6°C

Appendix B

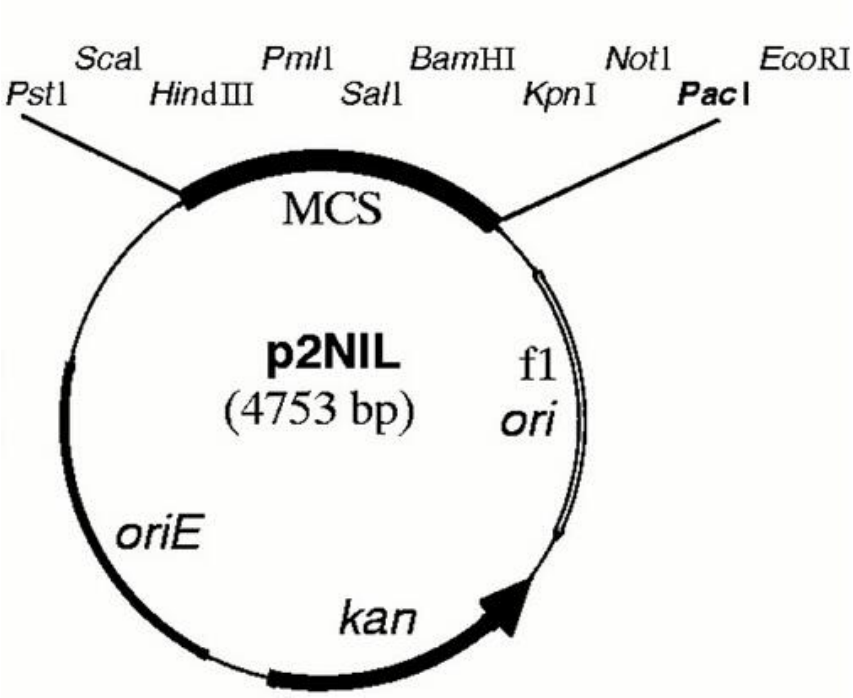

Figure B1: Vector map of p2NIL.

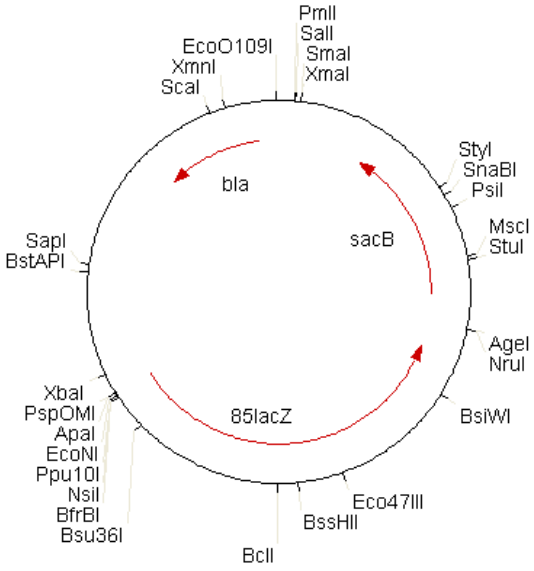

Figure B2: Vector map of pGOAL17.

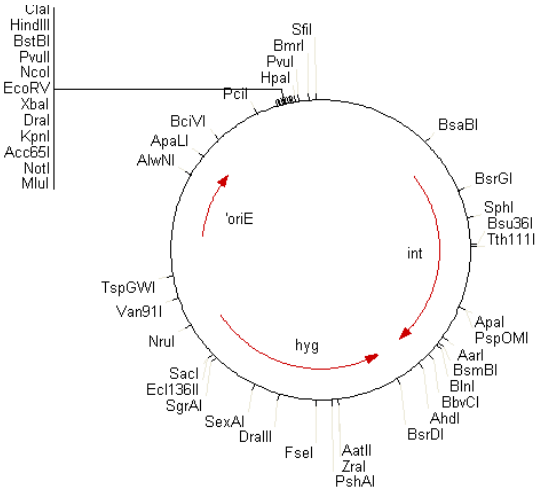

Figure B3: Vector map of pMV306H.

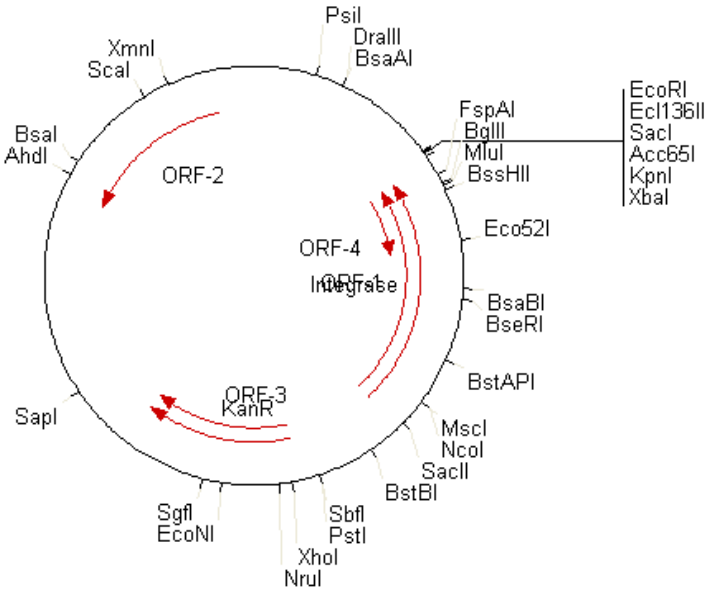

Figure B4: Vector map of pTweety.

Appendix C

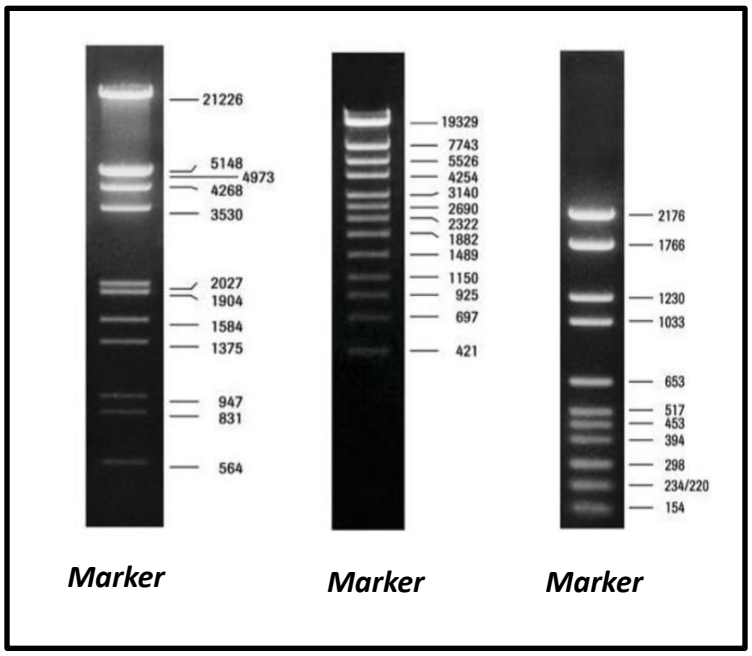

Molecular weight markers

References

Adams, D. W. A. E., J. (2009) Bacterial Cell Division: Assembly, Maintenance And Disassembly Of The Z Ring. *Nature Reviews Microbiology* 7**,** 642-653.

Adindla, S., Inampudi, K., Guruprasad, K. & Guruprasad, L. (2004). Identification and analysis of novel tandem repeats in the cell surface proteins of archaeal and bacterial genomes using computational tools. *Comparative and functional genomics,* 5, 2-16.

Allesen-Holm, M., Barken, K. B., Yang, L., Klausen, M., Webb, J. S., Kjelleberg, S., Molin, S., Givskov, M. & Tolker-Nielsen, T. (2006). A Characterization Of DNA Release In *Pseudomonas aeruginosa* Cultures And Biofilms. *Molecular Microbiology,* 59**,** 1114-1128.

Asano, K., Kakizaki, I. & Nakane, A. (2012). Interaction Of *Listeria monocytogenes* Autolysin Amidase With Glycosaminoglycans Promotes Listerial Adhesion To Mouse Hepatocytes. *Biochimie,* 94**,** 1291-1299.

Astarie-Dequeker, C., Le Guyader, L., Malaga, W., Seaphanh, F.-K., Chalut, C., Lopez, A. & Guilhot, C. (2009). Phthiocerol Dimycocerosates Of *Mycobacterium tuberculosis* Participate In Macrophage Invasion By Inducing Changes In The Organization Of Plasma Membrane Lipids. *Plos Pathogens,* 5**,** E1000289.

Atrih, A., Zöllner, P., Allmaier, G. & Foster, S. J. (1996). Structural Analysis Of *Bacillus subtilis* 168 Endospore Peptidoglycan And Its Role During Differentiation. *Journal Of Bacteriology,* 178**,** 6173-6183.

Bayer, M., Iberer, R., Bischof, K., Rassi, E., Stabentheiner, E., Zellnig, G. & Koraimann, G. (2001). Functional And Mutational Analysis Of P19, A DNA Transfer Protein With Muramidase Activity. *Journal Of Bacteriology,* 183**,** 3176-3183.

Bateman, A., Birney, E., Cerruti, L., Durbin, R., Etwiller, L., Eddy, S. R., Griffiths-Jones, S., Howe, K. L., Marshall, M. & Sonnhammer, E. L. (2002). The PFAM protein families database. *Nucleic acids research,* 30, 276-280.

Bayles, K. W. (2003). Are the molecular strategies that control apoptosis conserved in bacteria? *Trends In Microbiology*, 11, 306-311.

Bayles, K. W. (2014). Bacterial Programmed Cell Death: Making Sense Of A Paradox. *Nature Reviews Microbiology,* 12**,** 63-69.

Berendt, S., Lehner, J., Zhang, Y. V., Rasse, T. M., Forchhammer, K. & Maldener, I. (2012). Cell Wall Amidase Amic1 Is Required For Cellular Communication And Heterocyst Development In The *Cyanobacterium anabaena Pcc* 7120 But Not For Filament Integrity. *Journal Of Bacteriology,* 194**,** 5218-5227.

Bernhardt, T. G. & De Boer, P. A. (2003). The *Escherichia coli* Amidase Amic Is A Periplasmic Septal Ring Component Exported Via The Twin-Arginine Transport Pathway. *Molecular Microbiology,* 48**,** 1171-1182.

Bloos, F. & Reinhart, K. (2014). Rapid diagnosis of sepsis. *Virulence,* 5, 154-160.

Boshoff, H. I., Singh, R. & Barry, C. E. (2008). Virulence And Persistence Mechanisms Of *Mycobacterium tuberculosis*. *Handbook Of Tuberculosis***,** 151-191.

Boudreau, M. A., Fisher, J. F. & Mobashery, S. (2012). Messenger Functions Of The Bacterial Cell Wall-Derived Muropeptides. *Biochemistry,* 51**,** 2974-2990.

Boutte, C. C., Baer, C. E., Papavinasasundaram, K., Liu, W., Chase, M. R., Meniche, X., Fortune, S. M., Sassetti, C. M., Ioerger, T. R. & Rubin, E. J. (2016). A Cytoplasmic Peptidoglycan Amidase Homologue Controls Mycobacterial Cell Wall Synthesis. *Elife,* 5. doi:10.7554/eLife.14590

Brennan, P. J. (2003). Structure, Function, And Biogenesis Of The Cell Wall Of *Mycobacterium tuberculosis*. *Tuberculosis,* 83**,** 91-97.

Brodin, P., Poquet, Y., Levillain, F., Peguillet, I., Larrouy-Maumus, G., Gilleron, M., Ewann, F., Christophe, T., Fenistein, D. & Jang, J. (2010). High Content Phenotypic Cell-Based Visual Screen Identifies *Mycobacterium tuberculosis* Acyltrehalose-Containing Glycolipids Involved In Phagosome Remodeling. *Plos Pathogens,* 6**,** E1001100.

Bugg, T. D., Braddick, D., Dowson, C. G. & Roper, D. I. (2011). Bacterial Cell Wall Assembly: Still An Attractive Antibacterial Target. *Trends In Biotechnology,* 29**,** 167-173.

Bussiere, D. E., Pratt, S. D., Katz, L., Severin, J. M., Holzman, T. & Park, C. H. (1998). The Structure Of Vanx Reveals A Novel Amino-Dipeptidase Involved In Mediating Transposon-Based Vancomycin Resistance. *Molecular Cell,* 2**,** 75-84.

Büttner, F. M., Renner-Schneck, M. & Stehle, T. (2015). X-Ray Crystallography And Its Impact On Understanding Bacterial Cell Wall Remodeling Processes. *International Journal Of Medical Microbiology,* 305**,** 209-216.

Büttner, H., Mack, D. & Rohde, H. (2015). Structural Basis Of *Staphylococcus epidermidis* Biofilm Formation: Mechanisms And Molecular Interactions. *Frontiers In Cellular And Infection Microbiology,* 5**,** 14.

Cambier, C., O'leary, S. M., O'sullivan, M. P., Keane, J. & Ramakrishnan, L. (2017). Phenolic Glycolipid Facilitates Mycobacterial Escape From Microbicidal Tissue-Resident Macrophages. *Immunity,* 47**,** 552-565. E4.

Cambier, C., Takaki, K. K., Larson, R. P., Hernandez, R. E., Tobin, D. M., Urdahl, K. B., Cosma, C. L. & Ramakrishnan, L. (2014). Mycobacteria Manipulate Macrophage Recruitment Through Coordinated Use Of Membrane Lipids. *Nature,* 505**,** 218.

Cameron, T. A., Zupan, J. R. & Zambryski, P. C. (2015). The essential features and modes of bacterial polar growth. *Trends In Microbiology,* 23, 347-353.

Chao, M. C., Kieser, K. J., Minami, S., Mavrici, D., Aldridge, B. B., Fortune, S. M., Alber, T. & Rubin, E. J. (2013). Protein Complexes And Proteolytic Activation Of The Cell Wall Hydrolase RipA Regulate Septal Resolution In Mycobacteria. *Plos Pathogens,* 9**,** E1003197.

Chaput, C., Ecobichon, C., Cayet, N., Girardin, S. E., Werts, C., Guadagnini, S., Prévost, M.-C., Mengin-Lecreulx, D., Labigne, A. & Boneca, I. G. (2006). Role Of Amia In The Morphological Transition Of *Helicobacter pylori* And In Immune Escape. *Plos Pathogens,* 2**,** E97.

Charlier, P., Wery, J. P., Dideberg, O. & Frère, J. M. (2011). *Streptomyces albus* Gd-Ala-D-Ala Carboxypeptidase. *Encyclopedia Of Inorganic And Bioinorganic Chemistry*. doi.org/10.1002/9781119951438.eibc0498

Chen, Y., Fukuoka, S. & Makino, S. (2000). A Novel Spore Peptidoglycan Hydrolase Of *Bacillus cereus*: Biochemical Characterization And Nucleotide Sequence Of The Corresponding Gene, Slel. *Journal Of Bacteriology,* 182**,** 1499-1506.

Claessen, D., Emmins, R., Hamoen, L. W., Daniel, R. A., Errington, J. & Edwards, D. H. (2008). Control Of The Cell Elongation–Division Cycle By Shuttling Of Pbp1 Protein In *Bacillus subtilis*. *Molecular Microbiology,* 68**,** 1029-1046.

Cloud, K. A. & Dillard, J. P. (2002). A Lytic Transglycosylase Of *Neisseria gonorrhoeae* Is Involved In Peptidoglycan-Derived Cytotoxin Production. *Infection And Immunity,* 70**,** 2752-2757.

Collier-Hyams, L. S., Zeng, H., Sun, J., Tomlinson, A. D., Bao, Z. Q., Chen, H., Madara, J. L., Orth, K. & Neish, A. S. (2002). Cutting Edge: *Salmonella avra* Effector Inhibits The Key Proinflammatory, Anti-Apoptotic NF-Kb Pathway. *The Journal Of Immunology,* 169**,** 2846-2850.

Coulombe, F., Divangahi, M., Veyrier, F., De Léséleuc, L., Gleason, J. L., Yang, Y., Kelliher, M. A., Pandey, A. K., Sassetti, C. M. & Reed, M. B. (2009). Increased Nod2-Mediated Recognition Of N-Glycolyl Muramyl Dipeptide. *Journal Of Experimental Medicine,* 206**,** 1709-1716.

Crick, D. C., Mahapatra, S. & Brennan, P. J. (2001). Biosynthesis Of The Arabinogalactan-Peptidoglycan Complex Of *Mycobacterium tuberculosis*. *Glycobiology,* 11**,** 107r-118r.

Datta, P., Dasgupta, A., Singh, A. K., Mukherjee, P., Kundu, M. & Basu, J.(2006). Interaction Between Ftsw And Penicillin-Binding Protein 3 (PBP3) Directs PBP3 To Mid-Cell, Controls Cell Septation And Mediates The Formation Of A Trimeric Complex Involving Ftsz, Ftsw And PBP3 In Mycobacteria. *Molecular Microbiology,* 62**,** 1655-1673.

Davis, K. M. & Weiser, J. N. (2011). Modifications To The Peptidoglycan Backbone Help Bacteria To Establish Infection. *Infection And Immunity*, 79**,** 562-570.

Dhar, N. & Manina, G. (2015). Single-cell analysis of mycobacteria using microfluidics and time-lapse microscopy. *Mycobacteria Protocols*. Springer. 241-256

Domenech, P., Reed, M. B. & Barry, C. E. (2005). Contribution Of The *Mycobacterium tuberculosis* MmpL Protein Family To Virulence And Drug Resistance. *Infection And Immunity,* 73**,** 3492-3501.

Dörr, T., Alvarez, L., Delgado, F., Davis, B. M., Cava, F. & Waldor, M. K. (2016). A Cell Wall Damage Response Mediated By A Sensor Kinase/Response Regulator Pair Enables Beta-Lactam Tolerance. *Proceedings Of The National Academy Of Sciences,* 113**,** 404-409.

Doyle, R. J. & Marquis, R. E. (1994). Elastic, Flexible Peptidoglycan And Bacterial Cell Wall Properties. *Trends In Microbiology,* 2**,** 57-60.

Dziarski, R. & Gupta, D. (2006). Mammalian PGRPs: Novel Antibacterial Proteins. *Cellular Microbiology,* 8**,** 1059-1069.

Ehrt, S. & Schnappinger, D. (2009). Mycobacterial Survival Strategies In The Phagosome: Defence Against Host Stresses. *Cellular Microbiology,* 11**,** 1170-1178.

Engel, H., Smink, A. J., Van Wijngaarden, L. & Keck, W. (1992). Murein-Metabolizing Enzymes From *Escherichia coli*: Existence Of A Second Lytic Transglycosylase. *Journal Of Bacteriology,* 174**,** 6394-6403.

Ercoli, G., Tani, C., Pezzicoli, A., Vacca, I., Martinelli, M., Pecetta, S., Petracca, R., Rappuoli, R., Pizza, M. & Norais, N. (2015). Lytm Proteins Play A Crucial Role In Cell Separation, Outer Membrane Composition, And Pathogenesis In Nontypeable *Haemophilus influenzae*. *mBio,* 6**,** E02575-14.

Erdemli, S. B., Gupta, R., Bishai, W. R., Lamichhane, G., Amzel, L. M. & Bianchet, M. A. (2012). Targeting the cell wall of Mycobacterium tuberculosis: structure and mechanism of L, D-transpeptidase 2. *Structure,* 20, 2103-2115.

Esmail, H., Barry, C., Young, D. & Wilkinson, R. (2014). The Ongoing Challenge Of Latent Tuberculosis. *Phil. Trans. R. Soc. B,* 369**,** 20130437.

Fernández-Tornero, C., López, R., García, E., Giménez-Gallego, G. & Romero, A. (2001). A Novel Solenoid Fold In The Cell Wall Anchoring Domain Of The Pneumococcal Virulence Factor Lyta. *Nature Structural And Molecular Biology,* 8**,** 1020.

Firczuk, M. & Bochtler, M. (2007). Folds And Activities Of Peptidoglycan Amidases. *Fems Microbiology Reviews,* 31**,** 676-691.

Flärdh, K. (2003). Essential Role Of Diviva In Polar Growth And Morphogenesis In *Streptomyces coelicolor* A3 (2). *Molecular Microbiology,* 49**,** 1523-1536.

Folkesson, A., Eriksson, S., Andersson, M., Park, J. T. & Normark, S. (2005). Components Of The Peptidoglycan-Recycling Pathway Modulate Invasion And Intracellular Survival Of *Salmonella Enterica Serovar typhimurium*. *Cellular Microbiology,* 7**,** 147-155.

Frirdich, E. & Gaynor, E. C. (2013). Peptidoglycan Hydrolases, Bacterial Shape, And Pathogenesis. *Current Opinion In Microbiology,* 16**,** 767-778.

Frirdich, E., Vermeulen, J., Biboy, J., Soares, F., Taveirne, M. E., Johnson, J. G., Dirita, V. J., Girardin, S. E., Vollmer, W. & Gaynor, E. C. (2014). Peptidoglycan LD-Carboxypeptidase PGP2 Influences Campylobacter Jejuni Helical Cell Shape And Pathogenic Properties And Provides The Substrate For The Dl-Carboxypeptidase PGP1. *Journal Of Biological Chemistry,* 289**,** 8007-8018.

Galli, E., Paly, E. & Barre, F.-X. (2017). Late Assembly Of The *Vibrio cholerae* Cell Division Machinery Postpones Septation To The Last 10% Of The Cell Cycle. *Scientific Reports,* 7**,** 44505.

Gee, C. L., Papavinasasundaram, K. G., Blair, S. R., Baer, C. E., Falick, A. M., King, D. S., Griffin, J. E., Venghatakrishnan, H., Zukauskas, A. & Wei, J.-R. (2012). A Phosphorylated Pseudokinase Complex Controls Cell Wall Synthesis In Mycobacteria. *Sci. Signal.,* 5**,** Ra7-Ra7.

Gilmore, M. E., Bandyopadhyay, D., Dean, A. M., Linnstaedt, S. D. & Popham, D. L. (2004). Production Of Muramic δ-Lactam In *Bacillus subtilis* Spore Peptidoglycan. *Journal Of Bacteriology,* 186**,** 80-89.

Gilmore, S. A., Schelle, M. W., Holsclaw, C. M., Leigh, C. D., Jain, M., Cox, J. S., Leary, J. A. & Bertozzi, C. R. (2012). Sulfolipid-1 Biosynthesis Restricts *Mycobacterium tuberculosis* Growth In Human Macrophages. *Acs Chemical Biology,* 7**,** 863-870.

Goldberg, M. F., Saini, N. K. & Porcelli, S. A. (2014). Evasion Of Innate And Adaptive Immunity By *Mycobacterium tuberculosis*. *Molecular Genetics Of Mycobacteria, Second Edition.* American Society Of Microbiology. Second Edition, 747-772

Gopal, R. & Khader, S. A. (2013). Vaccines Against Tuberculosis: Moving Forward With New Concepts. *Expert Review Of Vaccines,* 12**,** 829-831.

Goren, M. B., Hart, P. D. A., Young, M. & Armstrong, J. (1976). Prevention Of Phagosome-Lysosome Fusion In Cultured Macrophages By Sulfatides Of *Mycobacterium tuberculosis*. *Proceedings Of The National Academy Of Sciences,* 73**,** 2510-2514.

Hansen, J. M., Golchin, S. A., Veyrier, F. J., Domenech, P., Boneca, I. G., Azad, A. K., Rajaram, M. V., Schlesinger, L. S., Divangahi, M. & Reed, M. B. (2013). N-Glycolylated Peptidoglycan Contributes To The Immunogenicity But Not Pathogenicity Of *Mycobacterium tuberculosis*. *The Journal Of Infectious Diseases,* 209**,** 1045-1054.

Harding, C. V., Ramachandra, L. & Wick, M. J. (2003). Interaction Of Bacteria With Antigen Presenting Cells: Influences On Antigen Presentation And Antibacterial Immunity. *Current Opinion In Immunology,* 15**,** 112-119.

Heffron, J. D., Orsburn, B. & Popham, D. L. (2009). Roles Of Germination-Specific Lytic Enzymes CwlJ And SleB In *Bacillus anthracis*. *Journal Of Bacteriology,* 191**,** 2237-2247.

Heijenoort, J. V. (2001). Formation Of The Glycan Chains In The Synthesis Of Bacterial Peptidoglycan. *Glycobiology,* 11**,** 25r-36r.

Hempel, A. M., Cantlay, S., Molle, V., Wang, S.-B., Naldrett, M. J., Parker, J. L., Richards, D. M., Jung, Y.-G., Buttner, M. J. & Flärdh, K. (2012). The Ser/Thr protein kinase AfsK regulates polar growth and hyphal branching in the filamentous bacteria Streptomyces. *Proceedings Of The National Academy of Sciences*, 109, E2371-E2379.

Hett, E. C., Chao, M. C. & Rubin, E. J. (2010). Interaction And Modulation Of Two Antagonistic Cell Wall Enzymes Of Mycobacteria. *Plos Pathogens,* 6**,** E1001020.

Hett, E. C. & Rubin, E. J. (2008). Bacterial Growth And Cell Division: A Mycobacterial Perspective. *Microbiology And Molecular Biology Reviews,* 72**,** 126-156.

Höltje, J.-V. (1995). From Growth To Autolysis: The Murein Hydrolases In *Escherichia coli*. *Archives Of Microbiology,* 164**,** 243-254.

Höltje, J.-V., Kopp, U., Ursinus, A. & Wiedemann, B. (1994). The Negative Regulator Of β-Lactamase Induction AmpD Is A *N*-Acetyl-Anhydromuramyl-L-Alanine Amidase. *Fems Microbiology Letters,* 122**,** 159-164.

Humann, J. & Lenz, L. L. (2009). Bacterial Peptidoglycan-Degrading Enzymes And Their Impact On Host Muropeptide Detection. *Journal Of Innate Immunity,* 1**,** 88-97.

Iwase, T., Uehara, Y., Shinji, H., Tajima, A., Seo, H., Takada, K., Agata, T. & Mizunoe, Y. (2010). *Staphylococcus epidermidis* Esp Inhibits *Staphylococcus aureus* Biofilm Formation And Nasal Colonization. *Nature,* 465**,** 346.

Jackson, M., Mcneil, M. R. & Brennan, P. J. (2013). Progress In Targeting Cell Envelope Biogenesis In *Mycobacterium tuberculosis*. *Future Microbiology,* 8**,** 855-875.

Jacobs, C., Joris, B., Jamin, M., Klarsov, K., Beeumen, J., Mengin-Lecreulx, D., Heijenoort, J., Park, J. T., Normark, S. & Frère, J. M. (1995). AmpD, Essential For Both β-Lactamase Regulation And Cell Wall Recycling, Is A Novel Cytosolic *N*-Acetylmuramyl-L-Alanine Amidase. *Molecular Microbiology,* 15**,** 553-559.

Jani, C., Eoh, H., Lee, J. J., Hamasha, K., Sahana, M. B., Han, J.-S., Nyayapathy, S., Lee, J.-Y., Suh, J.-W. & Lee, S. H. (2010). Regulation Of Polar Peptidoglycan Biosynthesis By Wag31 Phosphorylation In Mycobacteria. *BMC Microbiology,* 10**,** 327.

Johnson, J. W., Fisher, J. F. & Mobashery, S. (2013). Bacterial Cell-Wall Recycling. *Annals Of The New York Academy Of Sciences,* 1277**,** 54-75.

Kadioglu, A., Weiser, J. N., Paton, J. C. & Andrew, P. W. (2008). The Role Of *Streptococcus pneumoniae* Virulence Factors In Host Respiratory Colonization And Disease. *Nature Reviews Microbiology,* 6 (4)**,** 288.

Kana, B. D., Gordhan, B. G., Downing, K. J., Sung, N., Vostroktunova, G., Machowski, E. E., Tsenova, L., Young, M., Kaprelyants, A. & Kaplan, G. (2008). The Resuscitation-Promoting Factors Of *Mycobacterium tuberculosis* Are Required For Virulence And Resuscitation From Dormancy But Are Collectively Dispensable For Growth In Vitro. *Molecular Microbiology,* 67**,** 672-684.

Kang, C.-M., Nyayapathy, S., Lee, J.-Y., Suh, J.-W. & Husson, R. N. (2008). Wag31, A Homologue Of The Cell Division Protein DivIVA, Regulates Growth, Morphology And Polar Cell Wall Synthesis In Mycobacteria. *Microbiology,* 154**,** 725-735.

Kato, M. & Goren, M. B. (1974). Synergistic Action Of Cord Factor And Mycobacterial Sulfatides On Mitochondria. *Infection And Immunity,* 10**,** 733-741.

Kerff, F., Petrella, S., Mercier, F., Sauvage, E., Herman, R., Pennartz, A., Zervosen, A., Luxen, A., Frère, J.-M. & Joris, B. (2010). Specific Structural Features Of The *N*-Acetylmuramoyl-L-Alanine Amidase Amid From *Escherichia coli* And Mechanistic Implications For Enzymes Of This Family. *Journal Of Molecular Biology,* 397**,** 249-259.

Kieser, K. J. & Rubin, E. J. (2014). How Sisters Grow Apart: Mycobacterial Growth And Division. *Nature Reviews Microbiology,* 12**,** 550.

Kikuchi, Y., Hosokawa, T. & Fukatsu, T. (2007). Insect-Microbe Mutualism Without Vertical Transmission: A Stinkbug Acquires A Beneficial Gut Symbiont From The Environment Every Generation. *Applied And Environmental Microbiology,* 73**,** 4308-4316.

Kumar, K., Awasthi, D., Berger, W. T., Tonge, P. J., Slayden, R. A. & Ojima, I. (2010). Discovery Of Anti-TB Agents That Target The Cell-Division Protein FtsZ. *Future Medicinal Chemistry,* 2**,** 1305-1323.

Kumar, P., Arora, K., Lloyd, J. R., Lee, I. Y., Nair, V., Fischer, E., Boshoff, H. I. & Barry, C. E. (2012). Meropenem Inhibits D, D-Carboxypeptidase Activity In *Mycobacterium tuberculosis*. *Molecular Microbiology,* 86**,** 367-381.

Lacks, S. & Neuberger, M. (1975). Membrane Location Of A Deoxyribonuclease Implicated In The Genetic Transformation Of *Diplococcus pneumoniae*. *Journal Of Bacteriology,* 124**,** 1321-1329.

Lambert, C., Fenton, A. K., Hobley, L. & Sockett, R. E. (2011). Predatory *Bdellovibrio* Bacteria Use Gliding Motility To Scout For Prey On Surfaces. *Journal Of Bacteriology,* 193**,** 3139-3141.

Lambris, J. D., Ricklin, D. & Geisbrecht, B. V. (2008). Complement Evasion By Human Pathogens. *Nature Reviews Microbiology,* 6**,** 132.

Lavollay, M., Arthur, M., Fourgeaud, M., Dubost, L., Marie, A., Veziris, N., Blanot, D., Gutmann, L. & Mainardi, J.-L. (2008). The Peptidoglycan Of Stationary-Phase *Mycobacterium tuberculosis* Predominantly Contains Cross-Links Generated By L, D-Transpeptidation. *Journal Of Bacteriology,* 190**,** 4360-4366.

Lee, J. B., Byeon, J. H., Jang, H. A., Kim, J. K., Yoo, J. W., Kikuchi, Y. & Lee, B. L. (2015). Bacterial Cell Motility Of *Burkholderia* Gut Symbiont Is Required To Colonize The Insect Gut. *Febs Letters,* 589**,** 2784-2790.

Lee, M., Zhang, W., Hesek, D., Noll, B. C., Boggess, B. & Mobashery, S. (2009). Bacterial AmpD At The Crossroads Of Peptidoglycan Recycling And Manifestation Of Antibiotic Resistance. *Journal Of The American Chemical Society,* 131**,** 8742-8743.

Lerner, T. R., Lovering, A. L., Bui, N. K., Uchida, K., Aizawa, S.-I., Vollmer, W. & Sockett, R. E. (2012). Specialized Peptidoglycan Hydrolases Sculpt The Intra-Bacterial Niche Of Predatory *Bdellovibrio* And Increase Population Fitness. *Plos Pathogens,* 8**,** E1002524.

Li, Y., Hsin, J., Zhao, L., Cheng, Y., Shang, W., Huang, K. C., Wang, H.-W. & Ye, S. (2013). FtsZ Protofilaments Use A Hinge-Opening Mechanism For Constrictive Force Generation. *Science,* 341**,** 392-395.

Limoli, D. H., Jones, C. J. & Wozniak, D. J. (2015). Bacterial Extracellular Polysaccharides In Biofilm Formation And Function. *Microbiology Spectrum,* 3 (3). doi:10.1128/microbiolspec.MB-0011-2014.

Lin, P. L. & Flynn, J. L. (2010). Understanding latent tuberculosis: a moving target. *The Journal of Immunology,* 185, 15-22.

Liu, C., Gelius, E., Liu, G., Steiner, H. & Dziarski, R. (2000). Mammalian Peptidoglycan Recognition Protein Binds Peptidoglycan With High Affinity, Is Expressed In Neutrophils, And Inhibits Bacterial Growth. *Journal Of Biological Chemistry,* 275**,** 24490-24499.

Liu, C., Xu, Z., Gupta, D. & Dziarski, R. (2001). Peptidoglycan Recognition Proteins A Novel Family Of Four Human Innate Immunity Pattern Recognition Molecules. *Journal Of Biological Chemistry,* 276**,** 34686-34694.

Lovering, A. L., Safadi, S. S. & Strynadka, N. C. (2012). Structural Perspective Of Peptidoglycan Biosynthesis And Assembly. *Annual Review Of Biochemistry,* 81**,** 451-478.

Lutkenhaus, J. (1993). FtsZ Ring In Bacterial Cytokinesis. *Molecular Microbiology,* 9**,** 403-409.

Lutkenhaus, J., Pichoff, S. & Du, S. (2012). Bacterial Cytokinesis: From Z Ring To Divisome. *Cytoskeleton,* 69**,** 778-790.

Machowski, E. E., Senzani, S., Ealand, C. & Kana, B. D. (2014). Comparative Genomics For Mycobacterial Peptidoglycan Remodelling Enzymes Reveals Extensive Genetic Multiplicity. *BMC Microbiology,* 14**,** 75.

Mahapatra, S., Scherman, H., Brennan, P. J. & Crick, D. C. (2005). N Glycolylation Of The Nucleotide Precursors Of Peptidoglycan Biosynthesis Of Mycobacterium Spp. Is Altered By Drug Treatment. *Journal Of Bacteriology,* 187**,** 2341-2347.

Maiga, M., Agarwal, N., Ammerman, N. C., Gupta, R., Guo, H., Maiga, M. C., Lun, S. & Bishai, W. R. (2012). Successful Shortening Of Tuberculosis Treatment Using Adjuvant Host-Directed Therapy With FDA Approved Phosphodiesterase Inhibitors In The Mouse Model. *Plos One,* 7**,** E30749.

Männik, J. & Bailey, M. W. (2015). Spatial Coordination Between Chromosomes And Cell Division Proteins In *Escherichia coli*. *Frontiers In Microbiology,* 6**,** 306.

Maphatsoe, M. (2017). Cellular localization of low-molecular-weight penicillin-binding proteins and other cell wall remodeling enzymes in Mycobacterium smegmatis. MSc unpublished.

Marrakchi, H., Lanéelle, M.-A. & Daffé, M. (2014). Mycolic Acids: Structures, Biosynthesis, And Beyond. *Chemistry & Biology,* 21**,** 67-85.

Mathew, B., Hobrath, J. V., Ross, L., Connelly, M. C., Lofton, H., Rajagopalan, M., Guy, R. K. & Reynolds, R. C. (2016). Screening And Development Of New Inhibitors Of FtsZ From *Mycobactarium tuberculosis*. *Plos One,* 11**,** E0164100.

Mcshane, H. (2011). Tuberculosis Vaccines: Beyond Bacille Calmette–Guérin. *Philosophical Transactions Of The Royal Society B: Biological Sciences,* 366**,** 2782-2789.

Meador-Parton, J. & Popham, D. L. (2000). Structural Analysis Of *Bacillus subtilis* spore Peptidoglycan During Sporulation. *Journal Of Bacteriology,* 182**,** 4491-4499.

Meniche, X., Otten, R., Siegrist, M. S., Baer, C. E., Murphy, K. C., Bertozzi, C. R. & Sassetti, C. M. (2014). Subpolar Addition Of New Cell Wall Is Directed By DivIVA In Mycobacteria. *Proceedings Of The National Academy Of Sciences,* 111**,** E3243-E3251.

Mesnage, S., Chau, F., Dubost, L. & Arthur, M. (2008). Role Of *N*-Acetylglucosaminidase And *N*-Acetylmuramidase Activities In *Enterococcus faecalis* Peptidoglycan Metabolism. *Journal Of Biological Chemistry,* 283**,** 19845-19853.

Molle, V., Saint, N., Campagna, S., Kremer, L., Lea, E., Draper, P. & Molle, G. (2006). Ph-Dependent Pore-Forming Activity Of OmpaTB From *Mycobacterium tuberculosis* And Characterization Of The Channel By Peptidic Dissection. *Molecular Microbiology,* 61**,** 826-837.

Moya, B., Juan, C., Albertí, S., Pérez, J. L. & Oliver, A. (2008). Benefit of having multiple ampD genes for acquiring β-lactam resistance without losing fitness and virulence in Pseudomonas aeruginosa. *Antimicrobial agents and chemotherapy*, 52, 3694-3700.

Mukamolova, G. V., Turapov, O. A., Kazarian, K., Telkov, M., Kaprelyants, A. S., Kell, D. B. & Young, M. (2002). The *rpf* gene of *Micrococcus luteus* encodes an essential secreted growth factor. *Molecular microbiology*, 46, 611-621.

Mukamolova, G. V., Yanopolskaya, N. D., Kell, D. B. & Kaprelyants, A. S. (1998). On Resuscitation From The Dormant State Of *Micrococcus luteus*. *Antonie Van Leeuwenhoek,* 73**,** 237-243.

Nair, N., Vinod, V., Suresh, M. K., Vijayrajratnam, S., Biswas, L., Peethambaran, R., Vasudevan, A. K. & Biswas, R. (2015). Amidase, A Cell Wall Hydrolase, Elicits Protective Immunity Against *Staphylococcus aureus* And *Staphylococcus epidermidis*. *International Journal Of Biological Macromolecules,* 77**,** 314-321.

Ng, V. H., Cox, J. S., Sousa, A. O., Macmicking, J. D. & Mckinney, J. D. (2004). Role Of Katg Catalase-Peroxidase In Mycobacterial Pathogenesis: Countering The Phagocyte Oxidative Burst. *Molecular Microbiology,* 52**,** 1291-1302.

Nikitushkin, V. D., Demina, G. R., Shleeva, M. O., Guryanova, S. V., Ruggiero, A., Berisio, R. & Kaprelyants, A. S. (2015). A Product Of RpfB And RipA Joint Enzymatic Action Promotes The Resuscitation Of Dormant Mycobacteria. *The Febs Journal,* 282**,** 2500-2511.

Núñez, M. E., Martin, M. O., Duong, L. K., Ly, E. & Spain, E. M. (2003). Investigations Into The Life Cycle Of The Bacterial Predator *Bdellovibrio bacteriovorus* 109j At An Interface By Atomic Force Microscopy. *Biophysical Journal,* 84**,** 3379-3388.

O'Brien, K. L., Wolfson, L. J., Watt, J. P., Henkle, E., Deloria-Knoll, M., McCall, N., Lee, E., Mulholland, K., Levine, O. S. & Cherian, T. (2009). Burden of disease caused by Streptococcus pneumoniae in children younger than 5 years: global estimates. *The Lancet*, 374, 893-902.

Ohno, N., Yadomae, T. & Miyazaki, T. (1982). Identification Of 2-Amino-2-Deoxyglucose Residues In The Peptidoglucan Of *Streptococcus pneumoniae*. *Carbohydrate Research,* 107**,** 152-155.

Ojha, A., Anand, M., Bhatt, A., Kremer, L., Jacobs Jr, W. R. & Hatfull, G. F. (2005). Groel1: A Dedicated Chaperone Involved In Mycolic Acid Biosynthesis During Biofilm Formation In Mycobacteria. *Cell,* 123**,** 861-873.

Osawa, M. & Erickson, H. P. (2013). Liposome Division By A Simple Bacterial Division Machinery. *Proceedings Of The National Academy Of Sciences,* 110**,** 11000-11004.

Otto, M. (2009). *Staphylococcus epidermidis*—The'accidental'pathogen. *Nature Reviews Microbiology,* 7**,** 555.

Parish, T. & Stoker, N. G. (2000). Use Of A Flexible Cassette Method To Generate A Double Unmarked *Mycobacterium tuberculosis* Tlya Plcabc Mutant By Gene Replacement. *Microbiology,* 146**,** 1969-1975.

Park, J. T. & Uehara, T. (2008). How bacteria consume their own exoskeletons (turnover and recycling of cell wall peptidoglycan). *Microbiology and Molecular Biology Reviews,* 72, 211-227.

Pérez-Gallego, M., Torrens, G., Castillo-Vera, J., Moya, B., Zamorano, L., Cabot, G., Hultenby, K., Albertí, S., Mellroth, P. & Henriques-Normark, B. (2016). Impact Of AmpC Derepression On Fitness And Virulence: The Mechanism Or The Pathway? *MBIO,* 7**,** E01783-16.

Pham, T. T., Jacobs-Sera, D., Pedulla, M. L., Hendrix, R. W. & Hatfull, G. F. (2007). Comparative Genomic Analysis Of Mycobacteriophage Tweety: Evolutionary Insights

And Construction Of Compatible Site-Specific Integration Vectors For Mycobacteria. *Microbiology,* 153**,** 2711-2723.

Pinheiro Da Silva, F., Cataldi, T. R., De Lima, T. M., Starzynski, P. N., Barbeiro, H. V., Labate, M. T. V., Cémachado, M. C. C., De Souza, H. P. & Labate, C. A. (2016). Proteomic Profiling Identifies *N*-Acetylmuramoyl-L-Alanine Amidase As A Novel Biomarker Of Sepsis. *Biomarkers In Medicine,* 10**,** 1225-1229.

Plocinski, P., Arora, N., Sarva, K., Blaszczyk, E., Qin, H., Das, N., Plocinska, R., Ziolkiewicz, M., Dziadek, J. & Kiran, M. (2012). *Mycobacterium tuberculosis* CwsA Interacts With CrgA And Wag31, And The CrgA-CwsA Complex Is Involved In Peptidoglycan Synthesis And Cell Shape Determination. *Journal Of Bacteriology,* 194**,** 6398-6409.

Plocinski, P., Martinez, L., Sarva, K., Plocinska, R., Madiraju, M. & Rajagopalan, M. (2013). *Mycobacterium tuberculosis* CwsA Overproduction Modulates Cell Division And Cell Wall Synthesis. *Tuberculosis,* 93**,** S21-S27.

Plocinski, P., Ziolkiewicz, M., Kiran, M., Vadrevu, S., Nguyen, H., Hugonnet, J., Veckerle, C., Arthur, M., Dziadek, J. & Cross, T. (2011). Characterization Of CrgA, A New Partner Of The *Mycobacterium tuberculosis* Peptidoglycan Polymerization Complexes. *Journal Of Bacteriology,* 193**,** 3246-3256.

Pompeo, F., Foulquier, E. & Galinier, A. (2016). Impact Of Serine/Threonine Protein Kinases On The Regulation Of Sporulation In *Bacillus subtilis*. *Frontiers In Microbiology,* 7**,** 568.

Popham, D. L., Helin, J., Costello, C. E. & Setlow, P. (1996). Muramic Lactam In Peptidoglycan Of *Bacillus subtilis* Spores Is Required For Spore Outgrowth But Not For Spore Dehydration Or Heat Resistance. *Proceedings Of The National Academy Of Sciences,* 93**,** 15405-15410.

Potluri, L. P., De Pedro, M. A. & Young, K. D. (2012). *Escherichia coli* Low-Molecular-Weight Penicillin-Binding Proteins Help Orient Septal FtsZ, And Their Absence Leads To Asymmetric Cell Division And Branching. *Molecular Microbiology,* 84**,** 203-224.

Prideaux, B., Via, L. E., Zimmerman, M. D., Eum, S., Sarathy, J., O'brien, P., Chen, C., Kaya, F., Weiner, D. M. & Chen, P.-Y. (2015). The Association Between Sterilizing Activity And Drug Distribution Into Tuberculosis Lesions. *Nature Medicine,* 21**,** 1223.

Qin, Z., Ou, Y., Yang, L., Zhu, Y., Tolker-Nielsen, T., Molin, S. & Qu, D. (2007). Role Of Autolysin-Mediated DNA Release In Biofilm Formation Of *Staphylococcus epidermidis*. *Microbiology,* 153**,** 2083-2092.

Ramos-Sevillano, E., Urzainqui, A., Campuzano, S., Moscoso, M., González-Camacho, F., Domenech, M., De Córdoba, S. R., Sánchez-Madrid, F., Brown, J. S. & García, E. (2015). Pleiotropic Effects Of Cell Wall Amidase LytA On *Streptococcus pneumoniae* Sensitivity To The Host Immune Response. *Infection And Immunity,* 83**,** 591-603.

Richards, J. P. & Ojha, A. K. (2014). Mycobacterial Biofilms. *Molecular Genetics Of Mycobacteria, Second Edition.* American Society Of Microbiology. Second Edition, 773-784

Rico-Lastres, P., Díez-Martínez, R., Iglesias-Bexiga, M., Bustamante, N., Aldridge, C., Hesek, D., Lee, M., Mobashery, S., Gray, J. & Vollmer, W. (2015). Substrate Recognition And Catalysis By LytB, A Pneumococcal Peptidoglycan Hydrolase Involved In Virulence. *Scientific Reports,* 5**,** 16198.

Rigden, D. J., Jedrzejas, M. J. & Galperin, M. Y. (2003). Amidase domains from bacterial and phage autolysins define a family of γ-D, L-glutamate-specific amidohydrolases. *Trends in Biochemical Sciences,* 28, 230-234.

Rivera, I., Molina, R., Lee, M., Mobashery, S. & Hermoso, J. A. (2016). Orthologous And Paralogous AmpD Peptidoglycan Amidases From Gram-Negative Bacteria. *Microbial Drug Resistance,* 22**,** 470-476.

Rocaboy, M., Herman, R., Sauvage, E., Remaut, H., Moonens, K., Terrak, M., Charlier, P. & Kerff, F. (2013). The Crystal Structure Of The Cell Division Amidase AmiC Reveals The Fold Of The Amin Domain, A New Peptidoglycan Binding Domain. *Molecular Microbiology,* 90**,** 267-277.

Rosenthal, R., Blundell, J. & Perkins, H. (1982). Strain-Related Differences In Lysozyme Sensitivity And Extent Of *O*-Acetylation Of Gonococcal Peptidoglycan. *Infection And Immunity,* 37**,** 826-829.

Rosser, A., Stover, C., Pareek, M. & Mukamolova, G. V. (2017). Resuscitation-Promoting Factors Are Important Determinants Of The Pathophysiology In *Mycobacterium tuberculosis* Infection. *Critical Reviews In Microbiology,* 43**,** 621-630.

Russell-Goldman, E., Xu, J., Wang, X., Chan, J. & Tufariello, J. M. (2008). A *Mycobacterium tuberculosis* Rpf Double-Knockout Strain Exhibits Profound Defects In Reactivation From Chronic Tuberculosis And Innate Immunity Phenotypes. *Infection And Immunity,* 76**,** 4269-4281.

Sacks, L. V. & Behrman, R. E. (2009). Challenges, Successes And Hopes In The Development Of Novel TB Therapeutics. *Future Medicinal Chemistry,* 1**,** 749-756.

Santi, I., Dhar, N., Bousbaine, D., Wakamoto, Y. & Mckinney, J. D. (2013). Single-Cell Dynamics Of The Chromosome Replication And Cell Division Cycles In Mycobacteria. *Nature Communications,* 4**,** 2470.

Sarathy, J., Dartois, V., Dick, T. & Gengenbacher, M. (2013). Reduced Drug Uptake In Phenotypically Resistant Nutrient-Starved Nonreplicating *Mycobacterium tuberculosis*. *Antimicrobial Agents And Chemotherapy,* 57**,** 1648-1653.

Sarathy, J. P., Dartois, V. & Lee, E. J. D. (2012). The Role Of Transport Mechanisms In *Mycobacterium tuberculosis* Drug Resistance And Tolerance. *Pharmaceuticals,* 5**,** 1210-1235.

Sasindran, S. J. & Torrelles, J. B. (2011). *Mycobacterium tuberculosis* Infection And Inflammation: What Is Beneficial For The Host And For The Bacterium? *Frontiers In Microbiology,* 2**,** 2.

Sauvage, E., Kerff, F., Terrak, M., Ayala, J. A. & Charlier, P. (2008). The Penicillin-Binding Proteins: Structure And Role In Peptidoglycan Biosynthesis. *Fems Microbiology Reviews,* 32**,** 234-258.

Schaub, R. E., Chan, Y. A., Lee, M., Hesek, D., Mobashery, S. & Dillard, J. P. (2016). Lytic Transglycosylases LtgA And LtgD Perform Distinct Roles In Remodeling, Recycling And Releasing Peptidoglycan In *Neisseria gonorrhoeae*. *Molecular Microbiology,* 102**,** 865-881.

Scherr, N. & Nguyen, L. (2009). Mycobacterium Versus Streptomyces—We Are Different, We Are The Same. *Current Opinion In Microbiology*, 12**,** 699-707.

Schoonmaker, M. K., Bishai, W. R. & Lamichhane, G. (2014) Nonclassical Transpeptidases Of *Mycobacterium tuberculosis* Alter Cell Size, Morphology, The Cytosolic Matrix, Protein Localization, Virulence, And Resistance To β-Lactams. *Journal Of Bacteriology,* 196**,** 1394-1402.

Senzani, S., Li, D., Bhaskar, A., Ealand, C., Chang, J., Rimal, B., Liu, C., Kim, S. J., Dhar, N. & Kana, B. (2017). An Amidase_3 Domain-Containing *N*-Acetylmuramyl-L-Alanine Amidase Is Required For Mycobacterial Cell Division. *Scientific Reports,* 7**,** 1140.

Shockman, G. & Höltje, J.-V. (1994). Microbial Peptidoglycan (Murein) Hydrolases. *New Comprehensive Biochemistry.* Elsevier, 27, 131-166

Sikhosana, N. (2015). Characterization of Amidas_2 domain proteins in *Mycobacterium smegmatis.* Honours project conducted at the CBTBR, Department of Molecular Medicine and Haematology, School of Pathology, Wits University. Unpublished.

Silver, L. L. (2006). Does The Cell Wall Of Bacteria Remain A Viable Source Of Targets For Novel Antibiotics? *Biochemical Pharmacology,* 71**,** 996-1005.

Simmons, D. P., Canaday, D. H., Liu, Y., Li, Q., Huang, A., Boom, W. H. & Harding, C. V. (2010). *Mycobacterium tuberculosis* And Tlr2 Agonists Inhibit Induction Of Type I IFNγ And Class I MHC Antigen Cross Processing By Tlr9. *The Journal Of Immunology,* 185**,** 2405-2415.

Singh, A., Mai, D., Kumar, A. & Steyn, A. J. (2006) Dissecting virulence pathways of *Mycobacterium tuberculosis* through protein-protein association. *Proc Natl Acad Sci U S A*, 103, 11346-51.snap

Singh, B., Nitharwal, R. G., Ramesh, M., Pettersson, B., Kirsebom, L. A. & Dasgupta, S. (2013). Asymmetric Growth And Division In Mycobacterium Spp.: Compensatory Mechanisms For Non-Medial Septa. *Molecular Microbiology,* 88**,** 64-76.

Singh, S. K., Saisree, L., Amrutha, R. N. & Reddy, M. (2012). Three Redundant Murein Endopeptidases Catalyse An Essential Cleavage Step In Peptidoglycan Synthesis Of *Escherichia* coli K12. *Molecular Microbiology,* 86**,** 1036-1051.

Smith, C. & Brun, Y. (2005). Bacterial Cell Differentiation. *ELS.* doi.org/10.1038/npg.els.0001422

Smith, T. J., Blackman, S. A. & Foster, S. J. (2000). Autolysins Of *Bacillus subtilis*: Multiple Enzymes With Multiple Functions. *Microbiology,* 146**,** 249-262.

Snapper, S., Melton, R., Mustafa, S., Kieser, T. & WR JR, J. (1990). Isolation and characterization of efficient plasmid transformation mutants of Mycobacterium smegmatis. *Molecular Microbiology,* 4, 1911-1919.

Somma, S., Gastaldo, L. & Corti, A.(1984). Teicoplanin, A New Antibiotic From *Actinoplanes teichomyceticus* Nov. Sp. *Antimicrobial Agents And Chemotherapy,* 26**,** 917-923.

Specht, S., Debrah, A., Klarmann, U., Mand, S., Hoerauf, A. & Pfarr, K. (2013). Chemotherapy Of Filariasis—Established Strategies And New Developments. *Gms Infect Dis,* 13**,** 2195-8831.

Steinberg, N. & Kolodkin-Gal, I. (2015). The Matrix Reloaded: How Sensing The Extracellular Matrix Synchronizes Bacterial Communities. *Journal Of Bacteriology,* 197**,** 2092-2103.

Stepkowski, T. & Legocki, A. B. (2001). Reduction Of Bacterial Genome Size And Expansion Resulting From Obligate Intracellular Lifestyle And Adaptation To Soil Habitat. *Acta Biochimica Polonica-English Edition-,* 48**,** 367-382.

Stubbs, K. A., Scaffidi, A., Debowski, A. W., Mark, B. L., Stick, R. V. & Vocadlo, D. J. (2008). Synthesis And Use Of Mechanism-Based Protein-Profiling Probes For Retaining B-D-

Glucosaminidases Facilitate Identification Of *Pseudomonas aeruginosa* NagZ. *Journal Of The American Chemical Society*, 130**,** 327-335.

Sugimoto, S., Iwamoto, T., Takada, K., Okuda, K.-I., Tajima, A., Iwase, T. & Mizunoe, Y. (2013). *Staphylococcus epidermidis* Esp Degrades Specific Proteins Associated With *Staphylococcus aureus* Biofilm Formation And Host-Pathogen Interaction. *Journal Of Bacteriology,* 195**,** 1645-1655.

Sureka, K., Hossain, T., Mukherjee, P., Chatterjee, P., Datta, P., Kundu, M. & Basu, J. (2010). Novel Role Of Phosphorylation-Dependent Interaction Between FtsZ And FipA In Mycobacterial Cell Division. *Plos One,* 5**,** E8590.

Swim, S., Gfell, M., Wilde, C. & Rosenthal, R. (1983). Strain Distribution In Extents Of Lysozyme Resistance And *O*-Acetylation Of Gonococcal Peptidoglycan Determined By High-Performance Liquid Chromatography. *Infection And Immunity,* 42**,** 446-452.

Szwedziak, P. & Löwe, J. (2013). Do The Divisome And Elongasome Share A Common Evolutionary Past? *Current Opinion In Microbiology,* 16**,** 745-751.

Tan, I. S. & Ramamurthi, K. S. (2014). Spore Formation In *Bacillus subtilis*. *Environmental Microbiology Reports,* 6**,** 212-225.

Terrasse, R., Amoroso, A., Vernet, T. & Di Guilmi, A. M. (2015). *Streptococcus pneumoniae* GAPDH Is Released By Cell Lysis And Interacts With Peptidoglycan. *Plos One,* 10**,** E0125377.

Thornberry, N. A. & Lazebnik, Y. (1998). Caspases: Enemies Within. *Science,* 281**,** 1312-1316.

Tidhar, A., Flashner, Y., Cohen, S., Levi, Y., Zauberman, A., Gur, D., Aftalion, M., Elhanany, E., Zvi, A. & Shafferman, A. (2009). The NLPD Lipoprotein Is A Novel *Yersinia pestis* Virulence Factor Essential For The Development Of Plague. *Plos One,* 4**,** E7023.

Tillman, G. E., Simmons, M., Garrish, J. K. & Seal, B. S. (2013). Expression Of A *Clostridium perfringens* Genome-Encoded Putative *N*-Acetylmuramoyl–L-Alanine Amidase As A

Potential Antimicrobial To Control The Bacterium. *Archives Of Microbiology,* 195**,** 675-681.

Torrens, G., Pérez-Gallego, M., Moya, B., Munar-Bestard, M., Zamorano, L., Cabot, G., Blázquez, J., Ayala, J. A., Oliver, A. & Juan, C. (2017). Targeting The Permeability Barrier And Peptidoglycan Recycling Pathways To Disarm *Pseudomonas aeruginosa* Against The Innate Immune System. *Plos One,* 12**,** E0181932.

Trautmann, M., Zick, R., Rukavina, T., Cross, A. S. & Marre, R. (1998). Antibiotic-Induced Release Of Endotoxin: In-Vitro Comparison Of Meropenem And Other Antibiotics. *The Journal Of Antimicrobial Chemotherapy,* 41**,** 163-169.

Typas, A., Banzhaf, M., Gross, C. A. & Vollmer, W. (2012). From The Regulation Of Peptidoglycan Synthesis To Bacterial Growth And Morphology. *Nature Reviews Microbiology,* 10**,** 123.

Uehara, T. & Bernhardt, T. G. (2011). More Than Just Lysins: Peptidoglycan Hydrolases Tailor The Cell Wall. *Current Opinion In Microbiology,* 14**,** 698-703.

Uehara, T. & Park, J. T. (2007). An Anhydro-*N*-Acetylmuramyl-L-Alanine Amidase With Broad Specificity Tethered To The Outer Membrane Of *Escherichia coli*. *Journal Of Bacteriology,* 189**,** 5634-5641.

Ulrichs, T. & Kaufmann, S. H. (2006). New Insights Into The Function Of Granulomas In Human Tuberculosis. *The Journal Of Pathology,* 208**,** 261-269.

Van Der Poll, T. & Opal, S. M. (2009). Pathogenesis, Treatment, And Prevention Of *Pneumococcal pneumonia*. *The Lancet,* 374**,** 1543-1556.

Vijay, S., Nagaraja, M., Sebastian, J. & Ajitkumar, P. (2014). Asymmetric Cell Division In *Mycobacterium tuberculosis* And Its Unique Features. *Archives Of Microbiology,* 196**,** 157-168.

Viljoen, A., Dubois, V., Girard-Misguich, F., Blaise, M., Herrmann, J. L. & Kremer, L. (2017). The diverse family of MmpL transporters in mycobacteria: from regulation to antimicrobial developments. *Molecular microbiology,* 104, 889-904.

Viollier, P. H. & Shapiro, L. (2003). A Lytic Transglycosylase Homologue, PleA, Is Required For The Assembly Of Pili And The Flagellum At The *Caulobacter crescentus* Cell Pole. *Molecular Microbiology,* 49**,** 331-345.

Vollmer, W., Blanot, D. & De Pedro, M. A. (2008). Peptidoglycan Structure And Architecture. *Fems Microbiology Reviews,* 32**,** 149-167.

Vötsch, W. & Templin, M. F. (2000). Characterization Of A β-*N*-Acetylglucosaminidase Of *Escherichia coli* And Elucidation Of Its Role In Muropeptide Recycling And β-Lactamase Induction. *Journal Of Biological Chemistry,* 275**,** 39032-39038.

Walport, M. J. (2001). Complement. *New England Journal Of Medicine,* 344**,** 1058-1066.

Wang, H., Gupta, D., Li, X. & Dziarski, R. (2005). Peptidoglycan Recognition Protein 2 (*N*-Acetylmuramoyl-L-Ala Amidase) Is Induced In Keratinocytes By Bacteria Through The P38 Kinase Pathway. *Infection And Immunity,* 73**,** 7216-7225.

Wells, V. L. & Margolin, W. (2012). A New Slant To The Z Ring And Bacterial Cell Branch Formation. *Molecular Microbiology,* 84**,** 199-202.

Whitchurch, C. B., Tolker-Nielsen, T., Ragas, P. C. & Mattick, J. S. (2002). Extracellular DNA Required For Bacterial Biofilm Formation. *Science,* 295**,** 1487-1487.

Wilmes, M., Meier, K., Schiefer, A., Josten, M., Otten, C. F., Klöckner, A., Henrichfreise, B., Vollmer, W., Hoerauf, A. & Pfarr, K. (2017). AmiD Is A Novel Peptidoglycan Amidase In Wolbachia Endosymbionts Of Drosophila Melanogaster. *Frontiers In Cellular And Infection Microbiology,* 7**,** 353.

World Health Organisation (WHO) (2017) Global tuberculosis report 2017

Wyckoff, T. J., Taylor, J. A. & Salama, N. R. (2012). Beyond growth: novel functions for bacterial cell wall hydrolases. *Trends In Microbiology,* 20, 540-547.

Yu, X. C. & Margolin, W. (1999). Ftsz Ring Clusters In Min And Partition Mutants: Role Of Both The Min System And The Nucleoid In Regulating FtsZ Ring Localization. *Molecular Microbiology,* 32**,** 315-326.

Zheng, Z., Omairi-Nasser, A., Li, X., Dong, C., Lin, Y., Haselkorn, R. & Zhao, J. (2017). An Amidase Is Required For Proper Intercellular Communication In The Filamentous *Cyanobacterium anabaena* Sp. Pcc 7120. *Proceedings Of The National Academy Of Sciences***,** 201621424.

Zhou, X. & Cegelski, L. (2012). Nutrient-Dependent Structural Changes In S. Aureus Peptidoglycan Revealed By Solid-State NMR Spectroscopy. *Biochemistry,* 51**,** 8143-8153.

Zhu, J., Jäger, K., Black, T., Zarka, K., Koksharova, O. & Wolk, C. P. (2001). HcwA, an autolysin, is required for heterocyst maturation in Anabaena sp. strain PCC 7120. *Journal Of Bacteriology*, 183, 6841-6851.

Zipperle Jr, G. F., Ezzell Jr, J. W. & Doyle, R. J. (1984). Glucosamine Substitution And Muramidase Susceptibility In *Bacillus aSnthracis*. *Canadian Journal Of Microbiology,* 30**,** 553-559.

Zug, R. & Hammerstein, P. (2015). Bad Guys Turned Nice? A Critical Assessment Of Wolbachia Mutualisms In Arthropod Hosts. *Biological Reviews,* 90**,** 89-111.

Zumla, A., Nahid, P. & Cole, S. T. (2013). Advances in the development of new tuberculosis drugs and treatment regimens. *Nature reviews Drug discovery,* 12, 388.